PORTLAND CEMENT pca ASSOCIATION
Research and Development
Construction Technology Laboratories

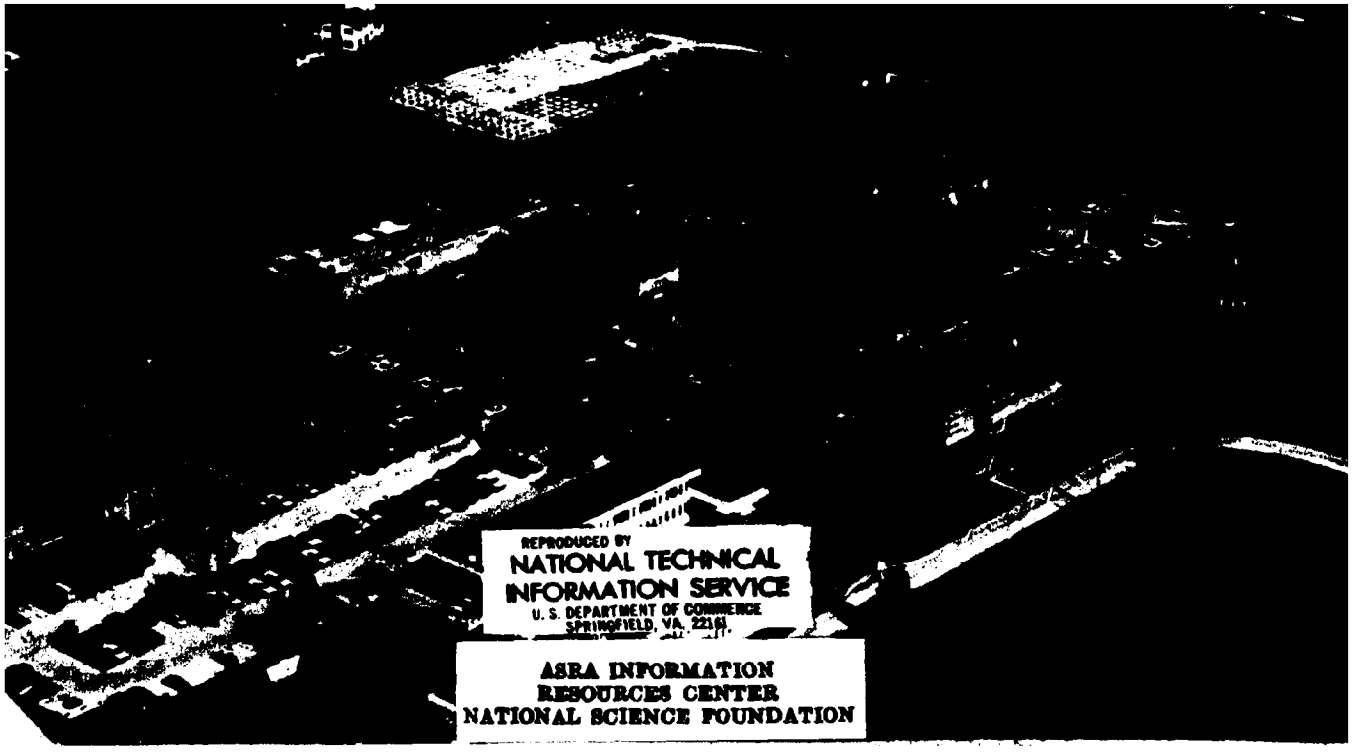

50272-101

REPORT DOCUMENTATION PAGE	1. REPORT NO. NSF/RA-750849	2.	3. Recipient's Accession No. PB281623
4. Title and Subtitle: Structural Walls in Earthquake Resistant Structures: Analytical Investigation, Dynamic Analysis of Isolated Structural Walls, Parts A&B			5. Report Date: October 1976 6.
7. Author(s): M. Fintel, A.T. Derecho, S.K. Ghosh, et al.			8. Performing Organization Rept. No.
9. Performing Organization Name and Address: Portland Cement Association, Engineering Services Department, Old Orchard Road, Skokie, Illinois 60076			10. Project/Task/Work Unit No. 11. Contract(C) or Grant(G) No. (C) (G) GI43880
12. Sponsoring Organization Name and Address: Applied Science and Research Applications (ASRA), National Science Foundation, 1800 G Street, N.W., Washington, D.C. 20550			13. Type of Report & Period Covered 14.

15. Supplementary Notes

16. Abstract (Limit: 200 words)

The objectives of the first part of this analysis are: (1) to evaluate the relative influence of various structural and ground motion parameters on the dynamic response to shear forces and deformations in critical regions of structural walls; (2) to determine estimates of critical force and deformation requirements in hinging regions of structural walls corresponding to different combinations of earthquake intensity and the significant structural parameters; and (3) to correlate data on critical dynamic response obtained in (2) with data from laboratory tests of isolated walls under reversing loads to arrive at recommendations on design force levels. The second part of the program which involves the static analysis of representative wall sections under combined flexure and axial load over the full range of deformation, includes: (1) determining the influence of different design parameters on the characteristics of moment-curvature diagrams, including ductility of typical wall sections; (2) developing charts (interaction diagrams) which can serve as bases for the design of walls in earthquake-resistant structures; and (3) examining the applicability of certain rules proposed to define the hysteretic moment-curvature characteristics of wall sections under reversing loads.

17. Document Analysis a. Descriptors

Earthquake resistant structures
Walls
Structural design
Construction
Dynamic structural analysis

b. Identifiers/Open-Ended Terms

Structural walls

c. COSATI Field/Group

18. Availability Statement: NTIS.	19. Security Class (This Report)	21. No. of Pages: 285
	20. Security Class (This Page)	22. Price: A13-A01

(See ANSI-Z39.18) See Instructions on Reverse

OPTIONAL FORM 272 (4-77)
(Formerly NTIS-35)
Department of Commerce

Report to
NATIONAL SCIENCE FOUNDATION
(RANN) Grant No. GI-43880

STRUCTURAL WALLS IN EARTHQUAKE RESISTANT STRUCTURES

Analytical Investigation
Dynamic Analysis of Isolated Structural Walls - Parts A & B

Overall Project Director: Mark Fintel

Principal Investigator: Arnaldo T. Derecho
Co-Investigators: Satyendra K. Ghosh
Mohammad Iqbal
George N. Freskakis
L. Erik Fugelso

Engineering Services Department
PORTLAND CEMENT ASSOCIATION
Old Orchard Road
Skokie, Ill. 60076

October 1976

TABLE OF CONTENTS

TABLE OF CONTENTS (contd.)

DYNAMIC ANALYSIS OF ISOLATED STRUCTURAL WALLS

INTRODUCTION

BACKGROUND AND NEED FOR THE STUDY

Although structural walls (shear walls)* have had a long history of satisfactory use in stiffening multistory buildings against wind, not enough information is available on the behavior of such elements under strong earthquake conditions.

The thinking among most engineers, starting in the early 1950's and persisting up to the present, has been that relatively flexible rigid frames perform best under earthquake conditions. This preference for the rigid frame in earthquake-resistant structures has been fostered, in part, by the full treatment given the subject in design codes. This preference for rigid frames tended to exclude consideration of alternative and equally satisfactory or possibly better solutions.

Observations of the performance of buildings subjected to earthquakes during the past decade have focused attention on the need to minimize damage in addition to ensuring the general safety of buildings during strong earthquakes. The need to control damage to both structural and nonstructural components during earthquakes becomes particularly important in buildings such as hospitals and other facilities which must continue operation following a major disaster. Damage control, in addition to life safety, is also economically desirable in tall buildings designed for residential and commercial occupancy, since the nonstructural components in such buildings usually account for 60 to 80 percent of the total cost.

There is little doubt that structural walls offer an efficient way to stiffen a building against lateral loads. When proportioned so that they possess adequate lateral stiffness to reduce the interstory

*In conformity with the nomenclature soon to be adopted both by the Applied Technology Council and in the forthcoming revised edition of Appendix A to ACI 318-71, Building Code Requirements for Reinforced Concrete,[1] the term "structural wall" is used in place of "shear wall".

distortions due to earthquake-induced motions, walls effectively reduce the likelihood of damage to the nonstructural elements contained in a building. When used with rigid frames, walls form a structural system that combines the gravity-load-carrying efficiency of the rigid frame with the lateral-load-resisting efficiency of the structural wall.

Observations of the comparative performance of rigid frame buildings and buildings stiffened by structural walls during recent earthquakes,[2,3,4] have clearly demonstrated the superior performance of buildings stiffened by properly proportioned and designed structural walls--from the point of view of safety and especially from the standpoint of damage control.

The recognition of the need to minimize damage under strong earthquakes, in addition to the primary requirement of life safety (i.e., no collapse), clearly imposes more stringent requirements on the design of our structures. This need to minimize damage provided the impetus for a closer examination of the structural wall as an earthquake-resisting element. Among the more immediate questions requiring answers for the establishment of a rational design procedure are:

1. What magnitude of deformation and associated forces can reasonably be expected at critical regions of structural walls under earthquakes of varying intensity?

2. How many cycles of large deformations can be expected corresponding to specific combinations of structure and ground motion characteristics?

3. What stiffness and strength should structural walls in typical plan configurations have in relation to the expected ground motion in order to limit the deformations in the structure to acceptable levels?

4. What design and detailing requirements must be met to provide walls with the strength and deformation capacities indicated by analysis?

The present analytical and experimental investigation was undertaken in an effort to provide answers to the above questions. This study is supported in major part by Grant No. GI-43880 from the National Science Foundation.

OBJECTIVES

Part I - Dynamic Inelastic Analysis of Structures

This part of the investigation has the following objectives:

Major Objectives:

(a) An evaluation of the relative influence of various structural and ground motion parameters on the dynamic response, particularly with respect to forces (especially shear) and deformations in critical regions of structural walls.

(b) The determination of estimates of critical force and deformation requirements in hinging regions of structural walls corresponding to different combinations of earthquake intensity and the significant structural parameters.

(c) The correlation of data on critical dynamic response obtained in (b) with data from laboratory tests of isolated walls under reversing loads to arrive at recommendations on design force levels. The design force levels would be intended to result in structures for which the force and deformation requirements under seismic conditions would be within the capacity indicated by laboratory data.

Secondary Objectives:

(d) The determination of the range of appropriate stiffness of walls corresponding to specified conditions in order to limit interstory distortions to acceptable levels. (The limits on the interstory distortions will depend on the tolerable deformations of specific nonstructural elements, including mechanical ductwork attached to the wall.)

(e) The evaluation of dynamic response histories for different parametric combinations in order to arrive at recommendations on a representative loading history which can be used in laboratory testing of structural walls under essentially static, reversed cycles of loading.

During Phase I of the program, dynamic analyses were carried out on isolated structural walls, with only exploratory runs made for frame-wall and coupled wall systems. The study of isolated walls was motivated not only by the need to obtain dynamic response data on the basic element of interest in this investigation, but also by a desire to establish a reference with which results for the more complex structural wall systems can be compared.

In certain cases, where the frame in a frame-wall structure or the coupling beams in a coupled wall structure are relatively flexible compared to the structural wall, the wall can be considered to act essentially as an isolated structural wall.

A detailed consideration of the dynamic response of frame-wall and coupled wall structures is planned for the subsequent phases of the investigation.

Part II - Sectional Analysis under Combined Flexure and Axial Load

This second part of the analytical program, which involves the static analysis of representative wall sections under combined flexure and axial load over the full range of deformation, has three main objectives.

1. To determine the influence of different design parameters on the characteristics of moment-curvature diagrams, including ductility, of typical wall sections.

   Since the basic input to dynamic inelastic structural analysis consists of the force-deformation relationship of the hinging regions of members, in addition to structural geometry and member dimensions, the effect of the design variables on structural response (mainly, deformation requirements) can be examined in terms of their influence on the primary M-φ curves of the critical sections.

2. To develop charts (interaction diagrams) which can serve as bases for the design of walls in earthquake-resistant structure. It is understood that such designs must allow for the effects of shear and reversed cyclic loads.

3. To examine the reasonableness and applicability of certain rules proposed to define the hysteretic moment-curvature characteristics of wall sections under reversing loads.

Work on this part during Phase I has consisted mainly of parametric studies to determine the effect of major design variables on the moment-curvature (M-φ) response curve for sections, as well as the moment-rotation (M-θ) curve for finite segments of structural walls. In addition, an initial effort was made towards objective No. 2 above by preparing a set of interaction diagrams applicable to wall sections covering a wide range of the significant design parameters.

ANALYSIS PROCEDURE - AN OVERVIEW

Part I - Dynamic Inelastic Analysis of Structures

It was recognized early in the study that if the design procedure to be developed was to be cast in practical form, it would have to involve only the most important parameters affecting the behavior of structural walls under seismic conditions. A parametric study considering reasonable variations in what were thought to be significant structural and ground motion variables was thus planned as a logical preliminary step to the compilation of data for the design procedure itself. Once the major variables were isolated, the formulation of the design procedure could proceed on the basis of these few major parameters.

The general procedure followed in the dynamic response study is described below:

1. A reference 20-story isolated structural wall, representing a typical element in a structural wall or "cross-wall" structure, was designed on the basis of the Uniform Building Code (UBC),[5] Zone 3 requirements.*

   A number of other designs were also considered to determine the practical range of variation of the required strength (yield level) corresponding to different stiffnesses and wall cross sections. On the basis of this study, the ranges of variation of the different structural parameters were established.

*It is pointed out that the use of UBC requirements to establish the dimensions (mainly relating to strength) of the reference structure has little bearing on the results of the analysis. The principal reason for the use of the UBC provisions (or of any code provisions for that matter) is to establish the practical range of variation of certain design parameters.

The major structural parameters considered were the fundamental period, T_1, and the flexural yield level, M_y, i.e., the force required to produce first yield in bending. For the purpose of defining the "first yield", a bilinear idealization was used to replace the actual curvilinear force-deformation relationship of structural members. For the basic 20-story structure studied, an initial fundamental period ranging from 0.8 sec. to 2.4 sec. and a yield level for the base of the wall ranging from 500,000 in-kips, to 1,500,000 in-kips were considered.

2. A number of strong-motion accelerograms and their corresponding velocity response spectra were examined for possible use as input in the dynamic analyses. Included in the study were several artificially generated accelerograms.

Because the number of analyses which could be undertaken to examine a particular parameter was obviously limited, it was necessary to limit consideration of input motions to those which would produce maximum or near-maximum response, and at the same time would represent realistic ground motions. An effort was made to examine the general characteristics of strong-motion records as a basis for judging the reasonableness of certain artificially generated accelerograms. However, the question of the reasonableness of an input motion for a given site was not considered.

In studying input motions, the following three characteristics affecting dynamic structural response were recognized:

(a) intensity - used here as a measure of the amplitude of the large acceleration pulses;

(b) duration of the large-amplitude pulses;

(c) frequency characteristics.

Except where duration was the parameter of interest, all the structures studied were subjected to 10 seconds of ground motion. The input motions were normalized with respect to intensity by multiplying the acceleration ordinates by a factor calculated to yield a "spectrum intensity"* equal to 0.75, 1.0 or 1.5 times that of the N-S component of the 1940 El Centro record.

The velocity response spectra of a total of 27 natural and 17 artificial accelerograms were examined for the purpose of determining the frequency characteristics of these motions. Characteristic variations of the frequency distribution within the period range from 0 to about 4 seconds were noted and used as a basis for selecting the input motions for use in the dynamic analyses.

3. A major requirement of the analysis to be used in the dynamic response study was the consideration of inelastic deformations at critical regions of structural members. Since economic considerations in design generally result in structural dimensions which allow inelasticity to develop when a structure is subjected to a major earthquake, the determination of the magnitude of the inelastic deformations (or the ductility requirement) clearly became the principal response parameter of interest.

*Defined here as the area under the 5%-damped relative velocity response spectrum between the periods of 0.1 and 3.0 seconds.

After examining a number of dynamic inelastic analysis computer programs and considering the availability of support for modifications which were deemed essential for the planned investigation, it was decided to use the program DRAIN-2D.[6] The program has been implemented on the CDC 6400 at Northwestern University. The present version of the program, used in the analysis of isolated structural walls, includes a capability for considering a 'degrading stiffness' model for reinforced concrete beams developed by R. W. Litton and G. H. Powell. Also included is an option to output compact time histories of response. Further modifications were introduced into the program by S. K. Ghosh and A. T. Derecho[7] at Portland Cement Association to allow plotting of response data*.

An effort was made to examine the feasibility of minimizing the cost per analysis without sacrificing accuracy in the relevant data, to permit a more extensive evaluation of the selected parameters. A preliminary series of analyses was undertaken to examine such possibilities as the use of a mathematical model of the isolated wall with lesser number of concentrated masses than floor levels and the use of a relatively longer time step for the numerical integration. Also considered was the question of the most appropriate model for the hinging region at the base of the wall.

*More recent (August 1976) modifications to Program DRAIN-2D, undertaken by I. Buckle and G. H. Powell at the request of PCA, include a model for a shear-shear slip mechanism at plastic hinges with an option to consider a third, descending branch of the M-θ and V-γ curves.

The frequency content of the input motion was considered first because of the significant effect it can have on the dynamic response of a given structure. It was deemed necessary to identify early in the study the frequency content distribution which would produce near-maximum response (for a fixed intensity and duration of the motion) in structures with specific periods and yield levels so that the appropriate input motion could be used in subsequent analyses where other parameters were varied.

The dynamic analyses assumed structural elements with unlimited deformation capacity (or ductility), since a major objective of these analyses is the determination of the magnitude of the deformation requirements corresponding to specific sets of parameter values. (The experimental investigation will then develop detailing procedures by which the indicated deformation requirements can be provided.)

To isolate the effect of individual variables on the response, only the particular parameter studied was varied in the reference structure at any one time. Although the process of modifying only one basic parameter of a structure while suppressing any change in other parameters* is artificial and may sometimes result in unrealistic structures, this device was considered necessary as a research procedure in order to avoid uncertainties in evaluating the effect of each variable.

4. For the purpose of the parametric study, the results of the dynamic analyses are presented mainly in the form of envelopes of selected response quantities, i.e., the maximum horizontal

*For instance, increasing the stiffness (and hence the frequency) of a structural wall by increasing its overall dimensions or its depth will ordinarily be accompanied by an increase in its strength or yield level.

displacements, interstory displacements, moments, shears, ductility ratios and cumulative plastic hinge rotations along the height of the structure. Time history plots of a number of response quantities were also obtained in the course of the analyses and are presented where they help in understanding the observed behavior. In addition, moment-rotation curves are also shown for some cases.

5. In the development of the design procedure, the principal concern was the determination of appropriate design force levels that would ensure adequate stiffness and strength and which, when combined with proper reinforcement details as indicated by laboratory tests, would provide the required deformation capacity.

To provide a broad base upon which the conclusions of this part of the study could rest, and to extend the results to structures with heights other than 20 stories and ground motions with intensities other than 1.5 ($SI_{ref.}$), a substantial number of analyses were made in addition to those undertaken for the parametric study. Much of this additional computation was necessitated by the observed sensitivity of the maximum base shear (an important design parameter) to higher modes of response and by the observation that when extensive yielding occurs, input motions which are critical with respect to displacements and rotational ductilities can in fact result in relatively low shears.

The procedure used in determining design force levels is based on a correlation of results from the dynamic analyses with data obtained from the experimental program.

6. The study aimed at formulating recommendations on a representative loading history (which can be used in testing specimens under essentially static reversing loads) was undertaken to establish reasonable bounds on the number of loading cycles which can be expected under various combinations of structure and ground motion parameters. To this end, the time history plots generated in the course of the parametric study and the development of the design procedure were examined, and characteristic measures of displacement response noted.

Part II - Sectional Analysis Under Combined Flexure and Axial Load

Work on this part of the project during Phase I was confined mainly to objective No. 1, with an intial effort made toward objective No. 2.

The main purpose of the study under objective No. 1 is to relate the type of structural wall section, as characterized by the significant design variables, to the expected deformation requirements. The design variables considered were:

(a) shape of structural wall cross-sections,

(b) percentage of longitudinal reinforcement,

(c) level of axial loading,

(d) degree of confinement of compression zone concrete.

The results of the study of the effect of sectional shape on the behavior of wall sections under combined bending and axial load were included in the Progress Report of August 1975.[8]

An initial effort was also made towards objective No. 2 by preparing a set of interaction diagrams applicable to wall sections covering a wide range of significant design parameters. These charts, which were presented in Supplement 3[9] to the Progress Report of August

1975, are intended to be used, in conjunction with data from the experimental program, in proportioning structural wall sections for earthquake-resistant structures.

In view of the fact that any recommendations on the detailed proportioning of structural wall sections will have to await final reduction and evaluation of the experimental data, it was decided to defer further work on Part II* in favor of completing Part I to the point where design force levels could be derived on the basis of the results of the dynamic analyses and the initial data from the experimental program.

*Beyond that reported in the Progress Report of August 1975, Reference 8.

COMPUTER PROGRAMS

Dynamic Inelastic Analysis of Structures

DRAIN-2D - General Features: The dynamic analysis studies were carried out using the computer program DRAIN-2D which was developed at the University of California at Berkeley. The program, with certain modifications and additions, has been implemented on the CDC 6400 computer at the Vogelback Computing Center of Northwestern University.

DRAIN-2D is a general purpose program for the dynamic analysis of plane inelastic structures subjected to earthquake excitation. Detailed information concerning the program is given in Reference 6 and 7. The essential features of the program, as presently implemented at Northwestern University, are discussed below.

1. The program considers only plane structures.
2. A structure may consist of a combination of beam or beam-column elements, truss elements or infill panel elements. The moment-rotation characteristics for the beam elements can be defined in terms of a bilinear relationship which may be stable hysteretic or may exhibit the "degrading stiffness" characteristic for deformation cycles subsequent to yielding.
3. The mass of the structure is assumed to be concentrated at nodal points.
4. Horizontal and vertical components of the input (base) acceleration may be considered simultaneously. The input motions are assumed applied directly to the base of the structure (no soil-structure interaction effects are considered).

5. Several types of damping may be specified, including mass-proportional and stiffness-proportional damping.

6. Shear deformations and the P-Δ effect in frame elements can be taken into account.

7. Output options include printouts of response quantities (e.g., displacement components and forces at node points and plastic rotations at member ends) corresponding to specified nodes as well as response envelopes at given time intervals. Envelopes of basic response quantities are automatically printed at the end of each computer run. Time histories of specified response quantities presented in compact form can also be obtained.

For structures consisting of beam elements (including columns under constant axial load) plots of a variety of response quantities can be obtained during each run.

The structural stiffness matrix is formulated by the direct stiffness method, with the nodal displacements as unknowns. The dynamic response is determined using step-by-step integration based on the assumption of a constant response acceleration during each time step.

The elements of particular interest in this study are beams and beam-columns, and especially beams characterized by a progressive decrease in reloading stiffness with cycles of loading subsequent to yield. In DRAIN-2D, both flexural and axial stiffnesses of these elements are considered. Variable cross sections may be taken into account by specifying the appropriate stiffness coefficients. Inelasticity is allowed in the form of concentrated plastic hinges at the element ends. For beam-column elements, the interaction between axial force and moment in causing yielding is taken into account in an approximate manner.

The moment-rotation characteristics of the inelastic hinges at the ends of beam and beam-column elements are specified in terms of an initial stiffness, k, and a post-yield or strain-hardening stiffness, pk, as shown in Fig. 1.

Two types of hysteretic loops can be specified for the moment-rotation curve characterizing the inelastic point hinges at element ends. The first one is the more common stable loop, shown in Fig. 2a, in which the unloading and reloading stiffnesses are equal to the initial stiffness. For this case the program accounts for the behavior of an element with inelastic hinges at its ends by assuming an equivalent element consisting of two parallel components, one elastic and the other elasto-plastic.

The second type of hysteretic loop is one which exhibits a decreasing stiffness for reloading cycles subsequent to yield. The basic or primary moment-rotation curve for the beam element with decreasing stiffness is defined in Fig. 1. After yielding occurs, however, the reloading branch, and to a minor degree the unloading branch, of the curve exhibits a decrease in slope (i.e., stiffness). This decrease in stiffness is assumed to be a function of the maximum rotation reached during any previous cycle; in DRAIN-2D it is determined by a set of rules representing an extended version of the rules proposed by Takeda and Sozen.[10] A single element model is used for this case. A typical plot of this moment-rotation hysteretic loop is shown in Fig. 2b.

Modifications Introduced into DRAIN-2D: Early runs using DRAIN-2D indicated the desirability of certain changes in the program. At the request of the Portland Cement Association, G. H. Powell and R. W. Litton at the University of California, Berkeley, introduced changes into the program to enable it to consider modifications of the basic

Takeda model for the decreasing stiffness beam element. The parameters α and β shown in Fig. 2b, which allow the basic decreasing stiffness model to be varied to correspond more closely to experimental results, were incorporated into the program. Powell and Litton also provided options for printing and storing on file the time histories of most response quantities in a compact and convenient form.

In addition to the above modifications, a major effort was made at the Portland Cement Association to incorporate plotting capabilities into the program. Plots of time histories of forces and deformations, as well as response envelopes, can be obtained automatically with each run. Options to punch cards for both envelopes and time histories of response, which can be used for plotting curves in comparative studies, have also been incorporated.

All modifications to the program DRAIN-2D as used in the study of isolated walls, have been documented and are discussed in detail in Reference 7.

A more recent (August 1976) modification in DRAIN-2D, undertaken by I. Buckle and G. H. Powell at the request of PCA, allows the modelling of the hinging region in a beam element in the form of a flexural 'point hinge' and a shear-shear slip mechanism designed to simulate the transverse relative displacement that can occur between the ends of the hinging region in walls subjected to high shears. The force-displacement relationships for both of these mechanisms can be specified in terms of a three-segment curve, the third segment representing the loss in strength accompanying displacements beyond the point of maximum strength. The behavior of the hysteresis loops under cyclic reversed loading can range from the 'stable loop' to Clough's model for degrading stiffness.[11] Plotting routines developed for earlier versions of the

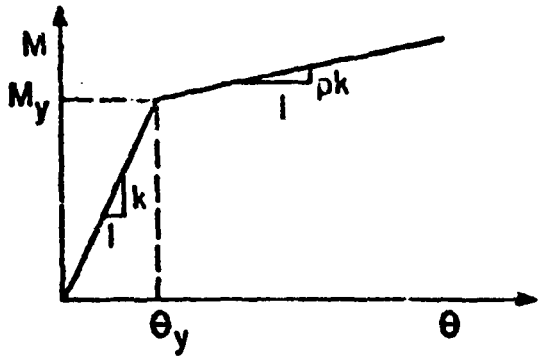

Fig. 1 Moment - Rotation Relationship

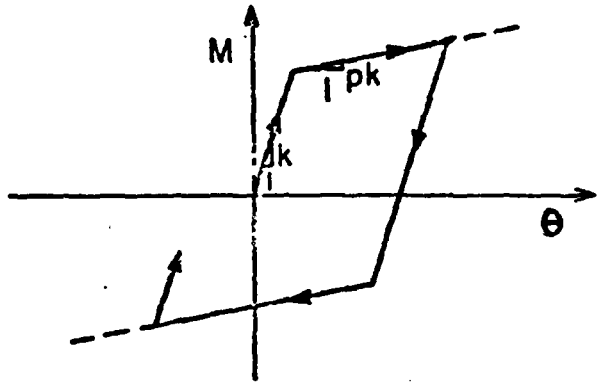

Fig. 2a Stable Hysteretic Loop

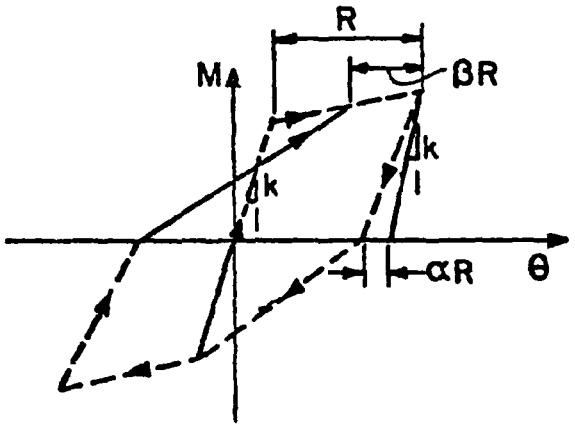

Fig. 2b Decreasing Stiffness Hysteretic Loop

program have already been adapted to the subroutines for this latest modification. These latest options added to DRAIN-2D have not been used in the study of isolated walls reported here; it is intended to use these options in the study of coupled walls and frame-wall systems.

Sectional Analysis Under Combined Flexure and Axial Load

The first step towards the realization of objectives No. 1 and 2 of this part of the analytical investigation was the development of a computer program for realistic nonlinear analyses of structural wall cross sections under flexure and axial compression. The developed program is quite general in that it allows a wide range in specifying the geometric and material properties of the sections to be analyzed. Sections of all commonly encountered shapes, containing a large number of reinforcement layers, can be dealt with. The stress-strain properties of steel and concrete are represented by realistic analytical relationships built into the program, or may be in the form of experimental data defined at discrete points. The output for each section analyzed is obtained in the form of a set of bending moment and curvature values, corresponding to a given magnitude of axial load applied on the section. Detailed documentation for this program is given in Reference 12.

Other Programs

Two dynamic analysis computer programs, DYMFR[13] and DYCAN,[14] developed at the Portland Cement Association, were used primarily to determine the undamped natural frequencies and mode shapes of the buildings considered in the parametric study. DYMFR is a program for the dynamic analysis of plane frame-wall systems, while DYCAN is designed specifically for the dynamic analysis of inelastic isolated cantilevers.

Both of these programs are implemented on the META4-1130 computing system at the PCA.

Another PCA-developed program, DYSDF,[15] for the dynamic analysis of single-degree-of-freedom systems (both linear and nonlinear) was used to calculate and plot the response spectra for the various input motions studied in connection with this investigation.

A number of other independent programs have been developed for various specific purposes. Among these is a program, AREAMR,[16] which utilizes the punched data from DRAIN-2D to compute the cumulative areas under moment-rotation diagrams, as well as the cumulative ductilities. The results can be plotted as functions of the elapsed time. Another useful program is ANYDATA.[17] Given a number of input arrays, this program can produce plots according to various specified arrangements. A number of smaller programs have been developed for preparing composite plots of response envelopes and time histories. A separate class of small programs has also been prepared for the processing of punched data from the sectional analysis program.

REFERENCES

1. Appendix A, Building Code Requirements for Reinforced Concrete, ACI 318-71, American Concrete Institute, P.O. Box 4754, Redford Station, Detroit, Michigan 48219.

2. "The Behavior of Reinforced Concrete Buildings Subjected to the Chilean Earthquakes of May 1960," Advanced Engineering Bulletin No. 6, Portland Cement Association, Skokie, Ill., 1963.

3. Fintel, M., "Quake Lesson from Managua: Revise Concrete Building Design?," Civil Engineering, ASCE, August 1973, pp. 60-63.

4. Anonymous, "Managua, If Rebuilt on Same Site, Could Survive Temblor," Engineering News Record, December 6, 1973, p. 16.

5. Uniform Building Code, 1973 Edition, International Conference of Building Officials, 5360 South Workman Mill Road, Whittier, California 90601.

6. Kanaan, A.E. and Powell, G.H., "General Purpose Computer Program for Inelastic Dynamic Reponse of Plane Structures," (DRAIN-2D), Report No. EERC 73-6, Earthquake Engineering Research Center, University of California, Berkeley, April 1973.

7. Ghosh, S.K. and Derecho, A.T., "Supplementary Output Package for DRAIN-2D, General Purpose Computer Program for Dynamic Analysis of Plane Inelastic Structures," Supplement No. 1 to an Interim Report on the PCA Investigation, "Structural Walls in Earthquake-Resistant Structures," NSF-RANN Grant No. GI-43880, August 1975.

8. Derecho, A.T., Freskakis, G.N., Fugelso, L.E., Ghosh, S.K. and Fintel, M., "Structural Walls in Earthquake-Resistant Structures - Analytical Investigation, Progress Report," Report to the National Science Foundation, RANN, under Grant No. GI-43880, Portland Cement Association, August 1975.

9. Ghosh, S.K., Derecho, A.T. and Fintel, M., "Preliminary Design Aids for Sections of Slender Structural Walls," Supplement No. 3 to the Progress Report on the PCA Analytical Investigation, "Structural Walls in Earthquake-Resistant Structures," NSF-RANN Grant No. GI-43880, Portland Cement Association, August 1975.

10. Takeda, T., Sozen, M.A. and Nielsen, N.N., "Reinforced Concrete Response to Simulated Earthquakes," Journal of the Structural Division, ASCE, Proceedings, Vol. 96, No. ST12, December 1970.

11. Clough, R.W. and Johnston, S.B., "Effect of Stiffness Degradation on Earthquake Ductility Requirements," Proceedings, Japan Earthquake Engineering Symposium, Tokyo, October 1966.

12. Ghosh, S.K., "A Computer Program for the Analysis of Slender Structural Wall Sections under Monotonic Loading," Supplement No. 2 to an Interim Report on an Investigation of Structural Walls in Earthquake Resistant Structures (PCA Project No. CR3675-4320, NSF-RANN Grant No. GI-43880, Portland Cement Association, Skokie, Ill., August 1975.

13. Derecho, A.T., "Program DYMFR - IBM 1130 Program for the Dynamic Analysis of Plane Multistory Frames," Portland Cement Association, 1971 (unpublished).

14. Derecho, A.T., "Program DYCAN - IBM 1130 Program for the Dynamic Analysis of Isolated Cantilevers," Portland Cement Association, 1974 (unpublished).

15. Derecho, A.T. and Fugelso, L.E., "Program DYSDF - for the Dynamic Analysis of Inelastic Single-Degree-of-Freedom Systems," Portland Cement Association, 1975 (unpublished).

16. Ghosh, S.K., "Program AREAMR - for the Computation of Cumulative Areas under Moment-Rotation Curves and Cumulative Ductilities," Portland Cement Association, 1976 (unpublished).

17. Ghosh, S.K., "Program ANYDATA - A General Purpose Plotting Routine," Portland Cement Association, 1976 (unpublished).

DYNAMIC ANALYSIS OF ISOLATED STRUCTURAL WALLS

PART A - INPUT MOTIONS

GENERAL

The primary objective of the analytical program is the estimation of the maximum forces and deformations which can reasonably be expected at critical regions in structural walls subjected to strong earthquakes. In view of this, the selection of an appropriate set of acceleration records for use as input horizontal base motions in the dynamic analyses was considered an essential preliminary step in the investigation.

The statistical character of structural response to earthquake motions requires the consideration of a sufficient number of input motions in the dynamic analysis. In an effort to minimize the necessary number of records for use in the analysis, an examination was made of the major parameters characterizing strong-motion accelerograms. If accelerograms can be classified into fairly broad categories according to certain basic properties, it should be possible to obtain, even with the deterministic approach used in the present study, good estimates of the maximum response of structures to earthquakes with a limited number of input records. For this purpose, a group of about 20 records were selected from a compilation of digitized strong-motion accelerograms published by the California Institute of Technology.[1] In addition to the natural records, a number of artificially generated accelerograms were considered.

The principal ground motion characteristics affecting dynamic structural response are intensity, duration and frequency content. Intensity indicates a characteristic measure of the amplitude of the acceleration record. Duration refers to the length of the record during which relatively large amplitude pulses occur, with due allowance for a reasonable build-up time. The frequency characteristics of a given

ferent component waves (having different frequencies) which make up the motion. Guzman, Crouse and Jennings[2] have pointed out that the best available indicators of the damage capability of the ground motion from earthquakes are the duration and the response spectra. The response spectra inherently contain the measures of intensity and frequency content.

By arbitrarily setting the duration of the input motion at 10 seconds, using Housner's "spectrum intensity" as a measure of intensity and noting certain trends in the damped relative velocity response spectra associated with the accelerograms, a basis is laid for the selection of records for use as input in the dynamic analysis. This is discussed in greater detail below.

DURATION

Because of the significant computer cost involved in dynamic inelastic analysis, particularly for the coupled-wall and frame-wall systems planned for the subsequent phases of this investigation, it was decided at the outset to use a duration of 10 seconds of the base excitation for most analyses. Only when studying the effect of duration on the response were 20-second records used.

A further justification for the use of a 10-second duration for the input motion is that most strong-motion accelerograms recorded on firm alluvial soil contain a short phase (5-15 seconds) of relatively consistent stationary high-intensity oscillations with dominant frequencies in the range of 2 to 5 cycles per second. Deterministic dynamic studies by Bogdanoff[3] have shown that structures subjected to a number of these ground motions experience their peak relative displacements during this short intense phase. Penzien and Liu,[4] on the basis of

the nonstationary response of linear systems to stationary "white noise", suggest that for typically damped (5-10% of critical) linear systems with fundamental periods up to 2 seconds, a 10-second duration of excitation gives ample time for structures to approach their steady state conditions; also, that increasing the duration of excitation beyond 10 seconds has a relatively small effect on the probability distribution of peak response. In a study of critical excitations for the design of earthquake-resistant structures, Drenick[5] also observed that damage to a structure is most likely to occur during the first 5 to 10 seconds of strong ground motion. For nonlinear structures, Clough and Benuska[6] have shown that the only significant effect of an increase in the duration of high-intensity base excitation is the cumulative plastic rotations in critically stressed members.

FREQUENCY CHARACTERISTICS

A typical strong-motion accelerogram shows an extremely complex series of oscillations. Examples of earthquake accelerograms, the NS and EW component of the May 18, 1940, Imperial Valley earthquake as recorded at El Centro, are shown in Fig. 1.[1] Any such record may be thought of as a superposition of simple, constant-amplitude waves, each with a different frequency, amplitude and phase. The importance of knowing the frequency characteristics of a given input motion lies in the phenomenon of resonance or quasi-resonance, which occurs when the frequency of the exciting force or motion approaches the frequency of the structure. Near-maximum response to earthquake excitation can be expected if the dominant frequency components occur in the same frequency (or period) range as the dominant effective frequencies (or periods) of a structure.

A convenient way of studying the frequency characteristics of an accelerogram is provided by the Fourier amplitude spectrum. Figure 2, from Reference 7, shows the Fourier amplitude spectra for the NS and EW components of the 1940 El Centro record. This spectrum provides a frequency decomposition of the accelerogram, indicating the amplitude (in units of velocity - a measure of the energy content) of the component at a particular frequency. Another commonly used measure of the frequency content of an accelerogram is the velocity response spectrum. This is a plot showing the variation of the maximum absolute value of the relative velocity of a linear single-degree-of-freedom system with the undamped natural period (or frequency) when subjected to a particular input motion. Figure 3 (Ref. 8) also shows the relative velocity response spectra for the NS and EW components of the 1940 El Centro record, for different values of the damping factor (specified as a fraction of the critical damping coefficient). Hudson has shown[9] that when the maximum response of a system occurs at the end of the record, the undamped relative velocity response spectrum has a form identical to that of the Fourier amplitude spectrum of the ground acceleration. Otherwise, these two plots are only roughly similar. As in the Fourier spectrum, the peaks in the velocity response spectrum reflect concentrations of the input energy at or near the corresponding frequencies. For damped systems, these peaks are reduced, the reduction being greater for the shorter period systems.

Although both Fourier amplitude and undamped velocity response spectra exhibit a jagged character, with peaks and troughs occurring at close intervals, it is usually possible to recognize a general trend in the overall shape of the curve. By noting the general shape of the spectrum in the frequency range of interest, a characterization of the input motion in terms of frequency content can be made.

In this study, where a viscous damping coefficient of .05 of critical for the first mode was used as the basic value for the dynamic analysis model, the 5% damped velocity response spectra corresponding to 10 seconds of each of 20 selected records were examined. Figures 4(a) and 4(b) show the velocity response spectra for the NS and EW component of the 1940 El Centro motion, based on the initial 10 seconds of the record. The remaining spectra considered are shown in Appendix A. On the basis of this examination, two general categories were recognized, namely:

1. A "peaking" accelerogram with a spectrum exhibiting dominant frequencies over a well-defined period range. The NS component of the 1940 El Centro record is an example of this class.
2. A "broad-band" accelerogram with a spectrum that remains more or less flat over the period range of interest. The vertical component of the 1940 El Centro record may be classified under this category.

   A sub-class of the broad-band category is a record with a spectrum which increases with increasing period within the period range of interest. This may be referred to as an "ascending" accelerogram. The EW component of the 1940 El Centro record is typical of this type of record.

While the procedure proposed above represents a rather crude method for classifying accelerograms in terms of frequency content, it nevertheless provides a sufficient basis for determining the potential severity of a given input motion in relation to a specific structure.

For a linear structure in which the dynamic behavior is dominated by the fundamental mode, as is the case in most reinforced concrete multistory buildings with structural walls, a strong response can be expected when the fundamental period falls within the peaking range of the input motion, i.e., within the period range where the dominant components of the input motion occur. Lesser response can be expected if the dominant period of the structure falls outside the peaking range.

The effective period of yielding structure changes with the extent of inelastic action and the general state of deformation of the structure (i.e., loading or unloading). Thus, different components of an input motion will exert varying influences on the behavior of the structure at different times. Since the general effect of yielding is to increase the period of vibration, the longer-period components in a record will tend to play a greater role as yielding progresses in the structure.

In a structure such as an isolated wall, where yielding at and near the base can produce a significant increase in the effective period of vibration, a peaking accelerogram with the spectrum peak centered about the initial fundamental period of the structure produces its maximum effect prior to yielding. After yielding, the effect of the dominant frequency components diminishes as the effective period of the structure moves beyond the peaking range. For such a structure, a broad-band accelerogram of the same intensity may produce a more severe response.

In isolated walls where only nominal yielding occurs, or in multiply-redundant structures such as frames and frame-wall systems, where yielding in some elements may not significantly change the effective period of the structure, the initial fundamental period may continue to provide a good indication of the dynamic properties of the structure even beyond first yield. A peaking accelerogram with its

spectrum peak centered about the initial fundamental period will likely produce more severe response when compared to a broad-band accelerogram of the same intensity.

The above two cases are illustrated schematically in Figures 5(a) and (b).

In order to have available a set of accelerograms for use as input in the dynamic analysis, a number of representative records were chosen from a compilation of natural records[1] and augmented by a selection of artificially generated accelerograms. The records were chosen to provide a set of peaking accelerograms with 5%-damped velocity response spectra peaking ranges covering the period range from about 0.5 to 3.0 seconds, as well as some broad-band accelerograms. The set of peaking accelerograms and their respective peaking ranges are listed in Table 1. Since the isolated structural walls considered in the dynamic analysis have fundamental periods varying from 0.8 sec. to 2.4 sec., there will be several records with their dominant frequency components near each of the basic structure periods.

The peaking ranges shown in Table 1 were determined visually such that the width of each range corresponds to an ordinate approximately equal to 2/3 of the peak value. The peaking ranges for the undamped spectra corresponding to the full records and those for the 5% damped spectra corresponding to the first 10 seconds of each record are given. In general, the peaks of the undamped spectra for the shorter, 10-second, segments of an accelerogram occur in the same period ranges as for the full records; however, the values are slightly lower. The period domain for peak ranges for the 5%-damped spectra differ slightly from those for the undamped case mainly because of the greater attenuation of the reponse due to damping for the shorter period structures.

In addition to the natural records listed, several artificially generated motions simulating earthquake accelerations were considered. These include six of the CalTech design earthquake accelerograms (A-1, A-2, B-1, B-2, C-1 and C-2) generated by Jennings, Housner and Tsai;[10] five records generated using the program PSEQGN (denoted here as P-1 through P-5), developed by Ruiz and Penzien;[11] and six records generated using the program SIMQKE, developed by Gasparini.[12] The CalTech accelerograms A, B, C were designed to simulate ground motions of varying intensity and duration corresponding to earthquakes of specific magnitude and epicentral distance. For instance, the A accelerograms are designed to represent the ground motions close to the causative fault of a magnitude 8.5 earthquake. The accelerograms P-1 through P-5 were generated to match, on the average, the spectrum, duration and peak acceleration of the NS component of the 1940 El Centro record.

The accelerograms generated using the program SIMQKE, denoted here as S-1 though S-6, are designed to match a target response spectrum while retaining the general duration and envelope shape of reasonably expected strong-motion records. The target spectrum used for these records was essentially a flat, broad-band spectrum over the period range from 0.3 to 3.0 seconds, which is similar in shape to the design response spectra proposed by Newmark, Blume and Kapur.[13]

For the purpose of the dynamic inelastic analyses planned for this study, the selected accelerograms were classified according to whether they could be considered as "peaking" or "broad-band" with respect to a particular basic structure fundamental period. The study considers basic structures with (initial) fundamental periods of 0.8, 1.4, 2.0 and 2.4 seconds. As a guide to the possible choice of input motions which could be used for any particular structure, Table 2 was prepared. Two

types of entries are shown under each period (where they apply) corresponding to a given accelerogram. An "A" is entered under a given period if the corresponding velocity response spectrum exhibits a narrow peak at or near the period of interest. A "B" is used to indicate that the velocity response spectrum shows a relatively high plateau extending from the period of interest to at least one second higher.

INTENSITY

The best parameter to use as a characteristic measure of the amplitude of the acceleration pulses within the period range of interest has not been clearly established. A commonly accepted measure of intensity is important if accelerograms are to be categorized according to intensity. Some investigators[14,15] have chosen to normalize accelerograms on the basis of the peak acceleration, velocity or displacement occurring within the portion of the record considered. Others have chosen to normalize their input accelerograms in terms of the "spectrum intensity"[8], i.e., the area under the relative velocity spectrum curve* between bounding values of the period representing the limits of the period range of interest. Still others have used the root-mean-square (rms) acceleration, defined as,

$$x_{rms} = \frac{1}{t} \int_0^t x^2 \, dt \, ^{1/2}$$

Figure 6 shows the (evolutionary) rms acceleration plot for the first 20 seconds of the NS component of the 1940 El Centro record.

If the intensity measure is to reflect the variation of acceleration amplitude over the period range of interest, the measure must have the character of an average. By this criterion, the peak acceleration

*Or the integral of the velocity response spectrum, corresponding to a particular damping value, between appropriate limits.

is a poor measure. The spectrum intensity taken over the period range of interest and using a reasonable damping value should yield a more representative measure of intensity. On the basis of a study of the statistical properties of a number of strong-motion records, Liu[16] concluded that the stationary root-mean-square (rms) acceleration provides a good measure of earthquake intensity. He further showed that, for the earthquakes he considered, there exists a close correlation between the stationary rms acceleration and Housner's spectrum intensity.[17]

The spectrum intensity and rms acceleration were calculated for the twenty horizontal components of the records listed in Table 1. The results are shown plotted in Fig. 7; the ordinate is the peak rms acceleration during the first 10 seconds of each record while the abscissa is the corresponding spectrum intensity defined between 0.1 and 3.0 seconds, for 5% damping and a 10 second duration. A linear relationship between the two quantities is suggested, viz.,

$$x_{rms} = (0.51 \pm 0.12)\ SI$$

As an additional check on the appropriateness of the spectrum intensity as a measure of the intensity of an accelerogram, a study of the nonlinear response of single-degree-of-freedom (SDF) systems was undertaken. The object here was to determine if a correlation could be established between the ductility requirement and the spectrum intensity. In SDF systems, the ductility ratio is defined as the ratio of the maximum relative displacement to the displacement corresponding to first yield. For a given earthquake, the ductility ratio serves as a good index of damage in structures or, for a given structure, it provides an indication of the potential destructiveness of an earthquake.

For this study, the first 10 seconds of nine sample records were considered and normalized in terms of spectrum intensity. Spectrum intensities equal to 0.75, 1.0 and 1.5 times the spectrum intensity of the initial 10 seconds of the NS component of the 1940 El Centro record at 5% damping were used. The yield displacements of the structures considered were calculated from the relation,

$$\Delta_y = \frac{.03gK}{2} T^{5/3},$$

which is based on the UBC-75 provision governing the design base shear, with Z = I = S = 1.0. For this purpose, a value of K = 0.80 was used and the yield force was assumed equal to twice the design base shear. A yield stiffness ratio, r_y = 0.05 (i.e., the ratio of the slope of the post-yield branch to the initial slope of the force-deformation curve) and a viscous damping coefficient, β = 0.05, were assumed. Ductility ratios corresponding to SDF systems having different initial periods when subjected to different base motions were determined for the three intensities of each of nine sample records.

Figures 8(a) and 8(b) show the displacement response spectra and the velocity response spectra, respectively, for the different intensities of the E-W component of the 1940 El Centro record. In both figures, the scale factor "f" is the ratio of the spectrum intensity of the input motion used to the reference spectrum intensity. The figures indicate that for the bilinear stable hysteretic systems considered, both the maximum displacements and velocities generally increase with an increase in the intensity of the input motion and the severity of the yielding. The curves corresponding to f = 1.0 in Fig. 8(a) show that the maximum displacements for both linear and bilinear systems are more or less the same over a broad period range, an observation also made by

earlier investigators. A similar behavior was observed by Veletsos[18] in a study using a slightly different normalization scheme. Figure 9 shows the variation of the ductility ratio with the period for the same acceleration record. Similar results were obtained by Clough and Johnston[19] using unscaled accelerograms and the same yielding displacement-period relation (with K = 0.67).

The mean ductility ratio and the mean ductility ratio plus one (unbiased) standard deviation are shown plotted against period in Fig. 10, for each of the intensity values of the nine-record sample. For any given period, the mean and the standard deviation both increase with increasing intensity. Figures 11(a) and (b) show the variation of the mean ductility with the spectrum intensity for two specific initial periods. For simple, stable hysteretic systems subjected to base motions normalized on the basis of spectrum intensity, the mean ductility ratio correlates reasonably well with the spectrum intensity.

On the basis of the above observations, it was decided to use the spectrum intensity as the characteristic measure of the intensity of an accelerogram. Thus, where several acceleration records are used as input in the parametric study, and intensity is not the parameter investigated, each accelerogram is normalized to a reference intensity. For this study, normalization of the intensity measure of the accelerograms is effected by scaling the amplitude of the acceleration records so that the spectrum intensity for 10 seconds of the record, at 5% of the critical damping, matches a specified proportion of a similarly defined spectrum intensity for the NS component of the 1940 El Centro record. Factors of 0.75, 1.0 and 1.5 have been used. The factor 1.5 is generally thought to represent the magnitude of the motion from the largest earthquake reasonably expected in California.[20] Using the

scaling procedure proposed by Guzman and Jennings,[21] this scale factor corresponds roughly to the motion expected from a shallow focus 8.5-magnitude earthquake at an epicentral distance of about 8-10 miles.

SUMMARY

A set of acceleration records for use as horizontal base motion input in structural dynamic analysis have been selected on the basis of intensity, duration and frequency content. From this set a minimum number of accelerograms can be chosen which will have the frequency content to excite any structure in this study in both its initial elastic condition and in the softened condition after yielding. The duration of the records has been limited to ten seconds of the most intense motion, which will generally be sufficient to determine the important features of the response. The amplitudes of the accelerograms have been normalized in terms of the spectrum intensity, which has been shown to be an adequate measure as it correlates well with other measures of intensity as well as with the response of simple linear and non-linear systems.

REFERENCES

1. Analysis of Strong Motion Earthquake Accelerograms, Vol. II, Corrected Accelerograms Parts A, B, C, Report EERL 72-79, California Institute of Technology, Earthquake Engineering Research Laboratory, 1972, 1973, 1974.

2. Guzman, R., Crouse, C.B. and Jennings, P.C., "Determination of Design Earthquakes for Nuclear Power Plants," Technical Report No. 50-T22, Fugro, Inc., 1975.

3. Bogdanoff, J.L., "Comments on Seismic Accelerograms and Response Spectra." (Preliminary Report) Joint U.S.-Japanese Seminar in Applied Stochastics, NSF-JSPS, Tokyo, May 1966.

4. Penzien, J. and Liu, S-C., "Nondeterministic Analysis of Nonlinear Structures Subjected to Earthquake Excitation," Proc. 4th World Conference on Earthquake Engineering, Vol. I, Chile, January 1969.

5. Drenick, R.F., "Prediction of Earthquake Resistance of Structures," Polytechnic Institute of Brooklyn, New York, Final Report to the National Science Foundation on Grant GK 14550, May 1972, 128 pp.

6. Clough, R.W. and Benuska, K.L., "FHA Study of Seismic Design Criteria for High-Rise Buildings," Report HUD TS-3, Federal Housing Administration, Washington, D.C., August 1964.

7. Analysis of Strong Motion Earthquake Accelerograms, Vol. IV, Fourier Spectra, Part A, Report EERL 71-81, California Institute of Technology, Earthquake Engineering Research Laboratory, 1972.

8. Analysis of Strong Motion Earthquake Accelerograms, Vol III - Response Spectra, Part A - Accelerograms IIA001 through IIA020, Report EERL 72-80, California Institute of Technology, Earthquake Engineering Research Laboratory, August 1972.

9. Hudson, D.E., "Some Problems in the Application of Response Spectrum Techniques to Strong-Motion Earthquake Analysis," Bulletin of the Seismological Society of America, Vol. 52, No. 2, April 1962.

10. Jennings, P.C., Housner, G.W. and Tsai, N.C., "Simulated Earthquake Motions for Deisgn Purposes," Proc. 4th World Conference on Earthquake Engineering, Vol. I, Chile, 1969.

11. Ruiz, P. and Penzien, J., "Probabilistic Study of the Behavior of Structures During Earthquakes," Earthquake Engineering Research Center Report No. EERC 69-3, University of California, Berkeley, March 1969.

12. Gasparini, D., "SIMQKE: A Program for Artificial Motion Generation," Internal Study Report No. 3, Dept. of Civil Engineering, Massachusetts Institute of Technology, January 1975.

13. Newmark, N.M., Blume, J.A. and Kapur, K.K., "Seismic Design Spectra for Nuclear Power Plants," Proc., ASCE Journal of the Power Division, PO2, 1973, pp. 287-303.

14. Frank, R. and Gasparini, D., "Evaluation of Seismic Safety of Buildings: Progress Report on Statistical Studies of Response of MDOF Systems to Real and Artificial Ground Motions," Internal Study Report No. 4, Dept. of Civil Engineering, Massachusetts Institute of Technology, January 1975.

15. Goel, S.C. and Berg, G.V., "Inelastic Earthquake Response of Tall Steel Frames," Journal of the Structural Division, ASCE, Paper No. 6061, August 1968.

16. Liu, S-C, "Statistical Analysis and Stochastic Simulation of Ground-Motion Data," The Bell System Technical Journal, 47, pp. 2273-2248, 1968.

17. Housner, G.W., "Behavior of Structures During Earthquakes," Journal of The Engineering Mech. Division, ASCE, Paper No. 2220, October 1959.

18. Veletsos, A.S., "Maximum Deformations of Certain Nonlinear Systems," Structural Research at Rice, Report No. 1, Dept. of Civil Enigneering, Rice University.

19. Clough, R.S. and Johnston, S.B., "Effect of Stiffness Degradation on Earthquake Ductility Requirements," Proc., Japan Earthquake Engineering Symposium, 1966.

20. Derecho, A.T. and Fintel, M., "Earthquake Resistant Design," Chapter 12 in Concrete Engineering Handbook, ed. by M. Fintel, Van Nostrand-Reinhold, New York, 1974.

21. Guzman, R. and Jennings, P.C., "Determination of Earthquake Design Spectra for Nuclear Power Plants," Technical Report No. 51-T22, Fugro, Inc., 1975.

PART A - INPUT MOTIONS

TABLES AND FIGURES

Table 1 - Period Ranges of Peak Velocity Response
for Selected Accelerograms

Earthquake Description	Cal Tech No.#	Component	Period Range of Dominant Velocity Response (sec.)	
			Undamped Spectrum for Entire Record	5% Damped Spectrum for Initial 10 sec. of Record
Imperial Valley, May 18, 1940	A001	S00E	0.4 - 1.2	0.4 - 1.2
El Centro Site, Imperial Valley Irrigation District	A001	S90W	0.3 - 1.6 (1.9 - 2.3)	1.9 - 3.0
	A001	Vert	0.1 - 3.0	0.1 - 3.0 (0.6 - 1.0)
Kern County, July 21, 1952	A002	S00E	0.9 - 2.1	2.4 - 3.0
Pasadena - Cal Tech Athenaeum*	A002	S90W	0.7 - 1.0 (1.4 - 2.5)	0.7 - 1.1
	A002	Vert	0.8 - 1.3	0.6 - 1.2
Kern County, July 21, 1952	A004	N21E	0.3 - 0.9	0.4 - 1.6
Taft Lincoln School Tunnel	A004	S69E	0.3 - 0.9	0.4 - 3.0
	A004	Vert	0.2 - 0.8	
Kern County, July 21, 1952 Hollywood Storage P. E. Lot	A007	S00N	0.9 - 1.4	0.8 - 1.2
Eureka, December 21, 1954 Eureka Federal Building	A008	N11W	1.0 - 1.6 (2.1 - 2.7)	1.0 - 1.6
Eureka, December 21, 1954	A009	N44E	1.4 - 1.7	1.3 - 2.4
Ferndale City Hall	A009	N46W	1.3 - 1.7	0.9 - 1.7
	A009	Vert	1.8 - 2.2	1.4 - 2.0

#See Reference (1). *Second 10 seconds of record.

Table 1 (contd.) - Period Ranges of Peak Velocity Response
for Selected Accelerograms

Earthquake Description	Cal Tech No.	Component	Period Range of Dominant Velocity Response (sec.)	
			Undamped Spectrum for Entire Record	5% Damped Spectrum for Initial 10 sec. of Record
El Almo, Baja, California	A011	S00W	0.8 - 1.2	1.2 - 1.9
February 9, 1956	A011	S90W	0.9 - 1.5	1.0 - 1.3
El Centro, Imperial Valley	A011	Vert	1.0 - 2.0	0.4 - 2.4
Borrego Mountain, April 8, 1968	A019	S00W	1.5 - 2.5	1.5 - 2.4
El Centro, Imperial Valley	A019	S90W	1.3 - 1.6 (2.1 - 2.4)	1.9 - 3.0
Borrego Mountain, April 8, 1968	A020	S00W	1.3 - 2.2	1.1 - 3.0
San Diego Light and Power Bldg.	A020	S90W	1.2 - 2.2	0.9 - 2.2
Parkfield, June 27, 1966	B036	N50E	1.3 - 1.7	1.2 - 1.6
Cholame, Shandon Array No. 12	B036	N40W	1.4 - 2.1	1.6 - 2.4
	B036	Vert	2.3 - 3.0	2.4 - 3.0
San Fernando, February 9, 1971	C041	S16E	0.8 - 1.8	0.9 - 2.0
Pacoima Dam	C041	S74W	0.3 - 0.6	0.4 - 1.7
	C041	Vert	0.2 - 0.6 (1.6 - 2.5)	
San Fernando, February 9, 1971	C048	S00W	1.3 - 2.4	1.5 - 2.2
8544 Orion Blvd., 1st Floor	C048	S90W	2.5 - 3.0	1.5 - 2.0
	C048	Vert	2.2 - 2.9	

NOTE: ( ) denotes secondary peak.

Table 2 - Classification of Selected Accelerograms in Terms of the Shape of Their 5%-Damped Velocity Response Spectra (Duration = 10 seconds)

Accelerogram	Component	Type of Record @ Period (sec.)			
		0.8	1.4	2.0	2.4
Imperial Valley, 5-18-40	NS	A	-	B	-
El Centro	EW	-	B	B	B
	Vert	B	B	B	B
Kern County, 2-21-52	N21E	A	-	-	-
Taft Lincoln School Tunnel	S69E	B	B	B	-
San Fernando, 2-9-71	S16E	-	A	-	-
Pacoima Dam	S74W	-	B	-	-
San Fernando, 2-9-71	NS	-	-	A	-
8544 Orion Blvd.	EW	-	-	A	-
Kern County, 2-21-52	NS	A	-	-	-
Cal Tech Athenaeum	EW	A	-	-	-
	Vert	A	-	-	A
Eureka, 12-21-52 Eureka Federal Building	N11W	B	B	-	-
Eureka, 12-21-52	N44E	-	B	-	-
Ferndale City Hall	N46W	B	A	-	-
	Vert	A	B	-	-
El Alamo, 2-9-56	NS	B	A	-	-
El Centro	Vert	-	B	-	-
Borrego Mt., 4-8-68	NS	-	-	B	B
El Centro	EW	-	-	B	B

@ A - "Peaking" relative to specified period value
B - "Broad band"

Table 2 (contd.) - Classification of Selected Accelerograms in Terms of the Shape of Their 5%-Damped Velocity Response Spectra (Duration = 10 seconds)

Accelerogram	Component	Type of Record			
		Period (sec.)			
		0.8	1.4	2.0	2.4
Borrego Mt., 4-8-68 San Diego L/P	EW	A	A	B	B
Kern County, 2-21-52 Hollywood Storage Building	NS	A	-	-	-
Parkfield, 5-27-66	N40W	B	B	B	B
Cholame, Shandon No. 12	N50E	-	A	-	-
Cal Tech-Artificial	A1	B	A	-	-
(Jennings, Housner, Tsai)	A2	B	B	A	-
	B1	B	-	-	B
	B2	B	A	-	-
	C1	B	B	-	-
	C2	B	B	-	-
PSEQGN-Artificial	P1	B	B	B	B
(Ruiz, Penzien)	P2	-	A	B	B
	P3	A	-	B	B
	P4	A	-	B	B
	P5	-	B	B	B
SIMQKE-Artificial	S1	B	B	B	B
(Gasparini)	S2	B	B	B	B
	S3	-	-	B	B
	S4	B	B	B	B
	S5	A	B	B	B

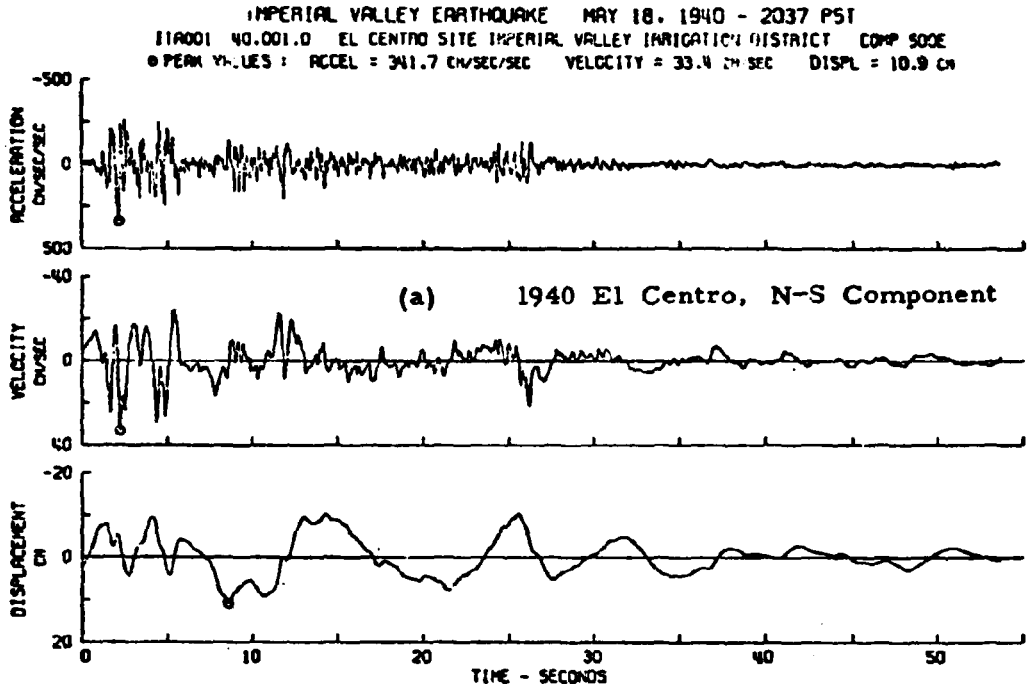

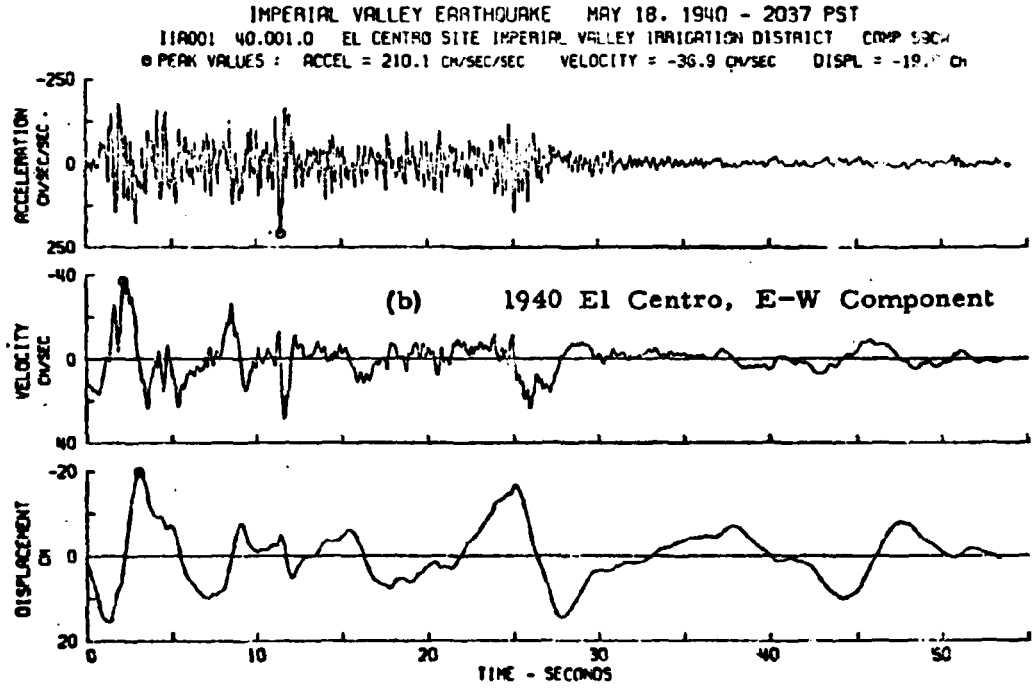

Fig. 1 Acceleration, Velocity and Displacement Histories 1940 El Centro record (from Ref. 1)

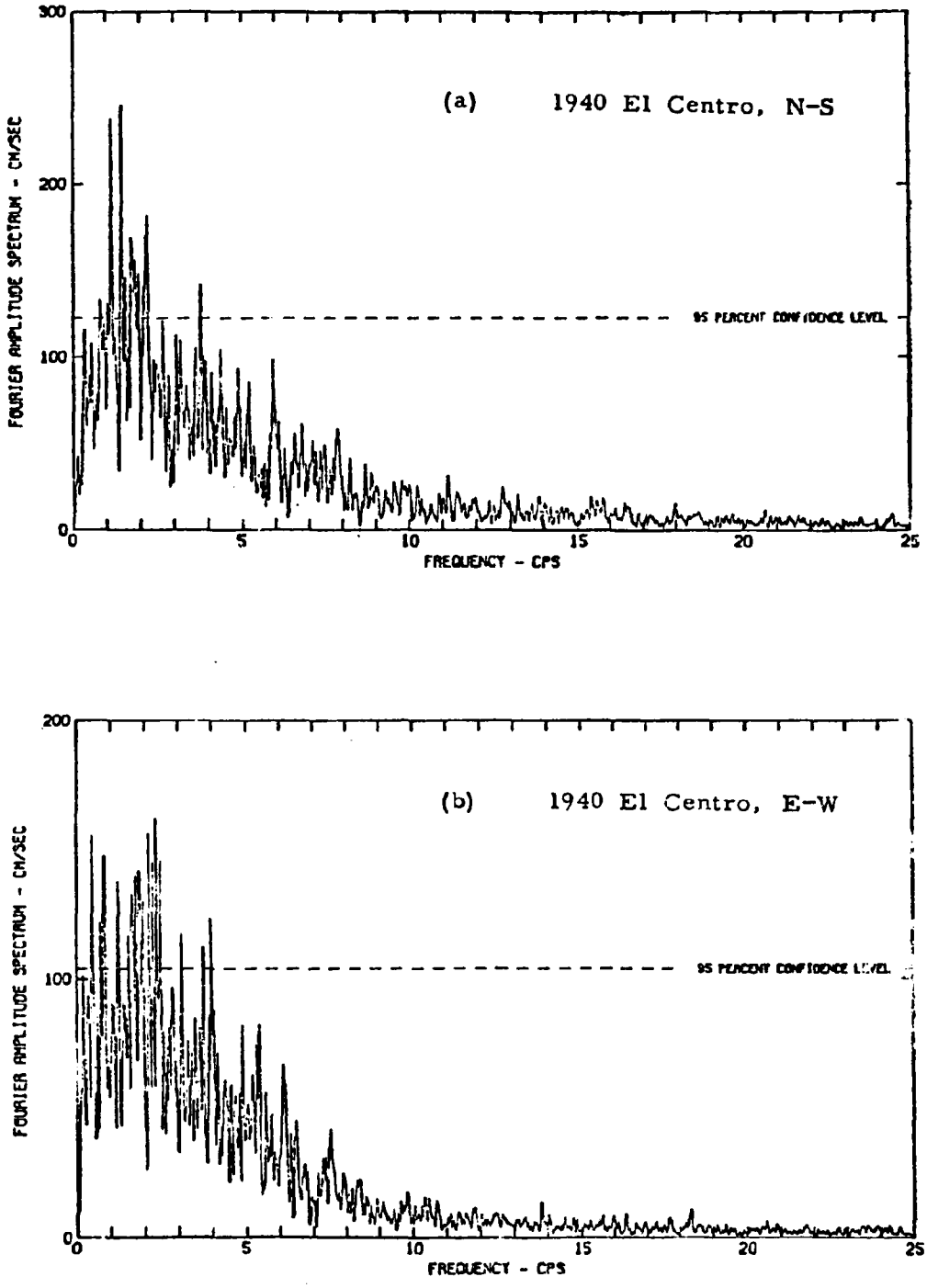

Fig. 2 Fourier Amplitude Spectrum - 1940 El Centro Record (from Ref. 7)

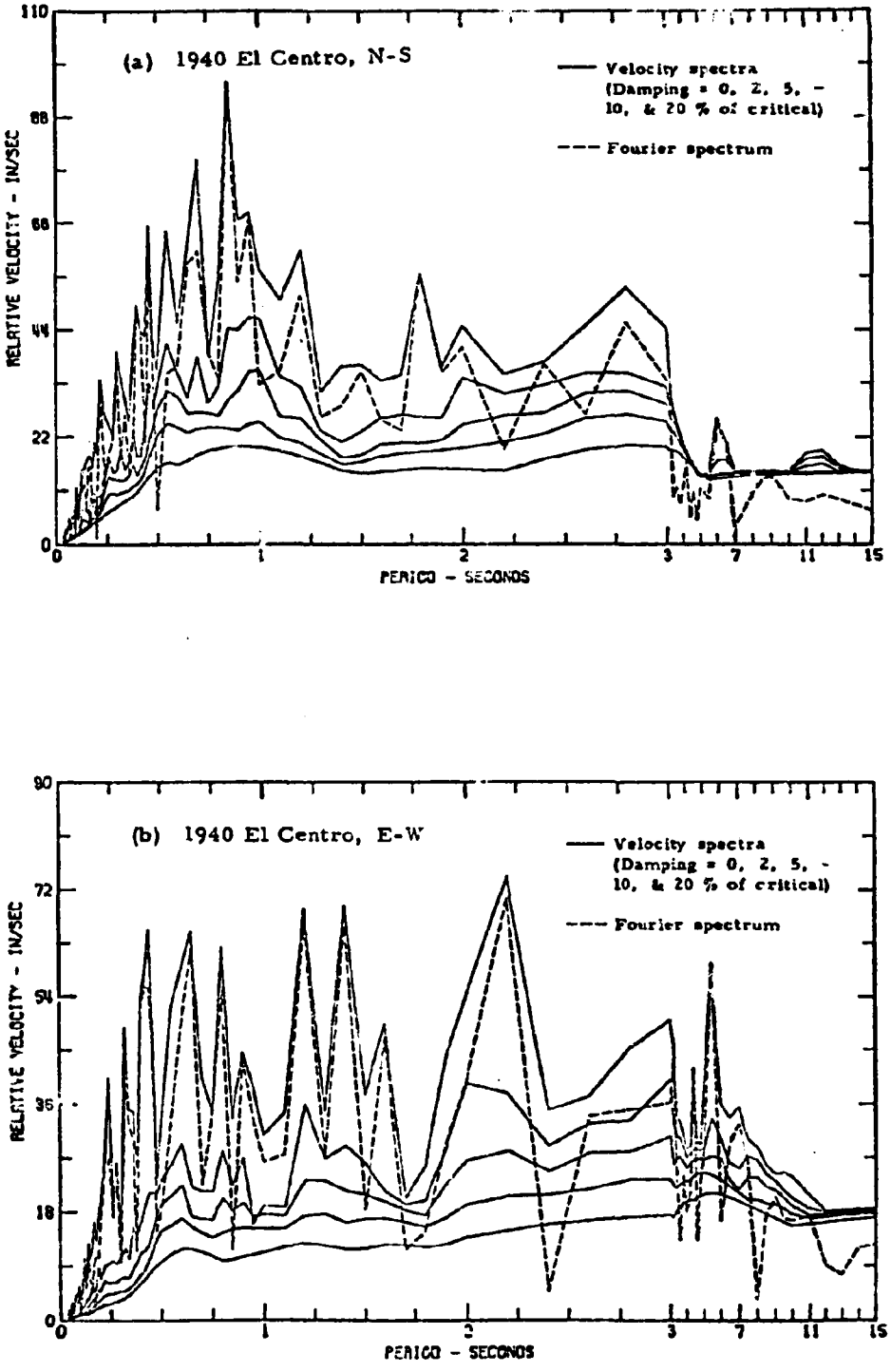

Fig. 3 Relative Velocity Response Spectra - 1940 El Centro Record (from Ref. 8)

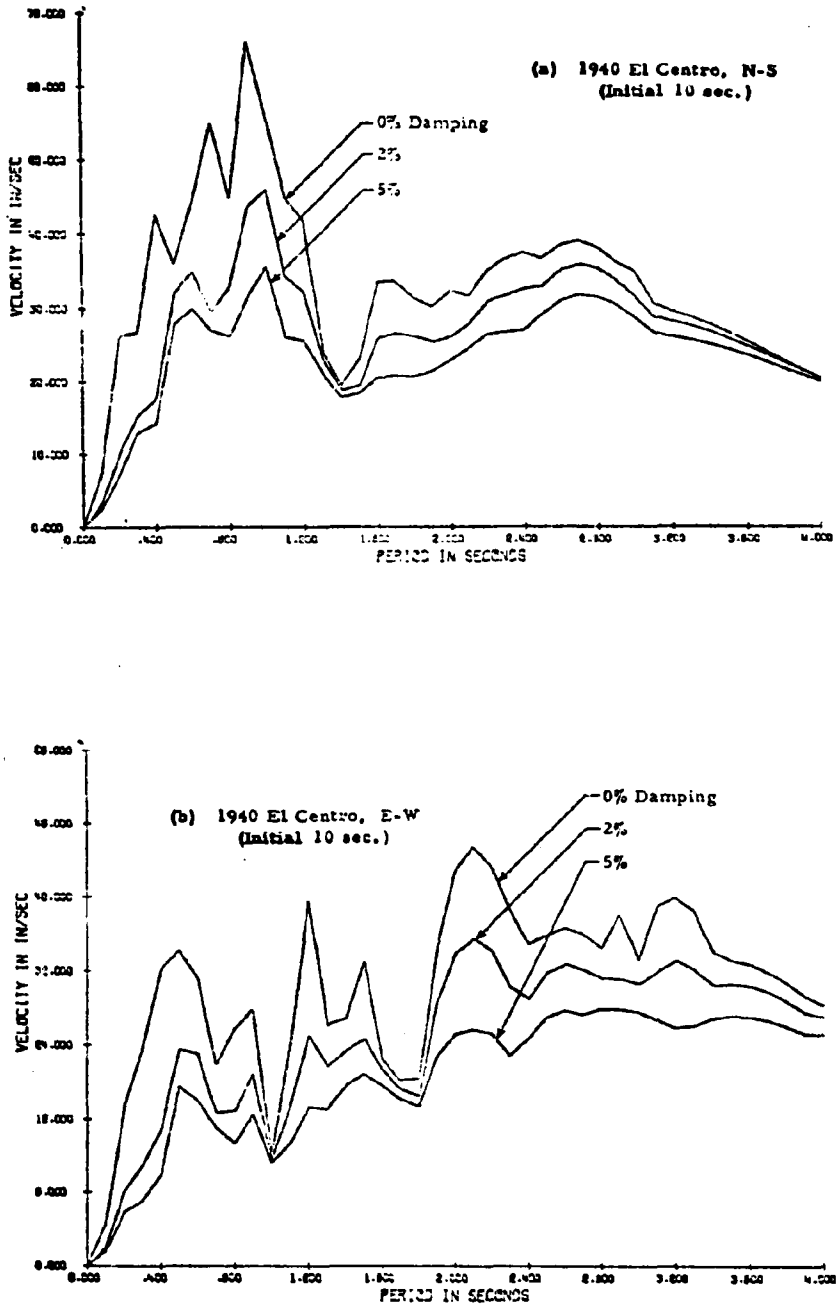

Fig. 4 Relative Velocity Response Spectrum
1940 El Centro Record

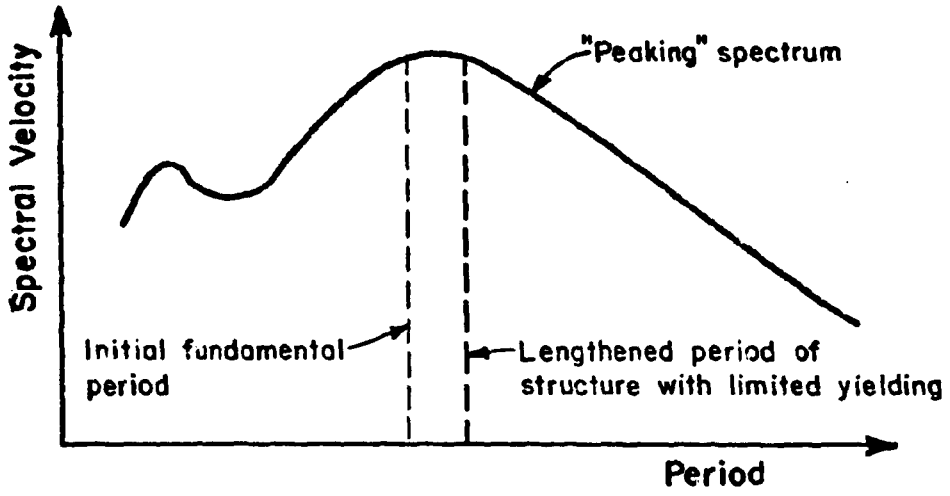

(a) Peaking Spectrum

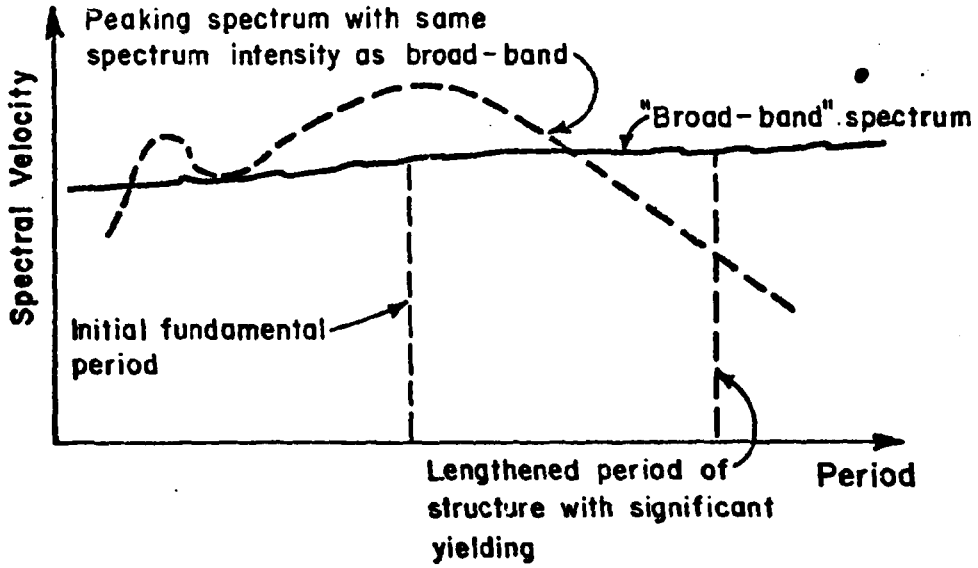

(b) Broad-band Spectrum

Fig. 5 Typical Basic Shapes of Damped Velocity Response Spectra

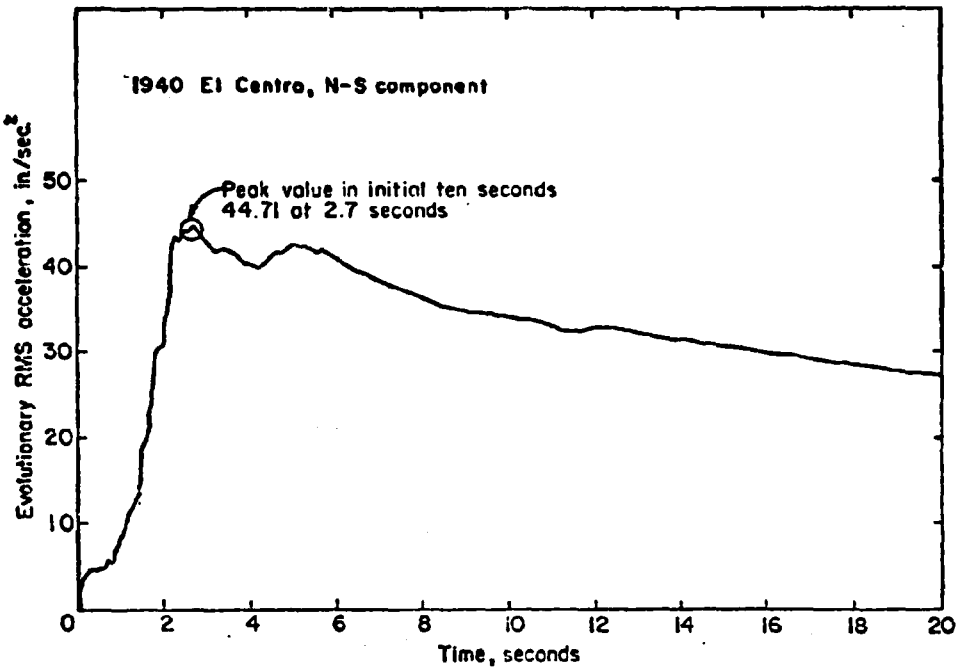

Fig. 6 Evolutionary RMS Acceleration versus Time

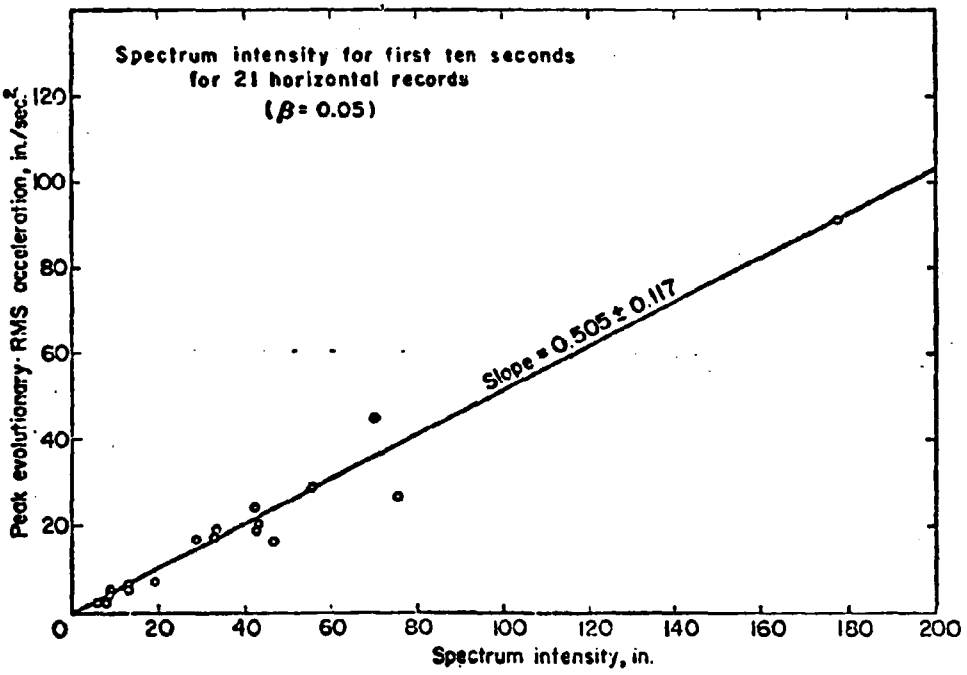

Fig. 7 Peak Evolutionary RMS Acceleration in First 10 Seconds vs. Spectrum Intensity for First 10 Seconds

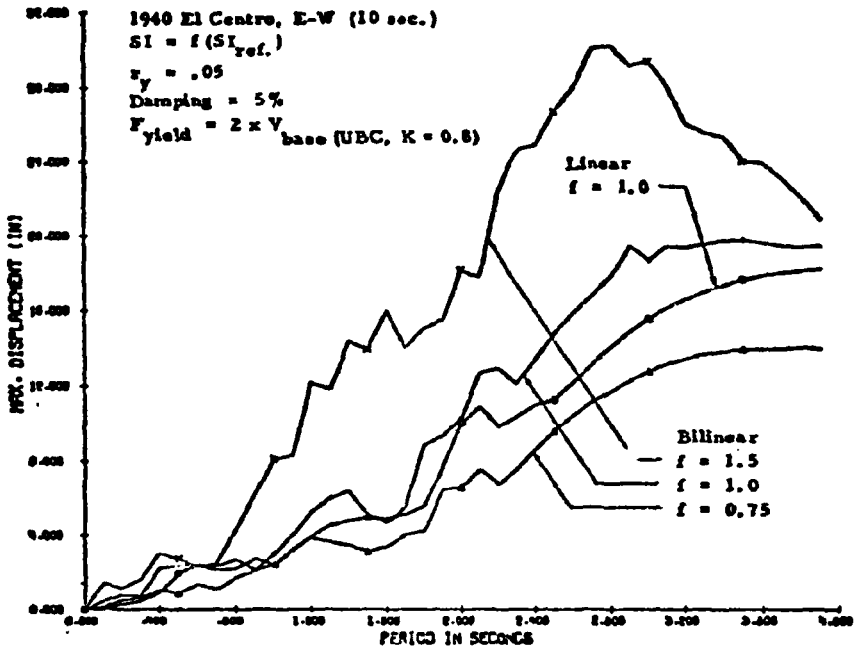

(a)

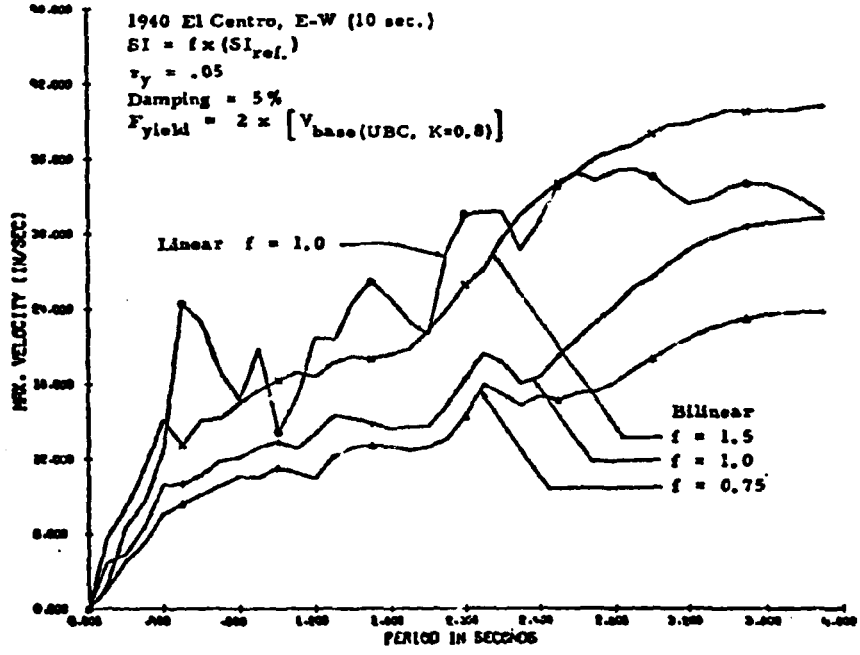

(b)

Fig. 8 Velocity Response Spectra for Linear and Bilinear Stable Hysteretic SDF Systems Subjected to Different Input Motion Intensities

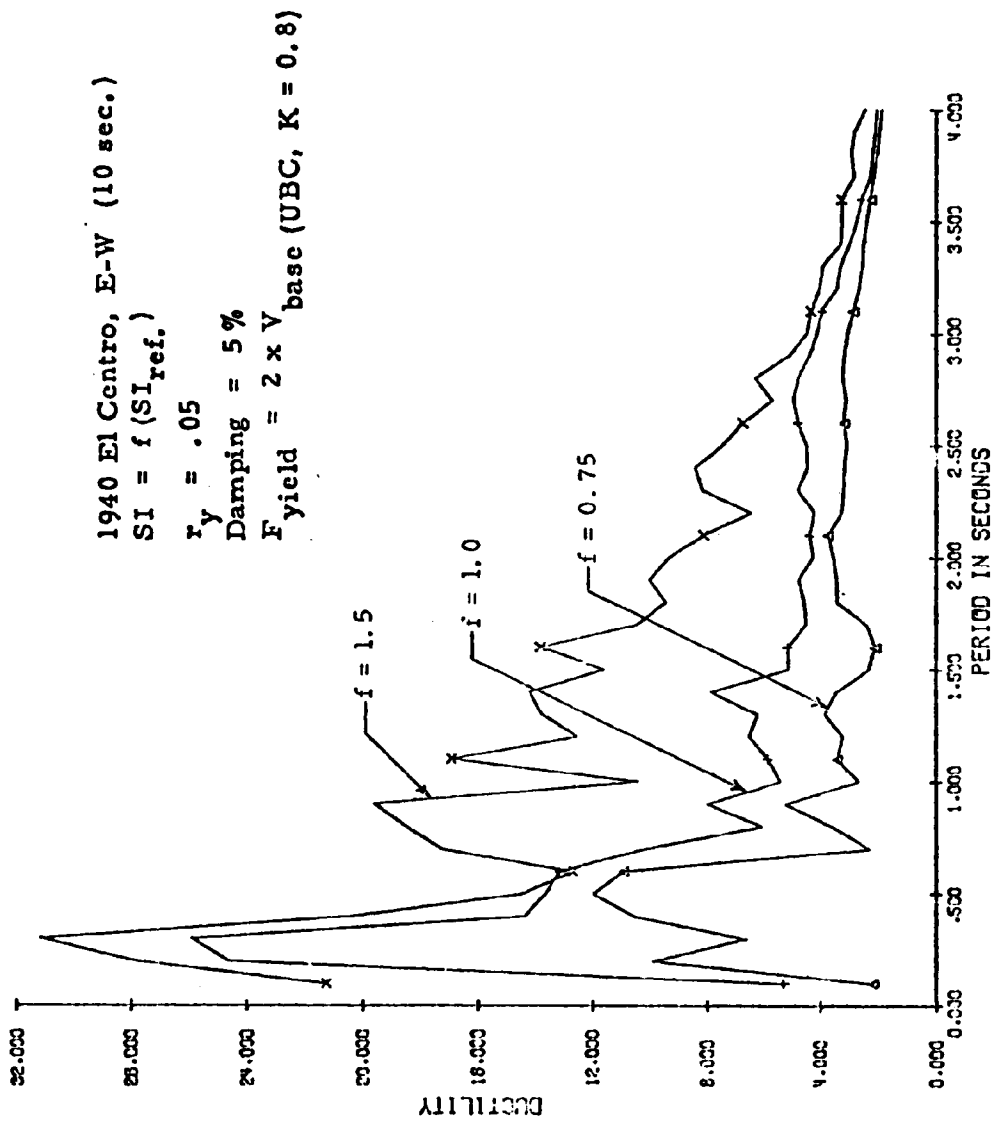

Fig. 9 Ductility Ratio versus Period for Bilinear Stable Hysteretic SDF Systems Subjected to Different Input Motion Intensities

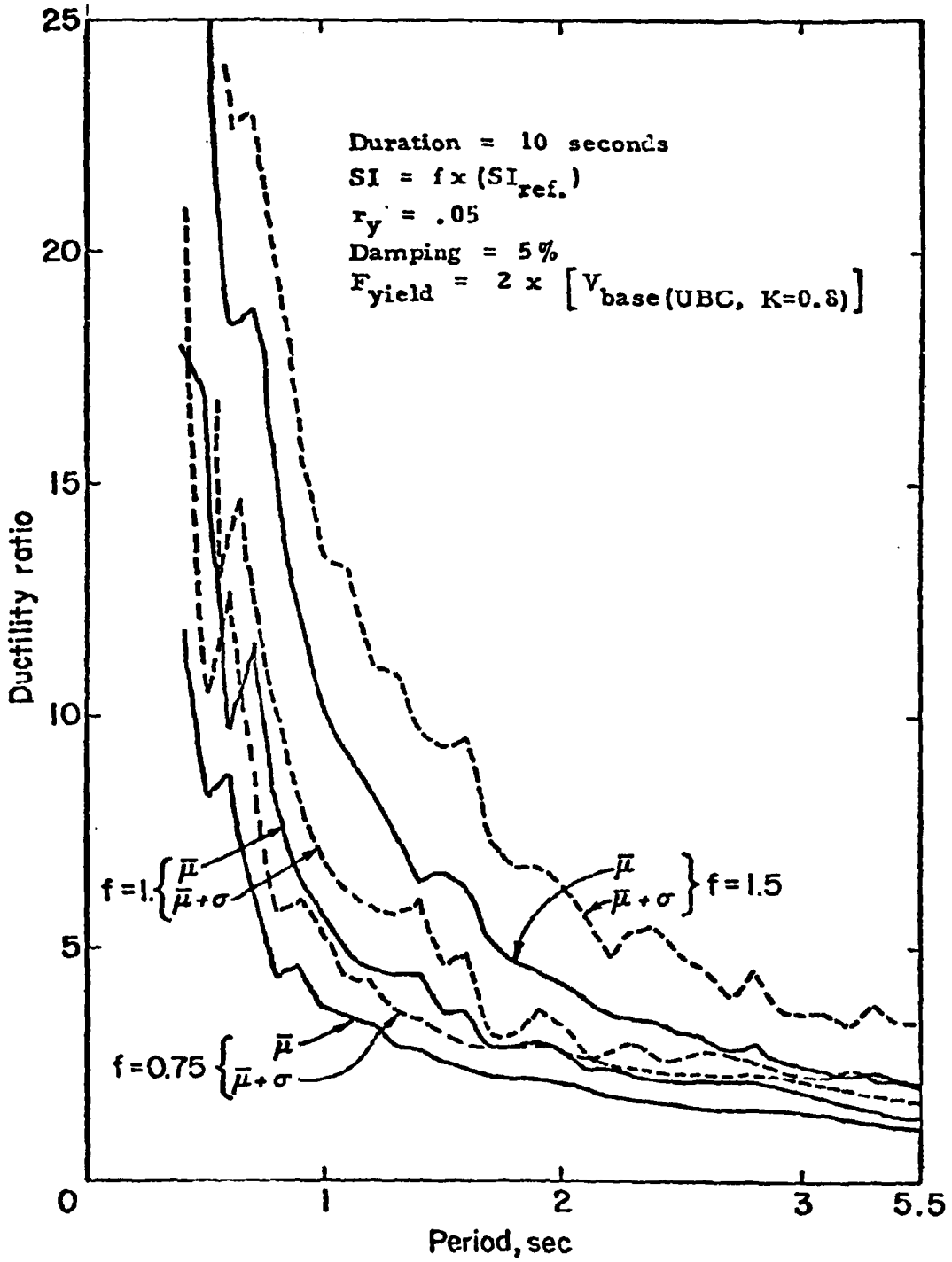

Fig. 10 Mean Ductility Ratio versus Period for Bilinear Stable SDF Systems

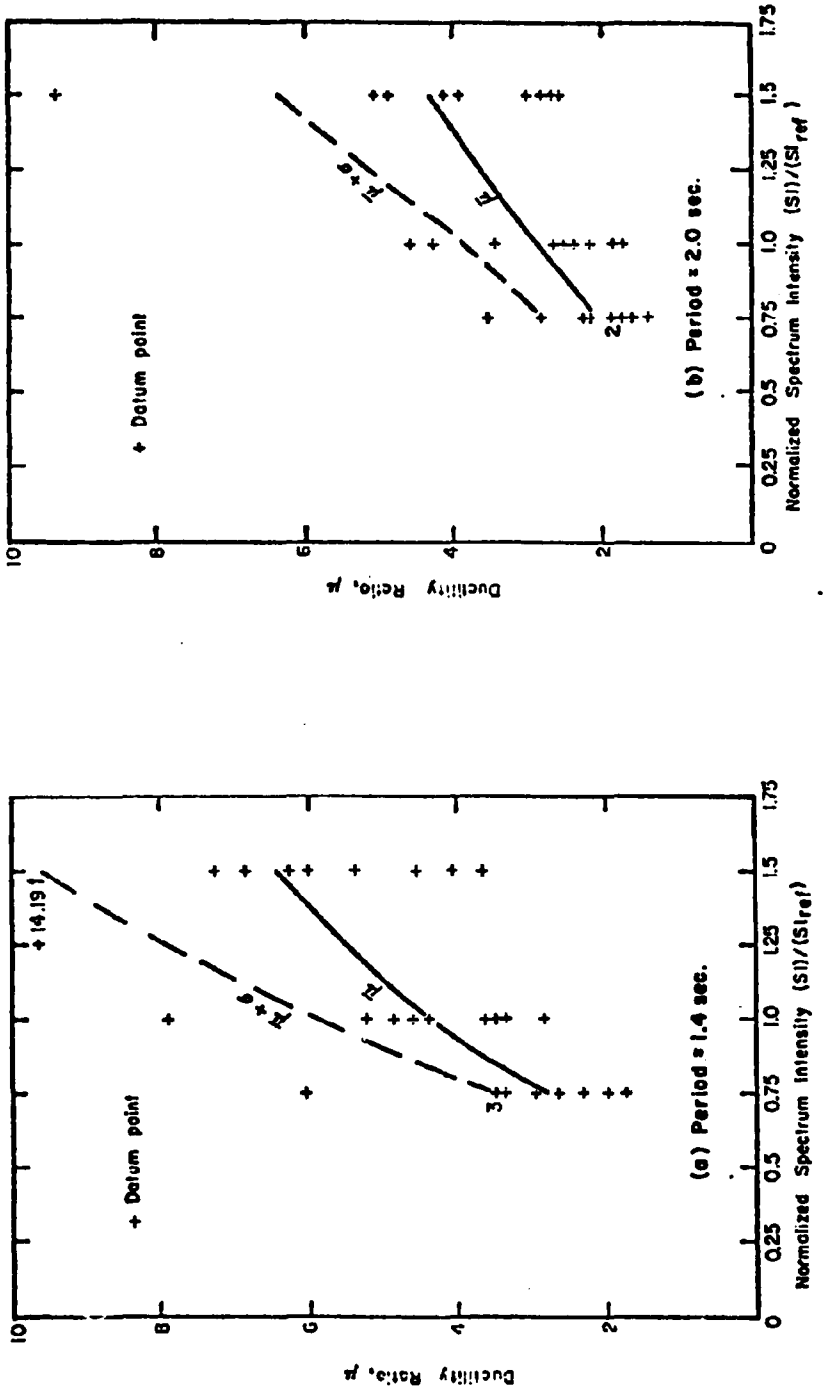

Fig. 11 Ductility Ratio versus Spectrum Intensity for Nine Input Motions - Bilinear Stable Hysteretic SDF Systems

APPENDIX A

Velocity Response Spectra for 10-Second Accelerograms

The velocity response spectra corresponding to the most intense portion of the natural and artificial accelerograms selected for this study are shown in Figures A-1 through A-42. Three values of damping, viz., 0%, 2% and 5% of critical were evaluated. The spectrum intensities for these records, based on the period interval 0.1 to 3.0 seconds, are listed in Table A-1.

Table A1 - Spectrum Intensities for Selected Accelerograms Corresponding to Initial 10 Seconds of Record*

Accelerogram	Component	Spectrum Intensity (inches)		
		0% Damping	2% Damping	5% Damping
El Centro, 5-18-40	NS	106.26	83.39	70.15
	EW	87.89	68.57	55.97
	Vert	22.90	17.76	14.69
Kern County, 2-21-52	N21E	44.35	34.61	28.67
Taft Lincoln School Tunnel	S69E	49.60	40.38	33.35
San Fernando, 2-9-71	S74W	182.02	141.19	116.20
Pacoima Dam	S16E	244.85	207.78	177.25
San Fernando, 2-9-71	NS	60.34	50.54	42.87
Holiday Inn, Orion Blvd.	EW	48.41	39.55	32.67
Kern County, 7-21-52	NS	18.43	15.34	13.06
Cal Tech Athenaeum	EW	29.48	23.48	19.30
(2nd 10 seconds)	Vert	9.97	8.03	6.66
Eureka, 12-21-52	N11W	59.06	50.13	43.39
Eureka Federal Building				
El Alamo, 2-9-56	NS	12.90	10.32	8.39
El Centro	EW	18.09	14.97	12.61
	Vert	2.99	2.34	1.90
Eureka, 12-21-52	N44E	96.63	85.50	75.18
Ferndale City Hall	N46W	61.65	53.81	46.88
	Vert	16.36	14.28	12.46
Kern County, 7-21-52	NS	20.02	15.31	12.47
Hollywood Storage Building				

*except where noted.

Table A1 (contd.) - Spectrum Intensities for Selected Accelerograms Corresponding to Initial 10 Seconds of Record

Accelerogram	Component	Spectrum Intensity (inches)		
		0% Damping	2% Damping	5% Damping
Borrego Mt., 4-8-68	NS	53.59	48.24	42.33
El Centro	EW	10.91	9.68	8.64
Borrego Mt., 4-8-68	NS	9.64	8.82	7.93
San Diego L/P	EW	7.49	6.50	5.71
Parkfield, 6-27-66	N40W	12.62	9.76	8.02
Cholame, Shandon	N50E	12.83	10.32	8.44
Array No. 12	Vert	7.08	5.67	4.71
Cal Tech-Artificial	A1	137.03	114.01	94.79
(Jennings, Housner, Tsai)	A2	117.11	101.15	86.33
	B1	94.29	77.28	65.36
	B2	92.59	76.58	62.93
	C1	19.30	16.37	14.38
	C2	17.24	13.89	11.50
SIMQKE-Artificial	S1	104.86	79.18	63.46
(Gasparini)	S2	106.67	82.86	67.57
	S3	54.00	44.01	36.43
	S4	55.87	43.05	34.84
	S5	90.47	67.78	56.60
	S6	93.85	70.22	58.21
PSEQGN-Artificial	P1	64.82	49.55	39.82
(Ruiz, Penzien)	P2	109.40	86.53	70.84
	P3	105.21	82.98	66.57
	P4	131.77	108.49	91.01
	P5	214.27	181.49	152.81

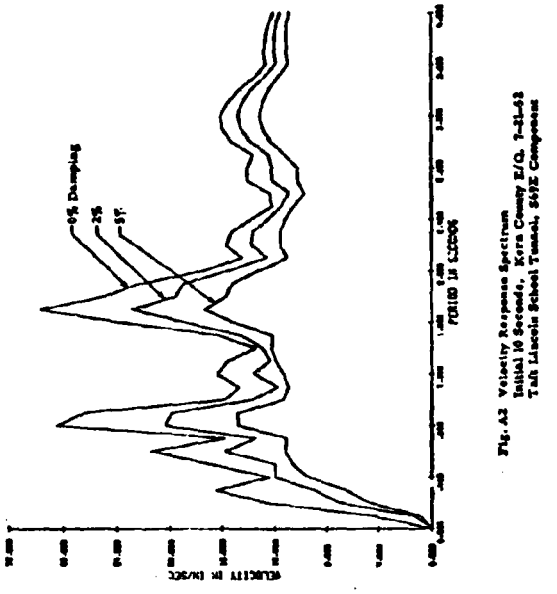

Fig. A1 Velocity Response Spectrum
Initial 10 Seconds, Kern County E/Q, 7-21-52
Taft Lincoln School Tunnel, N69E Component

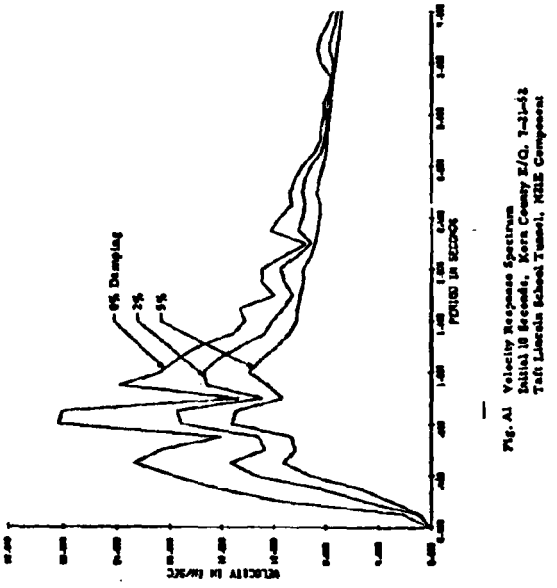

Fig. A2 Velocity Response Spectrum
Initial 10 Seconds, Kern County E/Q, 7-21-52
Taft Lincoln School Tunnel, S69E Component

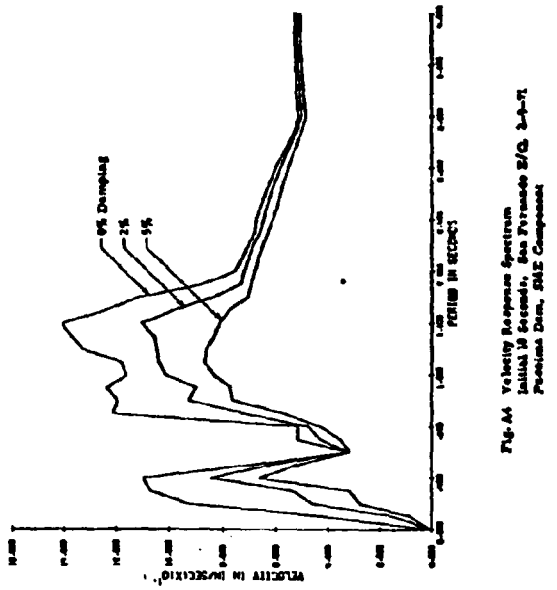

Fig. A3 Velocity Response Spectrum
Initial 10 Seconds, San Fernando E/Q, 2-9-71
Pacoima Dam, S74W Component

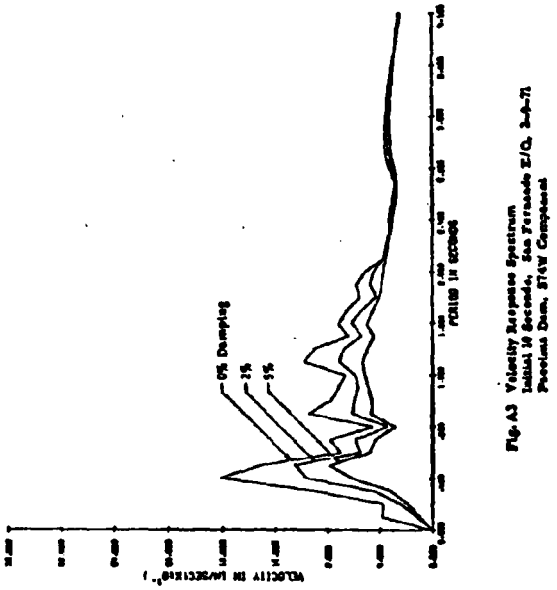

Fig. A4 Velocity Response Spectrum
Initial 10 Seconds, San Fernando E/Q, 2-9-71
Pacoima Dam, S16E Component

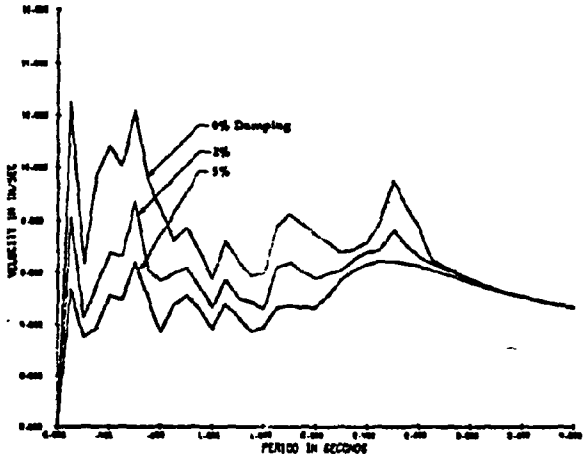

Fig. A5 Velocity Response Spectrum
Initial 10 Seconds, Imperial Valley E/Q, 5-18-40
El Centro, Vertical Component

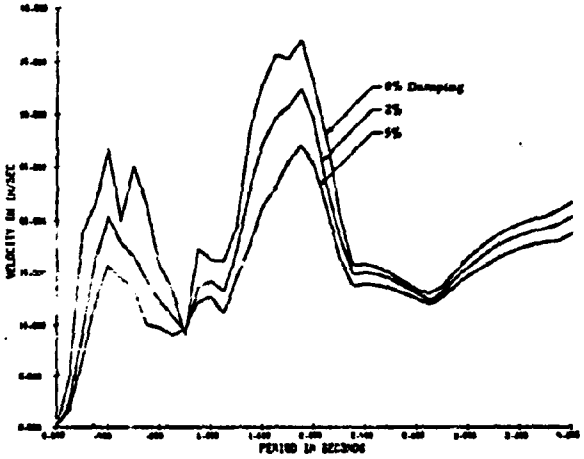

Fig. A6 Velocity Response Spectrum
Initial 10 Seconds, San Fernando E/Q, 2-9-71
8244 Orion Blvd., 1st Floor, NS Component

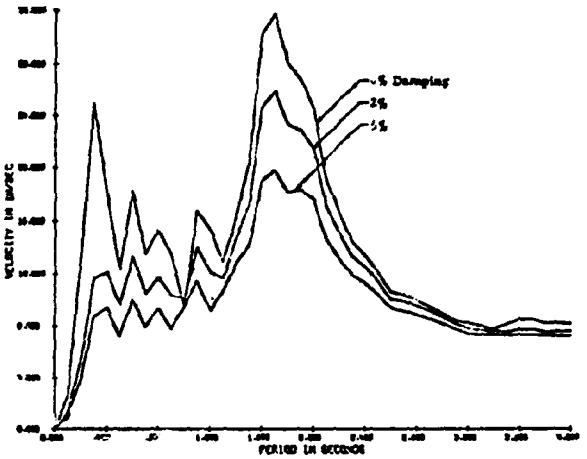

Fig. A7 Velocity Response Spectrum
Initial 10 Seconds, San Fernando E/Q, 2-9-71
8244 Orion Blvd., 1st Floor, EW Component

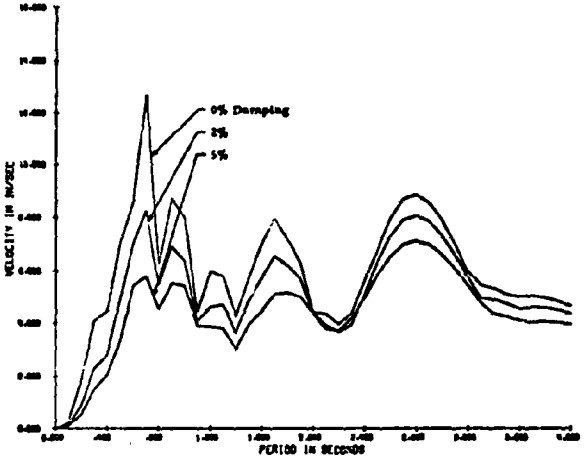

Fig. A8 Velocity Response Spectrum
Second 10 Seconds, Kern County E/Q, 7-21-52
Cal. Tech. Athenaeum, NS Component

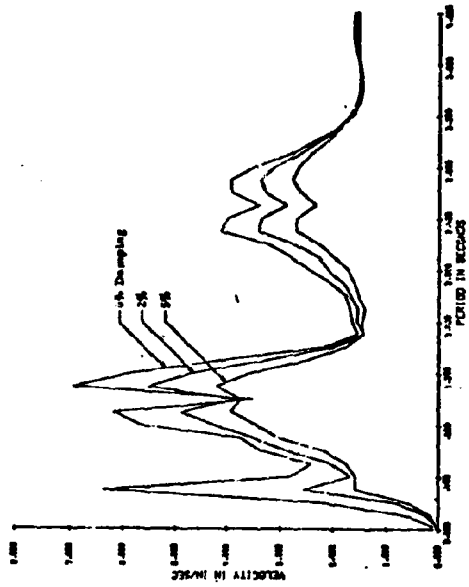

Fig.A10 Velocity Response Spectrum
Second 10 Seconds, Kern County E/Q, 7-21-52
Cal. Tech. Athenaeum, Vertical Component

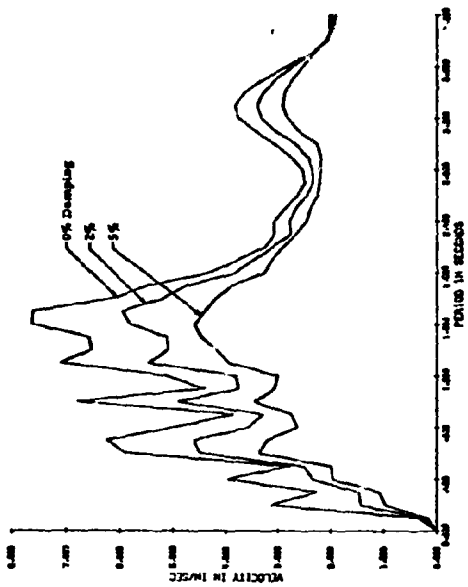

Fig.A11 Velocity Response Spectrum
Initial 10 Seconds, El Alsino E/Q, 5-18-40
El Centro, NS Component

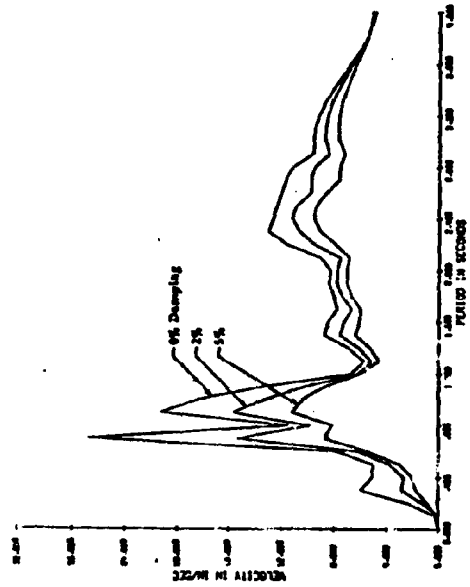

Fig.A9 Velocity Response Spectrum
Second 10 Seconds, Kern County E/Q 7-21-52
Cal. Tech. Athenaeum, EW Components

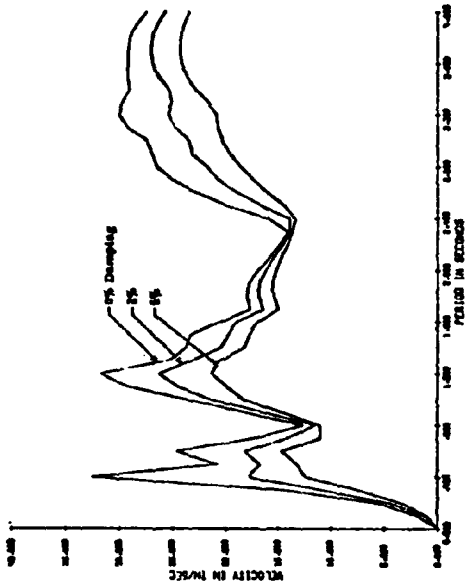

Fig.A12 Velocity Response Spectrum
Initial 10 Seconds, Eureka E/Q, 12-21-54
Eureka Federal Building, NUW Component

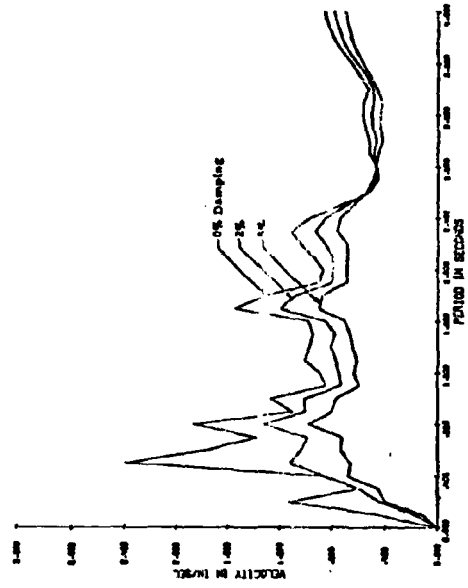

Fig. A14 Velocity Response Spectrum
Initial 10 Seconds, El Alamo E/Q 5-18-40
El Centro, Vertical Component

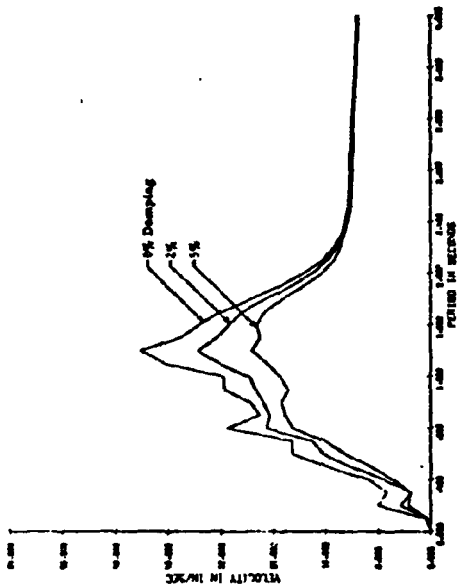

Fig. A15 Velocity Response Spectrum
Initial 10 Seconds, Eureka E/Q. 12-21-54
Ferndale City Hall, N16W Component

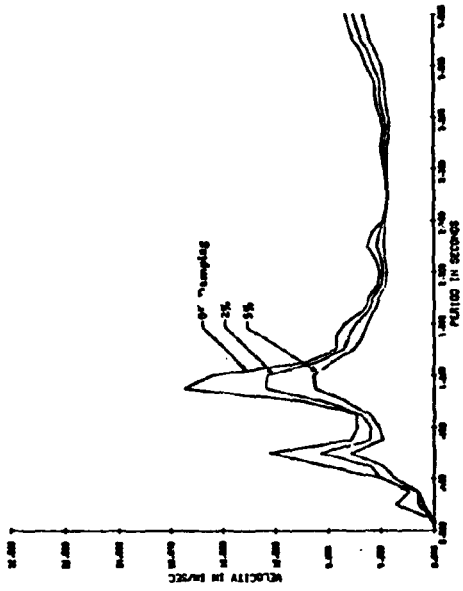

Fig. A13 Velocity Response Spectrum
Initial 10 Seconds, El Alamo E/Q 5-18-40
El Centro, EW Component

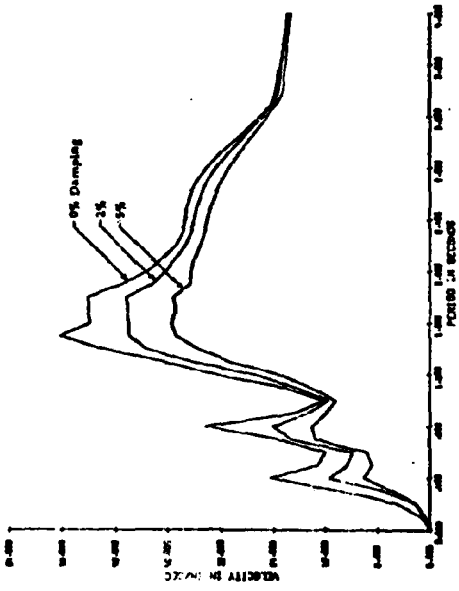

Fig. A16 Velocity Response Spectrum
Initial 10 Seconds, Eureka E/Q. 12-21-54
Ferndale City Hall, N44E Component

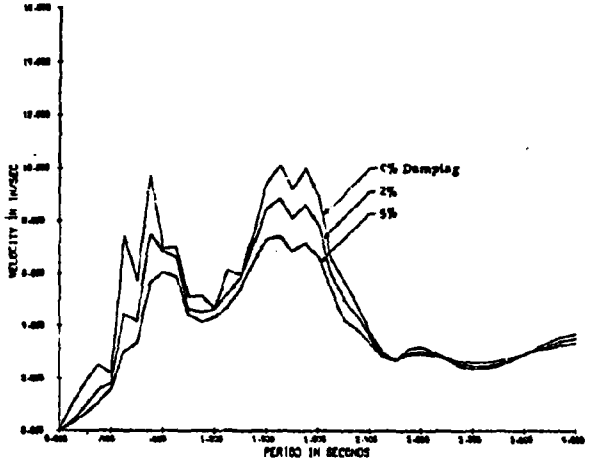

Fig. A17 Velocity Response Spectrum
Initial 10 Seconds, Eureka E/Q, 12-21-54
Ferndale City Hall, Vertical Component

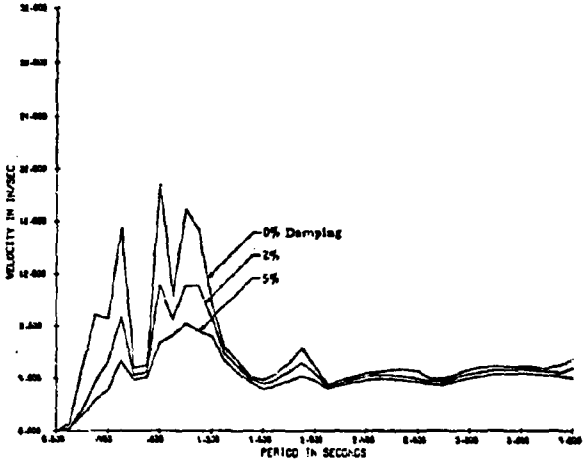

Fig. A18 Velocity Response Spectrum
Initial 10 Seconds, Kern County E/Q, 8-21-52
Hollywood Storage Building, P.E. Lot, NS Component

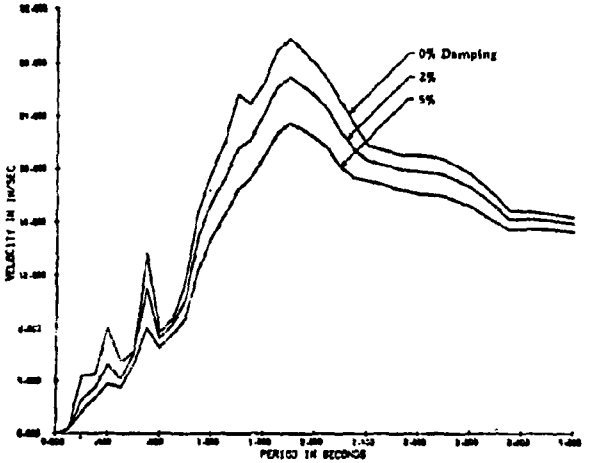

Fig. A19 Velocity Response Spectrum
Initial 10 Seconds, Borrego Mt. E/Q, 4-8-46
El Centro, NS Component

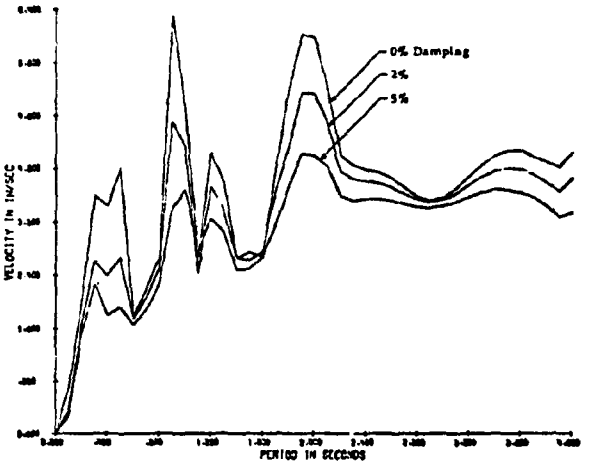

Fig. A20 Velocity Response Spectrum
Initial 10 Seconds, Borrego Mt. E/Q, 4-8-46
El Centro, EW Component

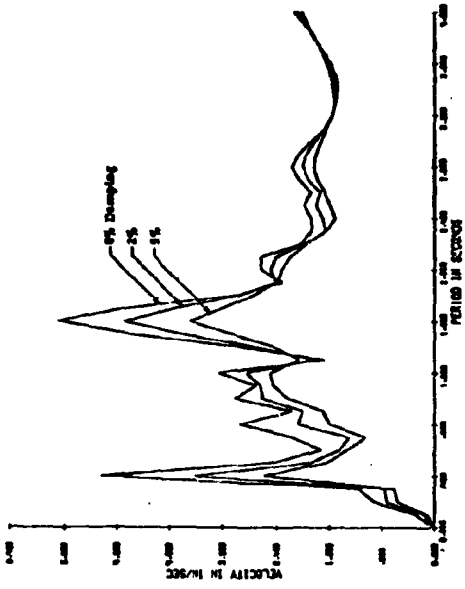

Fig. A22 Velocity Response Spectrum
Initial 10 Seconds, Borrego Mt. E/Q. 4-8-46
San Diego Light and Power Building, EW Component

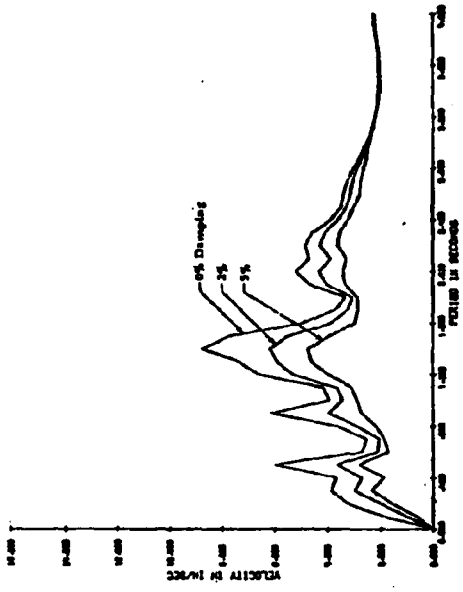

Fig. A24 Velocity Response Spectrum
Initial 10 Seconds, Parkfield E/Q. 4-17-66
Chalome - Shandon Array No. 12, NS45 Component

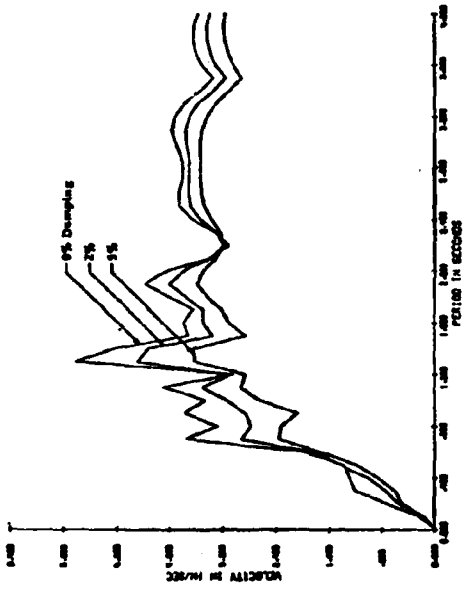

Fig. A23 Velocity Response Spectrum
Initial 10 Seconds, Borrego Mt. E/Q. 4-8-46
San Diego Light and Power Building, NS Component

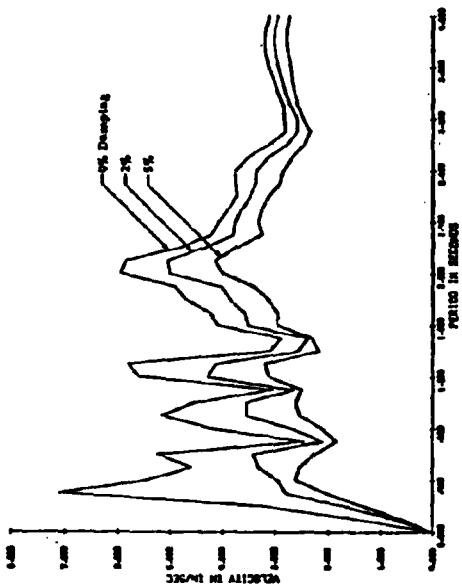

Fig. A25 Velocity Response Spectrum
Initial 10 Seconds, Parkfield E/Q. 4-17-66
Chalome - Shandon Array No. 12, N45W Component

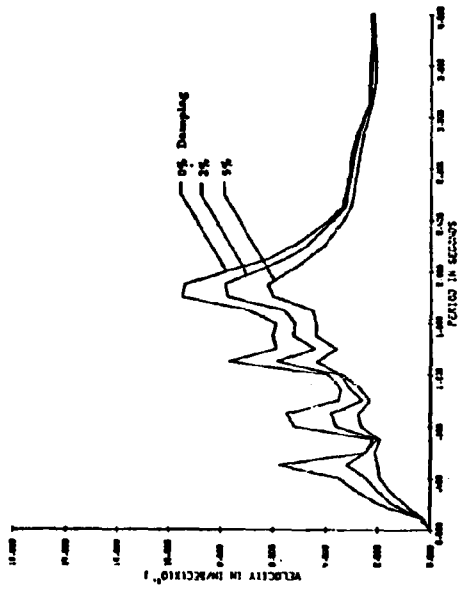

Fig. A24 Velocity Response Spectrum
Initial 10 seconds, Artificial Accelerogram A-1

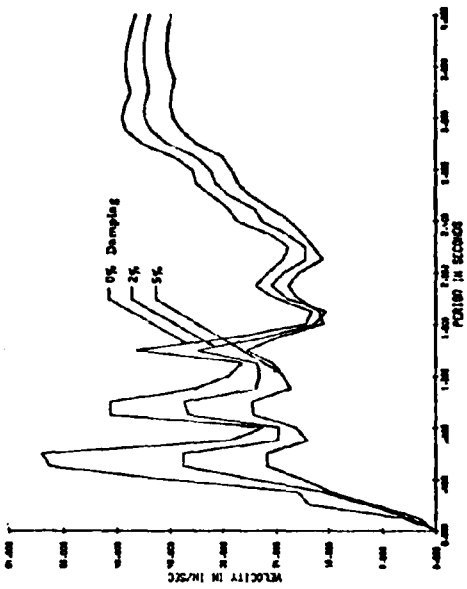

Fig. A25 Velocity Response Spectrum
Initial 10 seconds, Artificial Accelerogram B-1

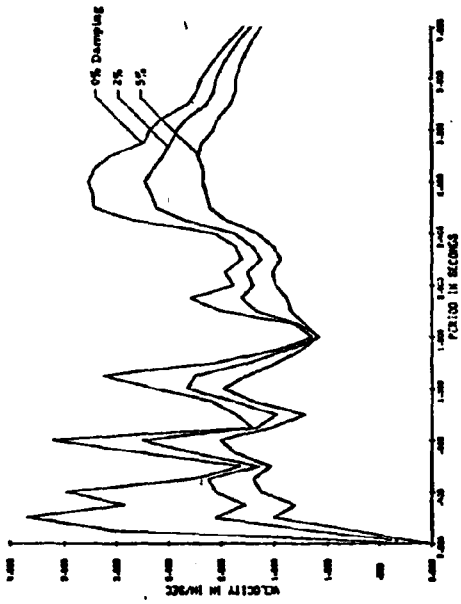

Fig. A25 Velocity Response Spectrum
Initial 10 Seconds, Parkfield E/Cn 6-47-46
Chalome - Shandon Array No. 12, Vertical Component

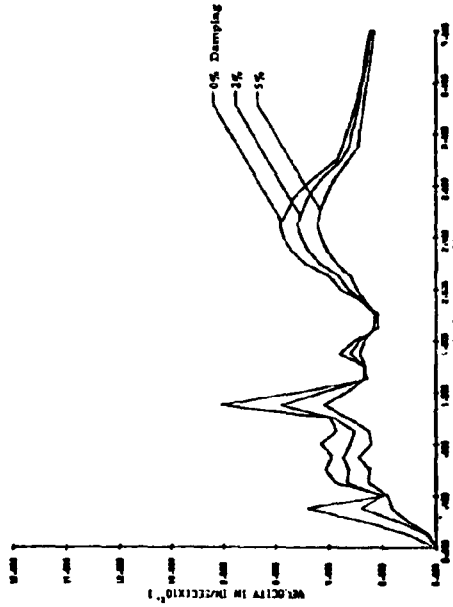

Fig. A27 Velocity Response Spectrum
Initial 10 seconds, Artificial Accelerogram A-2

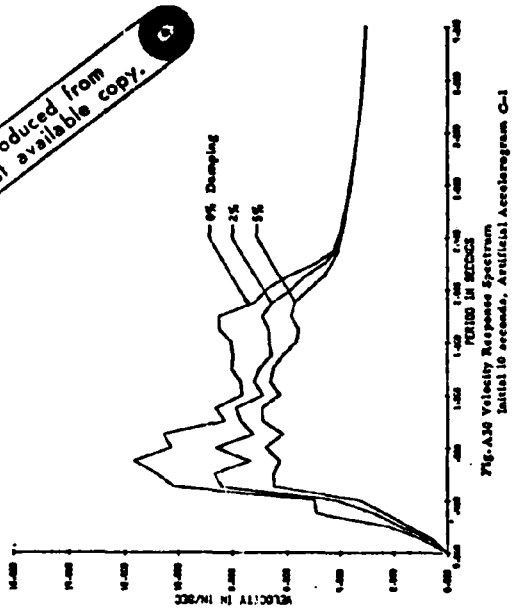

Fig. A30 Velocity Response Spectrum
Initial 10 seconds, Artificial Accelerogram C-1

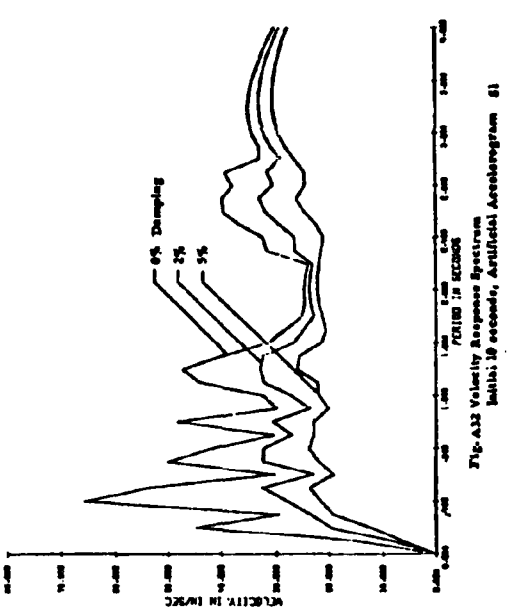

Fig. A32 Velocity Response Spectrum
Initial 10 seconds, Artificial Accelerogram E1

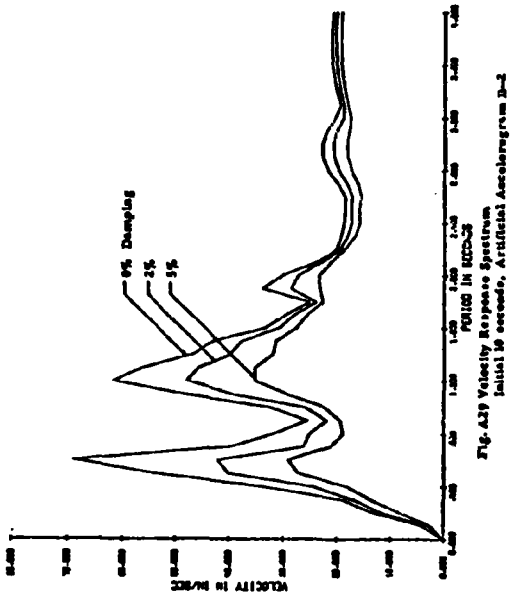

Fig. A31 Velocity Response Spectrum
Initial 10 seconds, Artificial Accelerogram E-2

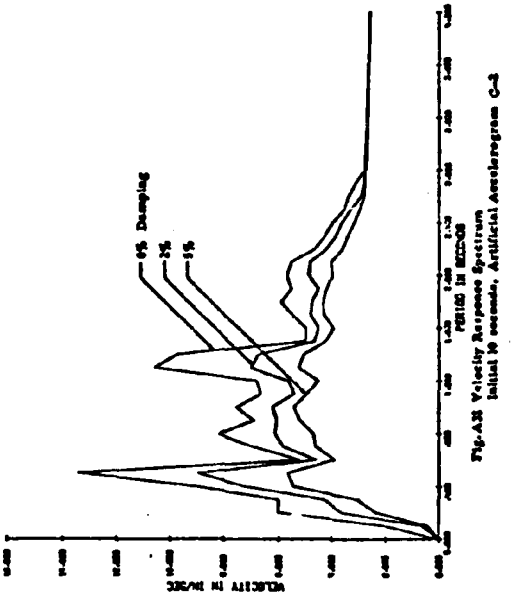

Fig. A33 Velocity Response Spectrum
Initial 10 seconds, Artificial Accelerogram C-2

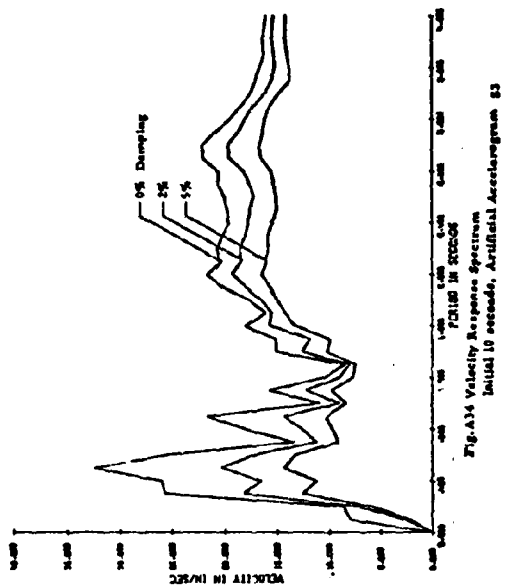

Fig. A34 Velocity Response Spectrum
Initial 10 seconds, Artificial Accelerogram #3

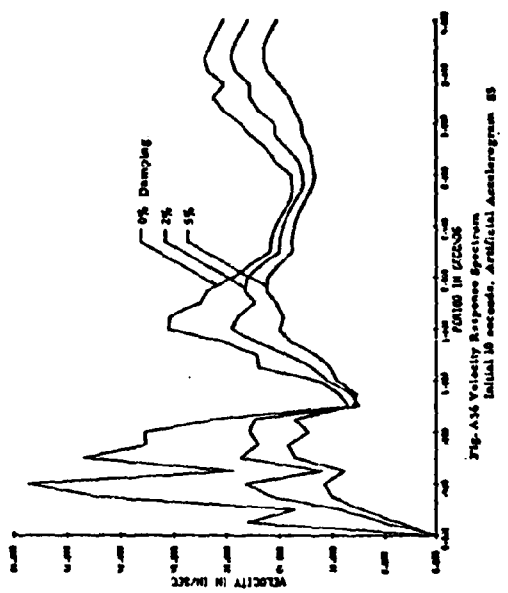

Fig. A36 Velocity Response Spectrum
Initial 10 seconds, Artificial Accelerogram #5

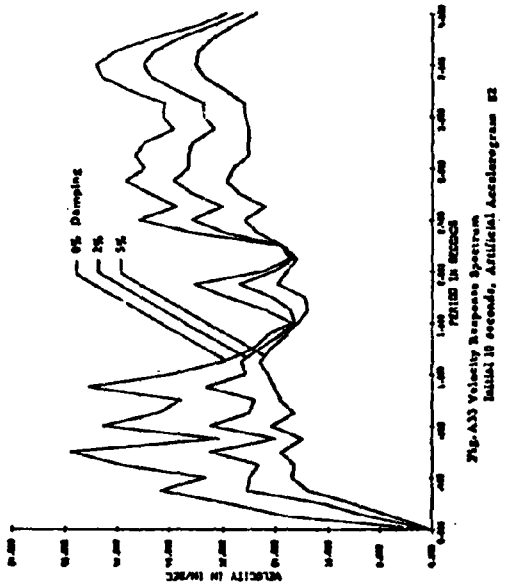

Fig. A33 Velocity Response Spectrum
Initial 10 seconds, Artificial Accelerogram #2

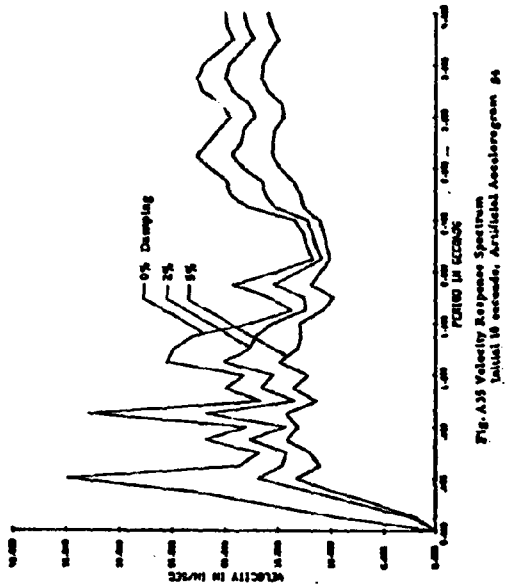

Fig. A35 Velocity Response Spectrum
Initial 10 seconds, Artificial Accelerogram #4

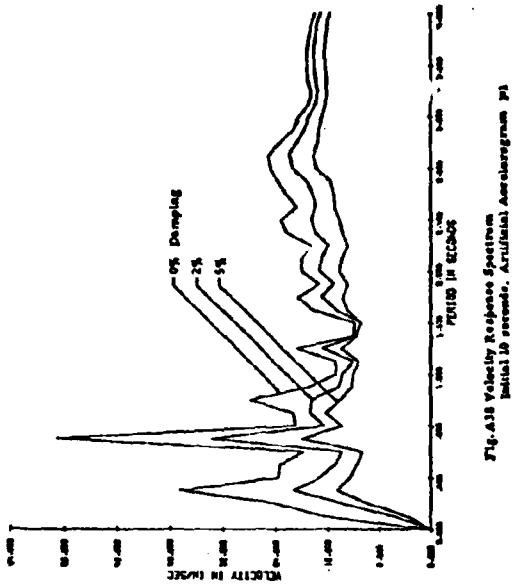

Fig. A38 Velocity Response Spectrum
Initial 10 seconds, Artificial Accelerogram #3

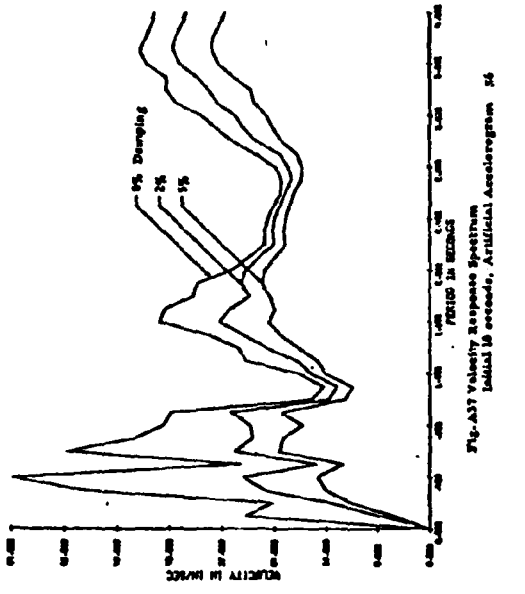

Fig. A37 Velocity Response Spectrum
Initial 10 seconds, Artificial Accelerogram #6

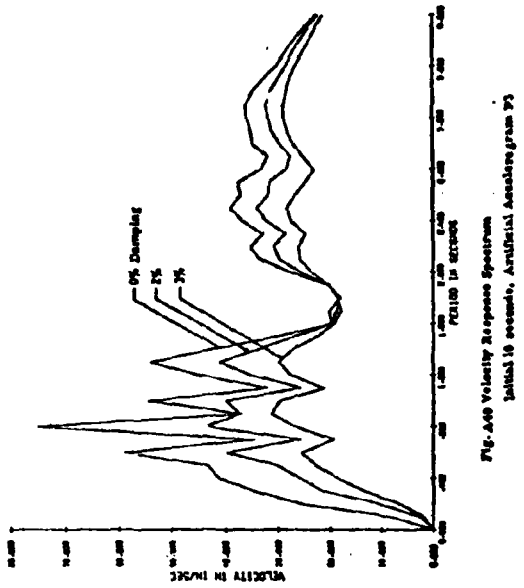

Fig. A40 Velocity Response Spectrum
Initial 10 seconds, Artificial Accelerogram #5

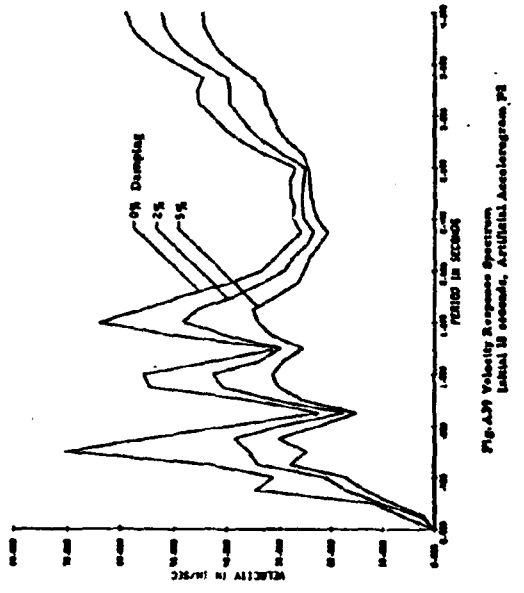

Fig. A39 Velocity Response Spectrum
Initial 10 seconds, Artificial Accelerogram #4

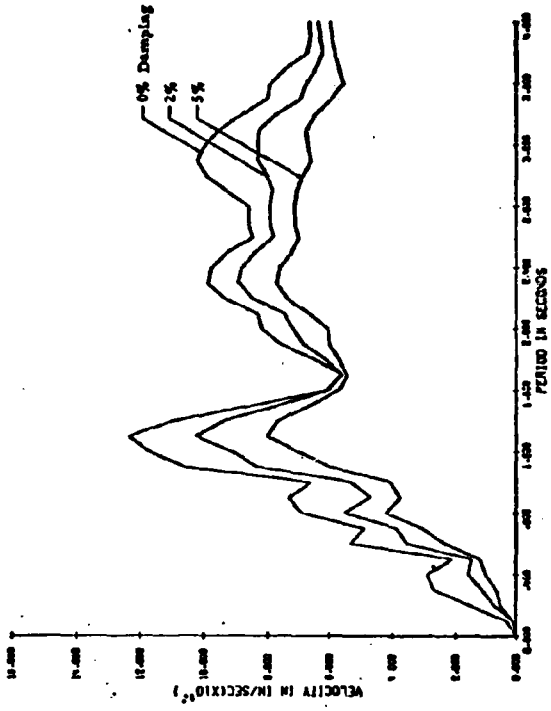

Fig. A42 Velocity Response Spectrum
Initial 10 seconds, Artificial Accelerogram #5

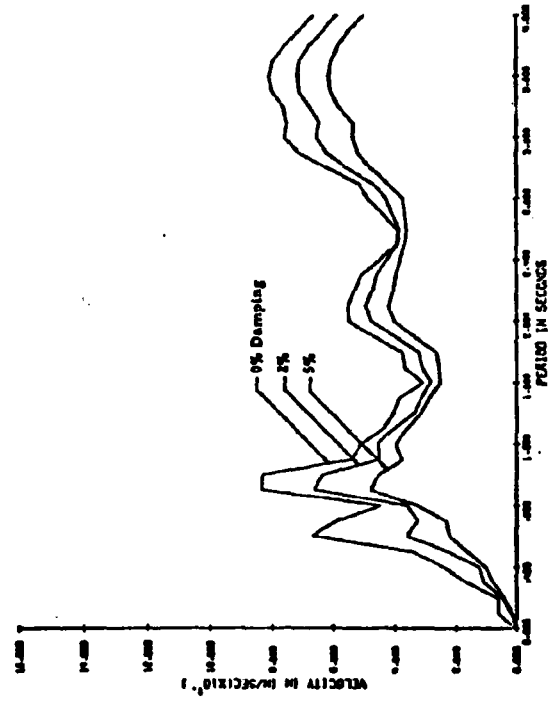

Fig. A41 Velocity Response Spectrum
Initial 10 seconds, Artificial Accelerogram #4

DYNAMIC ANALYSIS OF ISOLATED STRUCTURAL WALLS

PART B - PARAMETRIC STUDIES

GENERAL

A major step in the development of a design procedure for earthquake-resistant structural walls is the evaluation of the relative influence of the different structural and ground motion parameters on dynamic inelastic response. By allowing a comparison of the effects of the different variables on the relevant response quantities, the parametric studies serve to focus attention on the most significant variables. The subsequent development can then be formulated on the basis of these major variables, with due account taken of variations in response resulting from changes in the secondary variables.

PARAMETERS CONSIDERED

The behavior of a building subjected to earthquake motions is affected by a number of variables related to its dynamic and structural properties and the characteristics of the ground motion. The variables investigated in this study were those expected to have a significant effect on the response of the structure, particularly in relation to the deformation requirements on the individual members as well as the entire structure. These variables may be grouped as follows:

a. Structure characteristics:

   1. fundamental period of vibration, as affected by stiffness,
   2. strength or yield level,
   3. stiffness in post-yield range,
   4. character of the moment-rotation relationship of hinging regions,
   5. viscous damping,
   6. variations in stiffness and strength along the height,
   7. degree of fixity at the base of the structure,
   8. variations in height (number of stories).

b. Ground motion parameters:

1. intensity,
2. frequency characteristics,
3. duration.

The effects of these parameters on the seismic response of isolated structural walls were investigated by carrying out dynamic analyses of suitable mathematical models incorporating variations of the significant parameters over a reasonable range of values. The various structural models were obtained by changing the values of selected parameters in a basic reference structure. The properties of the reference structure and the range of variation in the individual parameters are discussed in the following sections.

BASIC BUILDING PROPERTIES

The basic structure considered in the parametric studies is a hypothetical 20-story building consisting mainly of a series of parallel structural walls, as shown in Fig. 1. The building is 60 ft. x 144 ft. in plan and rises some 178 feet above the ground. All story heights are 8'-9" except the first story, which is 12'-0" high.

For the purpose of the dynamic analysis, the mass of the structure was calculated to include the dead weight and 40 percent of the live load specified for apartment buildings by the Uniform Building Code.[1] This percentage of live load was deemed reasonable and is consistent with the current specifications for the design of columns in the lower stories of buildings. In calculating the design lateral forces (UBC Zone 3) for the purpose of proportioning the wall, however, only the dead weight of the building was used, as specified by UBC.

The stiffness of the structural wall in the basic building was assumed uniform along the height since this provides a better reference for the evaluation of the effect of stiffness taper.

The reference structure, here denoted by ISW 1.4 has an initial fundamental period of 1.4 sec. and a corresponding drift index (i.e., the ratio of lateral deflection at top to total height) of approximately 1/950 under the design seismic forces. The yield moment at the base was assumed equal to 500,000 in-kips*.

A constant wall cross section was also assumed throughout the height of the basic structure. However, a reduction in the yield level of sections above the base was included to reflect the effect of axial loads on the moment capacity. This, in effect, produced a moderate taper in the strength or yield level. The taper in strength used in the basic structure represents about the maximum that can be expected due to axial load only and was obtained on the basis of an examination of the interaction diagrams for several types of structural wall sections with varying percentages of longitudinal steel.

VARIATION OF STRUCTURAL PARAMETERS

The effects of the different structural and ground motion parameters on selected response quantities, particularly the shear and rotational ductility demand at the base of the wall as well as the interstory distortions, were determined by a controlled variation of each parameter in the reference structure. In most cases, only a single parameter was varied in the basic structure while the other parameters were held constant. Although this process sometimes resulted in unrealistic combinations of structural properties, it was considered essential to a proper evaluation of the effect of each variable on dynamic response.

*The design moment at the base of the wall, on the basis of UBC Zone 3 requirements, was calculated as 350,000 in-kips. This corresponds to a yield moment of approximately 500,000 in-kips when allowance is made for load factors, capacity reduction factors and the difference between the yield moment and the maximum moment capacity of typical reinforced concrete sections.

In varying the parameter values, the question of the appropriate range to consider in each case becomes important if the results of the parametric study are to have practical application. In the present study, the values of each parameter were chosen so that they represent a reasonable range of values commonly encountered in practice.

To examine the effect of the fundamental period of vibration, three other values were assumed in addition to the basic value of 1.4 sec., namely, 0.8, 2.0 and 2.4 sec. The stiffness of the reference structure was modified--while keeping the stiffness distribution and the mass constant--in order to arrive at the period variations. As an aid in selecting the appropriate stiffness, Fig. 2 was prepared, relating the stiffness with the fundamental period and the drift ratio corresponding to the code-specified forces. The above period values cover a relatively wide range of structural wall buildings.

In order to arrive at a reasonable range of values for the other major structural parameter, i.e., the yield level, an examination of various structural wall sections was undertaken. The yield strength corresponding to various combinations of rectangular and flanged wall sections of practical proportions and varying longitudinal steel percentages (0.5 to 4.0 percent) were determined for f_y = 60 ksi and f'_c = 4 ksi. Based on the results of these calculations, giving due consideration to current design practice, it was decided to use yield level values ranging from the 500,000 in-kips of the reference structure to 1,500,000 in-kips. Intermediate values of 750,000 in-kips and 1,000,000 in-kips were also considered.

Similar considerations were used in arriving at the ranges of values of the other structural parameters.

GROUND MOTION PARAMETERS

As explained in "Input Motions"*, a ground motion duration of 10 seconds was used for all analyses except when the effect of duration was investigated. The effect of the intensity of the ground motion was investigated by normalizing each input in terms of the 5%-damped spectrum intensity corresponding to the first 10 seconds of the NS component of the 1940 El Centro record--the "reference intensity", SI_{ref}. Intensities of 0.75, 1.0 and 1.5 relative to the 1940 El Centro (NS) were considered.

With the duration of the ground motion fixed and the intensity normalized, the only other ground motion parameter which could significantly affect the variability of results is the frequency characteristic. A basis for the broad classification of earthquake accelerograms according to frequency characteristics was proposed in "Input Motions". Using this system of classification, a number of typical records were chosen early in the study to investigate the effect of this parameter (frequency characteristic) on dynamic structural response. Once the effect of this particular parameter on response was determined, the number of input motions for use in the study of all the other parameters could be narrowed down to one or two. This procedure was considered necessary in order to limit the total number of analyses while still retaining a reasonable assurance that the calculated responses would provide a good estimate of structural requirements under a likely combination of unfavorable conditions.

A complete list of the parameter variations considered in this study is given in Tables 1(a) through 1(d). In preparing this list, it was found convenient to divide it into parts according to the structure's

*Part A of this report.

fundamental period. Thus, structures with a fundamental period of 0.8 sec. are listed under a basic structure denoted by ISW 0.8, and so on. The third column in the table clearly shows the variations in the basic value which were used in the parametric study.

Dynamic analyses were carried out for each combination of parameters shown in Table 1. Throughout the dynamic analyses it was assumed that structural elements possess unlimited inelastic deformation capacity (ductility) since a major objective of the study is the determination of the deformation requirements corresponding to particular values of parameter.

PRELIMINARY STUDIES

In the initial stages of the dynamic analysis study, a number of preliminary runs were made to: (a) explore the possibility of using a lesser number of lumped masses in the model than the number of floors in the prototype; (b) check the reasonableness of alternative techniques for modelling the hinging region at the base of the wall; and (c) determine the appropriate value of the integration time step to be used in the analysis. Questions (a) and (c) were considered mainly in an effort to reduce the amount of computer time required to undertake each analysis. Question (b) assumed importance in this particular study because of the need to obtain reliable estimates of the expected deformations in the hinging region and to correlate these with data from the experimental program.

Exploratory analyses were also carried out to assess the significance of the so-called P-Δ effect on dynamic response.

(1) Number of Lumped Masses in Model

The effect of the number of lumped masses on the accuracy of the results was studied using the models shown in Fig. 3. The 20-mass model represents a full model for the 20-story building shown in Fig. 1. The reduced models of five and eight masses have the nodes spaced at closer intervals near the base so that the behavior of the hinging region could be determined more accurately.

The results of dynamic analyses compared very favorably for the full model and the 8-mass model. The 5-mass model yielded the same maximum top displacement, but somewhat different moments, shears and plastic rotations in the lower part of the wall. Based on these results and considering the desired accuracy for relative story displacements, it was decided to lump the masses at alternate story levels in the upper portion of the wall. In the lower portion, the masses were lumped at each story level. The resulting 12-mass model is shown in Fig. 4. A comparison of results obtained with this model and the full 20-mass model of the reference structure ISW 1.4 showed excellent agreement.

(2) Modelling of the Plastic Hinge Region

The proper modelling of the region of potential hinging at and near the base of the wall is important if a reliable assessment of the deformation requirements in this critical region is expected. The model of the plastic hinging region should not only be realistic but should allow meaningful

interpretation of the dynamic analysis results in terms that relate to measurable quantities in the experimental investigation.

As previously explained, program DRAIN-2D[2] accounts for inelastic effects by allowing the formation of concentrated "point hinges" at the ends of elements when the moments at these points equal the specified yield moment. The moment-rotation characteristics of these point hinges can be defined in terms of a basic bilinear relationship which develops into either a stable hysteretic loop or exhibits a decrease in reloading stiffness with loading cycles subsequent to yield. Since the latter model represents more closely the behavior of reinforced concrete members under reversed inelastic loading, it was used throughout this study.

In modelling an element with bilinear moment-rotation characteristics using DRAIN-2D, a major problem is the determination of the properties to be assigned to the hinge. These properties can be derived by considering the model used in the program and relating its properties to a real member (Fig. 5) subjected to the same set of forces. The initial hinge stiffness, K_s, can then be taken as a very large number so that the two systems are identical up to the point when yielding occurs. In the post-elastic range the hinge properties can be derived by imposing the condition that the total rotation in the model, θ_2, be equal to the total rotation in the real element, θ_1. This yields the following expression for the yield stiffness ratio of the point hinge, r_2, (i.e., the ratio of the slope of the post-yield branch to the slope of the initial branch of the bilinear moment-rotation curve):

$$r_2 = \left[\frac{r_1}{K_s (1 - r_1) (1 - \gamma)}\right] \frac{2EI}{\ell} \qquad (1)$$

where:

r_1 = yield stiffness ratio for the cantilever element.

K_s = rotational stiffness of the point hinge in the model before yielding

γ = ratio of the tip moment to the moment at the fixed end

The main difficulty in using the above expression is that the ratio of the end moments, γ, is not known beforehand and, in fact, varies throughout the analysis. In addition, if the bending moment in the element is not uniform, the moment-rotation relationship for the element or a segment of it does not have the same shape as the sectional moment-curvature relationship. Thus, the yield stiffness ratio, r_1, and the yield moment, M_y, corresponding to the moment-rotation relationship of the element, are unknowns. One way to overcome these problems is to divide each member into short elements so that the moments at the two ends are approximately equal and thus $\gamma \sim 1$. For this case, the moment-rotation relationship is proportional to the moment-curvature relationship so that the desired properties can be easily obtained.

In this study it was found desirable to use the minimum number of nodal points consistent with an accurate determination of deformations in the hinging region, in order to economize on the cost of each run and thus allow a wider range of parametric values to be examined. Preliminary studies indicated that if nodal points were established at every story level near the

base of the wall (where hinging is expected), the ratio of end moments for each segment could be taken approximately equal to 0.9. For the model with nodal points as shown in Fig. 6a (the same as those shown in Fig. 4) this ratio was used to determine r_1 and M_y from the moment-curvature relationship and r_2 using equation (1). Analyses were then made using this model and one where the lower region of the wall was divided into much shorter elements (Fig. 6b) over which the curvature is approximately uniform. The results of the dynamic analyses were almost identical for rotations and forces in the hinging region. The displacements in the upper stories also compared very well although some discrepancies occurred in the displacements of the lower stories. It was thus decided that for the parametric studies, it would be sufficiently accurate to use element lengths equal to the height of a story near the base of the wall and to assume a ratio equal to 0.9 for the end moments in a segment.

(3) Integration Time Step

The time step, Δt, to be used in the dynamic analysis is of primary concern since it affects both the accuracy of the results and the cost of the computer runs. Some preliminary analyses using simple models indicated that an integration step as long as 0.02 second would result in sufficiently accurate results. Using the final 12-mass model for the reference structure ISW 1.4 (with fundamental period, T_1 = 1.4 sec.), a comparison of results was made using values of Δt = 0.02 sec. and 0.005 sec. The results showed very good agreement. The plastic deformations were within 1 percent and

the top displacements within 2.5 percent of each other. On the basis of these results, an integration time step $\Delta t = 0.02$ sec. was used for structures with initial fundamental periods of 1.4 sec. or longer.

In using a time step of 0.02 sec., irregularities in the solution were noticed in two cases: in walls with significant discontinuities in stiffness, etc., and in input accelerograms where large changes in the values of acceleration occurred in one time step. For both of these cases, the analyses were carried out using $\Delta t = 0.005$ sec. For structures with initial fundamental period, $T_1 = 0.8$ sec., a time step of 0.02 sec. appeared to be too large, even when extensive yielding occurred. For these cases, values of $\Delta t = 0.01$ and 0.005 yielded almost identical results.

(4) The P-Δ Effect

The nonlinear effect of gravity loads on deformations was examined for the reference structure ISW 1.4. Although extensive yielding took place in the structure and the lateral displacements were significant, the gravity load appeared to have no appreciable effect on the response. On this basis, the P-Δ effect was not considered in the subsequent analyses.

DISCUSSION OF RESULTS

GENERAL

Data from the dynamic analyses consist of plots of response quantities directly relating to the specific objectives set for this study. In selecting the response quantities to be plotted, primary importance was given to the behavior of the hinging region at the base of the wall. Generally, the base of the wall represents the most critical region from the standpoint of expected deformations and its importance to the behavior of the wall and other structures which may be attached to the wall.

In addition to quantities characterizing the response of the hinging region, the horizontal interstory distortions along the height of the wall have also been recorded. Here, a distinction should be drawn between two measures of interstory distortion. In isolated structural walls, which exhibit predominantly cantilever flexure-type behavior, the interstory "tangential deviation", (i.e., the deviation or horizontal displacement of a point on the axis of the wall at a given floor level measured from the tangent to the wall axis at the floor immediately below it (see Fig. 7)), rather than the "interstory displacement", provides a better measure of the distortion that the wall suffers. In fact, the tangential deviations vary in the same manner as, and are directly reflected in, the bending moments that are induced by the lateral deflection of the wall. For open frame structures characterized by a 'shearing type' deformation (resulting from the flexural action of the individual columns of the frame), the interstory displacement varies in about the same manner along the height of the structure as the tangential deviation and has been used as a convenient index of

the potential damage to both structural and nonstructural components of this type of building.[4] Figure 8 shows the typical variation with height of these two quantities for the case of a statically-loaded cantilever wall.

TYPICAL RESULTS OF ANALYSIS

The results of a typical analysis are obtained in the form of envelopes of maximum displacements, forces and ductility requirements along the height of the structure. In addition, response history plots of a variety of quantities, including plots of moment-plastic hinge rotation, moment-nodal hinge rotation and plots of moment vs. shear values throughout the response, have been obtained. To allow convenient comparison of responses for the parametric study, composite plots of envelopes and composite response history plots were prepared from cards punched during each run.

Figures 9 through 17 have been included to give an indication of the types of results obtained from each analysis through the plotting options introduced into Program DRAIN-2D.[5] Figure 9(a), for instance, shows the time history of horizontal displacement of the top of the reference structure ISW 1.4 (with fundamental period, T_1 = 1.4 sec. and yield level, M_y = 500,000 in-kips) when subjected to the E-W component of the 1940 El Centro record, normalized so as to yield a 5%-damped spectrum intensity equal to 1.5 times the spectrum intensity of the N-S component of the same record. Figure 9(b) shows the same type plots for the intermediate story levels of the same structure.

Figures 10(a) and (b) are time history plots of the interstory displacements between the different story levels of the same reference structure. Rotation time histories are of particular interest in the

lower part of the wall. Figure 11 shows the variations with time of the total rotations from the base of the wall to story levels 1 and 2, while Fig. 12 shows the time history of the plastic hinge rotation in the first story. Plots of moment and shear at the base versus time are shown in Figs. 13 and 14. Sample plots of two types of moment-rotation curve are shown in Figs. 15 and 16 for the same reference structure. Plots of moment vs. total rotation were used to determine the required rotational ductility at the base of the wall.

The change with time in the cumulative nodal rotation at the first story level (split into primary and secondary components as illustrated in Fig. 31) is shown in Fig. 17. The nodal rotation at the first story level represents the total rotation in the segment of the wall between the base and the first story level and serves as a convenient measure of the deformation within this region. Figure 18 shows the variation with time of the cumulative area under the base moment-nodal rotation hysteresis loop for the basic structure 15W 1.4. In calculating the areas for Fig. 18, the base moment was nondimensionalized by dividing by the corresponding value of the base moment at first yield.

In order to study the variation of the ratio of moment-to-shear, as well as the absolute values of these quantities, moment vs. shear plots were obtained with each analysis. Figure 19 shows an example of such a plot.

In presenting the results of the analyses the basic plots which have been used for the purpose of the parametric study are envelopes of maximum values of horizontal story displacements, interstory displacements, bending moments, horizontal shears, rotational ductility requirements, and cumulative plastic hinge rotations over the entire height of the structure.

The rotational ductility requirement for a member as plotted in these response envelopes is defined as:

$$\mu_r = \frac{\theta_{max}}{\theta_y} \tag{2a}$$

where θ_{max} is the maximum member rotation and θ_y is the rotation corresponding to yield. In terms of moments, this definition becomes:

$$\mu_r = 1 + \frac{(M_{max} - M_y)}{r_y M_y} \tag{2b}$$

where r_y is the ratio of the slope of the second, post-yield branch to the slope of the initial or elastic branch of the primary bilinear moment-rotation curve of the member, i.e., the yield stiffness ratio.

For the purpose of comparing histories of response for different values of a particular parameter, histories of normalized forces and deformations were obtained by dividing the value of the particular response quantity at any time by the corresponding value at first yield. Figure 23, for example, shows the time variation of the normalized total rotation between the base of the wall and story level 1. The dashed, horizontal lines through ordinates +1.0 and -1.0 correspond to first yield in each case.

GROUND MOTION PARAMETERS

Effect of Frequency Characteristics

As mentioned previously, it was considered desirable to study the effect of the frequency characteristics of the input motion on dynamic response early in the study in order to decide on the record(s) to use for the analysis of other parameters. This question is basic to the problem of determining the critical input motion in relation to the properties of a given structure. For this purpose, and to confirm the qualitative observations made in connnection with the response spectra of single-degree-of-freedom systems under "Input Motions", three separate sets of analyses were made. These are listed in Table 2.

The first set corresponds to the reference structure with fundamental period, T_1 = 1.4 sec. and consists of the four accelerograms listed under set (a) in Table 2. All the accelerograms were normalized to 1.5 times the 5%-damped spectrum intensity (SI) of the N-S component of the 1940 El Centro record*; the normalization factors are listed in Table 2. The normalized accelerograms are shown in Fig. 20, and the corresponding 5%-damped velocity spectra are shown in Fig. 21. Also shown for comparison is the velocity spectrum for the N-S component of the 1940 El Centro record. The entries in the fourth column of Table 2 indicate the classification of the accelerogram in terms of the general features of its velocity spectra relative to the initial fundamental period of the structure. Thus, a "peaking (0)" classification indicates that the 5%-damped velocity response spectrum for this accelerogram shows a pronounced peak at or close to the fundamental period of the

*In the following discussion, the 5%-damped spectrum intensity (SI) of the first 10 seconds of the N-S component of the 1940 El Centro record, for the period range 0.1 sec. to 3.0 sec., will be denoted by "$SI_{ref.}$" (which has a value of 70.15 in.).

structure considered (in this case, T_1 = 1.4 sec.). A "peaking (+)" classification indicates that the peak in the velocity spectrum occurs at a period value greater than that of the fundamental period of the structure considered. A "broad band" classification, as discussed under "Input Motions", refers to an accelerogram with a 5%-damped velocity spectrum which remains more or less flat over a region extending from the fundamental period of the structure to at least one second greater. A "broad band ascending" classification is similar to a "broad band" accelerogram, except that the velocity spectrum exhibits increasing spectral values for periods greater than the initial fundamental period.

The second and third sets of analyses undertaken to study the effect of frequency characteristics of the input motion include two and three accelerograms, respectively, and are also listed in Table 2. These sets correspond to structures with fundamental periods of 0.8 sec. and 2.0 sec. each.

In addition to the above three sets, a set of two analyses was made using an input motion intensity equal to 0.75 ($SI_{ref.}$) to illustrate the interaction between the intensity of the input motion and the yield level of a structure in determining the critical frequency characteristic of the input motion.

(a) Fundamental Period of Structure, T_1 = 1.4 sec., M_y = 500,000 in-kips

Envelopes of response values for the structure with period of 1.4 sec. and yield level, M_y = 500,000 in-kips, are shown in Fig. 22*. Figures 22(a), (b) and (e) indicate that the E-W component of the 1940 El Centro record, classified as

*In the envelopes for rotational ductility requirements, values less than 1.0 represent ratios of the calculated maximum moments to the yield moment, M_y.

"broad band ascending" with respect to frequency characteristics, produces relatively greater maximum displacements, interstory displacements and ductility requirements than the other three input motions considered. However, the same record produces the lowest value of the maximum horizontal shear, with the artificial accelerogram S1 producing the largest shear, as shown in Fig. 22(d). Because all the structures yielded and the slope of the second, post-yield branch of the assumed moment-rotation curve is relatively flat, the moment envelopes shown in Fig. 22(c) do not show any significant differences among the four input motions used.

An idea of the variation with time of the flexural deformation at the base of the wall under each of the four input motions of Set (a) in Table 2 is given by Fig. 23. This figure shows the normalized rotations of the node at story level "1", which represent the total rotations occurring in the first story. To plot the curves in Fig. 23, the absolute values of the rotations have in each case been divided by the corresponding rotation when yielding first occurred. The two dashed lines on each side of the zero axis (at ordinates +1.0 and -1.0) thus represent the initial yield level for all cases. The actual location of the 'state point' describing the deformation of the first story segment relative to its moment-rotation curve at each instant of time is indicated in Fig. 24, for the structure subjected to the 1940 El Centro, E-W motion.

It is interesting to note in Fig. 23 that although the intense motion starts relatively early under the artificial accelerogram S1 (see Fig. 20), yielding occurs first under the 1940 El Centro E-W motion. The relative magnitude of the rotation at first yielding, however, is greater under both S1 and the Pacoima Dam S16E record, a "peaking (0)" accelerogram.

As expected, the Holiday Inn, Orion record, a "peaking (+)" accelerogram, produced a much lower response during the first few seconds, since the velocity spectrum for this motion (see Fig. 21) peaks at a period greater than the initial fundamental period (T_1 = 1.4 sec.) of the structure. As the structure yields and the effective period increases, however, the response under this excitation increases gradually.

It is significant to note in Fig. 23 that as yielding progresses and the effective period increases, it is the "broad band ascending" type of accelerogram (in this case, the 1940 El Centro E-W component) which excites the structure most severely, while response to the other types of accelerogram--and particularly the peaking accelerograms--tend to diminish.

An indication of the change in fundamental period of a structure as the hinging (yielded, "softened") region progresses from the first story upward is given by Fig. 25, for different values of the yield stiffness ratio, $r_y = EI_2/EI_1$ or $(EI)_{yield}/(EI)_{elastic}$. The figure is based on the properties of the reference structure with initial fundamental period, T_1 = 1.4 sec. It is pointed out that since the structure goes through unloading and reloading stages as it oscillates in response to the ground motion (see Fig. 15), the

general behavior reflects the effects of the "elastic" or unloading stiffness, as well as its yield or reloading stiffness. The effect of each stiffness value will depend on the duration of the response under each stiffness value, and this in turn will depend on the character of the input motion. When yielding occurs early, and for the type of structure considered here in which the condition at the critical section (i.e., the base of the wall) determines to a large degree the response of the structure, it seems reasonable to assume that both elastic and yield stiffness play about equal roles in influencing the "effective period" of the structure. In the Takeda model[3] of the hysteretic loop, the initial portions of the reloading branches of the moment-rotation loops (see Fig. 15) have stiffness values intermediate between the initial elastic and the yield stiffness of the primary curve.

Figure 22(f) shows the cumulative plastic hinge rotations, i.e., the sum of the absolute values of the inelastic hinge rotations over the 10-second response period. This parameter reflects the combined effect of both the number and amplitude of inelastic cycles and provides another measure of the severity of the response. The fact that the artificial accelerogram S1 produces a slightly greater cumulative plastic hinge rotation at the base of the wall than does the 1940 El Centro E-W component, in spite of the lesser amplitude of the associated maximum rotation (see Fig. 22(e)), indicates that the response to S1 is characterized by a relatively greater number of cycles of inelastic oscillation than to El Centro E-W. This is indicated in the more jagged character of the

response history curve corresponding to S1 (shown in Fig. 23), and is a reflection of the considerably greater number of acceleration pulses over the 10-second duration in S1 than in any of the recorded accelerograms shown in Fig. 20.

It can be seen in Fig. 22(b) that the relative effect of the parameter considered (in this case, the frequency characteristics of the input motion) is similar on both interstory displacements and tangential deviations, the main difference between the two quantities being in their distribution along the height of the structure. For the subsequent cases, only the horizontal interstory displacement envelopes are shown. In considering these figures, the significance of the interstory displacement relative to the distortion in an isolated wall, and particularly its distribution along the height as compared to the corresponding tangential deviations, must be borne in mind.

(b) Fundamental Period of Structure, T_1 = 0.8 sec., M_y = 1,500,000 in-kips

To study the effects of frequency characteristics for the case of short-period structures with relatively high yield levels, a "peaking (0)" accelerogram (N-S component of the 1940 El Centro) and a "broad band ascending" type (E-W component of the 1940 El Centro) were considered.

Figure 26, which shows response envelopes of displacement, moments, etc., indicates that the peaking accelerogram consistently produces a greater response in the structure than does a broad band record. A comparison of Fig. 26(e) with Fig. 22(e), shows that the ductility requirements are not only

significantly less for this structure with a high yield level, but that yielding has not progressed as high up the structure as in the case of the structure considered under (a), with period T_1 = 1.4 sec. and a low yield level. For the type of structure considered here, where the displacements of the lower stories are generally in phase (fundamental mode predominating), the magnitude of the ductility requirements at the base of the wall is a direct function of the extent to which yielding has progressed up the height of the wall.

The greater response of the structure under the N-S component of the 1940 El Centro (peaking) follows from the fact than the dominant frequency components for this motion occur in the vicinity of the period of the structure, (see Fig. 21). In this region the E-W component has relatively low-power components. Also, because of the high yield level of the structure, yielding was not extensive, particularly under the E-W component and apparently did not cause the period of the yielded structure to shift into the range where the higher powered components of the E-W motion occur. On the other hand, Fig. 26(e) indicates that under the N-S component of 1940 El Centro, yielding in the structure extended up to the 4th story level, as against the 2nd story level under the E-W component. The greater extent of this yielding and the accompanying increase in the effective period of the structure could easily have put the structure within the next peaking range of the input motion (see Fig. 21).

(c) Fundamental Period of Structure, T_1 = 2.0 sec., M_y = 500,000 in-kips

For this structure, the peaking accelerogram used was the E-W component of the record taken at the first floor of the Holiday Inn on Orion Boulevard, Los Angeles, during the 1971 San Fernando earthquake. The record has a 5%-damped velocity spectrum that actually peaks at about 1.75 sec. and can thus be classified as a "peaking (-)" accelerogram relative to the structure considered. The other input motion considered is the E-W component of the 1940 El Centro record ("broad band ascending").

The response envelopes of Fig. 27 indicate, as in Set (a) with a structure period T_1 = 1.4 sec. and M_y = 500,000 in-kips, that where yielding is significant, the horizontal and interstory displacements, as well as the bending moments and ductility requirements near the base, are greater for the broad band accelerogram than for the peaking motion. Also, as in Set (a), the extensive yielding which occurs near the base results in a reduction of the maximum horizontal shears. Thus, Fig. 27(d), like Fig. 22(d), shows the maximum shears corresponding to the E-W component of the 1940 El Centro to be less than those for the other input motions. The greater base shears associated with these other input motions can be partially attributed to the effect of the higher (effective) modes of vibration. A comparison of Fig. 13 with Fig. 14 clearly indicates the greater sensitivity of the horizontal shears, as compared to bending moments (and displacements), to higher mode response. Figure 21 shows that most of the other

input motions considered have spectral ordinates in the low-period range that are generally greater than those of the 1940 El Centro E-W record.

The results of the preceding analyses serve to confirm the observations made earlier (see "Input Motions") in relation to the velocity spectrum. Thus, for structures where extensive yielding results in a significant increase in the effective period of vibration, the "broad band ascending" type of accelerogram can be expected to produce greater deformations than a "peaking" accelerogram of the same intensity. Where the expected yielding is of limited extent so that the increase in effective period is minor, a peaking type of accelerogram is more likely to produce greater deformations than a broad band accelerogram of the same intensity. Since the extent of yielding is a function of the earthquake intensity, the yield level of the structure, and the frequency characteristics of the input motion, these factors must be considered in selecting an input motion for a given structure to determine a reasonable estimate of the maximum response.

Interaction Between Earthquake Intensity and Structure Yield Level in Determining Critical Frequency Characteristic of Input Motion

In order to verify the above observation concerning the relationship of the input motion intensity and the structure yield level, the reference structure ISW 1.4 (T_1 = 1.4 sec., M_y = 500,000 in-kips) was subjected to two input motions with intensity equal to 0.75 ($SI_{ref.}$). The two motions used were the S16E component of the 1971 Pacoima Dam record and the E-W component of the 1940 El Centro record. As indicated in Table 2, the Pacoima Dam record is a "peaking (0)" type relative to the initial fundamental period of the structure, while the El Centro motion is of the "broad band ascending" type.

The resulting envelopes of response, shown, in Fig. 28, serve to further confirm the observation made earlier that when yielding in the structure is not extensive enough to cause a significant increase in the effective period of the structure, the peaking type accelerogram is likely to produce the more critical response. Figure 28(e) shows that in this case, yielding in the structure has not extended far above the base when compared to Case (a) where the input motion was twice as intense; see Fig. 22(e).

Note that in Case (a) considered earlier, the 1940 El Centro, E-W record (a "broad band" accelerogram), with intensity equal to 1.5 (SI_{ref}), represents the critical motion, while the Pacoima Dam record (a "peaking" motion) produces a relatively lesser response. By reducing the intensity of the motions by one-half so that yielding in this structure is significantly reduced, the Pacoima Dam record becomes the more critical motion, as Fig. 28 shows.

To summarize, it is pointed out that because the extent of yielding in a structure is influenced by the yield level of the structure, M_y, as well as the intensity of the input motion, both parameters must be taken into account when selecting the appropriate type of motion to use as input with particular reference to its frequency characteristics.

In selecting an input motion for use in the analysis of a structure at a particular site, the probable epicentral distance and intervening geology should be considered. These considerations, which affect the frequency content of the ground motion at the site, may logically rule out the possibility of dominant components occurring in certain frequency ranges. Because in seismic waves the high-frequency components tend to be attenuated more rapidly with distance than the low-frequency components, it is reasonable to expect that beyond certain distances, depending on

the geology, most of the high-frequency components from a given source are damped out so that only the low-frequency (long-period) components need be reckoned with.

Effect of Duration of Earthquake Motion

In studying the effect of duration of the earthquake motion, the response of the reference structure, with period T_1 = 1.4 sec. and M_y = 500,000 in-kips, to the first 10 seconds of the E-W component of the 1940 El Centro record was compared with its response to an accelerogram with a 20-second duration. Both accelerograms were normalized to yield a spectrum intensity equal to 1.5 ($SI_{ref.}$).

The 20-second accelerogram consists of the first 12.48 seconds of the E-W component of the 1940 El Centro record followed by that portion of the same record between 0.98 sec. and 8.5 sec. The intent in putting together this composite accelerogram was to subject the structure to essentially the same first 10 seconds of input motion but to extend the period of excitation using acceleration pulses of about the same intensity as those occurring in the first 10 seconds. Because the 1940 El Centro, E-W component has its peak acceleration at about 11.5 seconds, it was decided to include this peak in the composite record and add a segment from the more intense portion of the first 10 seconds to make a 20-second record. The inclusion of the peak acceleration at 11.5 sec. and the addition of the extra 7.5 sec. of fairly intense pulses, however, sufficiently altered the velocity response spectrum so that a normalizing factor smaller than that used for the 10-sec. input motion was indicated in order to yield a spectrum intensity equal to 1.5 times that of the 1940 El Centro, N-S component. Thus, a normalizing factor of 1.54 was calculated for the 20-second composite accelerogram,

compared to a factor of 1.88 used for the 10-second input record. This means that the amplitude of the pulses in the 10-second record was larger than in the first 10 seconds of the 20-second composite accelerogram by a factor of 1.88/1.54 or 1.22. A plot of the unnormalized 20-sec. composite accelerogram is shown in Fig. 29(a), with the corresponding relative velocity response spectra given in Fig. 29(b).

In Fig. 30, showing response envelopes, the curves corresponding to the 20-sec. composite accelerogram described above are marked "20 sec.-(a)". This figure shows that the displacements, interstory displacements, moments, shears and ductility requirements are greater for the 10-sec. record than for the 20-sec. composite record having the same spectrum intensity. In spite of this, the cumulative ductility, i.e., the sum of the absolute values of the plastic rotations in the hinging region, is greater for the 20-sec. long record, as shown in Fig. 30(f). This, of course, follows from the fact that the structure goes through a greater number of inelastic oscillations when subjected to longer excitation. The cumulative plastic hinge rotation plotted in Fig. 30(f) represents the sum of the "primary" and the "secondary" plastic rotations illustrated in Fig. 31. Because it is a measure of the number and extent of the excursions into the inelastic region which the critical segment in a member undergoes, the cumulative plastic hinge rotation represents an important index of the severity of deformation associated with dynamic response. This is particularly true for members which tend to deteriorate in strength with repeated cycles of inelastic deformation, i.e., with relatively short low-cycle-fatigue lives.

The time history of rotation of the node at the first story level of the wall when subjected to the two input motions discussed above is shown in Fig. 32. The curve marked "10 sec." actually corresponds to

the first 20 seconds of the 1940 El Centro, E-W record, normalized so that the spectrum intensity for the first 10 seconds equals 1.5 times $SI_{ref.}$. As might be expected, the response of the structure during the second 10 seconds of the normalized 1940 El Centro E-W record (marked "10-sec." in Fig. 32) decays after 12 seconds while the structure continues to oscillate through several cycles of relatively large amplitude under the 20-sec. composite accelerogram.

The third curve in Figures 30 and 32, marked "20 sec.-(b)", represents the response of the structure to the 20-sec. composite accelerogram when scaled by the same factor used in normalizing the 10-sec. record. Note that the curves marked "10-sec." and "20 sec.-(b)" in Fig. 32 coincide over the first 10 seconds.

Both Figures 30(f) and 32 indicate that the major effect of increasing the duration of the large-amplitude pulses in the input accelerogram is to increase the number of cycles of large-amplitude deformations which a structure will undergo. This conclusion assumes that the intensity and frequency characteristics of the additional motion do not differ significantly from those of the shorter duration input.

Effect of Earthquake Intensity

For the purpose of examining the effect of earthquake intensity, three sets of analyses were run corresponding to different combinations of the fundamental period, T_1 and the yield level, M_y. In all the cases considered, the input motion used was the first 10 seconds of the E-W component of the 1940 El Centro record, normalized to different intensity levels in terms of $SI_{ref.}$.

Table 3 shows the values of the periods and yield levels assumed for the structure, together with the different intensity levels of input motion used for each set. The envelopes of response for all of these cases are shown in Figures 33, 34 and 35. In all cases, there is a consistent increase in the response parameters considered with increasing intensity, a behavior also observed by other investigators.

Figure 33 shows that the displacements, interstory displacements and ductility requirements increase with increasing intensity in an almost proportional manner. The maximum moments and shears, however, do not show a proportional increase to reflect the increase in intensity. Thus, Figs. 33(c) and (d) show that an increase in intensity level from 1.0 to 1.5 produces about the same increase in the maximum moments and shears as an increase from 0.75 to 1.0 in intensity level.

Figure 34(e) indicates that with a yield level, M_y = 1,000,000 in-kips, the yielding, even under a 1.5 intensity level input motion, does not extend too high up the structure. For this case, the N-S component of the 1940 El Centro record, which has a velocity spectrum that peaks at about 0.8 sec. produces a greater response--for the same intensity (see Case (b) of "Effect of Frequency Characteristics").

STRUCTURAL PARAMETERS

The combinations of significant structural parameters used in investigating the effect of each parameter on dynamic response have been summarized for convenient reference in Table 4. In almost all cases, the parameter values in each set have been chosen so that only the parameter of interest is varied while the other variables remain constant.

The fundamental period, T_1, and the yield level, M_y, (the basic parameters characterizing the force-deformation curve of the structure), were extensively studied using different combinations of structural parameters. The slope of the post-yield branch of the primary bilinear moment-rotation curve, as defined by the yield stiffness ratio, r_y, was also considered in detail. Studies were also made to determine the sensitivity of the dynamic response to varying degrees of stiffness degradation in hinging regions of the wall. The effect of the shape of the hysteretic loop was examined by assuming different values of the parameters α and β which define the slopes of the unloading and reloading branches of the Takeda model of the M-θ loop (see Fig. 51) of potential inelastic hinges. Other parameters investigated included viscous damping, taper in stiffness and strength along the height of the structure, the fixity condition at the base, and the number of stories.

Based on the study of the effects of the frequency characteristics of the input motion, it was decided to use the first 10 seconds of the E-W component of the 1940 El Centro record, (with intensity adjusted so that its 5%-damped spectrum intensity equaled 1.5 times $SI_{ref.}$), as input motion for the analyses of the effects of all the structural parameters on dynamic response.

Effect of Fundamental Period, T_1

The effect of the initial fundamental period of the structure, T_1, was investigated by using four sets of data as shown in Table 4, each corresponding to a different yield level, M_y. Because of the close interrelationship between these two major structural parameters, it was deemed necessary to study the effects of the structure period under varying values of the yield level.

(a) Yield Level, M_y = 500,000 in-kips

Corresponding to this value of the yield level, four values of the fundamental period were used, namely, 0.8, 1.4, 2.0 and 2.4 secs. Even though the stiffness associated with a period value, T_1, of 0.8 sec. is rather high for a structural wall section having a yield level of 500,000 in-kips, this parameter combination was considered in order to provide some indication of the behavior of structures which might fall in this range.

Figure 36 shows the envelopes of response quantities for this set. In Fig. 36(a) and (b), the maximum horizontal and interstory displacements show a consistent increase with increasing fundamental period (or decreasing stiffness) of the structure. The rotational ductility requirements expressed as a ratio of the maximum rotation to the rotation at first yield, however, become greater with decreasing fundamental period, a trend also observed by Ruiz and Penzien.[6] Figure 36(e) indicates, as do similar plots shown earlier, that the greater the ductility requirements at the base, the higher the yielding generally extends above the base.

As might be expected from the fact that all the structures considered in Fig. 36 have the same yield level, and also because of the relatively flat slope of the post-yield branch of the M-θ curve (r_y = .05), the maximum moments and shears shown in Figs. 36(c) and (d) do not differ significantly for all four cases considered; the shorter period structures show only slightly greater moments at the base. Figure 36(e) also indicates that for relatively low yield levels where yielding is significant, the ductility requirements do not decrease significantly with an increase in period beyond a certain value of the fundamental period. Thus, the ductility requirements for the structures with periods of 2.0 and 2.4 sec. are about the same.

It is worth noting that although Fig. 36(e) shows the rotational ductility requirements--expressed as multiples of the corresponding yield rotations--as increasing with decreasing period of the structure, the absolute value of the maximum rotation for the stiff structure is less than that for the more flexible structure. The distinction between these two measures of the deformation requirement is illustrated in Fig. 37, for the case of structures with M_y = 500,000 in-kips. Figure 36(f) shows the cumulative plastic hinge rotation, i.e., the sum of the absolute values of the inelastic hinge rotations, as increasing with increasing period of the structure. This trend follows directly from the larger deformations of the more flexible structures.

The variation with time of the flexural deformation in the first story for the four structures considered in this set is shown in Figs. 38(a) and (b). In Fig. 38(a) the rotations have been normalized by the respective yield levels of each structure. For instance, the rotations for the structure with T_1 = 0.8 sec. have been divided by its yield rotation value of 0.00014 radians and those for the structure with T_1 = 2.0 sec., by 0.00070 radians. Thus, the absolute magnitude of the rotations for the latter structure are actually 0.00070/0.00014 or 5.0 times those of the former on the basis of the ordinates shown in this figure. The variation with time of the actual magnitude of the rotations (in radians) for the four cases considered are shown in Fig. 38(b).

(b), (c) and (d) Yield Level, M_y = 750,000, 1,000,000 and 1,500,000 in-kips, respectively

The same general trends observed in Set (a) above with respect to displacements, moments and ductility requirements are also apparent in Figs. 39 through 41 for the higher values of the yield level, M_y. Thus, as in Set (a), an increase in period results in an increase in the horizontal and interstory displacements and a decrease in the moments and the ductility requirements (expressed as a ratio). Although the horizontal shears do not change much with changing period for a given yield level, no clear trend can be observed insofar as the effect of period variation on the base shear is concerned. Generally, though, the shears tend to be higher for the shorter-period structures.

A comparison of Figs. 38(f) and 39(f) with Figs. 40(f) and 41(f) shows that while for structures with relatively low yield levels (i.e., M_y = 500,000 and 750,000 in-k) the cumulative plastic hinge rotation tends to decrease with decreasing period of the structure, the reverse trend holds as M_y increases beyond a certain value. As noted earlier in Set (a), the ratio of the maximum rotation to the yield rotation (as expressed by the rotational ductility) diminishes with increasing period of the structure, for a given yield level, M_y. This means that the relative extent of yielding (with respect to the corresponding yield level), diminishes with increasing period of a structure. Also, as the yield level increases, the degree of inelastic action generally diminishes, as might be expected and as indicated by a comparison of Figs. 36(e), 39(e), 40(e) and 41(e). Thus, an increase in both yield level and fundamental period would combine to reduce the amount of inelastic action in a structure; and where this combined effect is such as to make yielding in a structure insignificant, the cumulative plastic rotation becomes less for the long-period structure than for the short-period structure. Figure 40(e) shows that for the structure with M_y = 1,000,000 in-kips and T_1 = 2.0 sec., yielding is not too significant, while Fig. 41(e) indicates that the structure with M_y = 1,500,000 in-kips and T_1 = 2.4 sec. remains essentially elastic under a base motion with intensity SI = 1.5 ($SI_{ref.}$).

Effect of Yield Level, M_y

For this study, three sets of yield level values were considered corresponding to fundamental period values of 0.8, 1.4, and 2.0 sec. The different values included in each set are listed in Table 4.

Envelopes of maximum response values showing the effect of yield level are given in Figs. 42, 44 and 45 for the three values of the fundamental period assumed.

The following general comments apply to all cases shown in these figures. For the same fundamental period, the horizontal and interstory displacements decrease sharply as the yield level increases from 500,000 in-kips to a value associated with nominal yielding at the base (a value which tends to decrease with increasing value of the fundamental period, as is evident from a comparison of Figs. 42(a) and (b) with Figs. 45(a) and (b)). Above this value, the trend is reversed and an increase in yield level is accompanied by an increase in horizontal and interstory displacements. The maximum moments and shears increase almost proportionally with the yield level, as shown in plots (c) and (d) of Figs. 42, 44 and 45. As observed earlier under "Effect of Fundamental Period", the rotational ductility requirements increase significantly as the yield level decreases. This qualitative trend has also been observed in connection with the response of single-degree-of-freedom systems.[7] Figure 42(f) shows that the cumulative plastic hinge rotations also increase as the yield level decreases. A normalized time history plot of the total rotation in the first story is shown in Fig. 43 for the four structures with fundamental period, T_1 = 1.4 sec.

Fundamental Period and Yield Level Effects on Dynamic Response--Summary

The interrelationship between the effects of the initial fundamental period, T_1, and the yield level, M_y, on the dynamic response of 20-story isolated structural walls is summarized in Fig. 46, (a) through (f). The plots in the figure correspond to only one input motion, i.e., the E-W component of the 1940 El Centro record, with the acceleration amplitude adjusted to yield a 5%-damped spectrum intensity equal to 1.5 ($SI_{ref.}$). The properties of the structures considered are those for the basic structures listed in Table 1.

Figure 46 shows the effects of both T_1 and M_y on the maximum horizontal displacement of the top of the structure, the maximum interstory displacement along the height of the wall and the maximum moment, (in terms of the yield moment, M_y), the maximum shear, rotational ductility (expressed as a ratio of the maximum rotation to the corresponding yield rotation) and the cumulative plastic hinge rotation at the base of the wall. The maximum values of the response parameters are also listed in Table 5.

The following significant points, noted earlier in relation to the study of the separate effects of the fundamental period and the yield level, are summarized below for convenience in considering the curves shown in Fig. 46.

(a) Maximum Top Displacement and Maximum Interstory Displacement

For a particular value of the yield level, M_y, an increase in the fundamental period (indicating a decrease in the stiffness of the structure) results in an increase in horizontal and interstory displacements.

For a given fundamental period and for relatively low values of the yield level so that significant yielding occurs, the maximum displacements decrease with increasing yield level. Beyond a certain value of the yield level (which tends to decrease with increasing value of the fundamental period) associated with nominal yielding, the above trend is reversed, i.e., the maximum displacements increase with increasing yield level.

Figure 46(a) shows a dotted curve representing the top displacement resulting from the distributed design base shear, V_b, as specified in the Uniform Building Code (1976 Edition)--with the factors Z, S and I set equal to 1.0.

(b) Maximum Moment and Rotational Ductility at Base

For a particular value of the yield level, the ratios M_{max}/M_{yield} and $\theta_{max}/\theta_{yield}$ as measures of the maximum moment and rotational ductility at the base, respectively, generally decrease with increasing fundamental period, the decrease being more rapid for the lower yield levels. For a constant fundamental period, the above ratios consistently increase with decreasing yield level.

It should be pointed out that the yield level of 500,000 in-kips is not too realistic for structural walls having stiffnesses associated with fundamental period values less than 1.4 sec.

(c) Maximum Base Shear

For a particular yield level, M_y, the maximum base shear decreases as the fundamental period increases from 0.8 sec. to

a certain value which increases with increasing yield level. Beyond this value of the fundamental period, the maximum base shear increases with increasing period of the structure.

For a fixed furdamental period, the base shear increases consistently with increasing yield level, the rate of increase being greater for the stiffer (shorter-period) structures.

(c) Cumulative Plastic Hinge Rotation at Base

Figure 46(f) indicates, as noted earlier, that for structures with relatively low yield levels (i.e., M_y = 500,000 and 750,000 in-k) in which significant yielding occurs, the cumulative plastic hinge rotation at the base increases with increasing fundamental period over the entire period range (0.8 - 2.4 sec.) considered. For higher values of the yield level, the cumulative plastic hinge rotation increases with increasing period up to a point where the combination of high yield level and long period results in only nominal yielding. Beyond this value of the fundamental period (which decreases with increasing yield level) the trend is reversed and the cumulative plastic hinge rotation decreases with increasing fundamental period until the case is reached where no yielding occurs.

Curves corresponding to the design base shear as specified in the Uniform Building Code (UBC-76), multiplied by load factors of 1.4 and 2.0, are shown in Fig. 46(d) for comparison with the results of the dynamic analysis.

Effect of Yield Stiffness Ratio, r_y

The effect of the slope of the second, post-yield branch of the primary bilinear moment-rotation curve of the members which make up the structural wall was investigated by considering a value of the yield stiffness ratio, r_y, (i.e., the ratio of the slope of the second, post-yield branch to the slope of the initial, elastic branch of the M-θ curve), equal to 15%, in addition to the value of 5% used for most cases. As indicated in Table 4, these two values of the yield stiffness ratio were used with three combinations of the fundamental period and yield level. In addition, a value of $r_y = 0.01$ was considered for the case of structures with $T_1 = 1.4$ sec. and $M_y = 500{,}000$ in-kips.

Envelopes of response quantities for the three sets considered are given in Figs. 47, 48 and 49. These figures show that even when there is significant yielding at the base, as indicated by the plots for rotational ductility, an increase in the value of the yield stiffness ratio from 5% to 15% generally does not produce any significant effect on the response. As might be expected, the effect of a change in the value of the yield stiffness ratio, r_y, is more apparent in structures with relatively low yield levels ($M_y = 500{,}000$ in-k). There is a substantial (50%) reduction in the rotational ductility requirement at the base for the long-period ($T_1 = 2.0$ sec.) structures and a 20% reduction in the horizontal and interstory displacements for the moderately-long period ($T_1 = 1.4$ sec.) structures accompanying an increase in the yield stiffness ratio from 5% to 15%. The effect of increasing the yield stiffness ratio is less apparent in structures with relatively high yield levels, as shown by Fig. 48.

A decrease in the yield stiffness ratio from 5% to 1% results in an increase in the rotational ductility requirement at the base by a factor of 1.85 (see Fig. 47(e)) with a lesser increase in the cumulative plastic hinge rotation. Except for these, the effect of r_y on the response is relatively minor for the range of values considered. An increase in the slope of the post-yield branch of the M-θ curve tends to reduce the horizontal and interstory displacements as well as the ductility requirements at the base while increasing the moments and shears slightly.

It will be noted that for the Takeda model of the hysteretic M-θ loop, the effective stiffness of an element during most of the response after yielding may be governed not so much by the primary M-θ curve as by the rules governing the slope of the reloading stiffness associated with this model. The effect of r_y becomes significant only when the motion of the structure proceeds in a particular direction long enough for the primary curve to govern. However, because the post-yield slope in the bilinear M-θ curve represents the least value of the stiffness of the structure, it can be expected to have a greater effect on the maximum displacements and rotations than the subsequent "reduced" stiffnesses. The effect becomes most pronounced for structures with low yield levels (relative to the intensity of the input motion), and significant displacements and ductility requirements can then be expected particularly for low values of r_y. An idea of the percentage of the total response time during which the post-yield branch of the primary curve governs the effective stiffness of the structure can be obtained from Fig. 50, which shows the moment-rotation loop for the base of the structure with T_1 = 1.4 sec., M_y = 500,000 in-kips and r_y = 15%.

Effect of Character of M-θ Hysteretic Loop

In the analyses undertaken to investigate the effects of other parameters, the quantities α and β defining the slopes of the unloading and reloading branches of the Takeda model hysteretic loop (see Fig. 51) were assigned values of 0.10 and 0.0, respectively. The sensitivity of the calculated response to variations in the values of these two parameters was examined by analyzing structures using different values of α and β.

A value of 0.30 was considered for the unloading parameter α in addition to the basic value of 0.10 (with $\beta = 0$), for a structure with $T_1 = 1.4$ sec. and $M_y = 500{,}000$ in-k. For the Takeda model reloading parameter β, values of 0.4 and 1.0 were assumed in addition to the basic value of 0 (with $\alpha = 0.10$). Furthermore, results for a model with a stable bilinear hysteretic loop (see Fig. 51) were obtained for comparison with the response of structures with different values of β. The effect of the reloading parameter β was investigated for two sets of structures, one set representing low yield levels ($M_y = 500{,}000$ in-k, $T_1 = 1.4$ sec.) and the other relatively higher yield levels ($M_y = 1{,}000{,}000$ in-k, $T_1 = 0.8$ sec.). The various combinations used in this study are also listed in Table 4.

Figure 52, which shows response envelopes for cases where the parameter α is allowed values of 0.10 and 0.30 (with $\beta = 0$) indicates practically no difference in the maximum response values corresponding to the two assumed values of α.

Figures 53 and 54 show the response envelopes for cases when the reloading parameter β is varied. Both figures indicate that the effect of this parameter on dynamic response is not significant.

For the case of structures with low yield level (M_y = 500,000 in-k, see Fig. 53), an increase in the slope of the reloading curve--corresponding to increasing values of β--results in slight reductions in horizontal and interstory displacements and cumulative plastic hinge rotations. Where yielding is not as extensive as in structures with M_y = 1,000,000 in-k (compare Fig. 54(e) with 53(e)), the effects of variations in the value of β are even less significant. For this case, the trend with respect to maximum horizontal displacements is reversed, so that the structure with the stable bilinear hysteretic loop exhibits slightly greater displacements than any of the structures with decreasing-stiffness loops. The cumulative plastic hinge rotations, however, still increase as the value of β decreases (see Fig. 54(f)). Note that this same trend in the maximum response values was observed in the study of the effect of the yield level, M_y (see Fig. 42).

In each of the two sets of analyses where the reloading parameter β was varied, the maximum moments, shears and rotational ductility requirements at the base are practically the same in spite of the significant difference in the slopes of the reloading curves.

The variation with time of the nodal rotations at the first story level for the structures with T_1 = 1.4 sec. and M_y = 500,000 are shown in Fig. 55. For all cases the figure shows that the maximum response to the particular input motion used occurs very early when the primary bilinear curve (which is identical for all cases) governs; the envelopes of maximum response values do not differ significantly from each other. However, after the first major inelastic cycle of response occurs and the rules assumed for the reloading stiffness in each case take effect, the responses reflect the different characteristics of the M-θ hysteretic

loop. Thus, after first yield, the rotations tend to be greater for the lesser values of β (corresponding to reloading branches with flatter slopes or lesser stiffness).

Moment vs. nodal rotation plots for the structure with a stable hysteretic loop and that with $\beta = 0.40$ are shown in Fig. 56. The corresponding plot for the structure with $\beta = 0$ is shown in Fig. 16.

Effect of Damping

The viscous damping assumed for the structures considered in this study consists of a linear combination of stiffness-proportional and mass-proportional damping. The damping distribution among the initial component modes is defined in terms of the percentage of the critical damping for the first mode and the second mode, which are assumed to be equal. For most of the analyses, a damping coefficient of 0.05 was assumed.

To study the effect of damping, a second value of the damping coefficient, equal to 0.10, was considered. The responses corresponding to these two values of damping were compared for two combinations of the fundamental period, T_1, and the yield level, M_y, as shown in Table 4.

Envelopes of response corresponding to structures with intermediate period and low yield level (i.e., $T_1 = 1.4$ sec., $M_y = 500{,}000$ in-k) are shown in Fig. 57. As observed in other studies, the general effect of increasing the damping in a structure is to reduce the response. For the structures considered in this particular set, increasing the damping coefficient from 0.05 to 0.10 produced only a relatively small (about 12% in the maximum top displacement) reduction in response.

Figure 58 shows the response envelopes of structures with low period and relatively high yield level, i.e., T_1 = 0.8 sec., M_y = 1,000,000 in-k. The effect of increasing the value of the damping coefficient from 0.05 to 0.10 for this set is likewise insignificant. When compared with the results for the first set of structures with low yield level, Fig. 58 indicates that the increase in the viscous damping coefficient from 5% to 10% produces a slightly lower reduction (9%) in the maximum top displacement. However in terms of deformation requirements, the increase in damping produces a relatively greater percentage reduction in the high-yield-level (M_y = 1,000,000 in-k) structure than in the structure where extensive yielding occurs (M_y = 500,000 in-k): 19% as against 8% for the rotational ductility requirement and 41% as compared to 13% for the cumulative plastic hinge rotation. This increase in the energy dissipated through damping as the extent of inelasticity diminishes, and vice versa, was also noted by Ruiz and Penzien.[7]

Effect of Stiffness Taper

In examining the effect of other parameters the structures considered all have uniform stiffness throughout their entire height. To study the effect of a taper in stiffness, the response of a structure with the stiffness variation shown in Fig. 59 was compared to that of a structure with uniform stiffness. A ratio of $(EI)_{base}$ to $(EI)_{top}$ equal to 2.8 was used (corresponding to A/B = 4.0, see Fig. 59), the absolute value of the stiffness being adjusted to yield a fundamental period of 1.4 sec.

Figure 60, which shows the corresponding response envelopes, indicates that for the period and yield level (M_y = 500,000 in-kips) considered, the horizontal and interstory displacements as well as the

cumulative plastic rotations at the base are less for the tapered than for the uniform structure. However, the moments, shears and rotational ductility requirements at and near the base are greater for the tapered structure than for the wall with uniform stiffness.

Effect of Strength Taper

In order to evaluate the effect of a taper in the strength (yield level) of the wall, the following three cases were considered:

(a) A taper ratio, (i.e., the ratio of the yield level at the base to that at the top of the wall) of 2.0, with equal changes in strength occurring regularly at every story level. This is the taper used in the reference structure, which reflects the effects of axial loads on the moment capacity.

(b) A taper ratio of 3.8, with equal changes in strength occurring at every fourth story level, in a manner similar to the stiffness taper shown in Fig. 59. In addition, changes reflecting the effect of the axial load occur at every story level.

(c) A taper ratio of 1.0, representing uniform strength throughout the height of the wall.

Response envelopes for this set are shown in Fig. 61. Except for the increased rotational ductility requirement in the intermediate stories of the structure with a taper ratio of 3.8 as shown in Fig. 61(e), the effect of strength taper for the particular period and yield level considered appears to be negligible.

Effect of Fixity Condition at Base

The effect of yielding of the foundation at the base of the wall was considered by introducing a rotational spring (with linear M-θ characteristic) at the base of the analytical model. If the base fixity factor, F, is defined as the ratio of the moment developed at the base to that which would be developed if the base were fully fixed, under the same deformation, the spring stiffness, K_s, for the model shown in Fig. 62 is given by

$$K_s = \left(\frac{1}{1-F}\right)\frac{3EI}{\ell} \qquad (3)$$

In the analysis, the (linear) spring representing the rotational restraint of the foundation was modelled by an extension of the wall below the base having the appropriate flexural stiffness. This is shown in Fig. 63. The stiffness of the element used to simulate foundation restraint corresponding to each degree of base fixity assumed is also shown in the figure for the two sets considered.

Figure 64 shows a comparison of response envelopes for the first set in which the reference structure (T_1 = 1.4 sec., M_y = 500,000 in-k) has a fully fixed base (i.e., F = 1.0), with cases in which the base fixity factor was assigned values of 0.75 and 0.50. Note that the initial fundamental period value of 1.4 sec. applies only to the fully-fixed-base structure. The calculated fundamental period for the structure with F = 0.75 was 1.43 sec. and for the structure with F = 0.50, 1.52 sec.

Increases in the maximum horizontal and interstory displacements, in almost the same proportion as the increase in the fundamental period, accompany the decrease in the base fixity factor, F, from the fully fixed value of 1.0 to 0.75 (20% increase in the maximum top displacement)

and then to 0.50 (80% increase). It is interesting to note that for this group of low-yield-level structures where significant yielding occurs, the relaxation in the base fixity results in increases (though slight) in the maximum moment and shears and in the rotational ductility requirement at the base. In the case of the rotational ductility requirement, there is a 20% increase accompanying a decrease in the base fixity factor from 1.0 (fully fixed) to 0.50.

Figure 64(f) indicates that even though the ductility requirement at the base increases with decreasing base fixity as shown in Fig. 64(e), the cumulative plastic hinge rotation decreases with decreasing base fixity. Since the yield rotation is the same for all three structures in each set and the periods do not differ significantly from each other, this reversal in trend for these two measures of deformation may at first appear contrary to expectation. Figure 65, which shows the variation with time of the plastic hinge rotation at the bases of the walls, provides some explanation for this reversal in trend. The figure shows that although the maximum plastic hinge rotation increases with decreasing base fixity, the number of oscillations and hence the cumulative plastic hinge rotation tends to increase as the base fixity increases (and the period decreases).

To examine the effect of the base fixity condition on structures with high yield levels, a second set of analyses was undertaken for a basic structure with T_1 = 0.8 sec. and M_y = 1,500,000 in-k. Values of the base fixity factor equal to 0.75 (T_1 = 0.83 sec.) and 0.50 (T_1 = 0.88 sec.) were considered in addition to the fully fixed case.

Figure 66 shows envelopes of response quantities for this set. As in Set (a), Figs. 66 (a) and (b) show the expected increase in maximum displacements due to a relaxation of the base fixity. However, for the

structures in this set in which yielding was relatively small (compare Fig. 66(e) with Fig. 64(e)), the maximum moments and shears as well as the rotational ductility and the cumulative plastic hinge rotation at the base tend to decrease with a decrease in the base fixity factor. A 60% decrease in the rotational ductility requirement at the base accompanies a decrease in the base fixity factor from 1.0 to 0.50.

Apart from the increase in the maximum displacement which consistently results from a relaxation of the base fixity, the following points are worth noting from the above comparisons: when the yield level is relatively low so that extensive yielding results, a reduction in the base fixity factor can result in slight increases in the maximum forces and the rotational ductility requirement at the base of a wall; for structures with high yield levels, a relaxation of the base rotational restraint results in reductions in the maximum forces and deformations at the base. The effect of a change in the base fixity condition is more significant in structures with high yield levels where yielding is not extensive than in walls with relatively low yield levels.

Effect of Number of Stories

The effect of the number of stories or the height of the structure on dynamic response was investigated by considering 10-, 30- and 40-story variations of the basic 20-story reference structure. The stiffness of the structure in each case was adjusted to yield the same fundamental period (T_1 = 1.4 sec.) as the basic structure. Two sets of analyses were made, as listed in Table 4. In the first set, a common value of the yield level, M_y, equal to 1,000,000 in-kips, was assumed for all four structures. The purpose here was to isolate the effect of the number of stories on the response. In practice, however, the

strength of walls would normally be expected to increase with the height of the building. In recognition of this, a second set of analyses was made with the value of the yield level in each case adjusted to result in a ductility ratio of about 4 to 6 at the base of the wall.

A 12-mass model was used for both the 10- and 40-story walls, with the masses spaced at every half-story in the lower two stories of the 10-story wall and at every other floor in the lower eight stories of the 40-story structure. For the 30-story structure, a 14-mass model was used, with the lumped masses spaced at every floor in the lower five floors.

Figure 64 shows response envelopes corresponding to the first set, i.e., with a constant yield level, M_y, equal to 1,000,000 in-kips, assumed for all four structures. As indicated in Fig. 67(e), all structures except the 10-story wall yielded at the bases in varying degrees, the extent of yielding increasing with increasing height of structure. In the case of the 40-story structure, yielding extended above mid-height.

Except for the 10-story structure, which responded elastically, the maximum displacements and interstory displacements for the 20-, 30- and 40-story structures were essentially the same at corresponding floors above the base. For the same yield level, the maximum bending moments, shears and ductility requirements (expressed as a ratio of maximum to yield rotations) generally increase with increasing height of structure. The cumulative plastic hinge rotations, however, tend to decrease with increasing height of structure. This behavior follows from the fact that in order to obtain the same fundamental period of 1.4 sec., the 40-story wall had to be relatively much stiffer than say, the 20-story wall. In this case, the sectional stiffness of the 40-story wall had to

be 15.8 times that of the 20-story wall in order to obtain the same period, and for the same yield moment had a correspondingly lesser yield rotation. Thus, for about the same maximum rotation (see Fig. 67 (a)), the ductility ratio for the 40-story structure comes out greater than for the 20-story structure. Figure 68 shows a time history plot of the nodal rotations at a point corresponding to the 2nd floor above the base in each of the four structures considered under Set (a) as listed in Table 4.

Response envelopes for the second set of analyses--with the fundamental period, T_1, still equal to 1.4 sec. but with the yield level, M_y, adjusted so that the resulting ductility ratios at the base for all structures fall in the range of 4 to 6--are shown in Fig. 69. The yield level assumed in each case and the corresponding ductility ratios at the base are listed below, see Fig. 69(e).

No. of Stories	Assumed Yield Level, M_y (in-kips)	Ductility Ratio at Base
10	200,000	5.4
20	750,000	4.9
30	1,500,000	6.0
40	2,500,000	5.9

For the conditions assumed in this set, the maximum displacements at the top of all four structures are about the same, as shown in Fig. 69(a); the slight differences reflect the relative magnitudes of the base ductility ratio. The equal maximum deflection at the top for different heights of structure immediately implies increasing interstory distortions with decreasing height. This is shown in Fig. 69 (b). The increase in the yield level with height of structure leads to a very regular increase in the maximum bending moment and shear with the

number of stories. Figure 67(f), however, indicates that the cumulative plastic hinge rotations at the base tend to increase with decreasing yield level and structure height, the effect of the former apparently predominating.

SUMMARY AND CONCLUSIONS

The preceding essentially qualitative discussion of the effects of various structural and ground motion parameters was meant to establish the relative importance of these parameters with respect to the significant structural response quantities. The major considerations involved in assessing the effects of the various parameters are the magnitude and extent of the deformation requirements as well as the accompanying forces. At the base of the wall, which represents the critical region, the major concerns are the amplitude and number of deformation cycles associated with dynamic response to a specific input motion intensity. Along the height of the structure, the magnitude and distribution of the interstory distortions are of major interest, the interstory distortion* being a good index of the potential damage in buildings. The significant observations made in connection with this study are summarized below.

1. The most important parameters insofar as deformation demands are concerned are the intensity, duration and frequency content characterizing the ground motion, and the fundamental period and yield level of the structure. The other parameters studied had relatively lesser effects on the deformation demand for the range of values considered.

2. Where significant yielding can be expected in a structure, i.e., yielding which would appreciably alter the effective period of vibration, an input motion with a velocity spectrum of the "broad band ascending" type is likely to produce more

*Expressed appropriately as 'interstory tangential deviations' for isolated walls and as 'horizontal interstory displacements' for frame-wall systems.

severe deformation demands than other types of motion of the same intensity and duration. For cases where only nominal yielding is expected, "peaking" type accelerograms tend to produce more severe deformations.

The above considerations are important in determining near-maximum or critical response values for design purposes, or in specifying input motions for use in the analysis of particular types of structures.

3. The shear at the base of an isolated structural wall (which can significantly affect the deformation capacity of the hinging region) is more sensitive to higher mode response and generally undergoes a greater number of reversals than the moments or deformations (horizontal displacements and rotations). Because of this, the maximum base shear can be appreciably lower for input motions which produce extensive yielding and are critical with respect to moments and displacement than for motions which produce lesser displacements. The criticality of response with respect to shear will depend on the relationship of the frequency characteristics of the input motion to the significant higher effective mode frequencies of the yielded structure.

4. The major effect of the duration of ground motion is to increase the cumulative plastic rotations in hinging regions. (The cumulative plastic rotation is another useful index of the severity of the deformation demand in critical regions of a structure and reflects both the magnitude and the number of cycles of loading associated with dynamic response.)

5. The deformation requirements increase almost proportionally with an increase in the intensity of the ground motion.

The determination of the appropriate intensity to use in a particular case will depend on such factors as earthquake magnitude, epicentral distance and site geology, all of which are beyond the scope of this report. As a matter of fact, the selection of the proper intensity, duration, and to some extent, the frequency characteristics of the input motion for use in the analysis of a particular case will be determined to a large degree by factors not considered in this report. The observations based on this study, however, can help guide the selection of the input motion parameters in the sense of providing information concerning the influence that a particular parameter can have on the structural response.

6. The ductility requirement, expressed as a ratio of the maximum rotation to the rotation at first yield, generally increases with decreasing fundamental period (or increasing stiffness) of a structure. In structures with relatively low yield levels where significant yielding occurs, however, the cumulative plastic rotation in hinging regions tends to decrease with decreasing period. This trend is mainly a reflection of the lesser absolute magnitude of the rotations for the stiffer structures. When the yield level is high enough (relative to the intensity of the ground motion) so that only insignificant yielding results, the above trend is reversed, i.e., the cumulative plastic hinge rotation tends to decrease with increasing period.

A direct result of increasing the stiffness of a structure and thus decreasing its fundamental period (assuming essentially the same mass) is the reduction in the maximum horizontal displacements and the interstory distortions along the height of the structure.

7. The magnitude of the deformation requirements in hinging regions--in terms of ductility ratios and cumulative plastic hinge rotations--generally decreases with increasing values of the yield level. The maximum horizontal displacements and interstory distortions also tend to diminish with increasing yield levels, as long as significant yielding occurs. Within a narrow range, where only nominal yielding occurs, the maximum displacements--particularly in the upper stories of a structure--tend to increase with increasing yield level, until a value is reached when no yielding occurs, i.e., linear elastic response.

Altnough the yield level in a structure usually does not vary independently of the fundamental period (an increase in stiffness is generally accompanied by an increase in the yield level), the effect of this major variable is worth noting, because of its interaction with the initial fundamental period and also because it affects the dominant or effective period of a yielding structure. The latter has important bearing on the type of ground motion that is likely to produce near-maximum or critical response.

The work represented by the preceding discussion, undertaken in pursuance of the first objective stated at the beginning of this discussion, constitutes a major segment of Part I of the Analytical Investigation. A total of some 60 analyses are included in this study, covering variations in eleven parameters.

By making possible an assessment of the relative importance of the different parameters affecting structural response, these parametric studies allow the subsequent effort directed towards the second objective, i.e., the determination of estimates of critical force and deformation requirements in hinging regions of structural walls, to concentrate on a manageable few of the more significant parameters as bases for the design procedure to be developed.

REFERENCES

1. Uniform Building Code, 1973 Edition, International Conference of Building Officials, 5360 South Workman Mill Road, Whittier, California, 90601.

2. Kanaan, A.E. and Powell, G.H., "General Purpose Computer Program for Inelastic Dynamic Response of Plane Structure," (DRAIN-2D), Report No. EERC 74-6, Earthquake Engineering Research Center, University of California, Berkeley, April 1973.

3. Takeda, T., Sozen, M.A. and Nielsen, N.N., "Reinforced Concrete Response to Simulated Earthquake," Journal of the Structural Division, ASCE, Proceedings Vol. 96, No. ST12, December 1970.

4. Czernecki, R.M., "Earthquake Damage to Tall Buildings," Structures Publication No. 359, Department of Civil Engineering, Massachusetts Institute of Technology, January 1973.

5. Ghosh, S.K. and Derecho, A.T., "Supplementary Output Package for DRAIN-2D, General Purpose Computer Program for Dynamic Analysis of Plane Inelastic Structures," Supplement No. 1 to a Progress Report on the PCA Investigation: Structural Walls in Earthquake Resistant Structures, NSF Grant No. GI-43880, Portland Cement Association, Skokie, IL 60076, August 1975.

6. Ruiz, P. and Penzien, J., "Probabilistic Study of the Behavior of Structures During Earthquakes," Earthquake Engineering Research Center Report No. EERC 69-3, University of California, Berkeley, March 1969.

7. Blume, J.A., Newmark, N.M. and Corning, L.H., Design of Multistory Reinforced Concrete Buildings for Earthquake Motions, Portland Cement Association, Skokie, IL, 1961.

PART B - PARAMETRIC STUDIES
TABLES AND FIGURES

Table 1(a) - BASIC STRUCTURE PROPERTIES AND VARIATIONS
Structure ISW 0.8

PROPERTIES	BASIC VALUE OR CHARACTERISTIC	VARIATIONS
STRUCTURAL		
Fundamental pericd	0.8 seconds	
Number of stories	20	
Height	178.25 ft.	
Weight (for mass computation)	4370 k/wall	
Stiffness parameter EI	6.346×10^{11} k-in^2	
Yield level, M_y	1,000,000 in-k	500,000 750,000 1,000,000 1,500,000 in-k
Yield stiffness ratio, r_y	0.05	0.15
Character of M-θ curve	Decreasing stiffness $\alpha = .10$, $\beta = 0$	
Damping	5% of critical	10% of critical
Stiffness taper $\frac{(EI)\ base}{(EI)\ top}$	1.0	
Strength taper $\frac{(M_y)\ base}{(M_y)\ top}$	2.0	
Basic fixity condition	Fully fixed	
INPUT MOTION		
Intensity	SI = 1.5 ($SI_{ref.}$)*	1.0 ($SI_{ref.}$)
Frequency characteristics	1940 El Centro, E-W	1940 El Centro, N-S 1952 Taft, S69E Artificial Acc. S1
Duration	10 seconds	

* $SI_{ref.}$ = 5%-damped spectrum intensity - between 0.1 and 3.0 seconds - corresponding to the first 10 seconds of the N-S component of the 1940 El Centro record.

Table 1(b) - BASIC STRUCTURE PROPERTIES AND VARIATIONS

Structure TSW 1.4

PROPERTIES	BASIC VALUE OR CHARACTERISTIC	VARIATIONS
STRUCTURAL		
Fundamental period	1.4 seconds	
Number of stories	20	10.40
Height	178.25 ft.	
Weight (for mass computation)	4370 k/wall	
Stiffness parameter EI	2.052×10^{11} k-in^{2}*	
Yield level, M_y	500,000 in-k	750,000 1,000,000 1,500,000 in-k, and elastic
Yield stiffness ratio, r_y	0.05	0.01, 0.15
Character of M-θ curve	Decreasing stiffness α = .10, β = 0	α = .30, β = 0.4, 1.0 and sable loop
Damping	5% of critical	10% of critical
Stiffness taper $\frac{(EI)\ \text{base}}{(EI)\ \text{top}}$	1.0	2.8
Strength taper $\frac{(M_y)\ \text{base}}{(M_y)\ \text{top}}$	2.0	1.0, 3.8
Basic fixity condition	Fully fixed	50% and 75% of fully fixed condition**
INPUT MOTION		
Intensity	SI = 1.5 ($SI_{ref.}$)	0.75 and 1.0 x ($SI_{ref.}$)
Frequency characteristics	1940 El Centro, E-W	1971 Holiday Orion, E-W 1971 Pacoima Dam, S16E, Artificial Acc. S1
Duration	10 seconds	20 seconds

* EI = 5.004×10^{11} k-in for stiffness taper 2.8

** Period of 1.4 sec. corresponds to fully fixed condition.

Table 1(c) - BASIC STRUCTURE PROPERTIES AND VARIATIONS
Structure ISW 2.0

PROPERTIES	BASIC VALUE OR CHARACTERISTIC	VARIATIONS
STRUCTURAL		
Fundamental period	2.0 seconds	
Number of stories	20	
Height	178.25 ft.	
Weight (for mass computation	4370 k/wall	
Stiffness parameter EI	0.990×10^{11} k-in^2	
Yield level, M_y	500,000 in-k	750,000 1,000,000 in-k and elastic
Yield stiffness ratio, r_y	0.05	0.15
Character of M-θ curve	Decreasing stiffness $\alpha = .10$, $\beta = 0$	
Stiffness taper $\frac{(EI)\ \text{base}}{(EI)\ \text{top}}$	1.0	
Strength taper $\frac{(M_y)\ \text{base}}{(M_y)\ \text{top}}$	2.0	
Basic fixity condition	Fully fixed	
INPUT MOTION		
Intensity	SI = 1.5 ($SI_{ref.}$)	1.0 x ($SI_{ref.}$)
Frequency characteristics	1940 El Centro, E-W	1971 Holiday Orion, E-W
Duration	10 seconds	

Table 1(d) - BASIC STRUCTURE PROPERTIES AND VARIATIONS
Structure ISW 2.4

PROPERTIES	BASIC VALUE OR CHARACTERISTIC	VARIATIONS
STRUCTURAL		
Fundamental period	2.4 seconds	
Number of stories	20	
Height	178.25 ft.	
Weight (for mass computation)	4370 k/wall	
Stiffness parameter EI	0.684×10^{11} k-in^2	
Yield level, M_y	500,000 in-k	750,000 1,000,000 1,500,000 in-k
Yield stiffness ratio, r_y	0.05	
Character of M-θ curve	Decreasing stiffness $\alpha = .10$, $\beta = 0$	
Damping	5% of critical	10% of critical
Stiffness taper $\frac{(EI)\ \text{base}}{(EI)\ \text{top}}$	1.0	
Strength taper $\frac{(M_y)\ \text{base}}{(M_y)\ \text{top}}$	2.0	
Basic fixity condition	Fully fixed	
INPUT MOTION		
Intensity	$SI = 1.5\ (SI_{ref.})$	
Frequency characteristics	1940 El Centro, E-W	
Duration	10 seconds	

Table 2 - Summary of Input Motions Considered in Study of Frequency Characteristics

Set	Structure Period, T_1 (and M_y)	Input Motion	Frequency Content Characterization#	Intensity Normalization Factor*
a	1.4 sec. (500,000 in-k)	1971 Pacoima Dam, S16E component	Peaking (0)	0.59
		1971 Holiday Inn Orion, E-W component	Peaking (+)	3.22
		Artificial Accelerogram, S1	Broad band	1.65
		1940 El Centro, E-W component	Broad band, ascending	1.88
b	0.8 sec. (1,500,000 in-k)	1940 El Centro, N-S component	Peaking (0)	1.50
		1940 El Centro, E-W component	Broad band, ascending	1.88
c	2.0 sec. (500,000 in-k)	1971 Holiday Inn, Orion, E-W component	Peaking (-)	3.22
		1940 El Centro, E-W component	Broad band, ascending	1.88
		Artificial Accelerogram, S1	Broad band	1.65

* Calculated to yield a 5%-damped spectrum intensity (for the range 0.1 to 3.0 sec.) equal to 1.5 times the reference spectrum intensity, $SI_{ref.}$, i.e., the 5%-damped spectrum intensity of the N-S component of the 1940 El Centro record.($SI_{ref.}$ = 70.15 in.) In all cases, only a 10-second duration of each accelerogram was considered.

\# Relative to the initial fundamental period, T_1, of the structure considered.

Table 3 - Structure Properties and Earthquake Intensity Levels Considered

Set	Fundamental Period, T_1	Yield Level, M_y	Levels of Intensity Used*
a	1.4 sec.	500,000 in-k	0.75, 1.0, 1.5
b	0.8 sec.	1,000,000 in-k	1.0, 1.5
c	2.0 sec.	500,000 in-k	1.0, 1.5

*In terms of $SI_{ref.}$

Table 4 - SUMMARY OF STRUCTURAL PARAMETERS

PARAMETER	VALUES OF PARAMETER CONSIDERED	REMARKS
Fundamental period, T_1 (sec.)	(a) 0.8, 1.4, 2.0, 2.4	M_y = 500,000 in-k
	(b) 0.8, 1.4, 2.0, 2.4	M_y = 750,000 in-k
	(c) 0.8, 1.4, 2.0	M_y = 1,000,000 in-k
	(d) 0.8, 1.4, 2.4	M_y = 1,500,000 in-k (r_y = 0.05)
Yield level, M_y (in-k)	(a) 500,000, 1,000,000, 1,500,000	T_1 = 0.8 sec.
	(b) 500,000, 750,000, 1,000,000 1,500,000 (Elastic)	T_1 = 1.4 sec.
	(c) 500,000, 750,000, 1,000,000	T_1 = 2.0 sec.
Yield Stiffness ratio, r_y	(a) 0.05, 0.15	T_1 = 0.8 sec.; M_y = 1,000,000 in-k
	(b) 0.01, 0.05, 0.15	T_1 = 1.4 sec.; M_y = 500,000 in-k
	(c) 0.05, 0.15	T_1 = 2.0 sec.; M_y = 500,000 in-k

Table 4 (contd.) - SUMMARY OF STRUCTURAL PARAMETERS

PARAMETER	VALUES OF PARAMETER CONSIDERED	REMARKS
Parameters characterizing shape of M-θ hysteretic loop: Takeda model parameters α and β	(a) α = 0.10, 0.30	T_1 = 1.4 sec. M_y = 500,000 in-k β = 0
	(b) β = 0, 0.4, 1.0 & stable loop	T_1 = 1.4 sec. M_y = 500,000 in-k α = 0.10
	(c) β = 0, 0.4, 1.0 & stable loop	T_1 = 0.8 sec. M_y = 1,000,000 in-k α = 0.10
Viscous damping (percent of critical)	(a) 5, 10	T_1 = 1.4 sec. M_y = 500,000 in-k
	(b) 5, 10	T_1 = 0.8 sec. M_y = 1,000,000 in-k
Stiffness taper $\frac{EI\ (base)}{EI\ (top)}$	(a) 1.0, 2.8	T_1 = 1.4 sec. M_y = 500,000 in-k
Strength taper $\frac{M_y\ (base)}{M_y\ (top)}$	(a) 1.0, 2.0, 3.8	T_1 = 1.4 sec. M_y (base) = 500,000 in-k

Table 4 (contd.) SUMMARY OF STRUCTURAL PARAMETERS

PARAMETER	VALUES OF PARAMETER CONSIDERED	REMARKS
Base Fixity condition (percent of full fixity)	(a) 50, 75, 100	T_1 = 1.4 sec.* M_y = 500,000 in-k
	(b) 50, 75, 100	T_1 = 0.8 sec.* M_y = 1,500,000 in-k
Number of stories	(a) 10, 20, 30, 40	T_1 = 1.4 sec. M_y = 1,500,000 in-k
	(b) 10, 20, 30, 40	T_1 = 1.4 sec. M_y adjusted to yield ductility ratios $\sim$ 4 - 6

*Refers to the fully-fixed condition.

Table 5 - EFFECT OF FUNDAMENTAL PERIOD AND YIELD LEVEL ON DYNAMIC RESPONSE OF 20-STORY ISOLATED STRUCTURAL WALLS

Earthquake Input: 1940 El Centro, E-W Component (10 sec., SI = 1.5 $SI_{ref.}$)

Yield Level, M_y (in-kips)	Initial Fundamental Period, T_1 (sec.) 0.80	1.40	2.00	2.40
Max. Top Displacement (in.)				
500,000	8.33	14.97	20.50	25.12
750,000	4.74	10.87	17.00	23.72
1,000,000	4.04	9.19	19.98	22.43
1,500,000	4.50	10.99	23.06	24.49 (E)*
Elastic	5.17	11.01	23.16	24.49
Max. Interstory Displacement (in.)				
500,000	0.47	0.86	1.24	1.56
750,000	0.28	0.65	1.12	1.51
1,000,000	0.24	0.58	1.25	1.51
1,500,000	0.29	0.75	1.57	1.76 (E)
Elastic	0.35	0.76	1.57	1.76
Max. Horizontal Shear at Base (kips)				
500,000	1030	830	1050	1060
750,000	1190	950	1070	1179
1,000,000	1330	1190	1120	1240
1,500,000	1610	1300	1150	1300 (E)
Elastic	1700	1420	1240	1300

*Elastic, i.e., structure did not yield.

Table 5 (contd.) - EFFECT OF FUNDAMENTAL PERIOD AND YIELD LEVEL ON DYNAMIC RESPONSE OF 20-STORY ISOLATED STRUCTURAL WALLS

Earthquake Input: 1940 El Centro, E-W Component (10 sec., SI = 1.5 $SI_{ref.}$)

Yield Level, M_y (in-k)	Initial Fundamental Period, T_1 (sec.)			
	0.80	1.40	2.00	2.40
Moment at Base (in-k)				
500,000	813,000	711,000	651,000	648,000
750,000	996,000	941,000	862,000	903,000
1,000,000	1,214,000	1,149,000	1,126,000	1,107,000
1,500,000	1,701,000	1,583,000	1,609,000	1,519,000 (E)
Elastic	2,419,000	1,677,000	1,782,000	1,519,000
Rotational Ductility Ratio				
500,000	13.6	8.1	6.2	5.7
750,000	6.3	4.9	2.9	3.92
1,000,000	4.1	2.9	2.5	2.1
1,500,000	2.6	1.1	1.4	1.0
Cum. Plastic Hinge Rotation at Base (radians)				
500,000	1.06×10^{-2}	1.50×10^{-2}	1.76×10^{-2}	2.31×10^{-2}
750,000	$.92 \times 10^{-2}$	1.01×10^{-2}	1.13×10^{-2}	1.69×10^{-2}
1,000,000	0.73×10^{-2}	0.89×10^{-2}	$.66 \times 10^{-2}$	1.02×10^{-2}
1,500,000	$.50 \times 10^{-2}$	0.04×10^{-2}	$.09 \times 10^{-2}$	0.

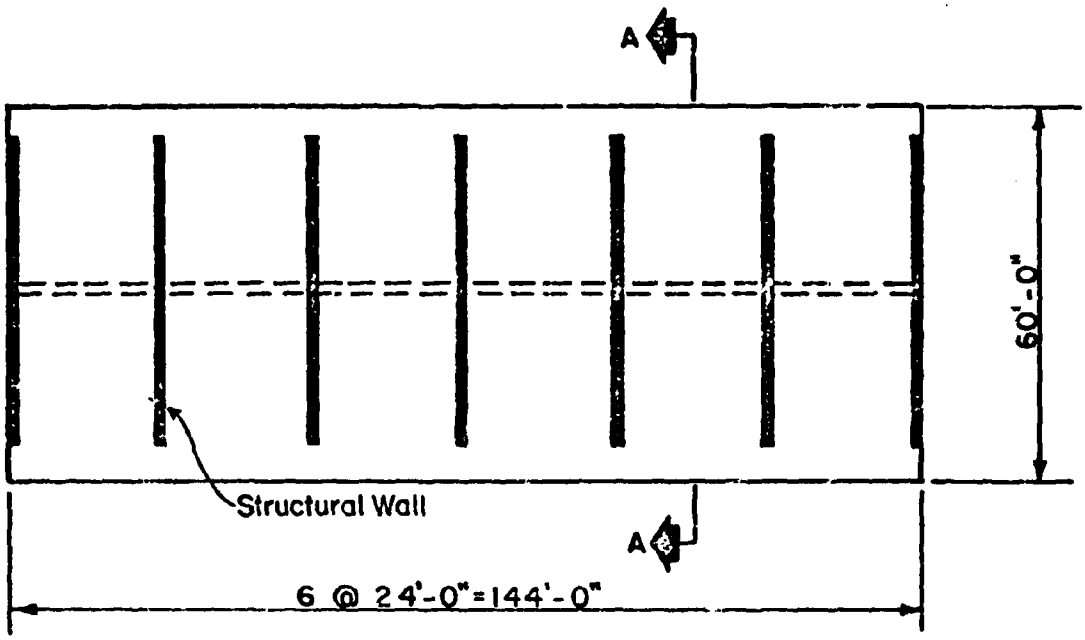

PLAN

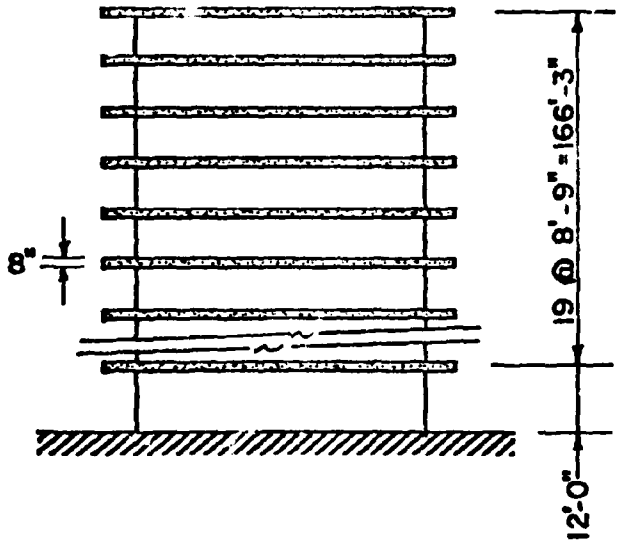

SECTION A-A

Fig. 1 Twenty Story Building with Isolated Structural Walls

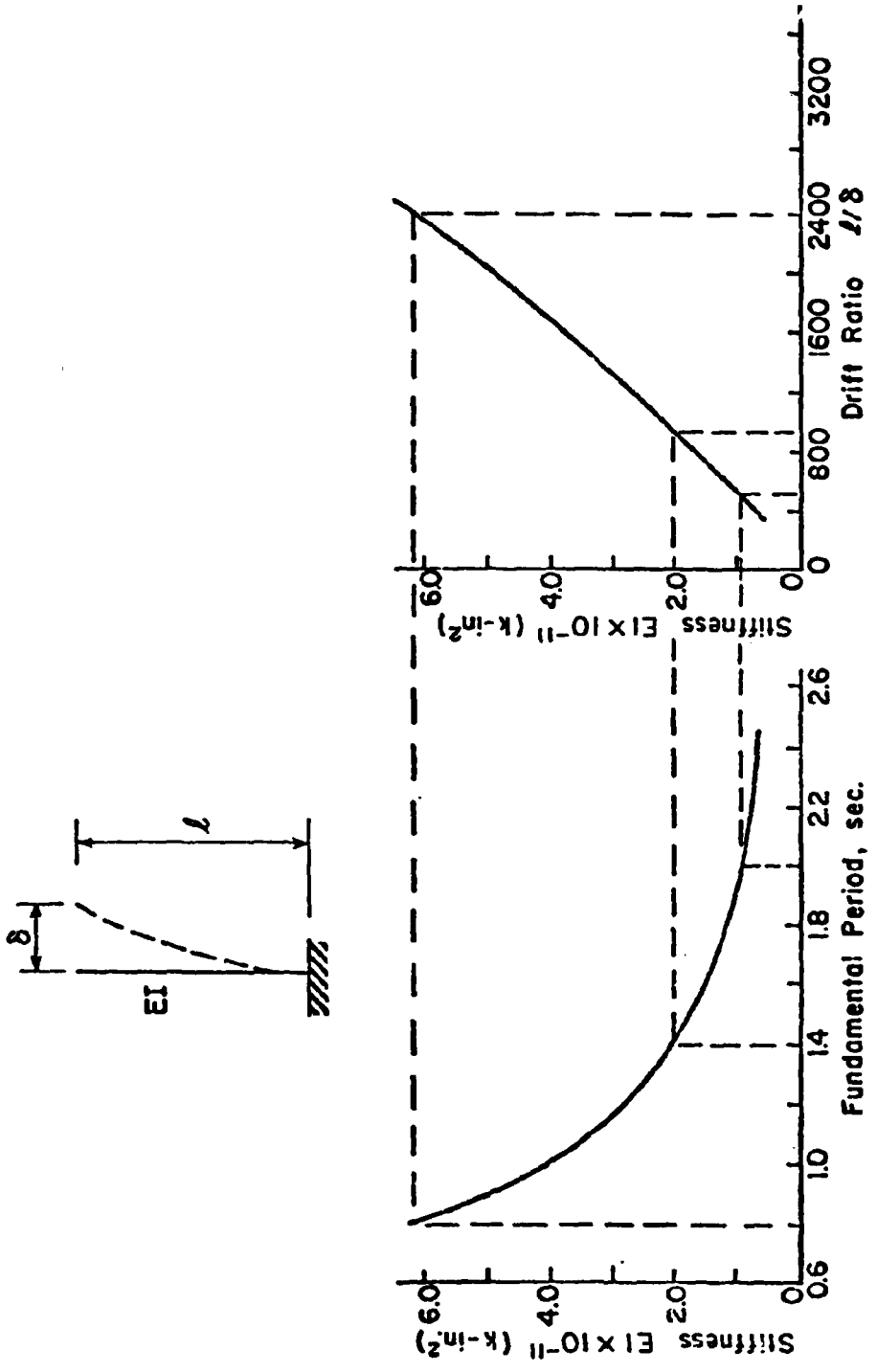

Fig. 2 Fundamental Period - Stiffness - Drift Relationship

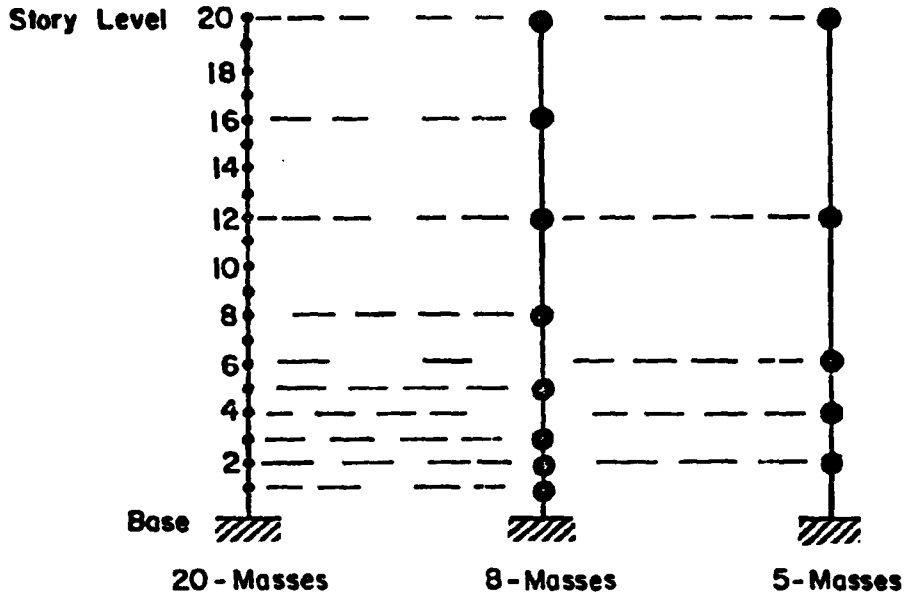

Fig. 3 Preliminary Models for 20 Story Building

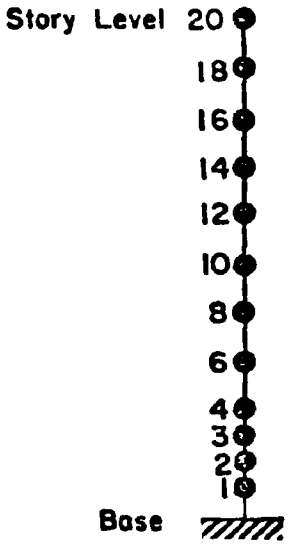

Fig. 4 Final Model - 12 Masses

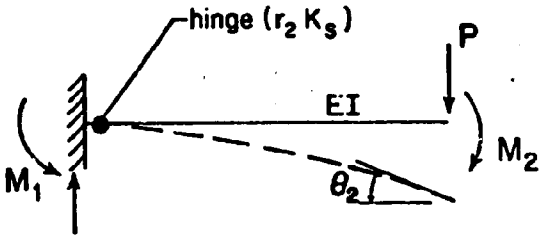

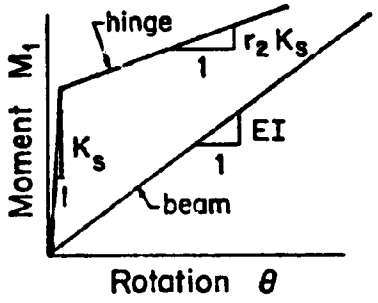

(a) Model in computer program

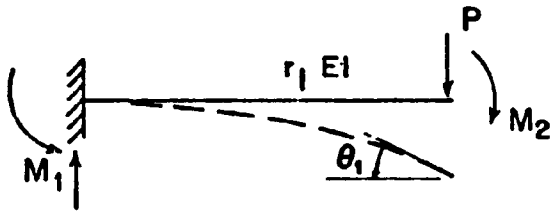

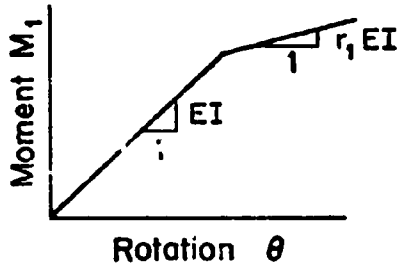

(b) Bilinear element

Fig. 5 Computer Model of Bilinear Element (After Yield)

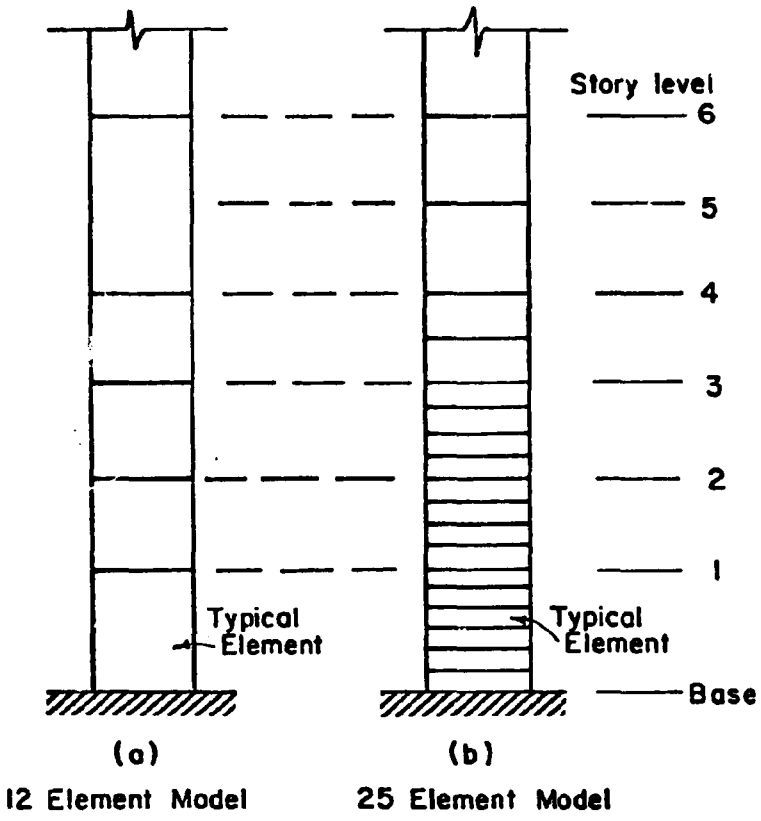

Fig. 6 Models for Lower Portion of Structural Wall

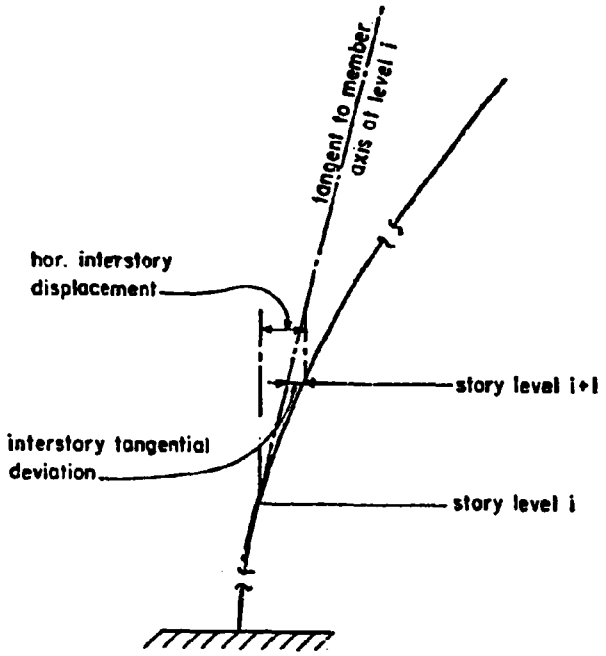

Fig. 7 Illustrating Tangential Deviation

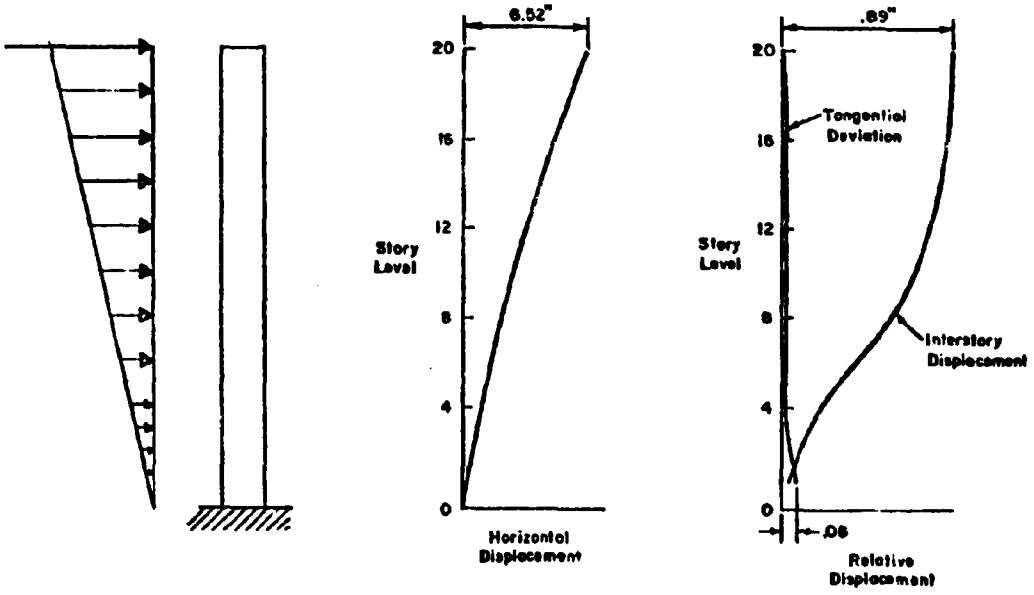

Fig. 8 Tangential Deviations versus Interstory Displacement

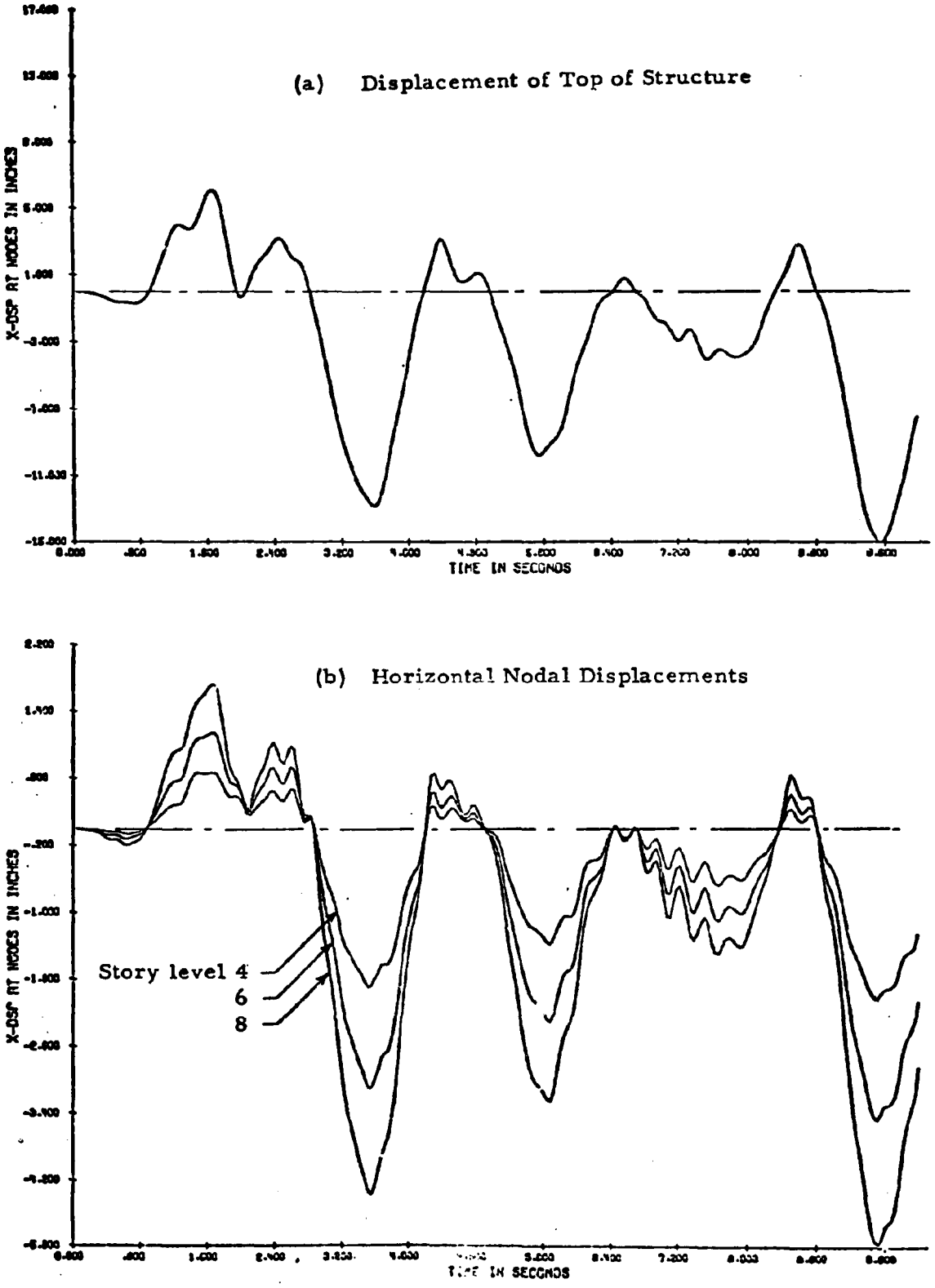

Fig. 9 Time Histories of Horizontal Displacements - Bldg. ISW1.4

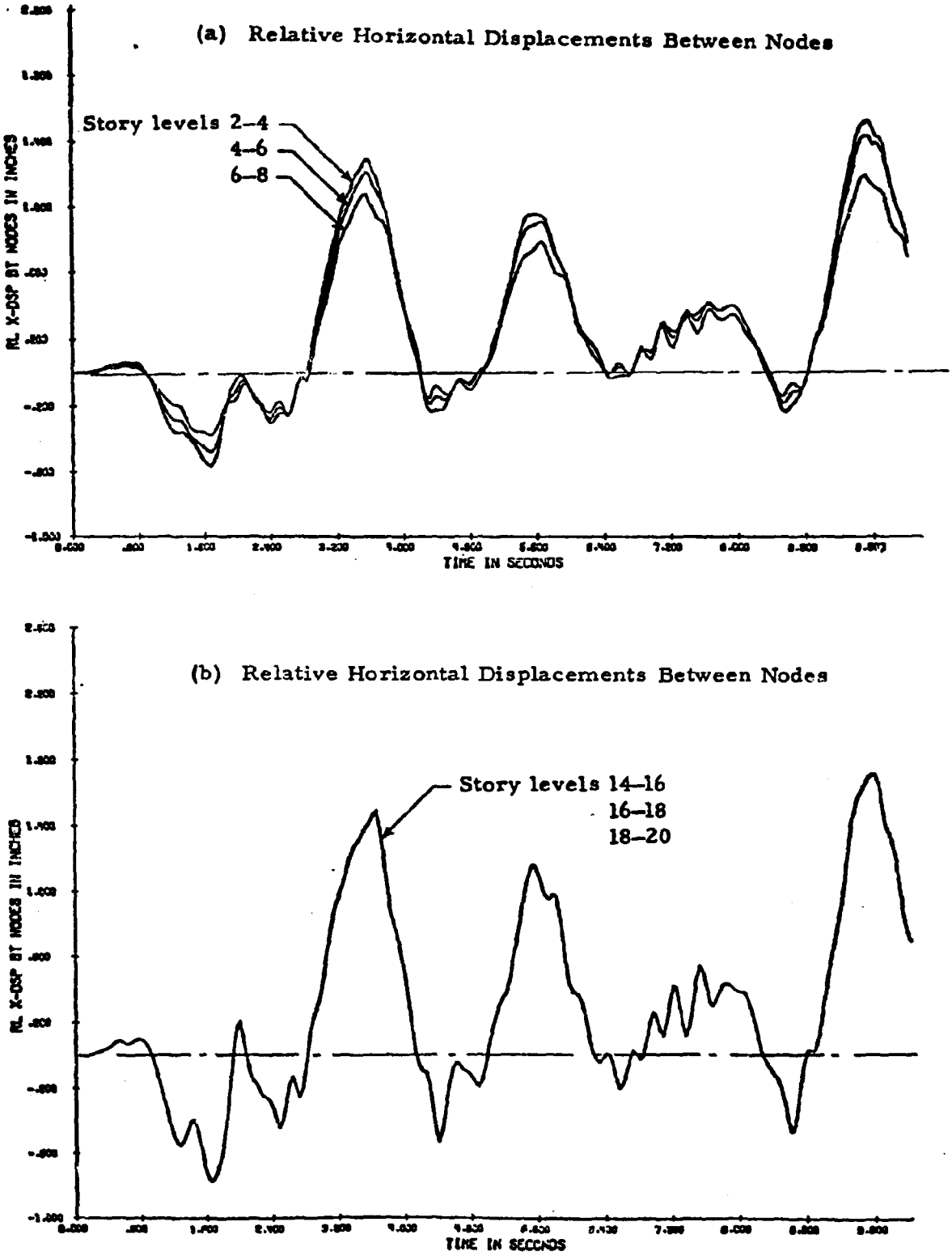

Fig. 10 Time Histories of Relative Horizontal Displacements - Bldg. ISW1.4

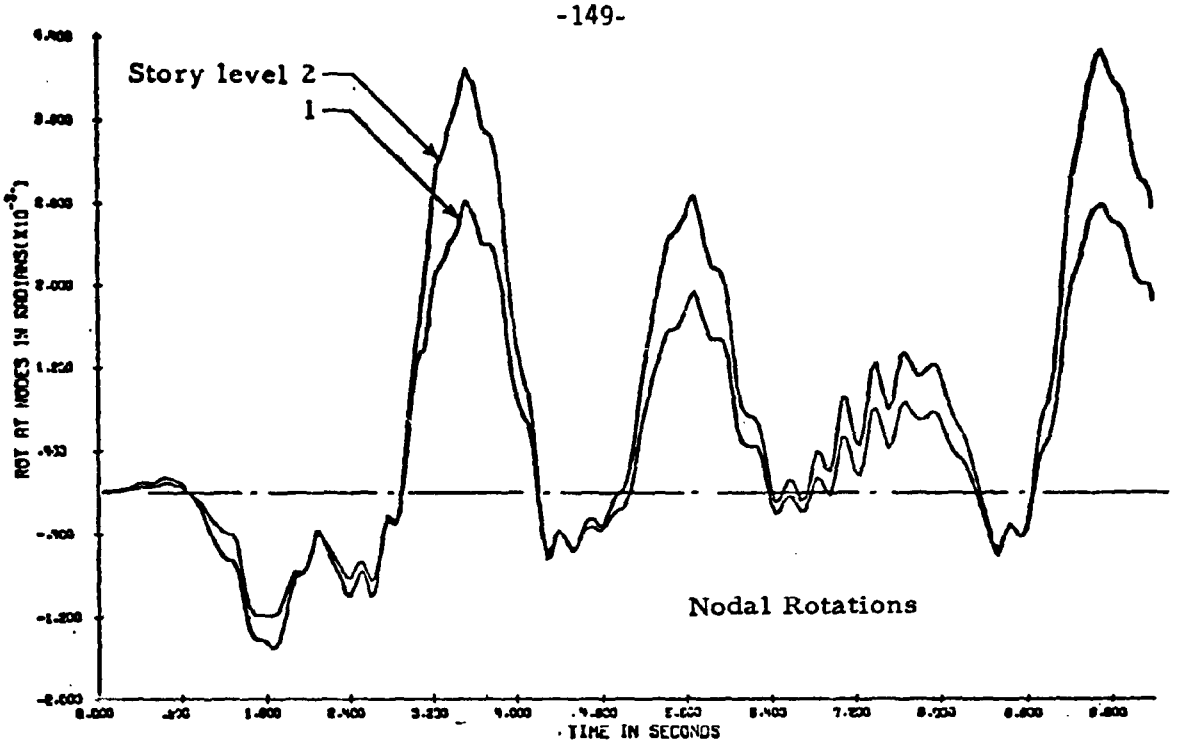

Fig. 11 Time Histories of Nodal Rotations - Bldg. ISW1.4

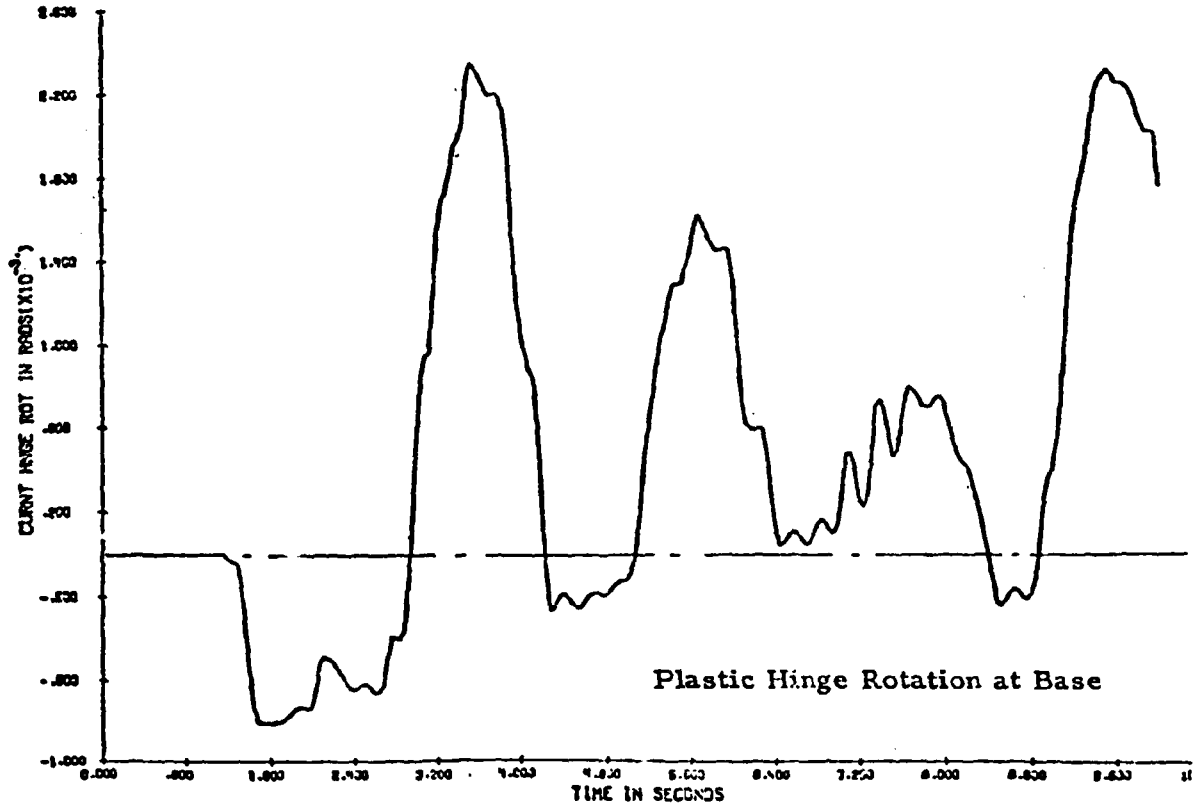

Fig. 12 Time History of Plastic Hinge Rotation at Base - Bldg. ISW1.4

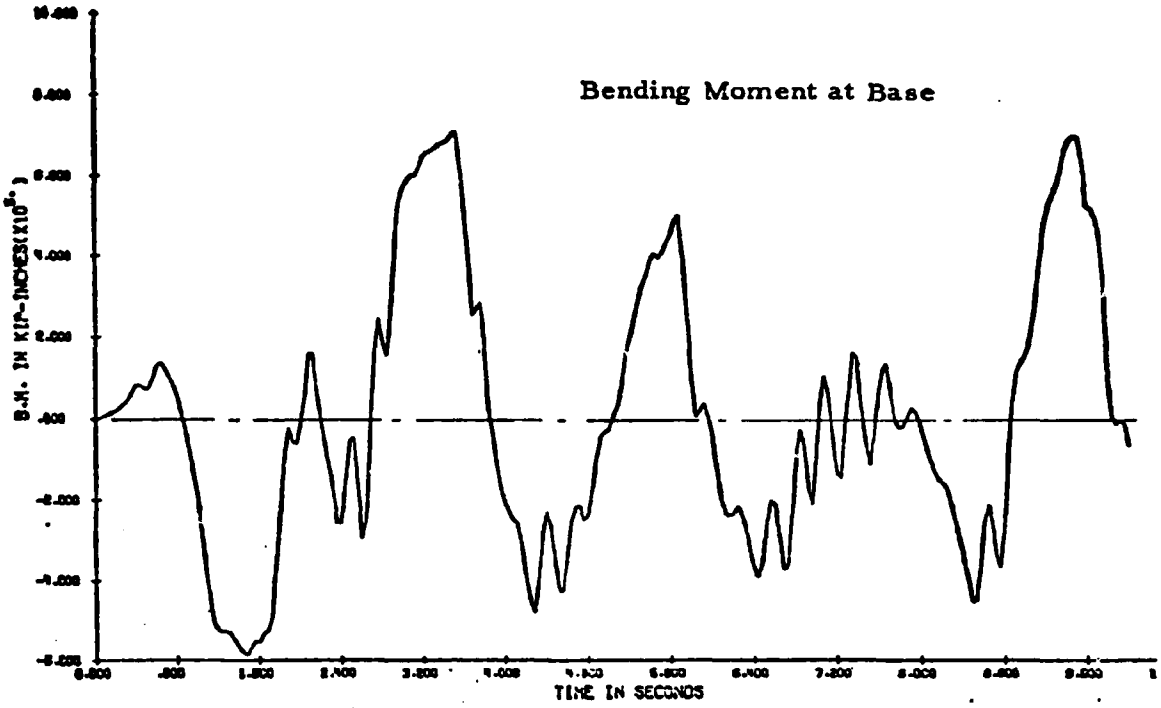

Fig. 13 Time History of Bending Moment at Base - Bldg. ISW1.4

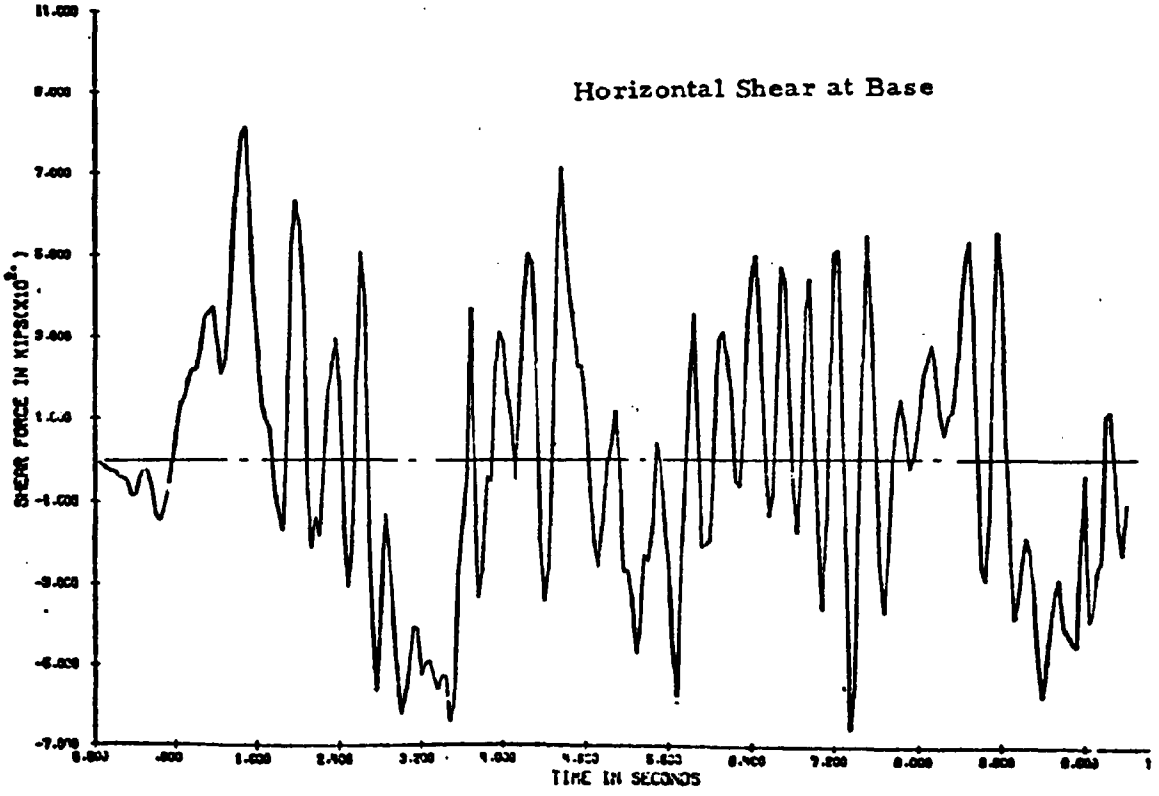

Fig. 14 Time History of Horizontal Shear at Base - Bldg. ISW1.4

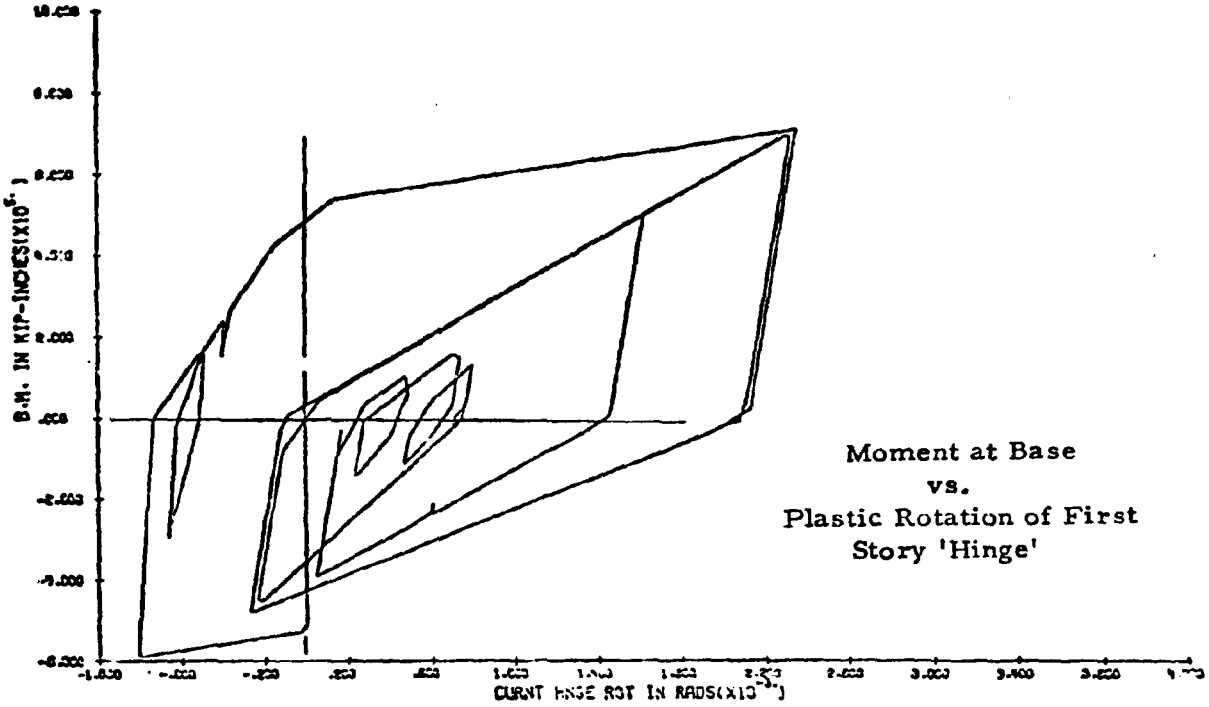

Fig. 15 Moment - Plastic Hinge Rotation Relationship - Bldg. ISW1.4

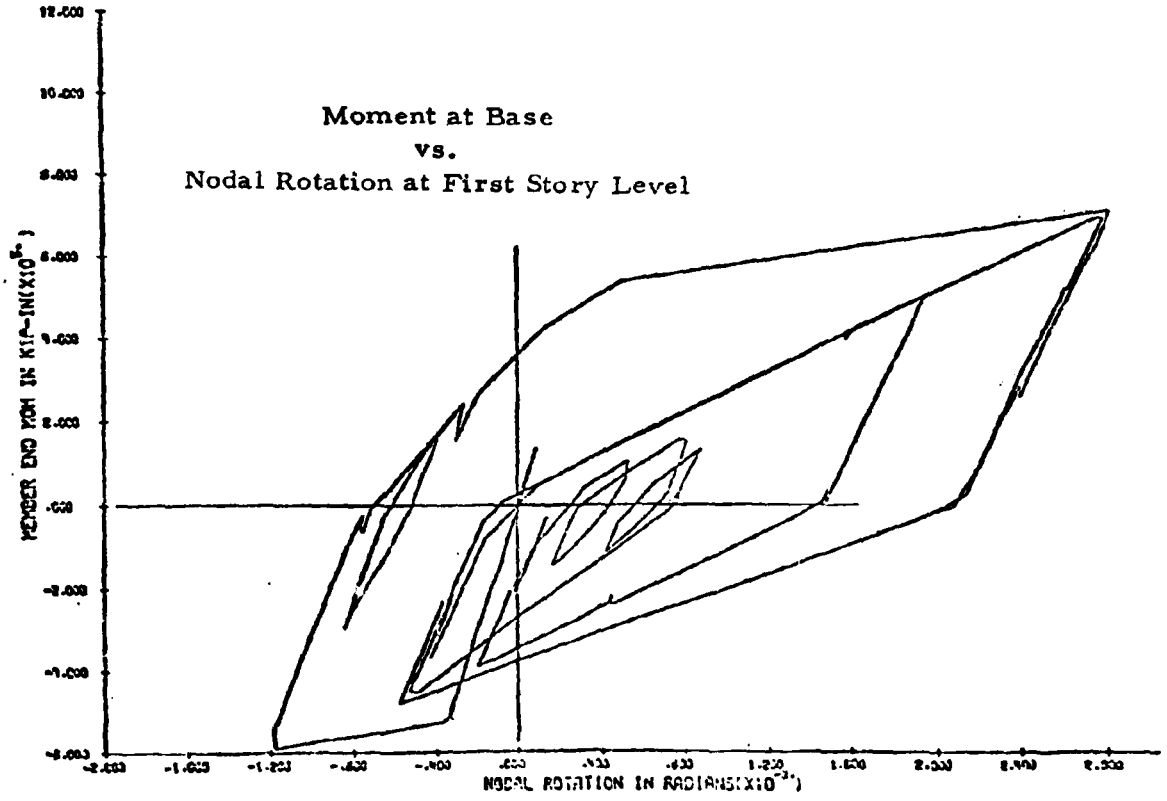

Fig. 16 Moment - Nodal Rotation Relationship - Bldg. ISW1.4

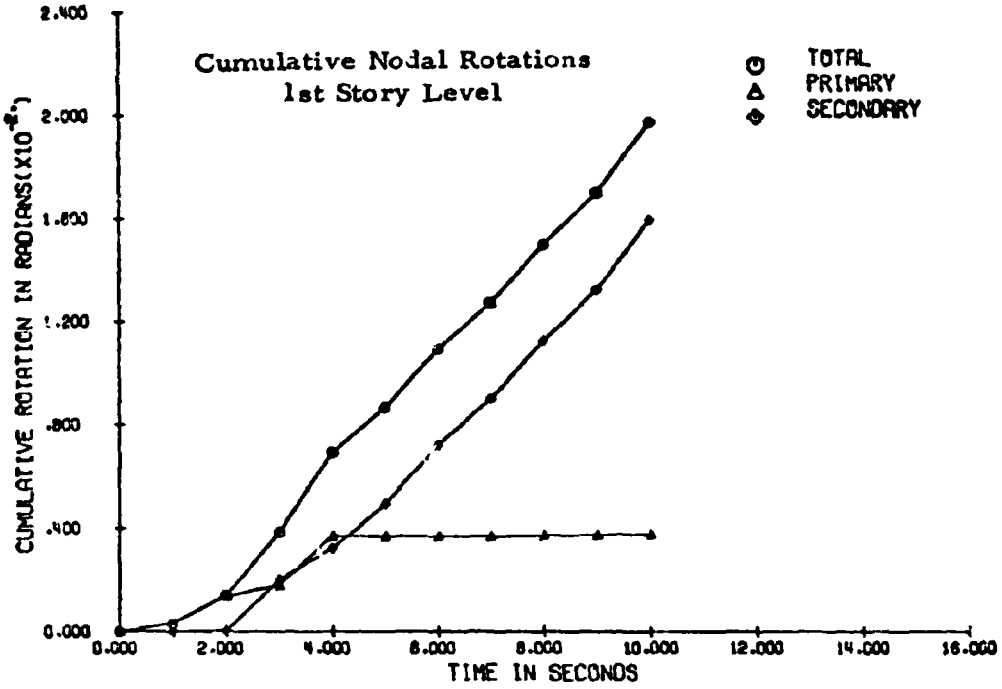

Fig. 17 Cumulative Nodal Rotations vs. Time for Node at First Story Level - Bldg. ISW1.4

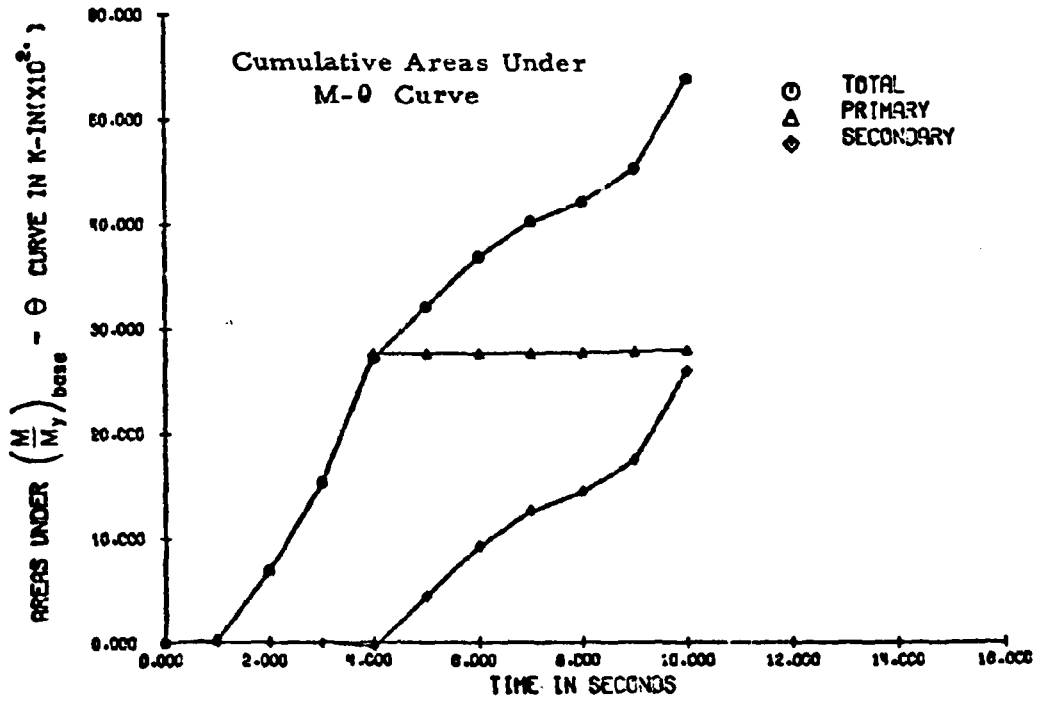

Fig. 18 Cumulative Areas Under $\left(\frac{M}{M_y}\right)_{base}$ - Θ Hysteresis Loop vs. Time for Node at First Story Level - Bldg. ISW1.4

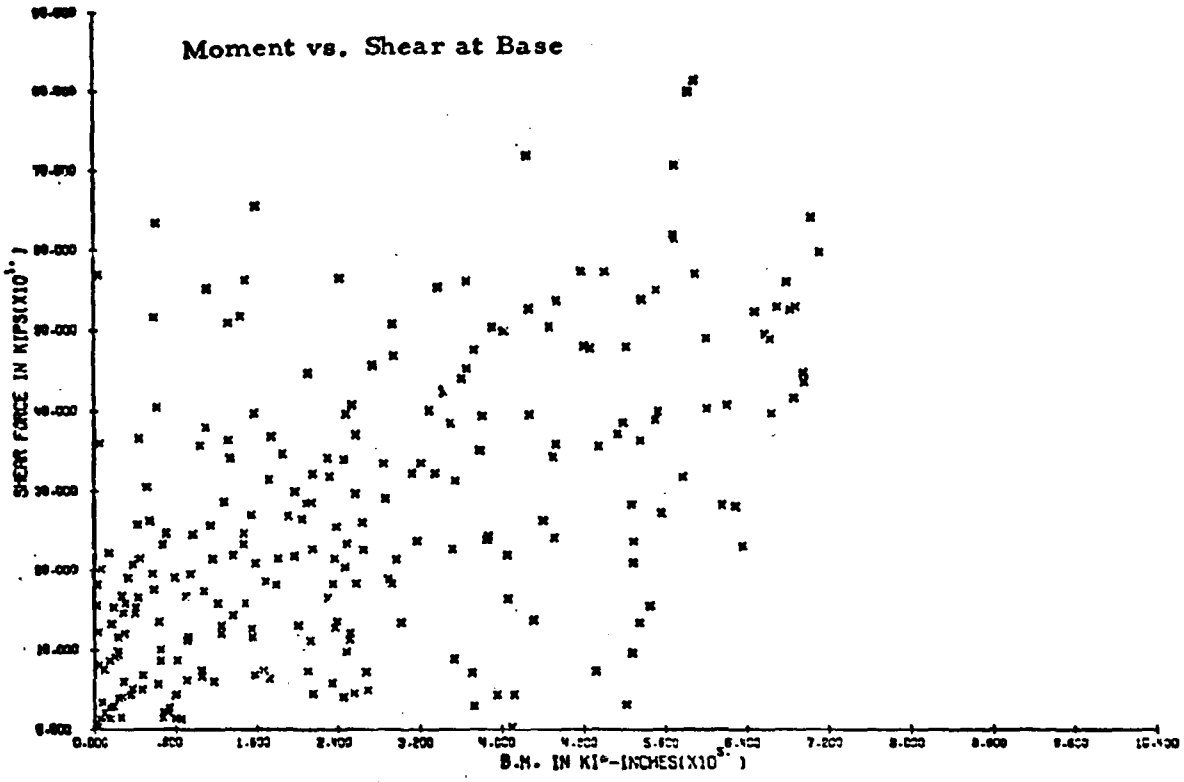

Fig. 19 Simultaneous Moment and Shear Values at Base at Each Time Interval During Response - Bldg. ISW1.4

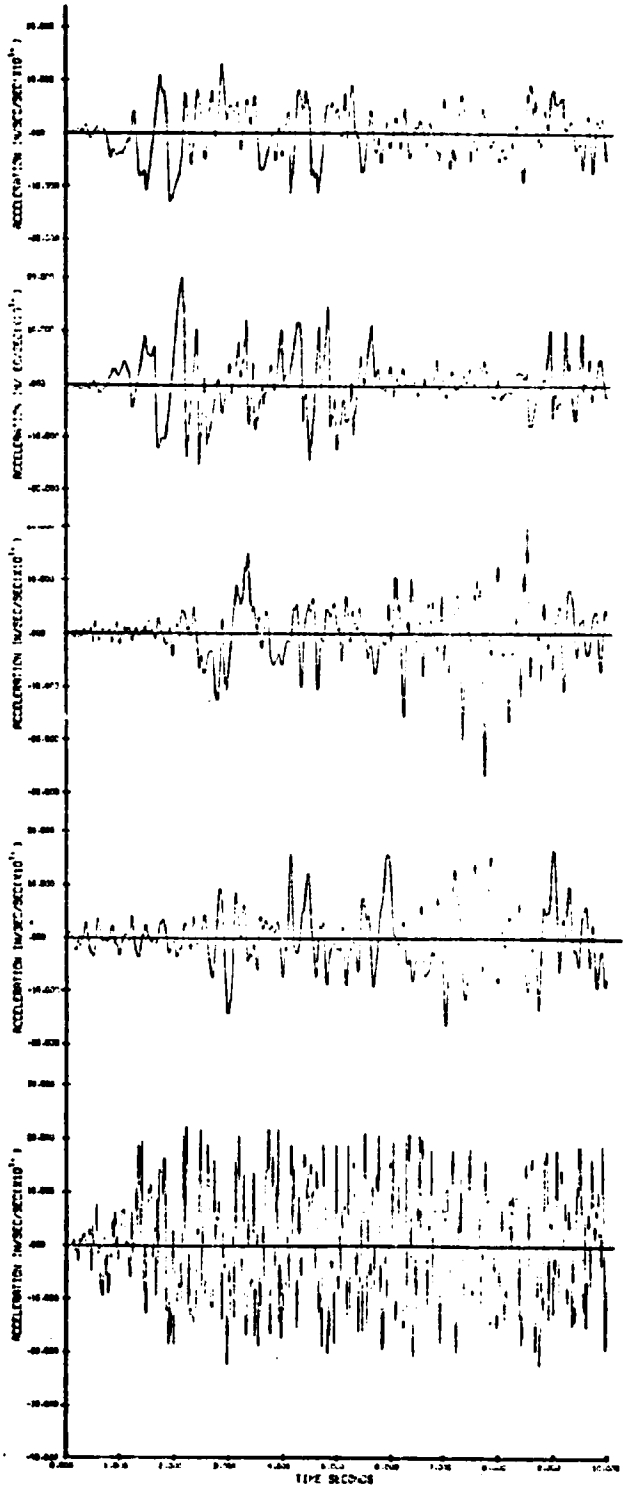

1940 El Centro, E-W
x 1.88

1940 El Centro, N-S
x 1.50

1971 Pacoima Dam, S16E
x 0.594

1971 Holiday Orion, E-W
x 3.22

Artificial Accelerogram, SI
x 1.66

Fig. 20 Ten-Second Duration Normalized Accelerograms

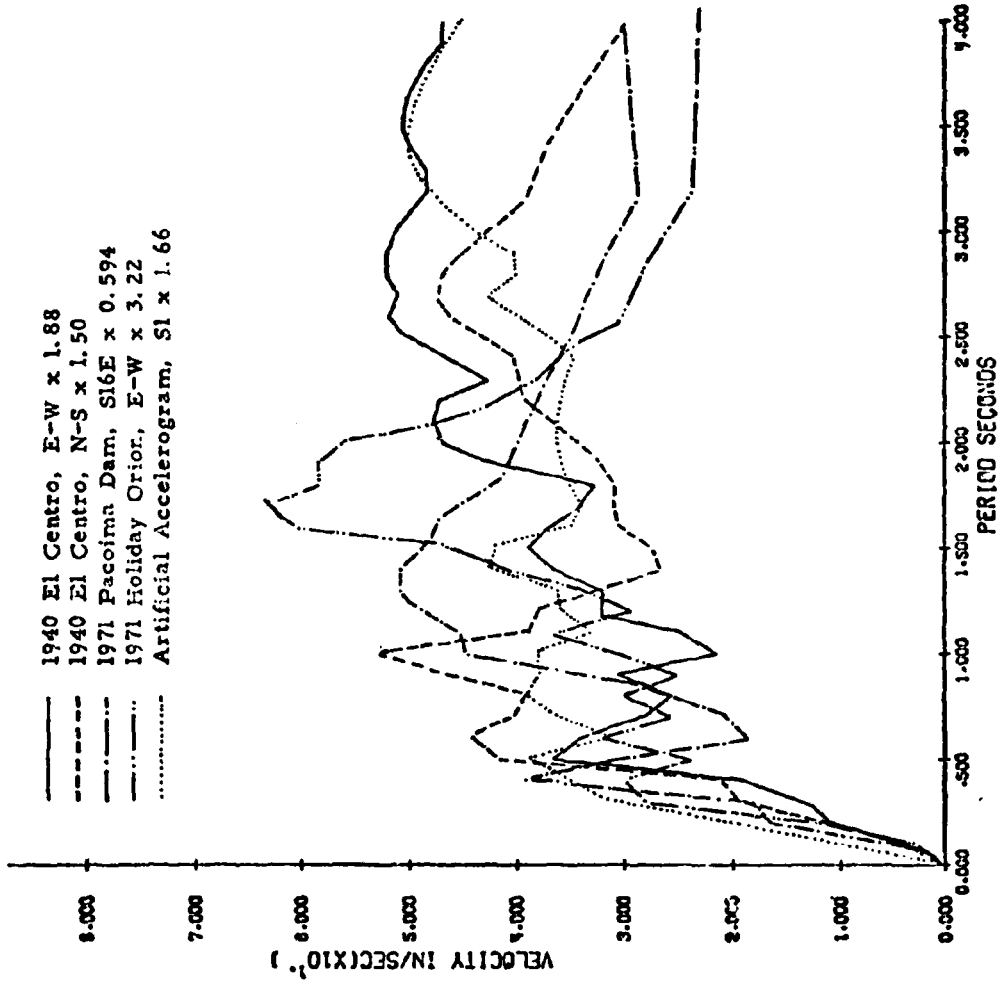

Fig. 21 Relative Velocity Response Spectra for First 10 Seconds of Normalized Input Motions

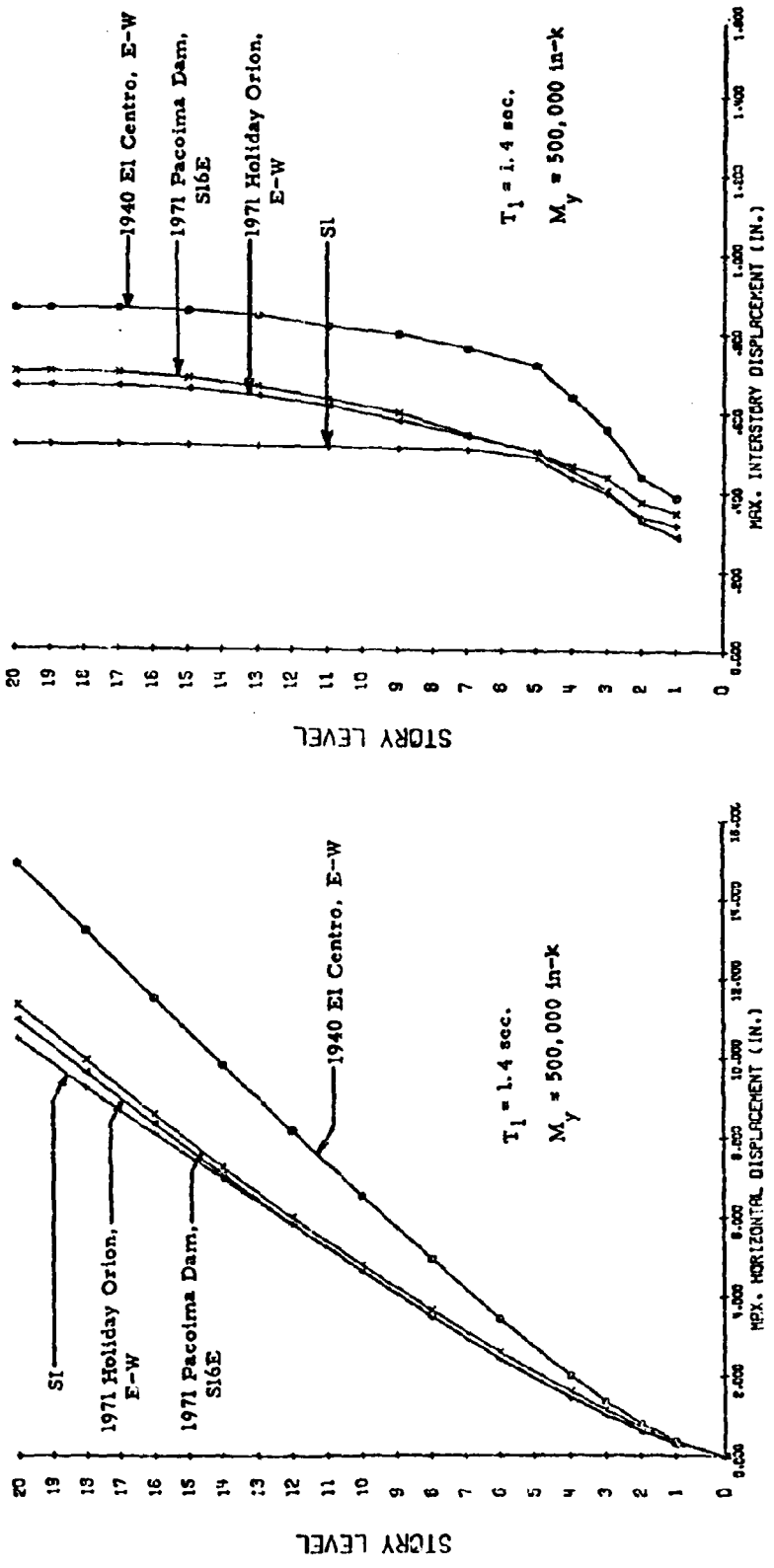

Fig. 22 Effect of Frequency Characteristics of Ground Motion

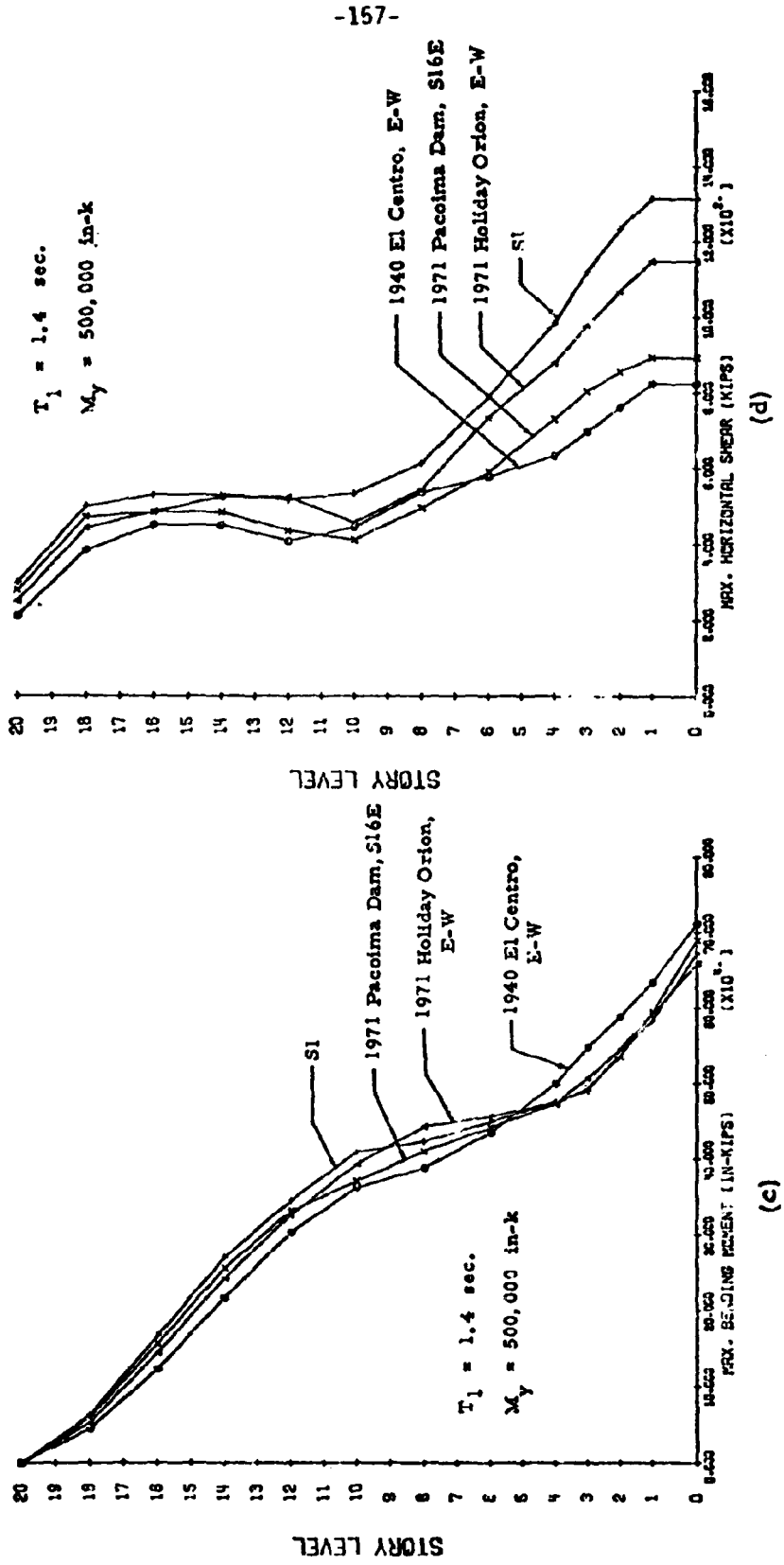

Fig. 22 (contd.) Effect of Frequency Characteristics of Ground Motion

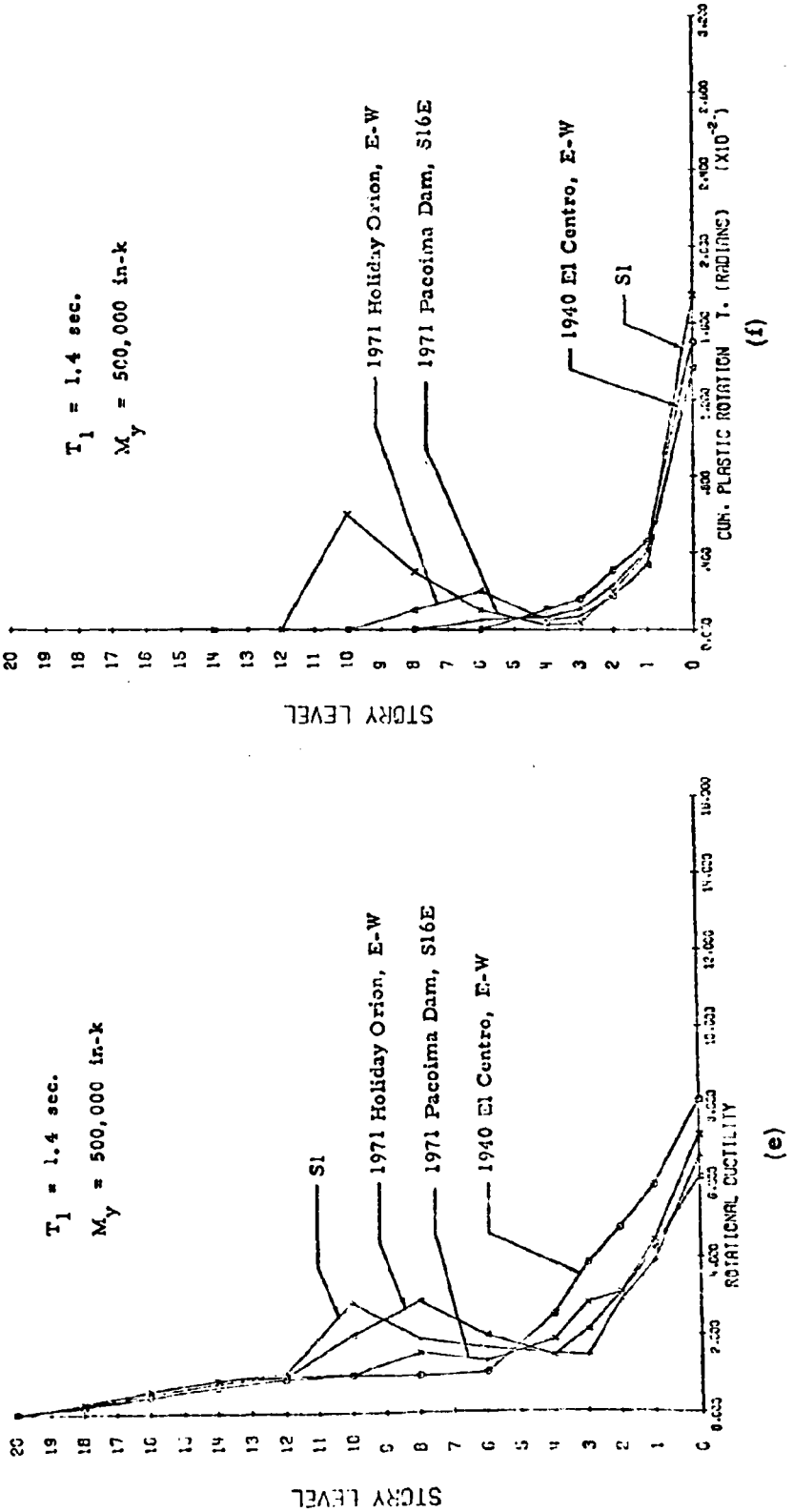

Fig. 22 (contd.) Effect of Frequency Characteristics of Ground Motion

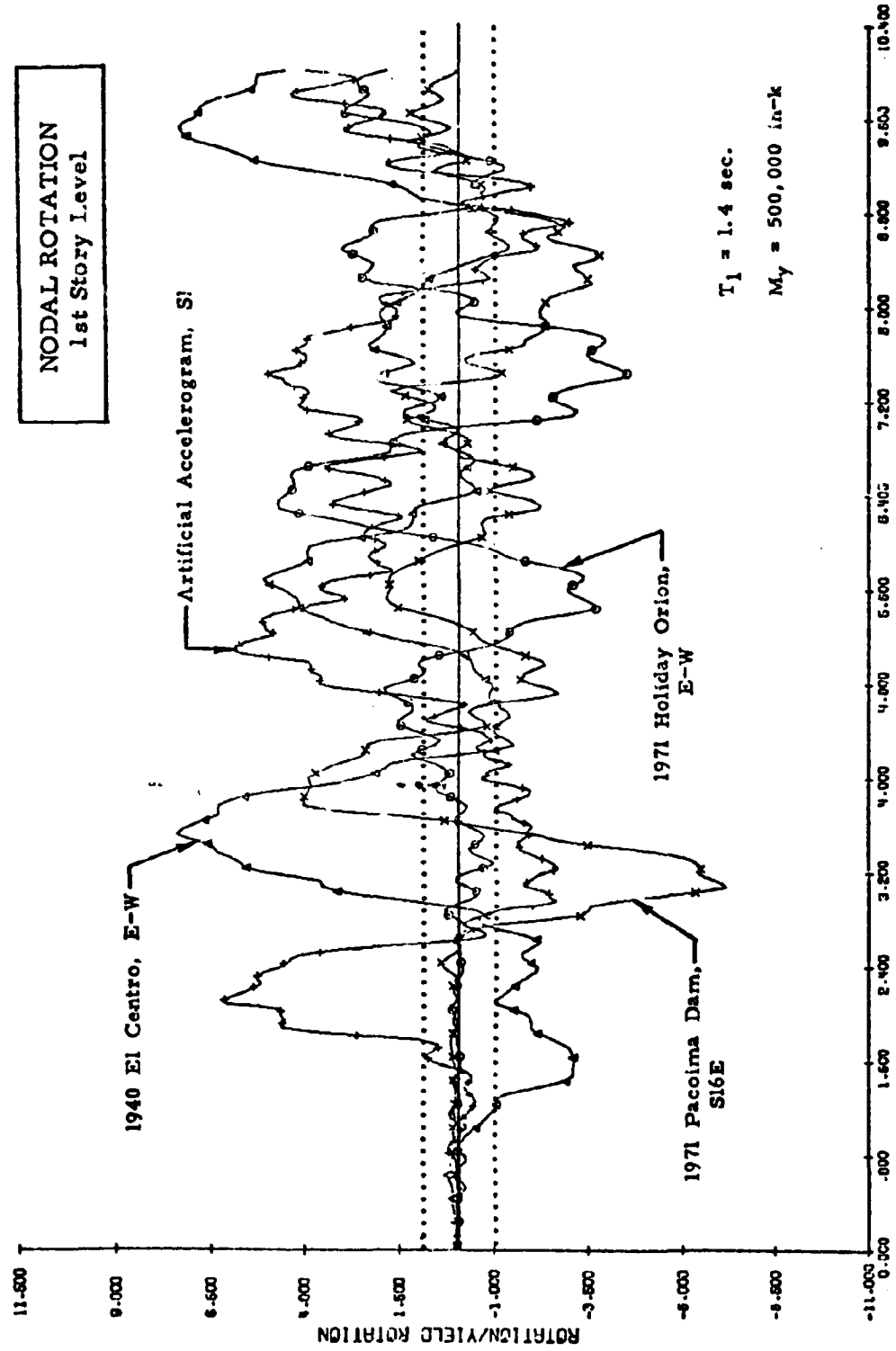

Fig. 23 Normalized Rotations in First Story vs. Time for Ground Motions with Different Frequency Characteristics

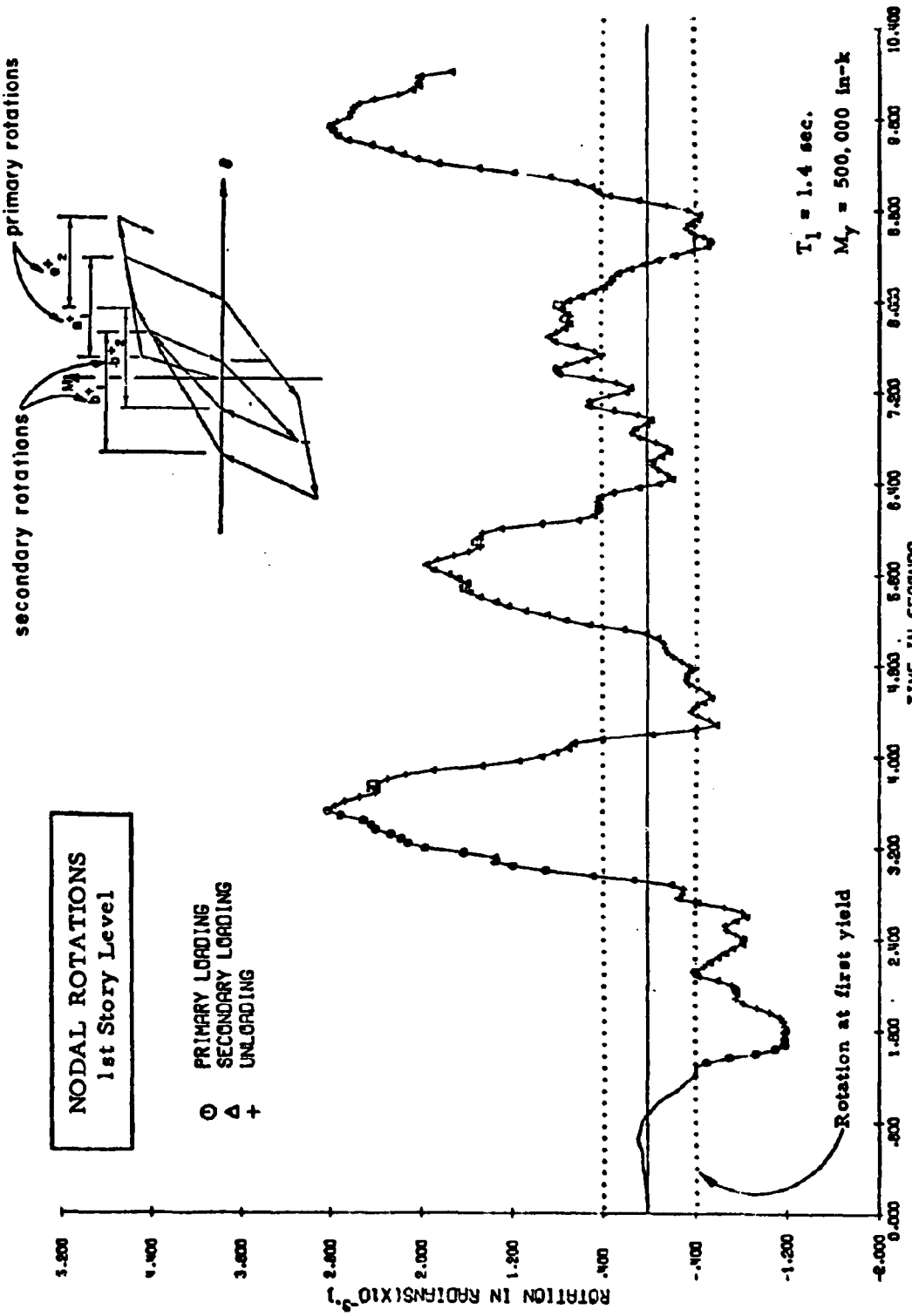

Fig. 24 Nodal Rotation History for Structure Subjected to 1940 El Centro, E-W Component

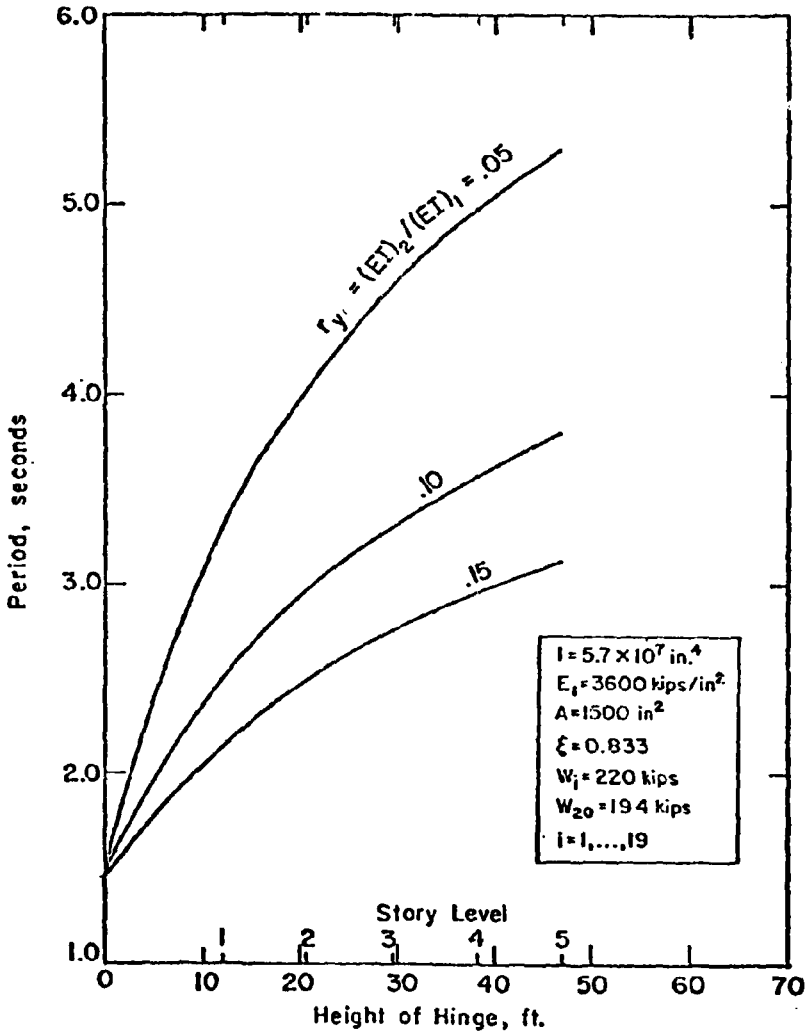

Fig. 25 Fundamental Period vs. Height of Yield Hinge, 20-Mass Cantilever

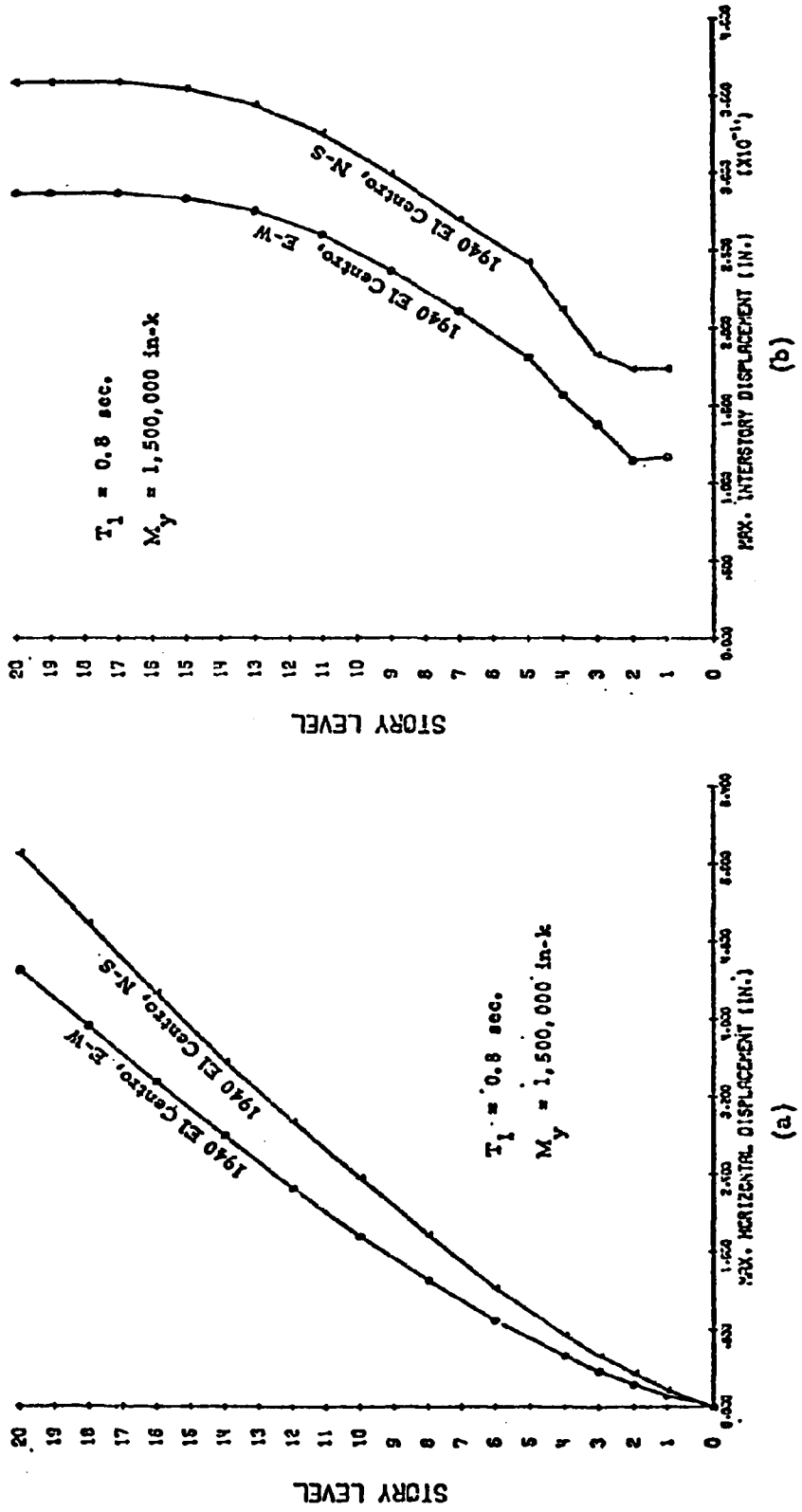

Fig. 26 Effect of Frequency Characteristics of Ground Motion

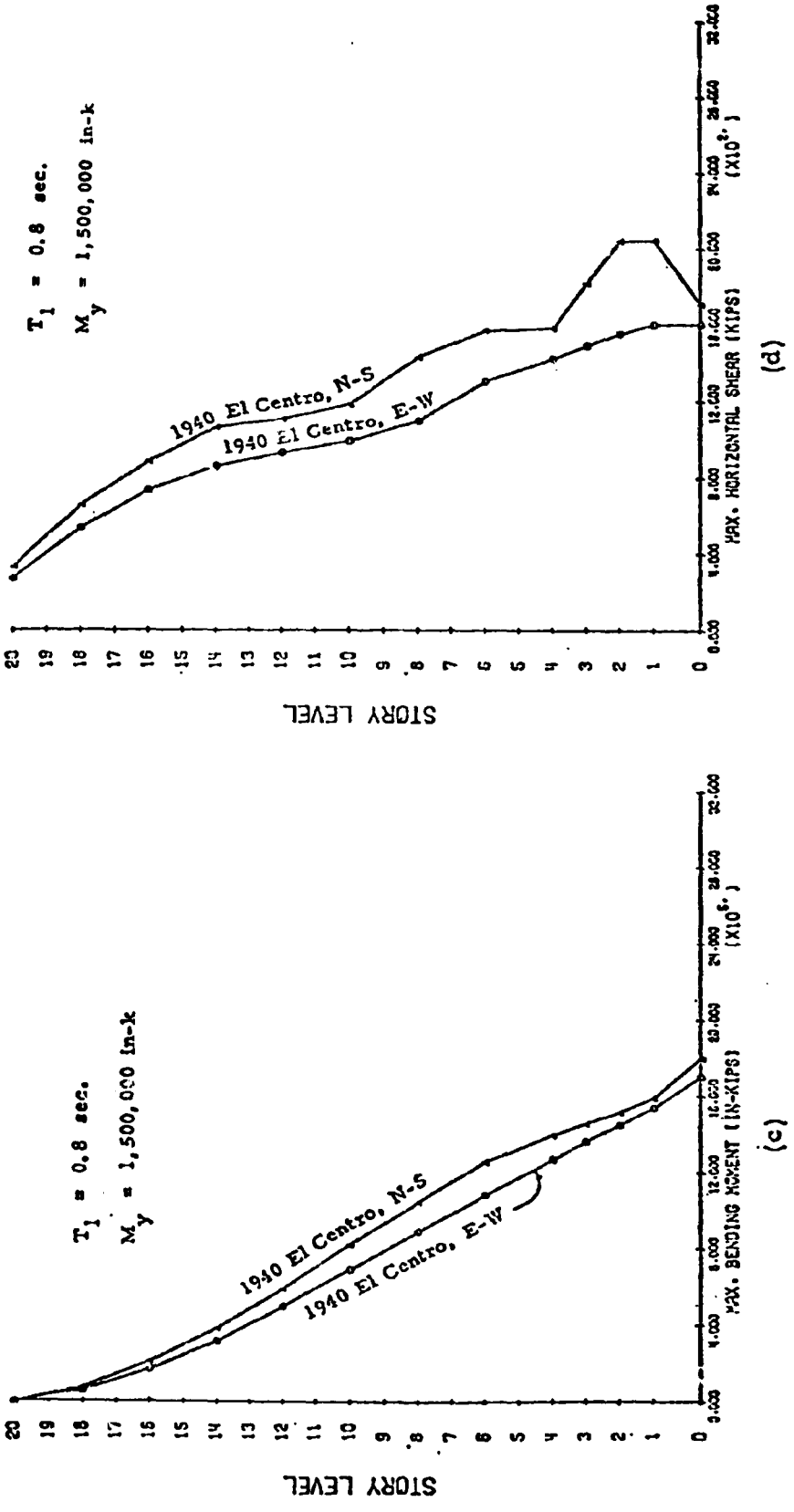

Fig. 26 (contd.) Effect of Frequency Characteristics of Ground Motion

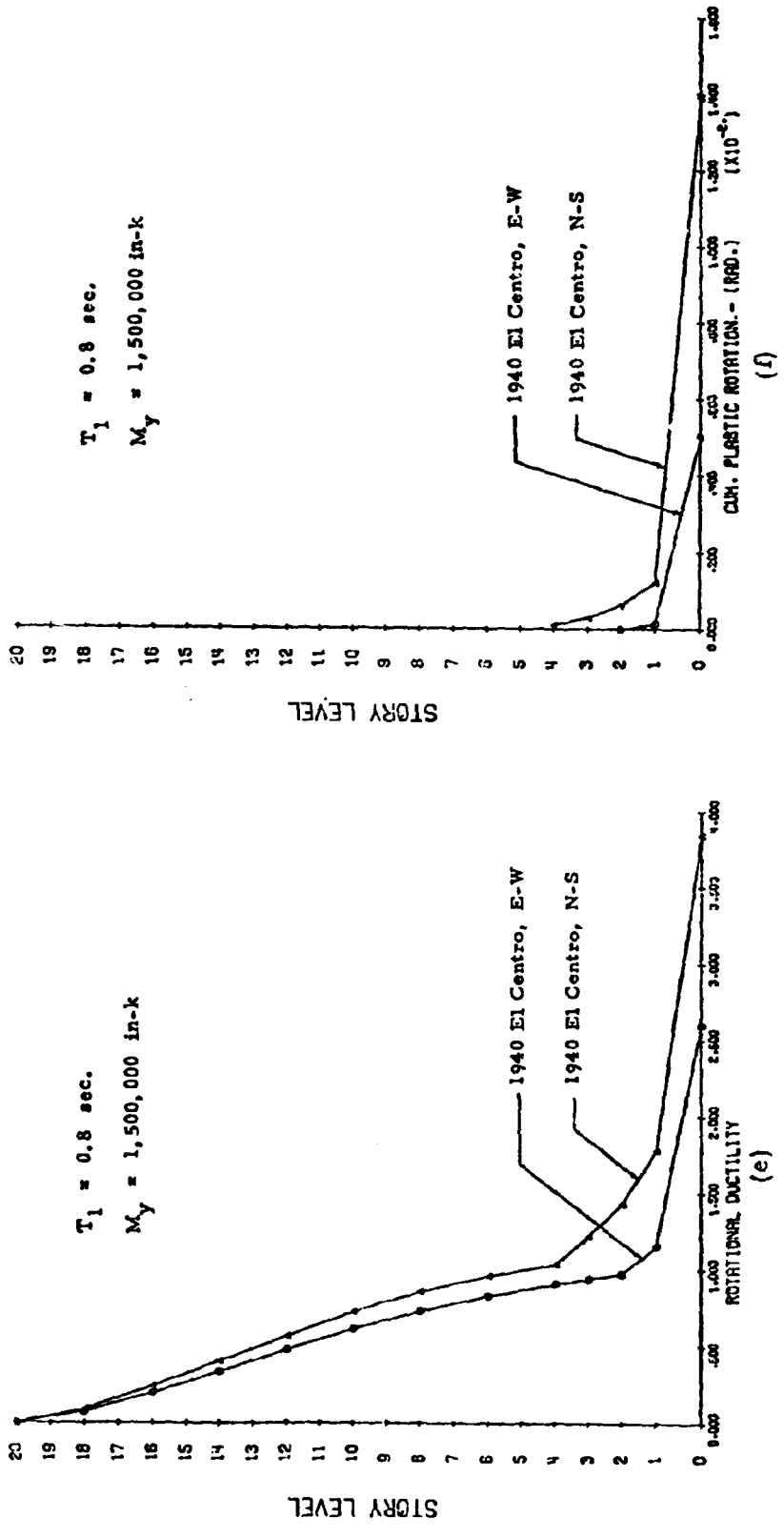

Fig. 26 (contd.) Effect of Frequency Characteristics of Ground Motion

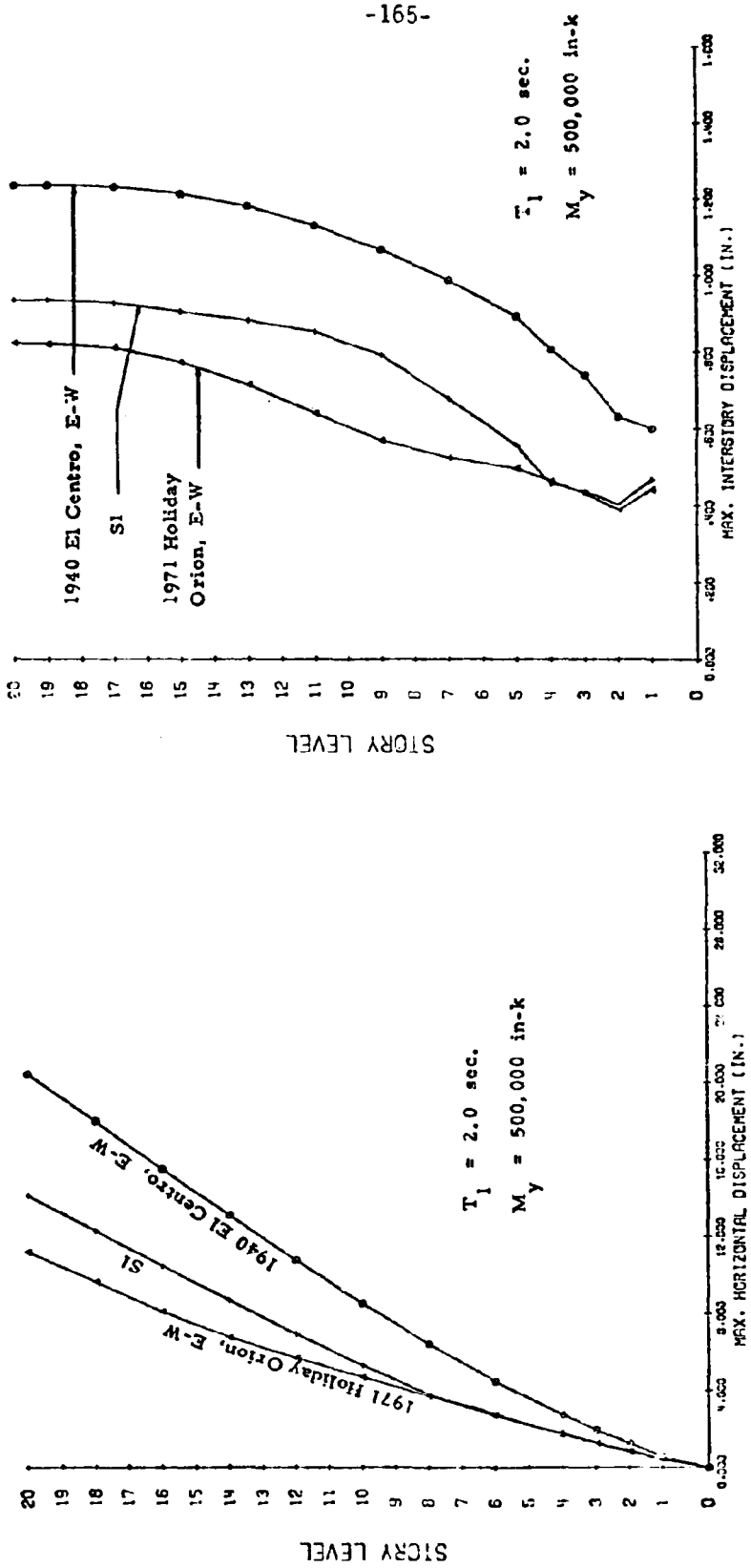

Fig. 27 Effect of Frequency Characteristics of Ground Motion

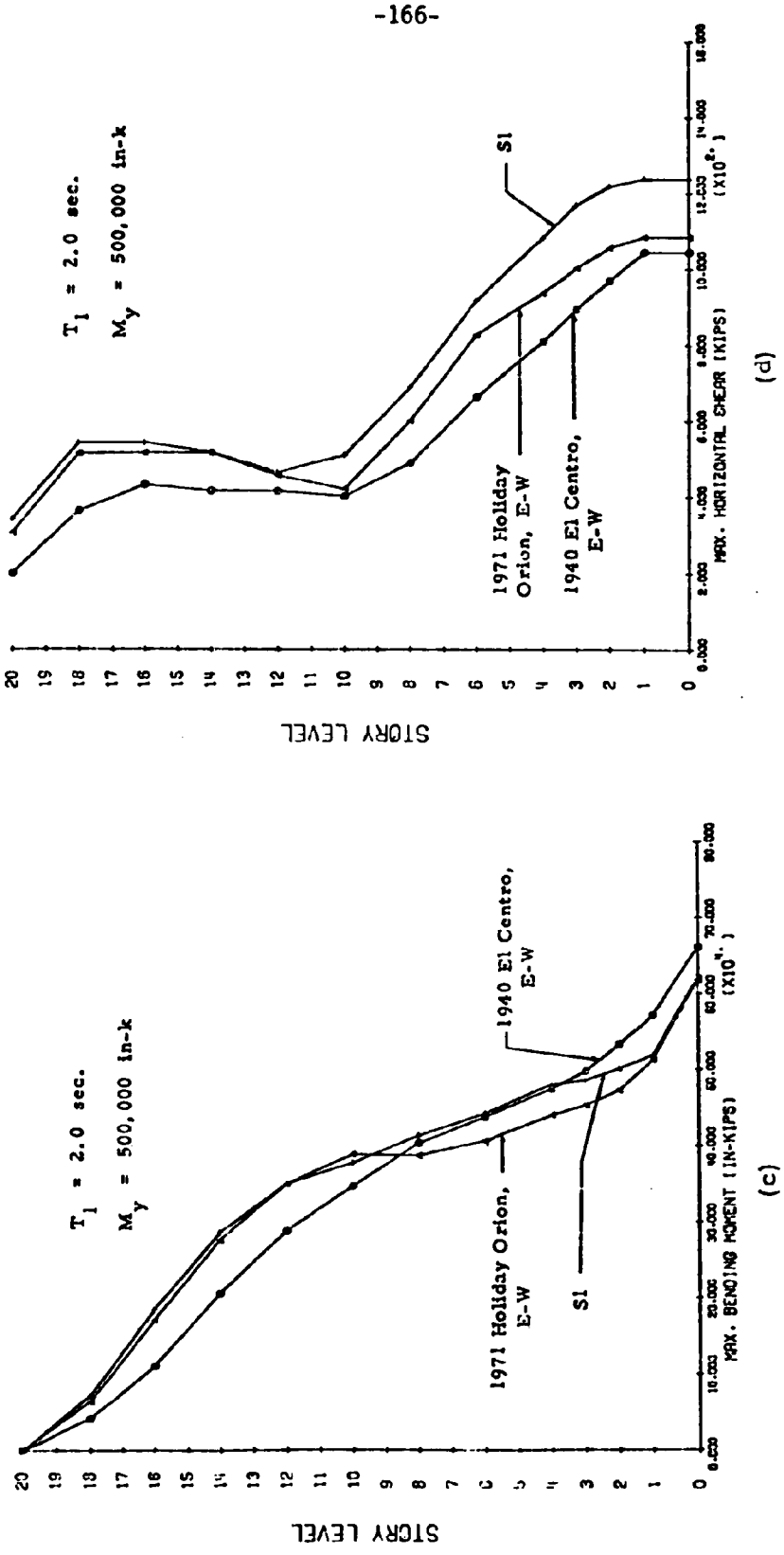

Fig. 27 (contd.) Effect of Frequency Characteristics of Ground Motion

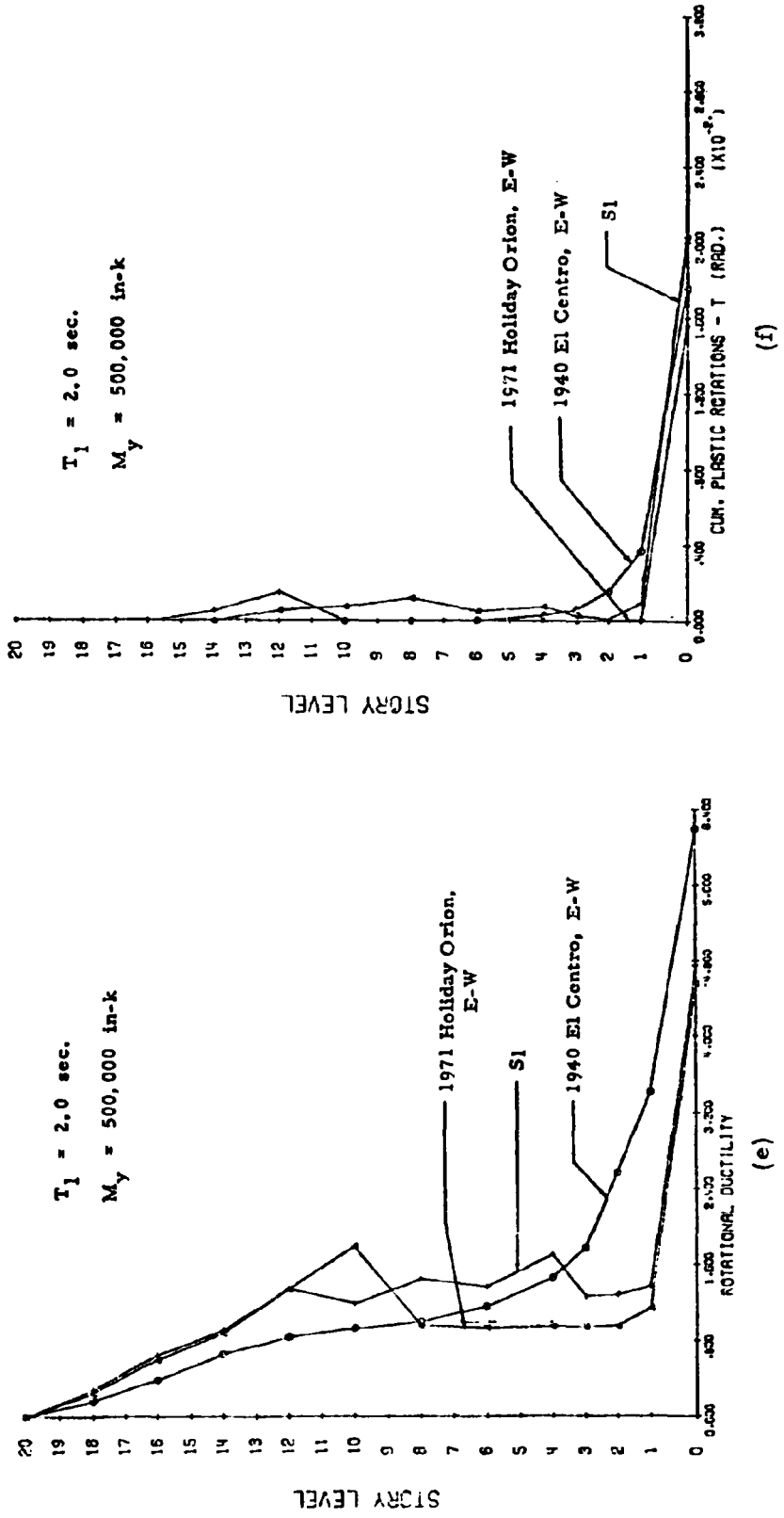

Fig. 27 (contd.) Effect of Frequency Characteristics of Ground Motion

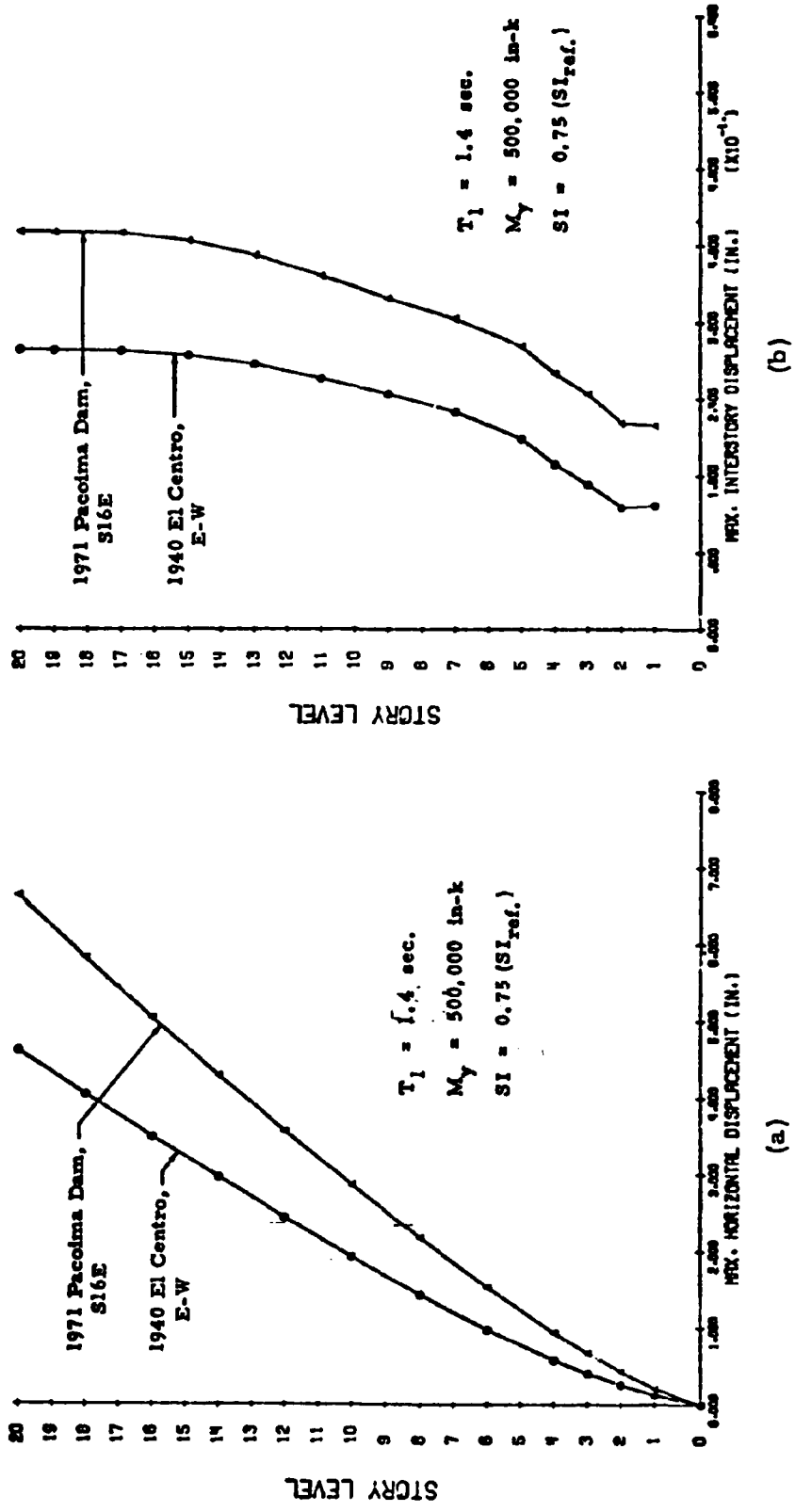

Fig. 28 Interacting Effects of Frequency Characteristics and Intensity of Ground Motion

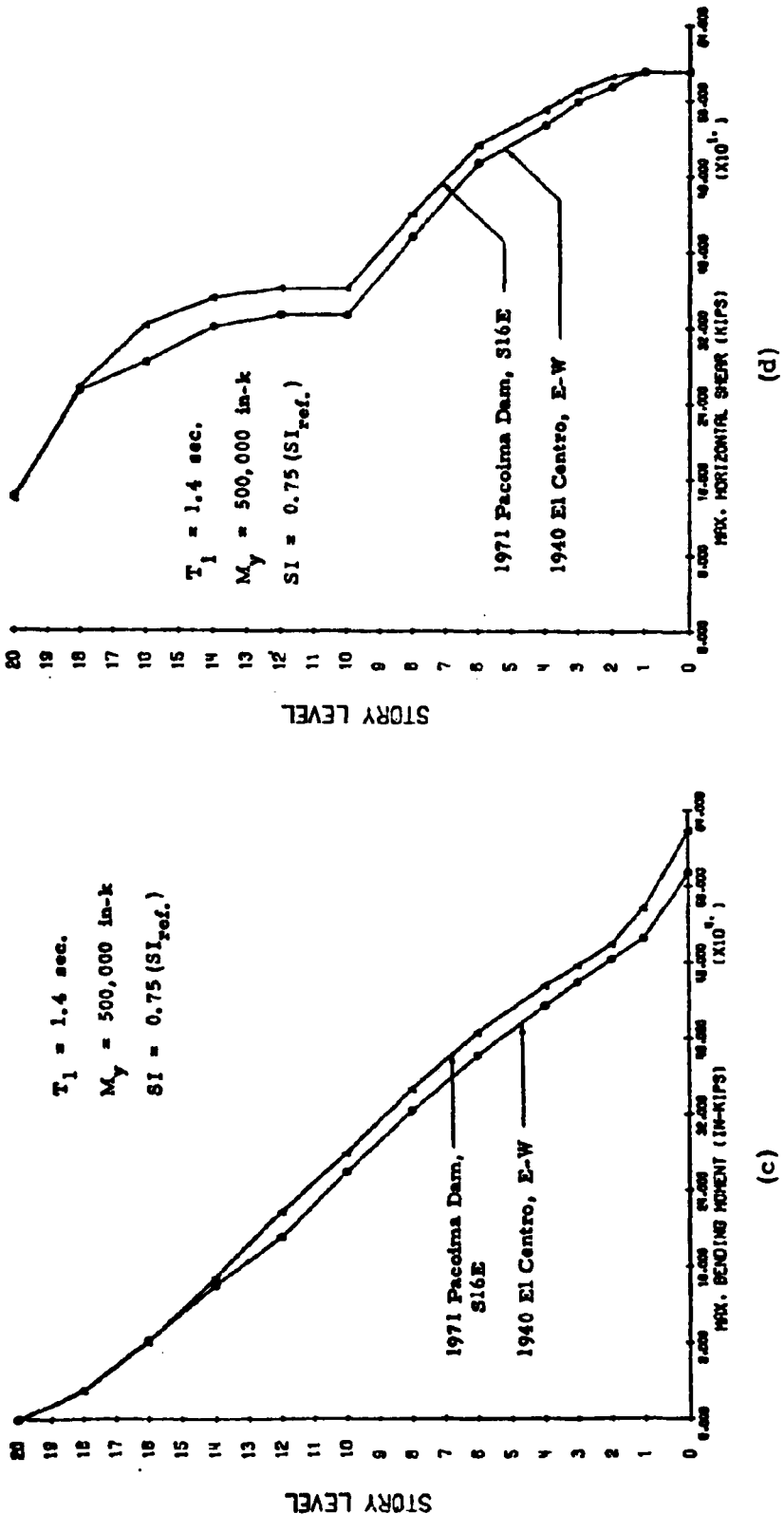

Fig. 28 (contd.) Interacting Effects of Frequency Characteristics and Intensity of Ground Motion

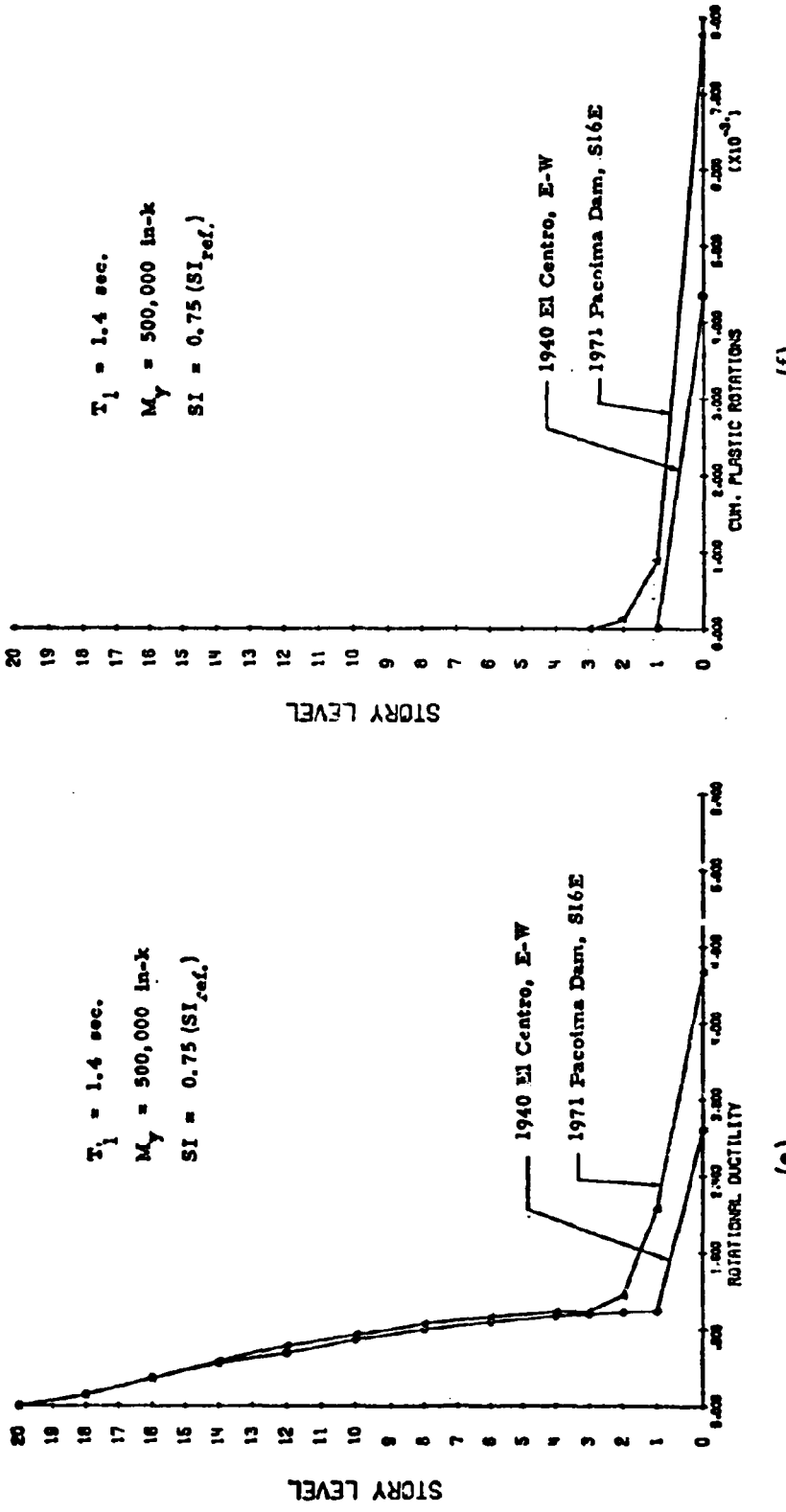

Fig. 28 (contd.) Interacting Effects of Frequency Characteristics and Intensity of Ground Motion

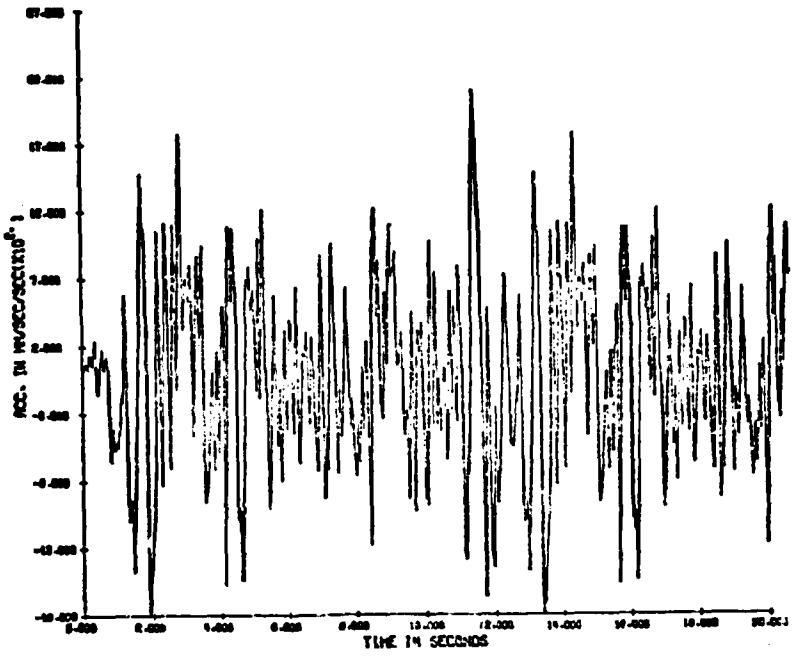

Fig. 29(a) 20-Second Composite Accelerogram

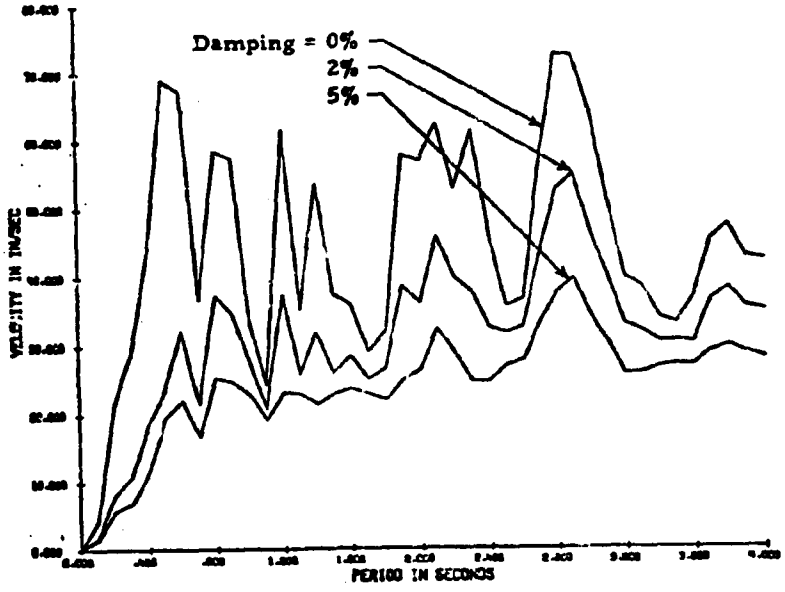

Fig. 29(b) Velocity Response Spectra for 20-sec. Composite Accelerogram

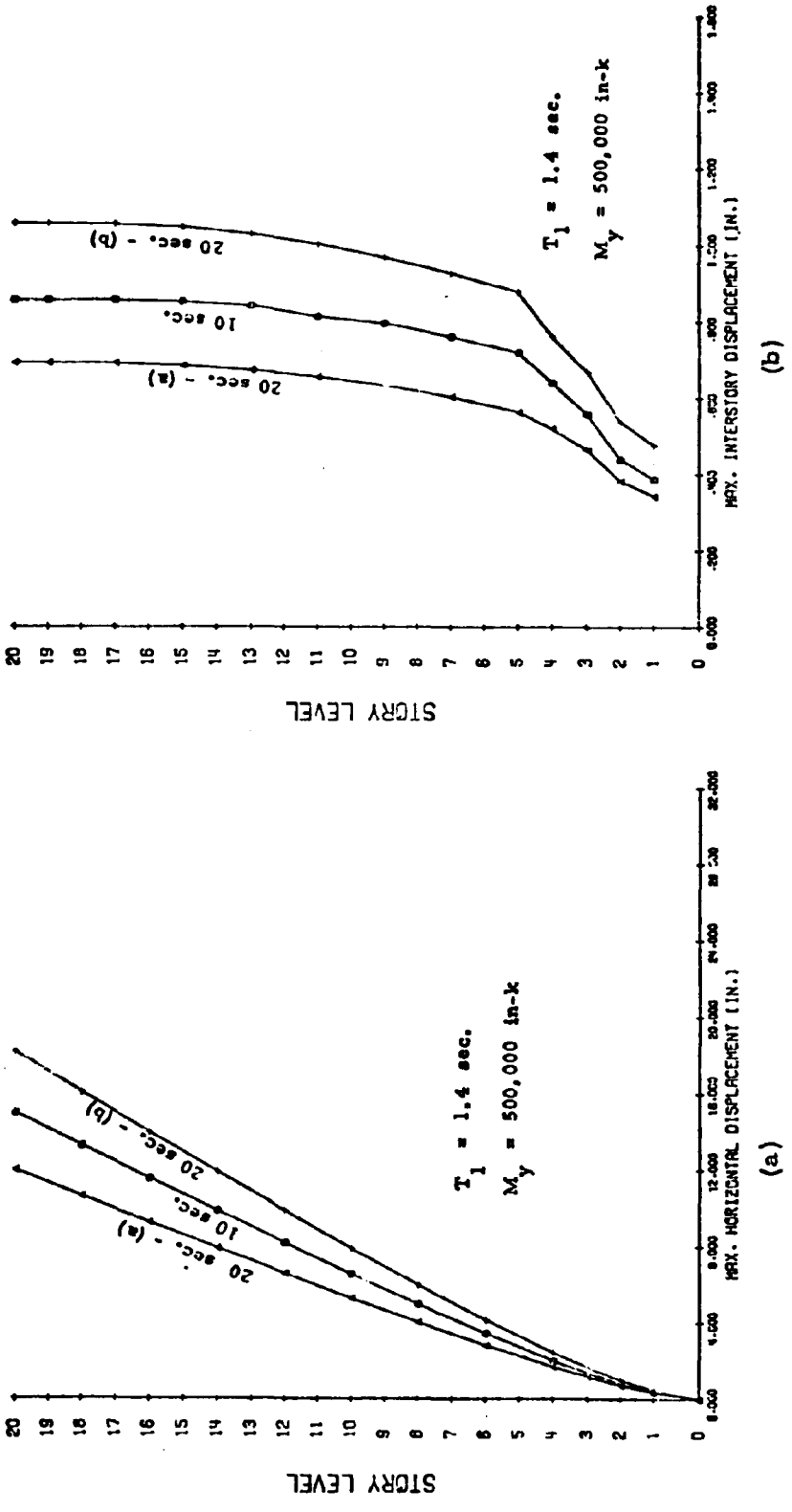

Fig. 30 Effect of Duration of Ground Motion

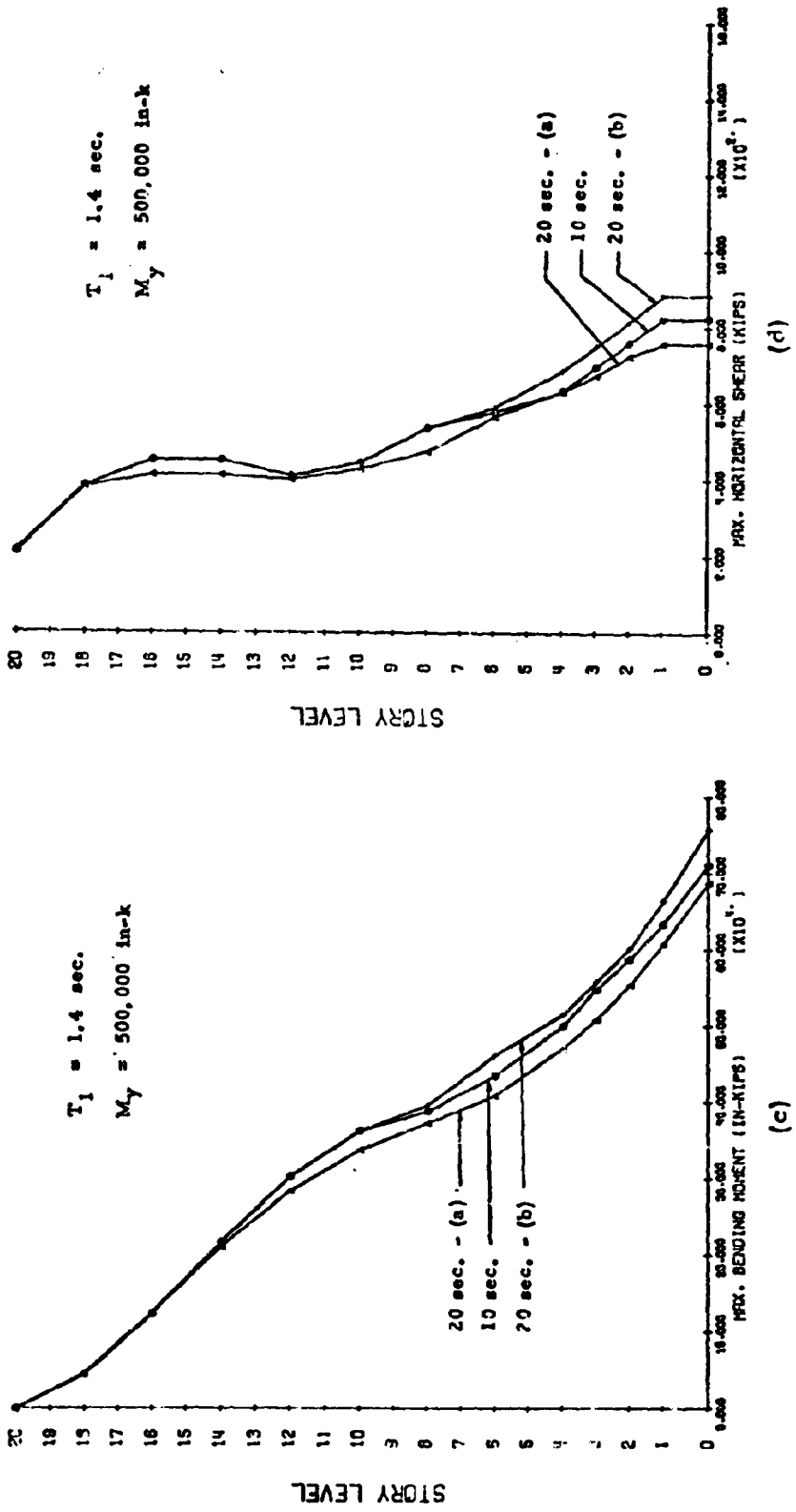

Fig. 30 (contd.) Effect of Duration of Ground Motion

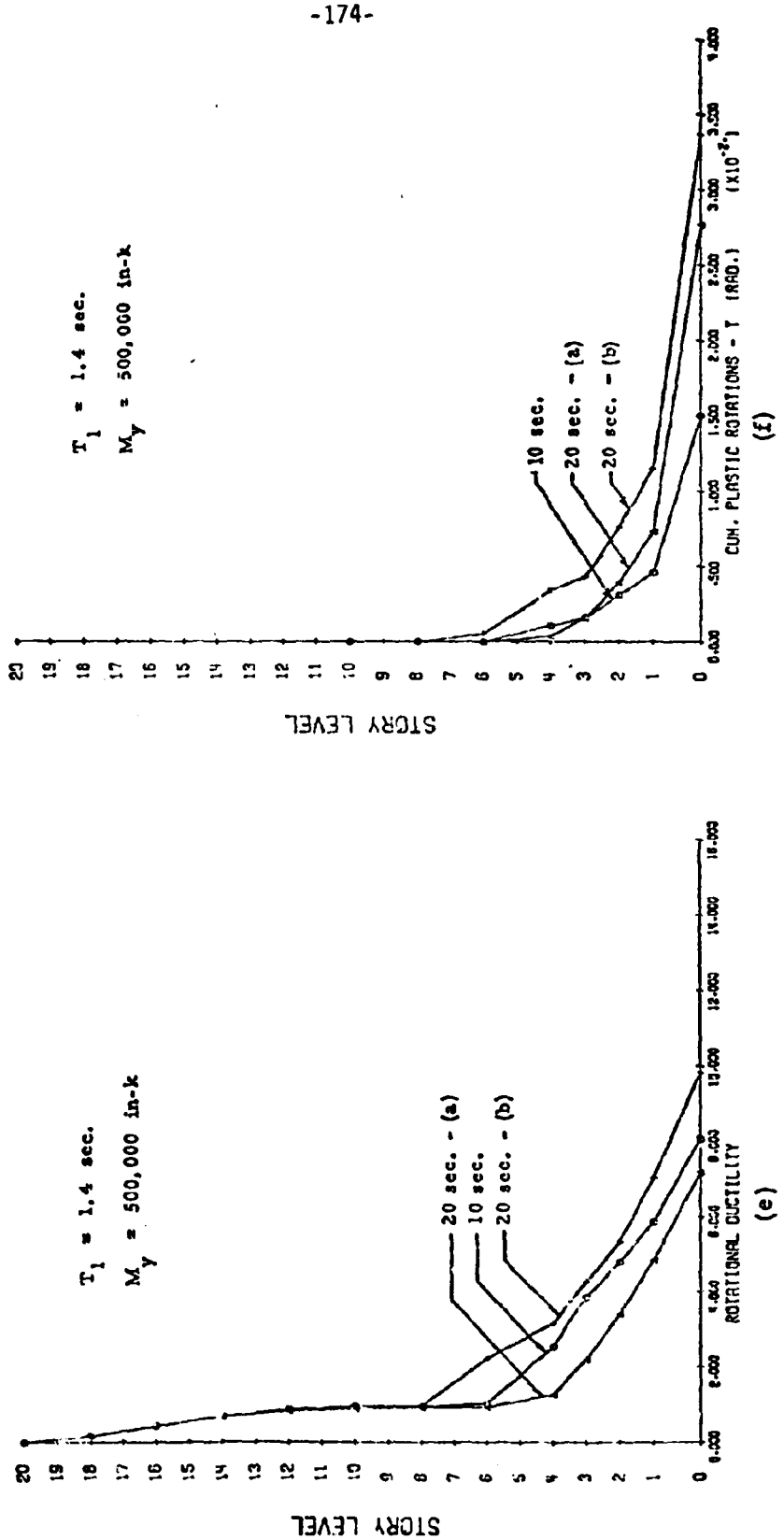

Fig. 30 (contd.) Effect of Duration of Ground Motion

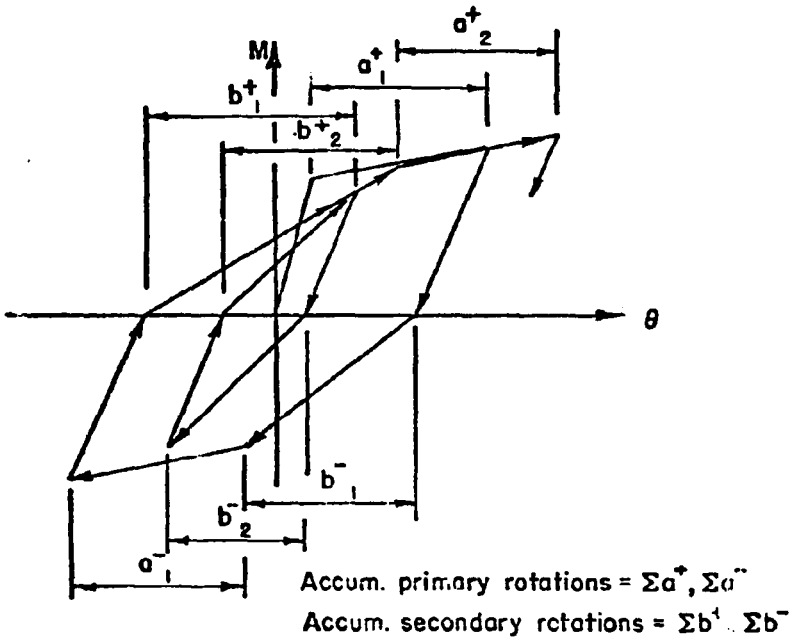

Fig. 31 Components of Cumulative Plastic Rotations for Takeda Stiffness Degrading Model

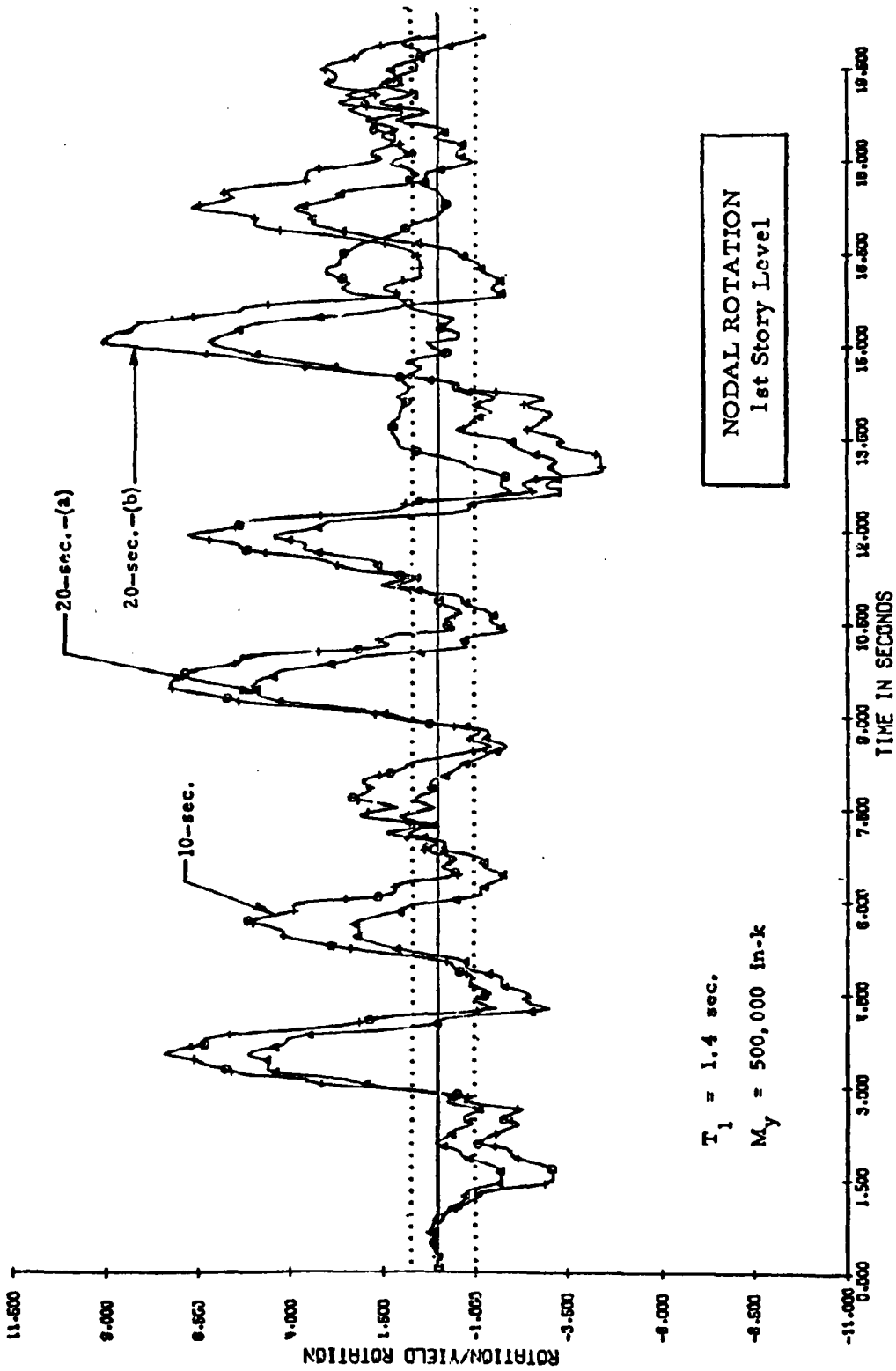

Fig. 32 Rotation in First Story vs. Time for Different Durations of Ground Motion

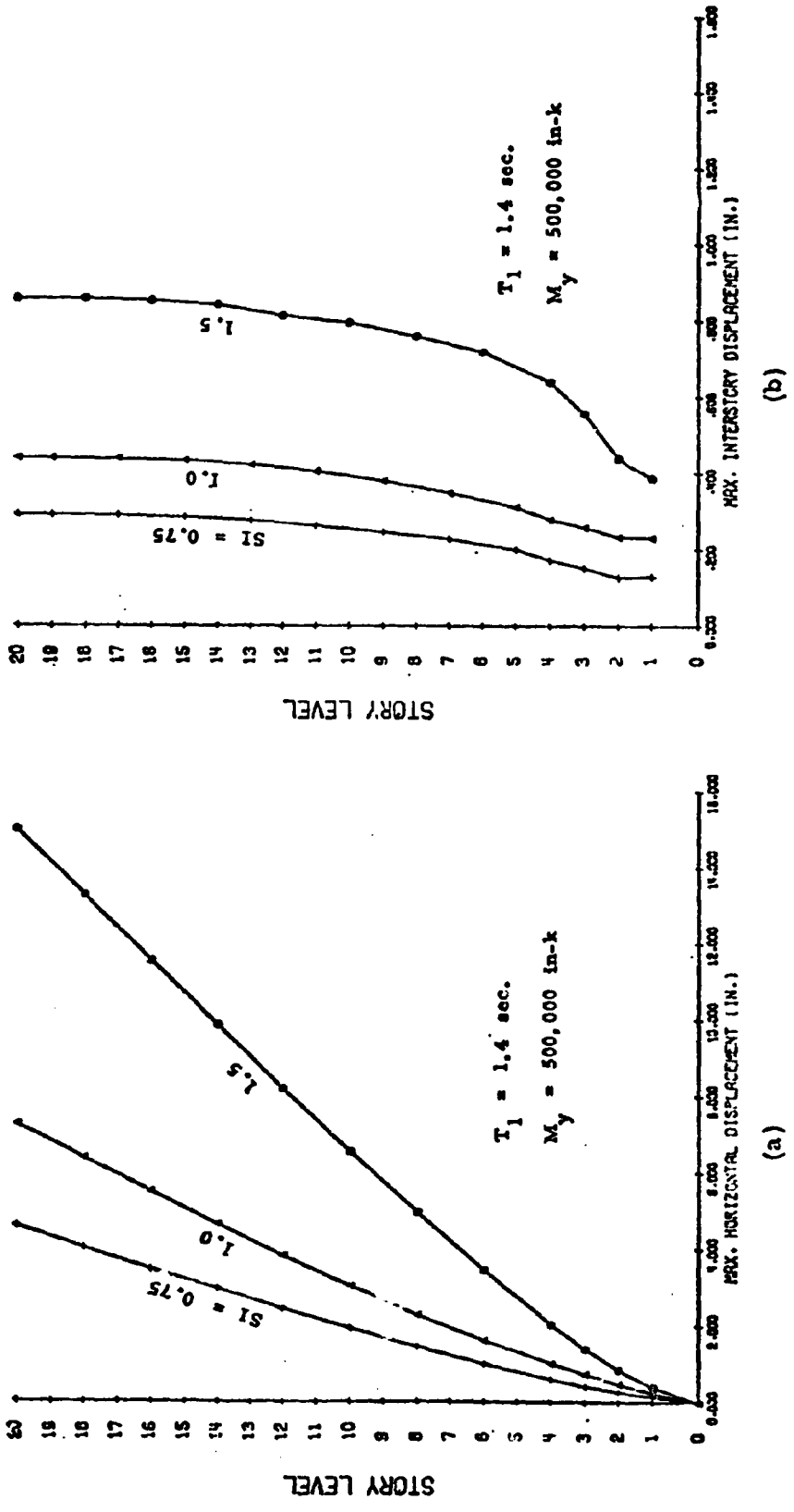

Fig. 33 Effect of Intensity of Ground Motion

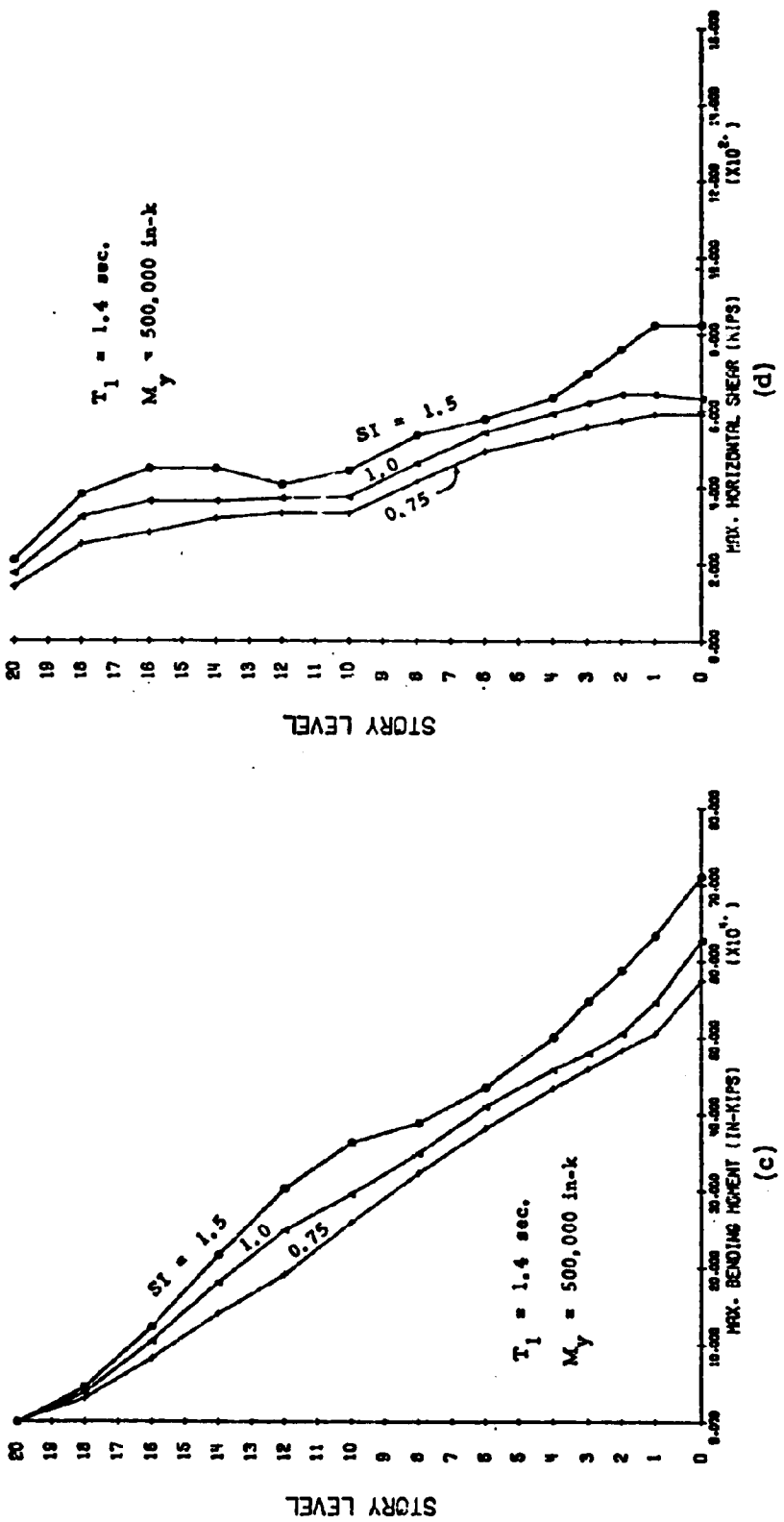

Fig. 33 (contd.) Effect of Intensity of Ground Motion

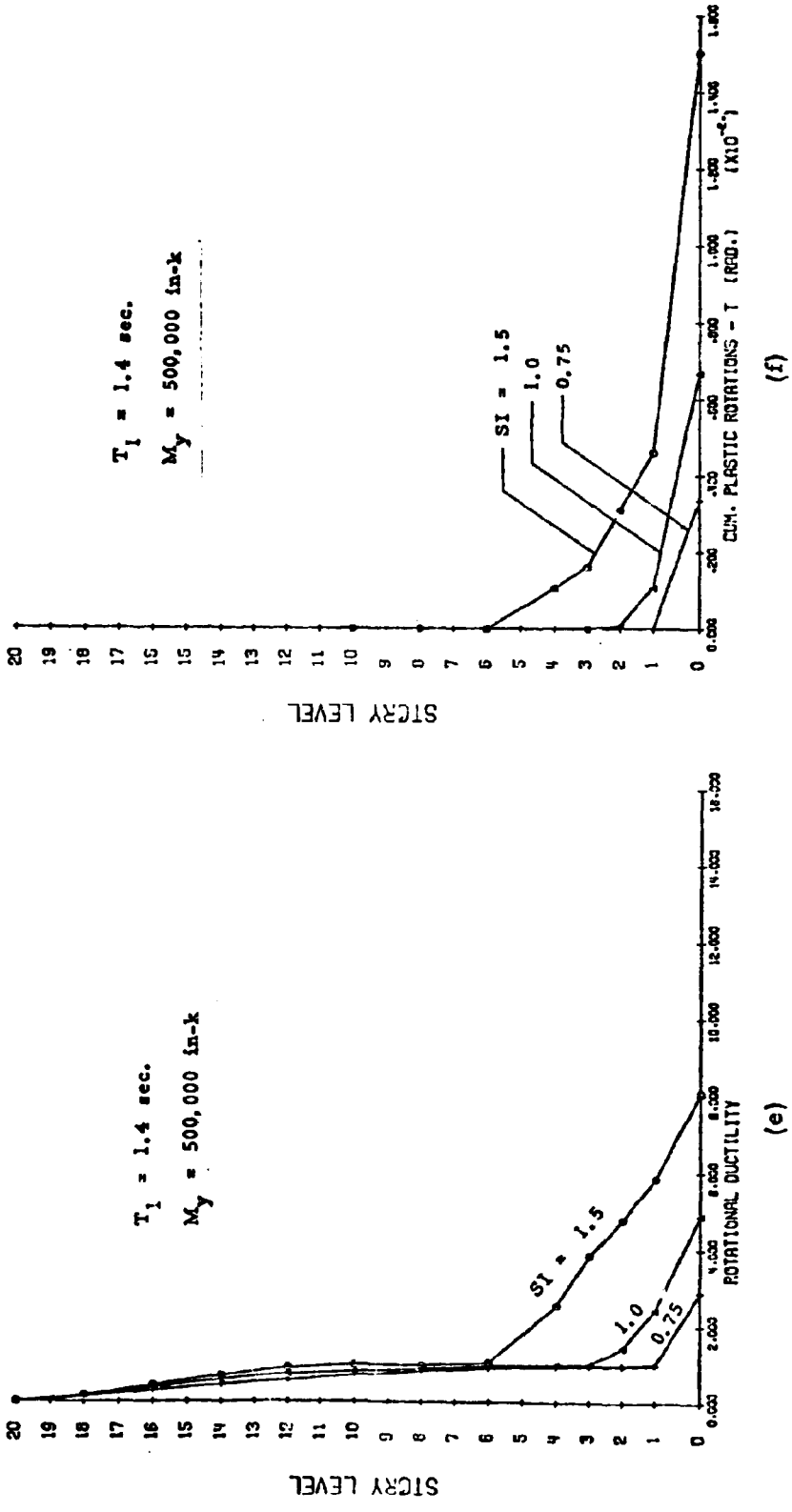

Fig. 33 (contd.) Effect of Intensity of Ground Motion

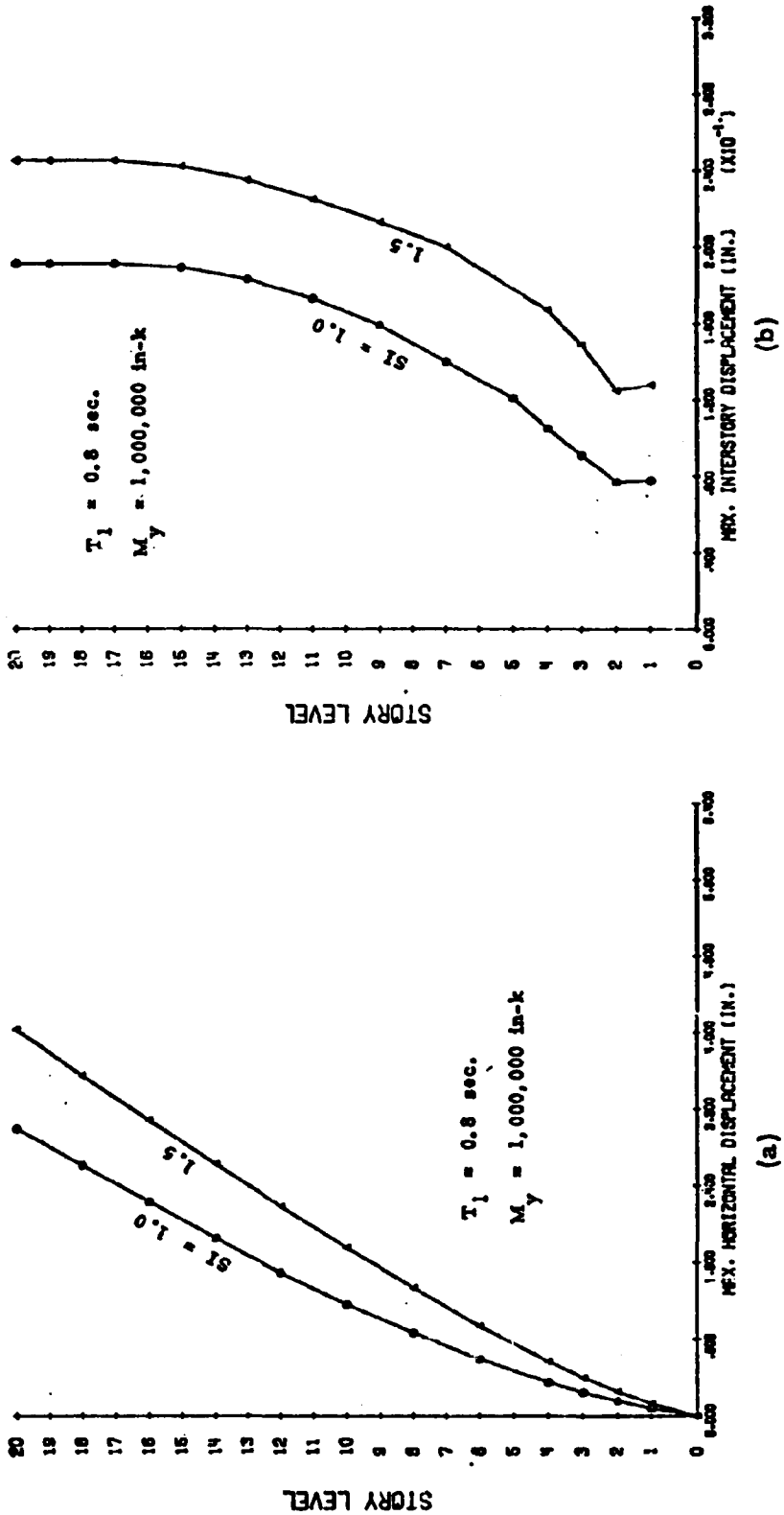

Fig. 34 Effect of Intensity of Ground Motion

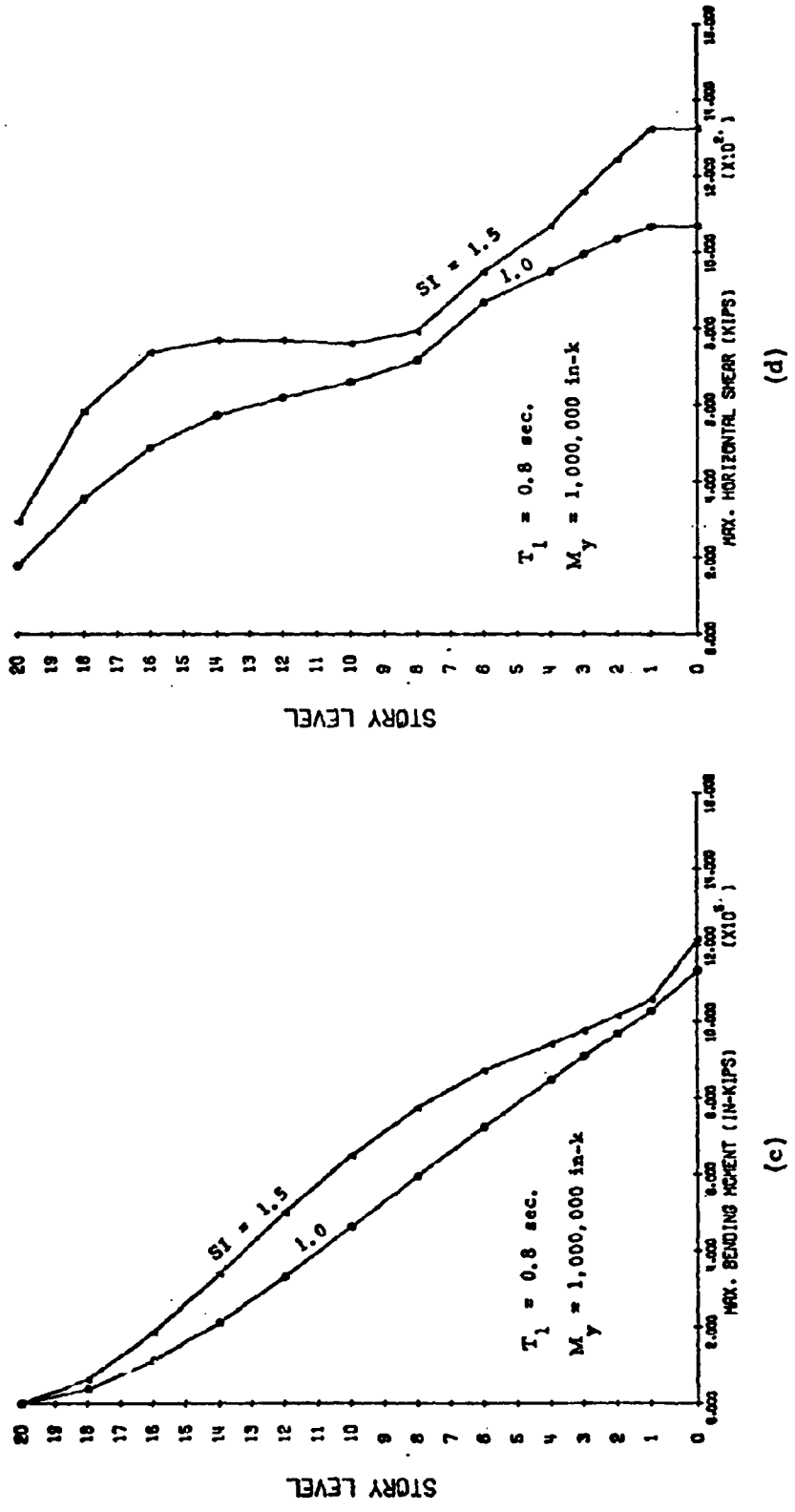

Fig. 34 (contd.) Effect of Intensity of Ground Motion

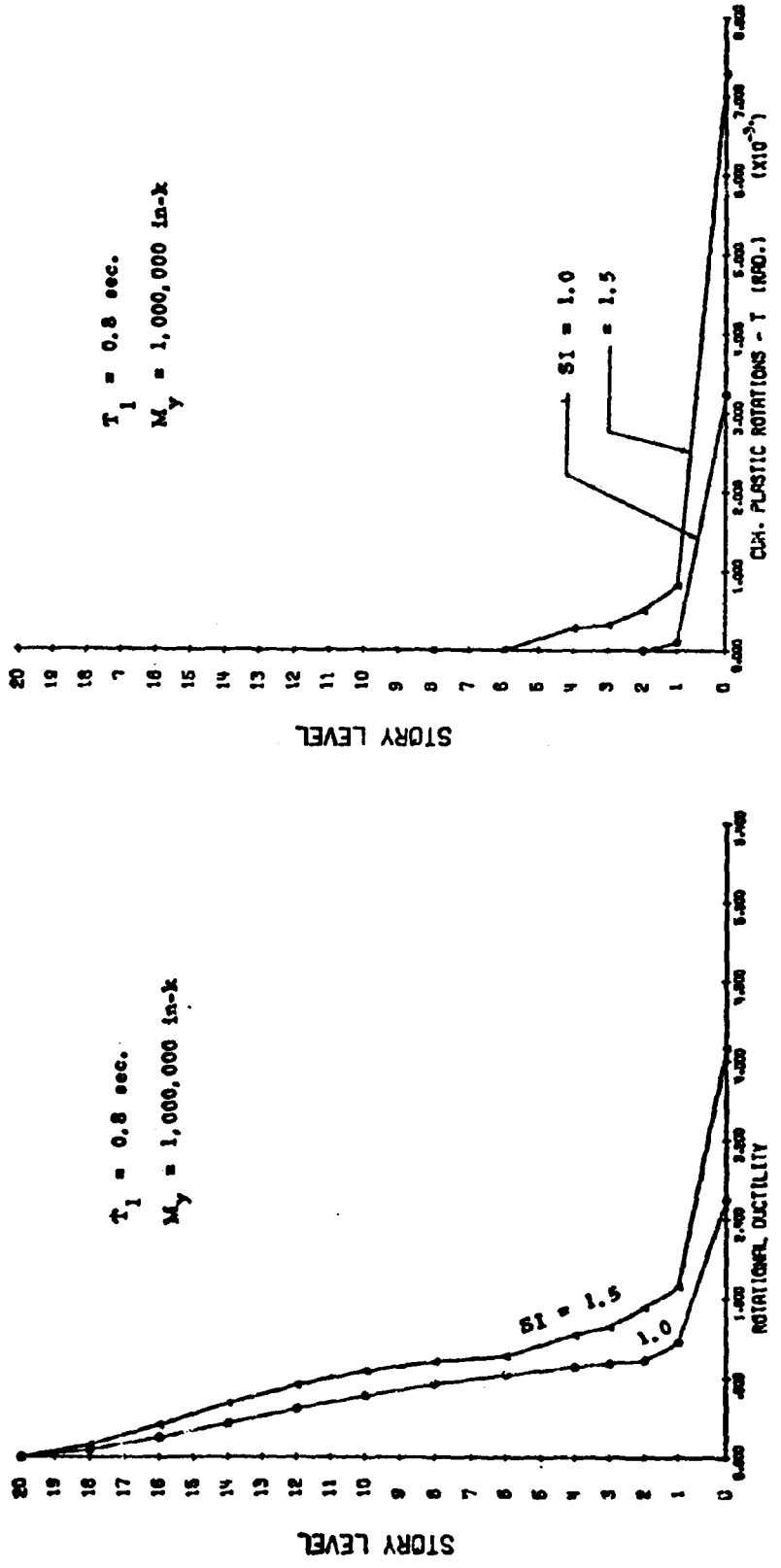

Fig. 34 (contd.) Effect of Intensity of Ground Motion

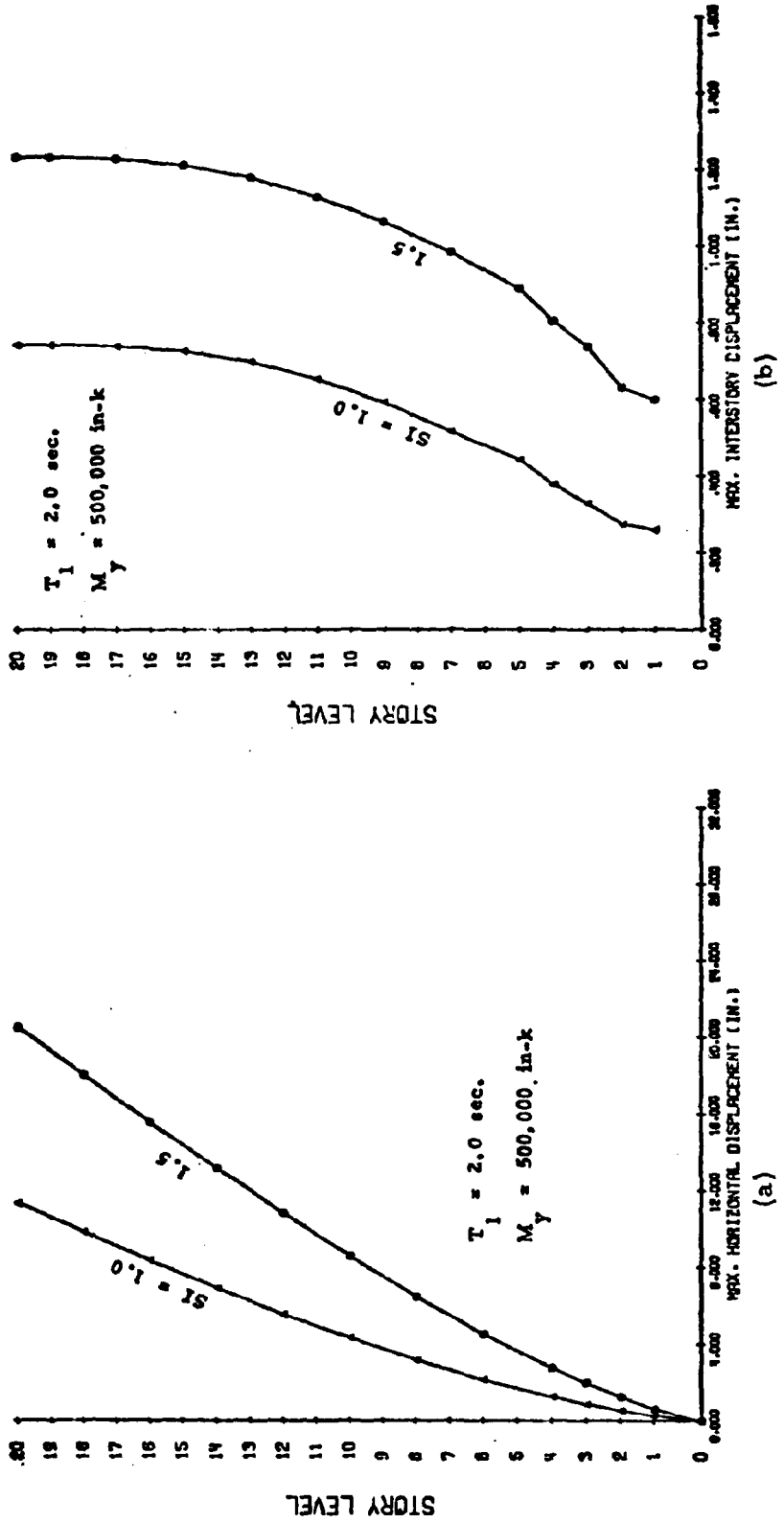

Fig. 35 Effect of Intensity of Ground Motion

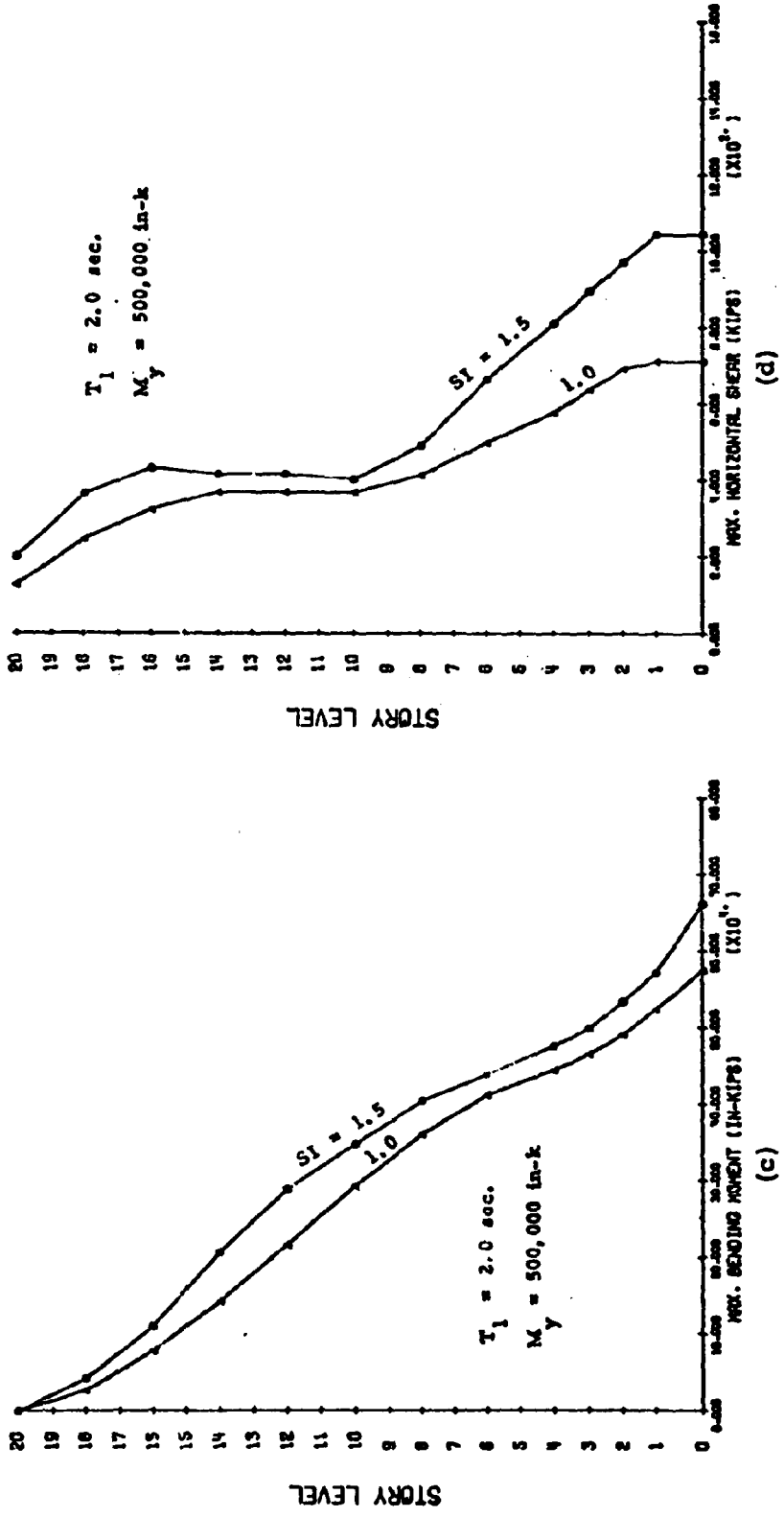

Fig. 35 (contd.) Effect of Intensity of Ground Motion

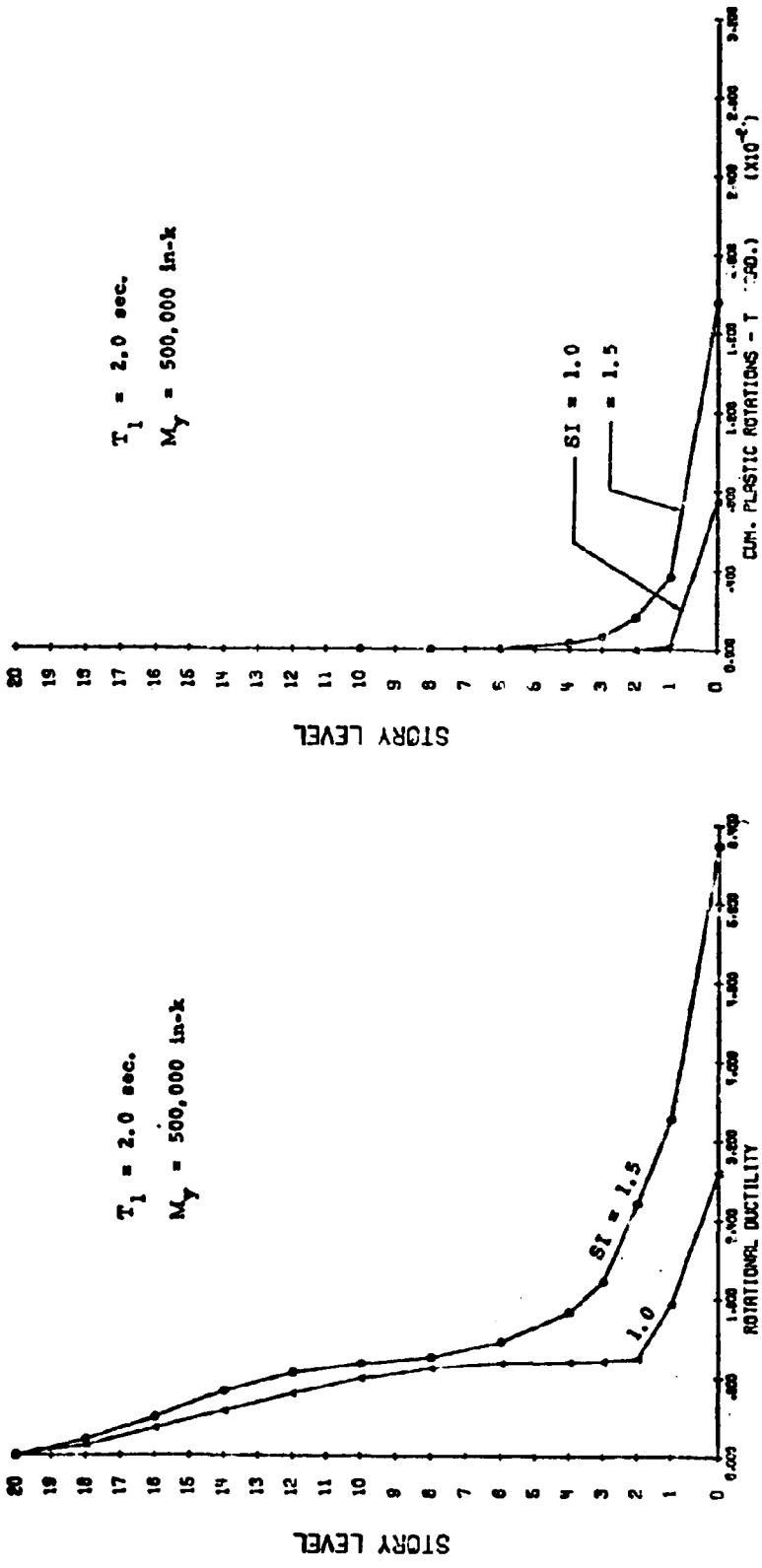

Fig. 35 (contd.) Effect of Intensity of Ground Motion

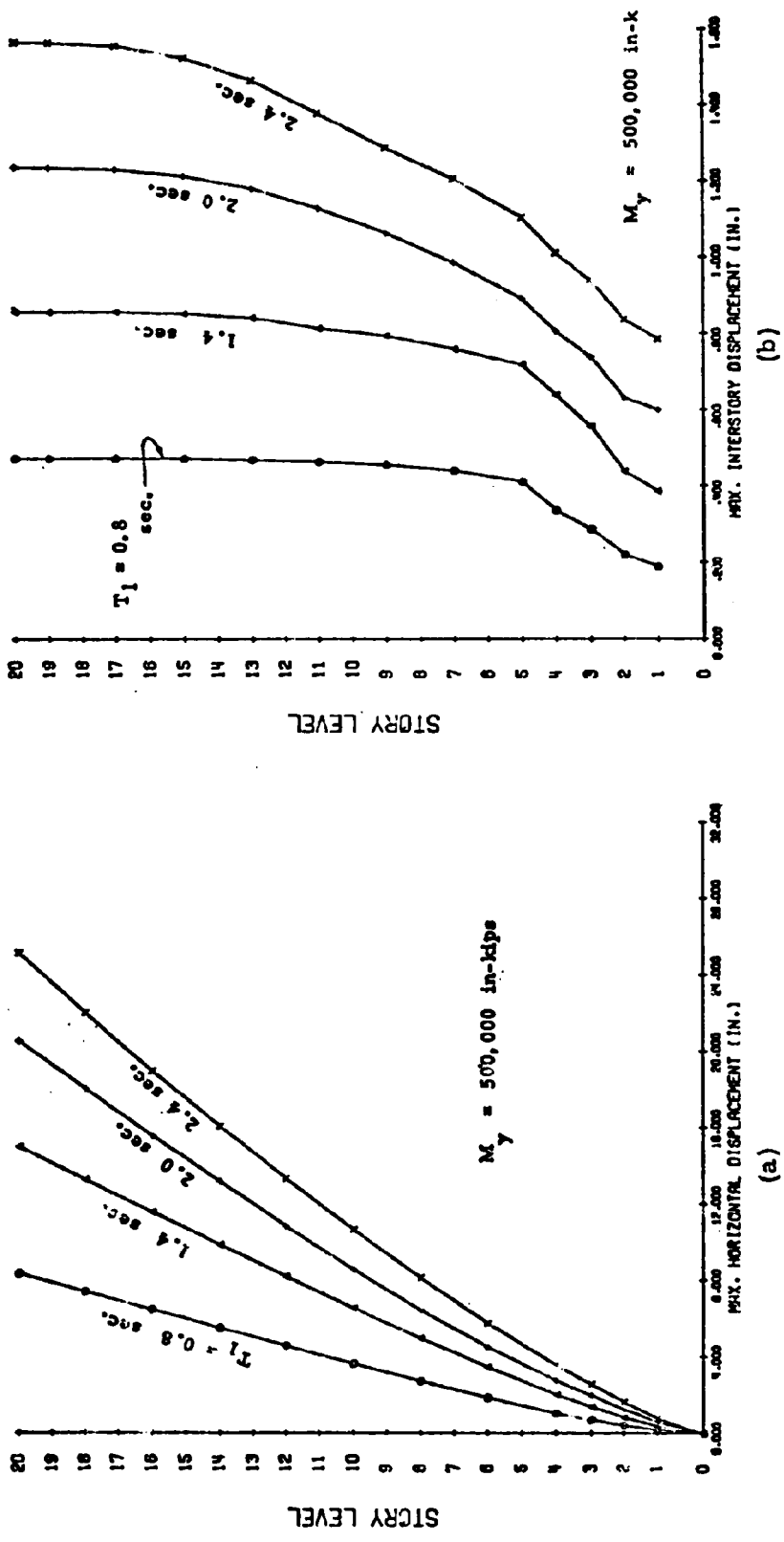

Fig. 36 Effect of Fundamental Period of Vibration, T_1

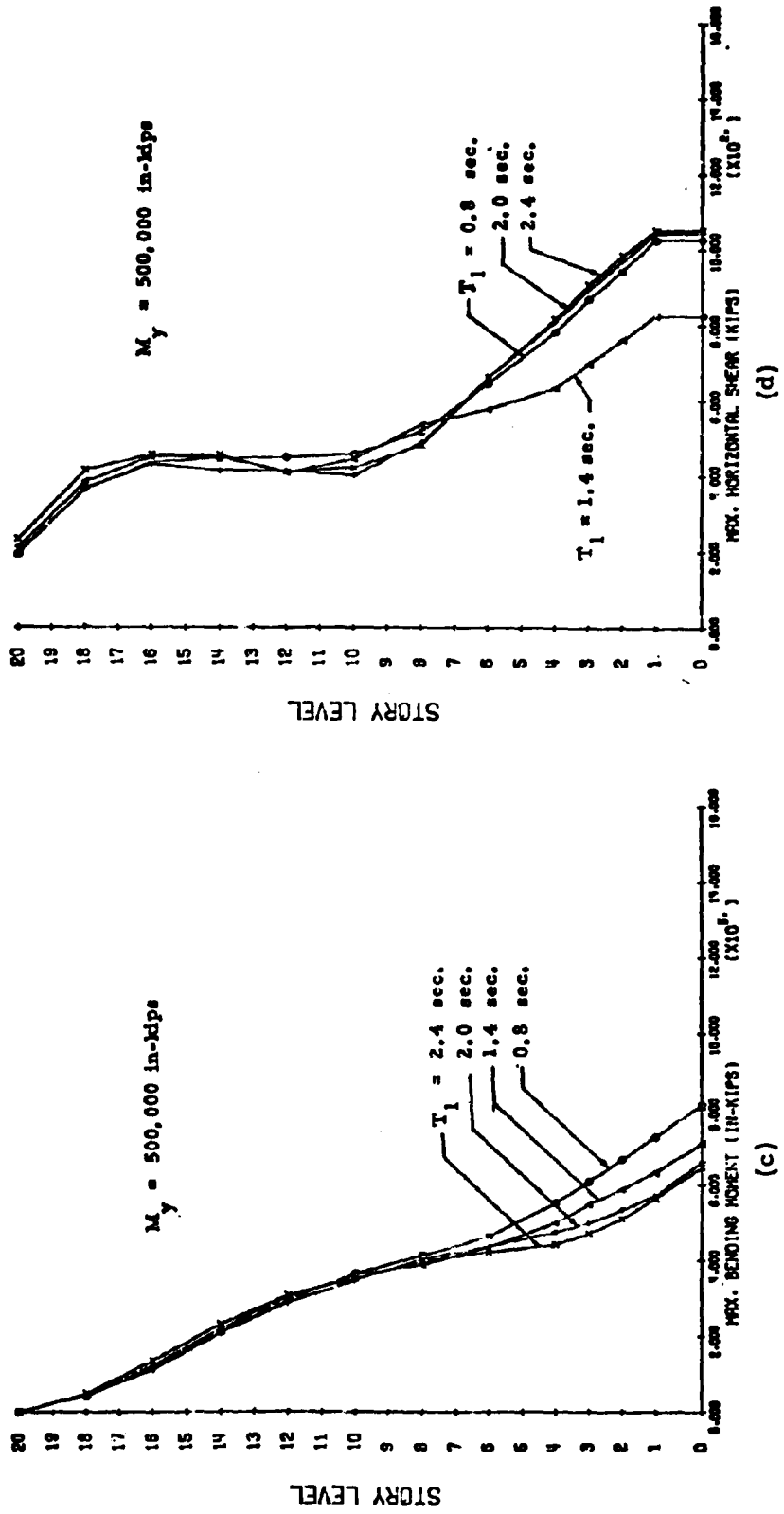

Fig. 36 (contd.) Effect of Fundamental Period of Vibration, T_1

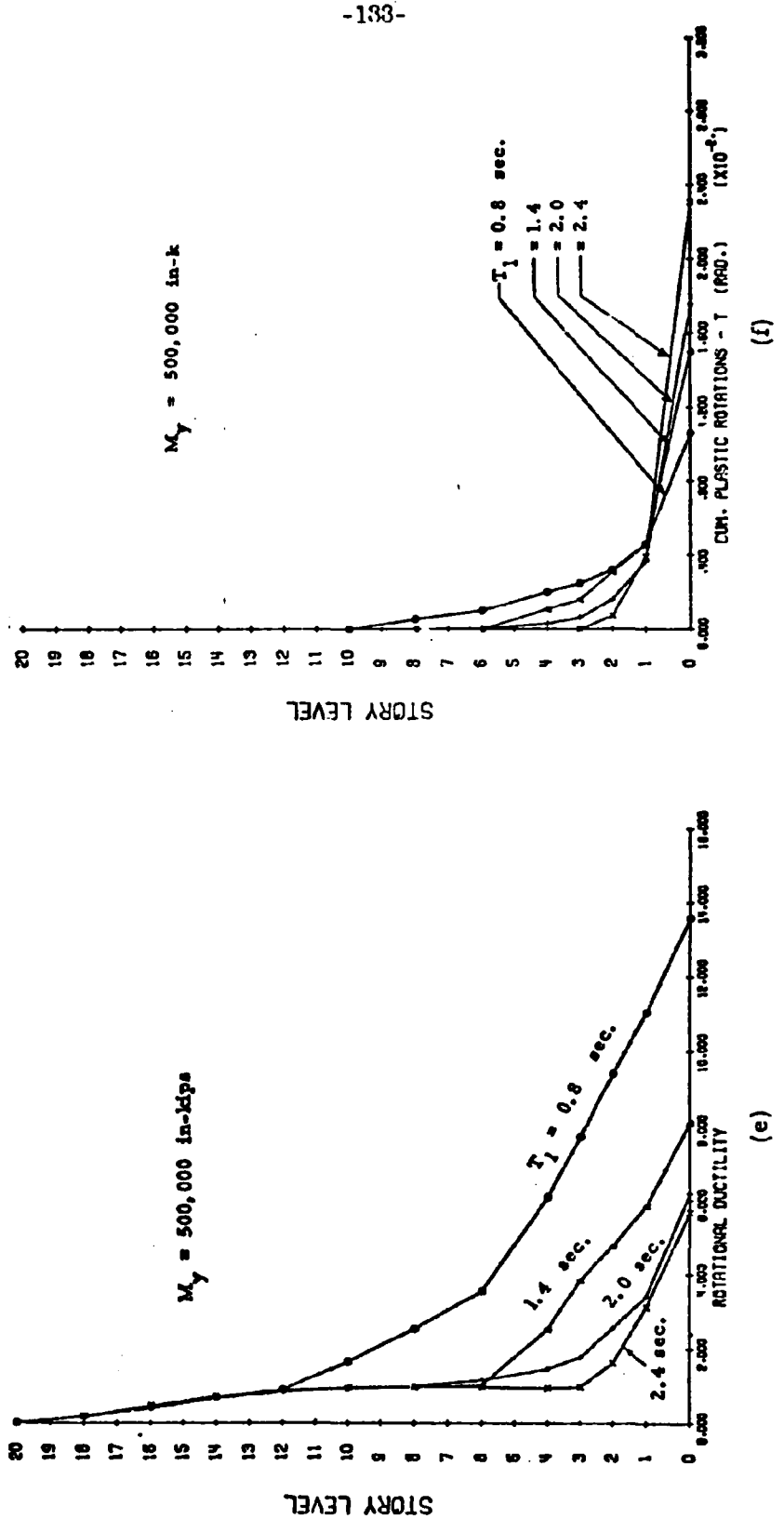

Fig. 36 (contd.) Effect of Fundamental Period of Vibration, T_1

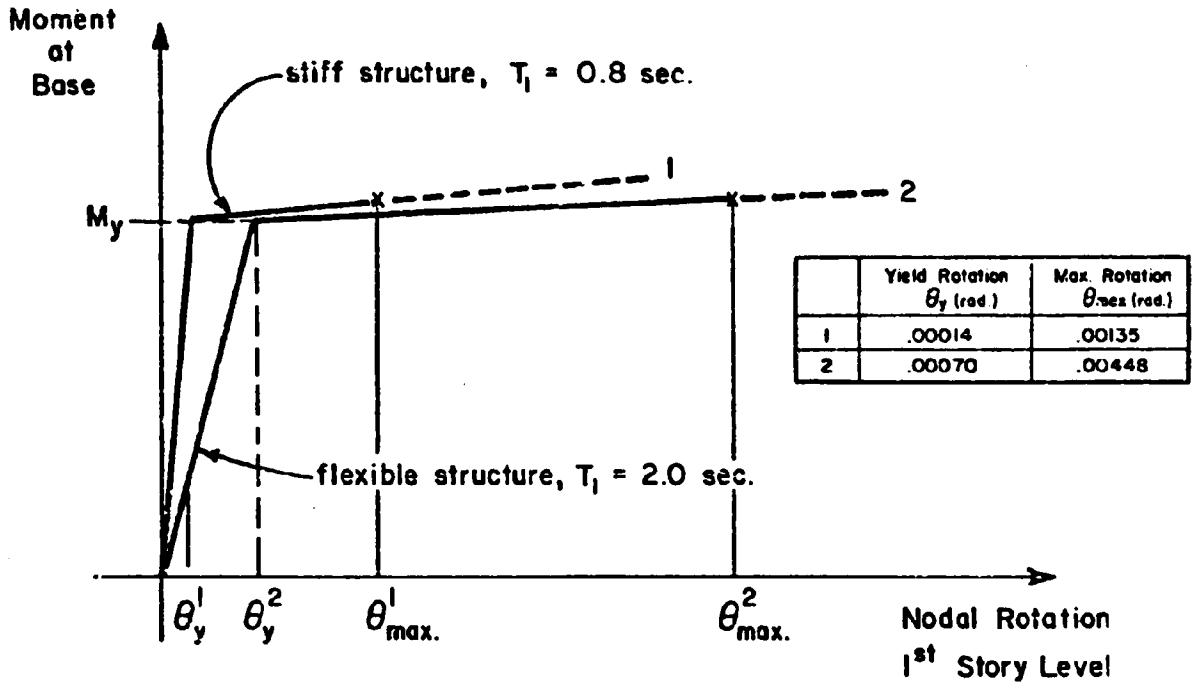

	Yield Rotation θ_y (rad.)	Max. Rotation θ_{max} (rad.)
1	.00014	.00135
2	.00070	.00448

MEASURES OF DEFORMATION

Ductility Ratio vs. **Absolute Rotations**

$$\mu_1 = \frac{\theta_{max.}^1}{\theta_y^1} = 9.6$$

$$\mu_2 = \frac{\theta_{max.}^2}{\theta_y^2} = 6.4$$

but note that:

$$\theta_{max.}^2 = 3.3\,\theta_{max.}^1$$

Fig. 37 Rotational Ductility Ratio vs. Maximum Absolute Rotation as Measures of Deformation Requirements

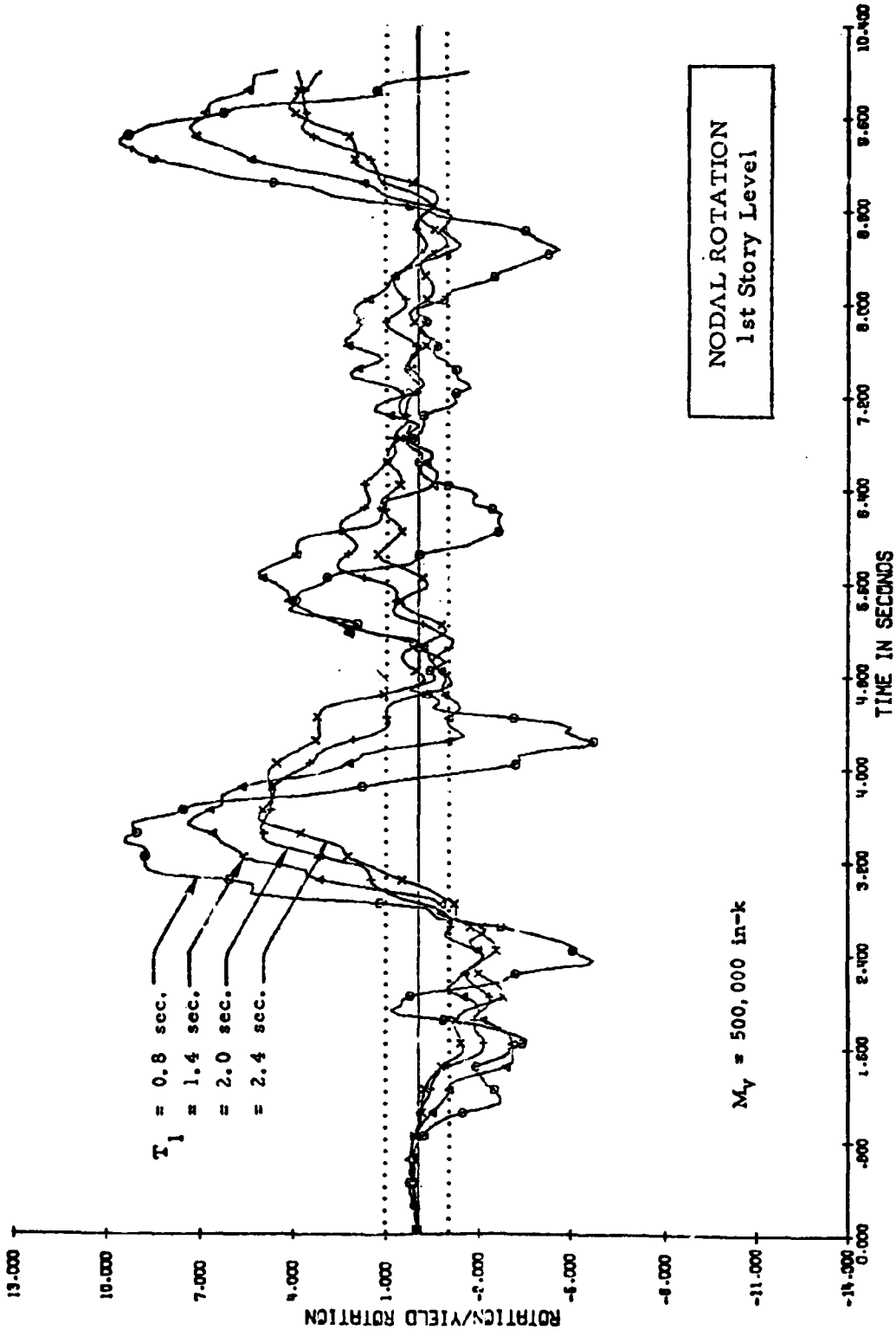

Fig. 38 (a) Normalized Rotations in First Story vs. Time for Different Values of Fundamental Period, T_1

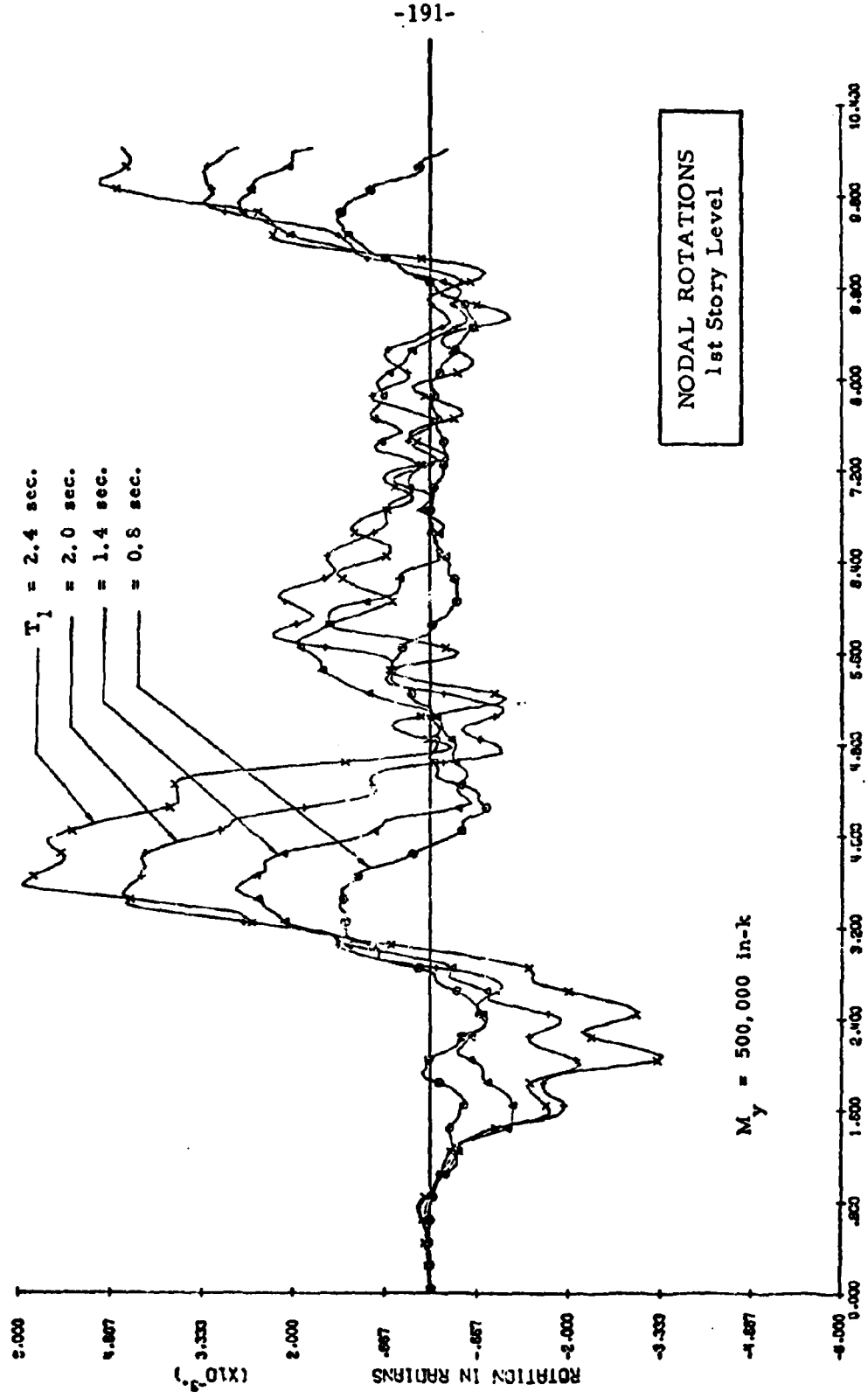

Fig. 38(b) Actual Values of Rotation in First Story vs. Time for Different Values of Fundamental Period, T_1

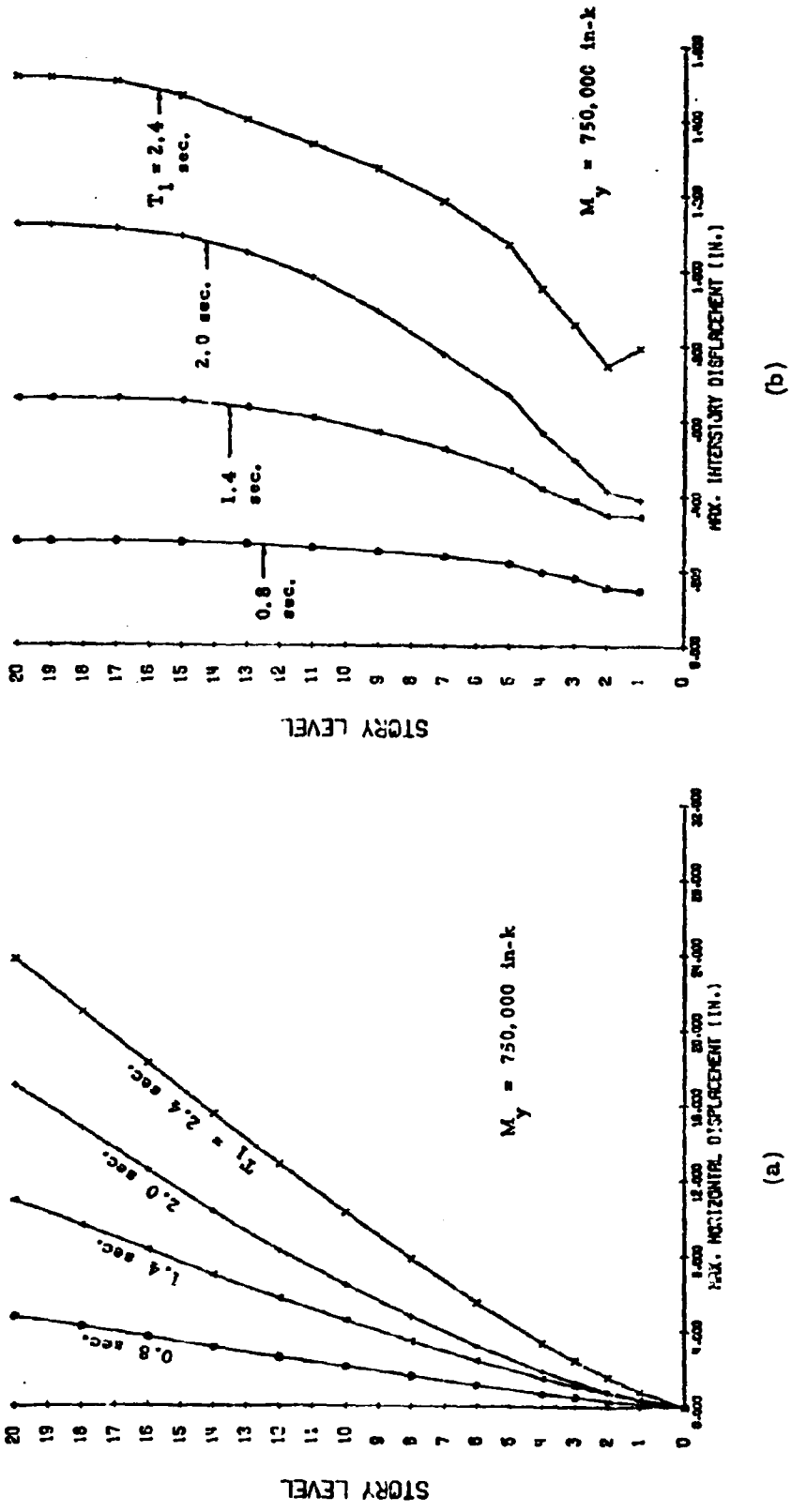

Fig. 39 Effect of Fundamental Period of Vibration, T_1

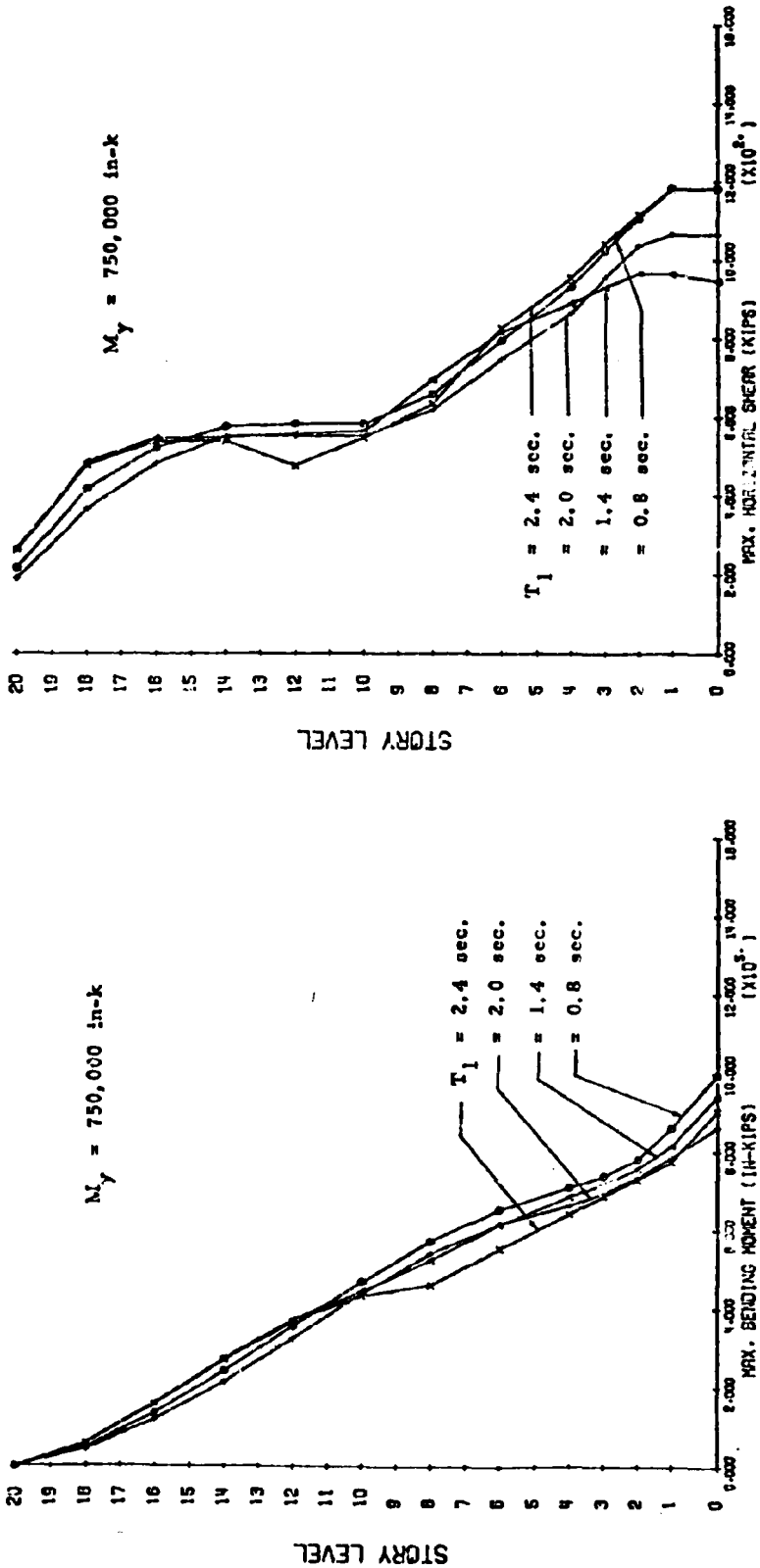

Fig. 39 (contd.) Effect of Fundamental Period of Vibration, T_1

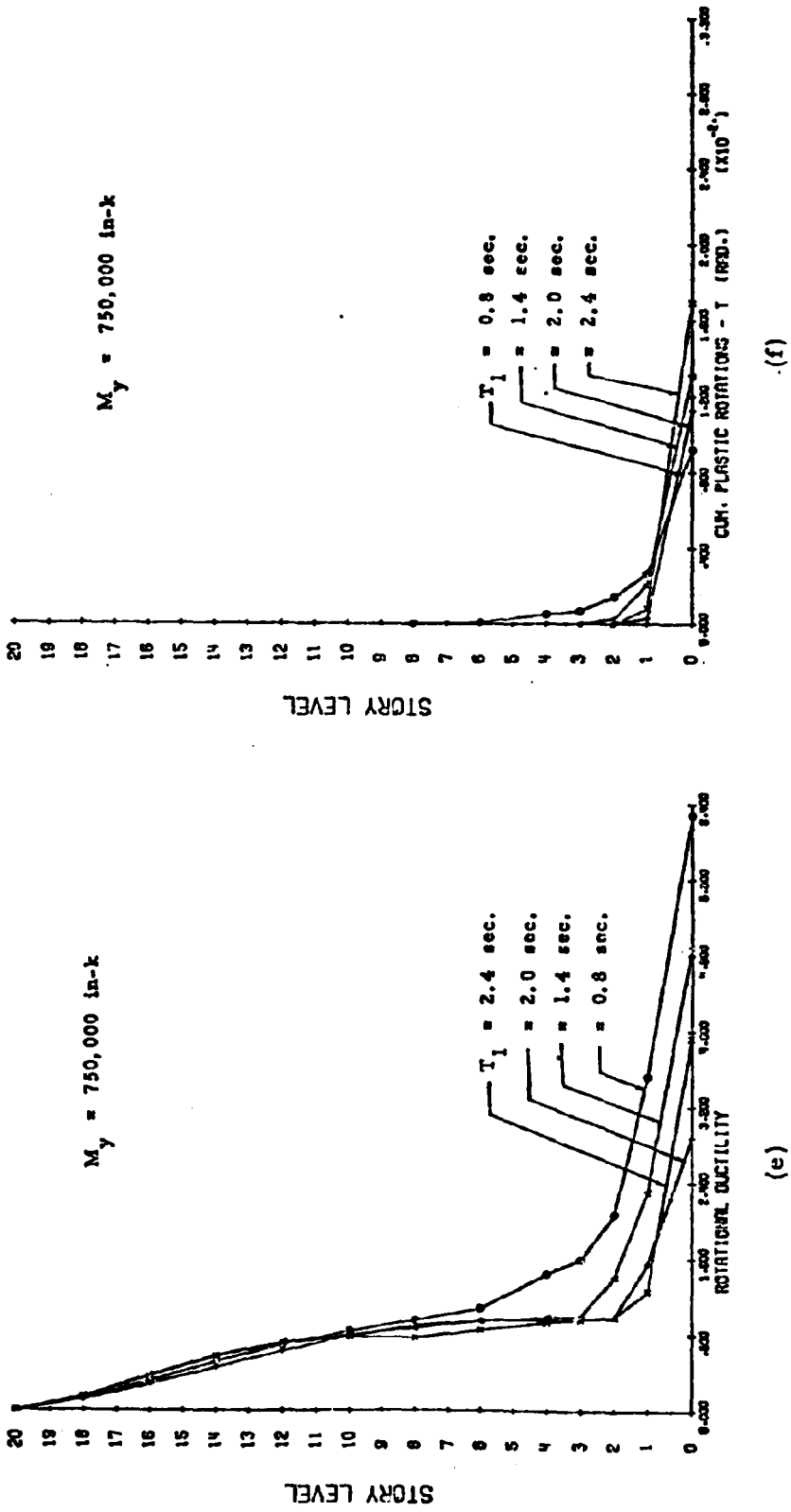

Fig. 39 (contd.) Effect of Fundamental Period of Vibration, T_1

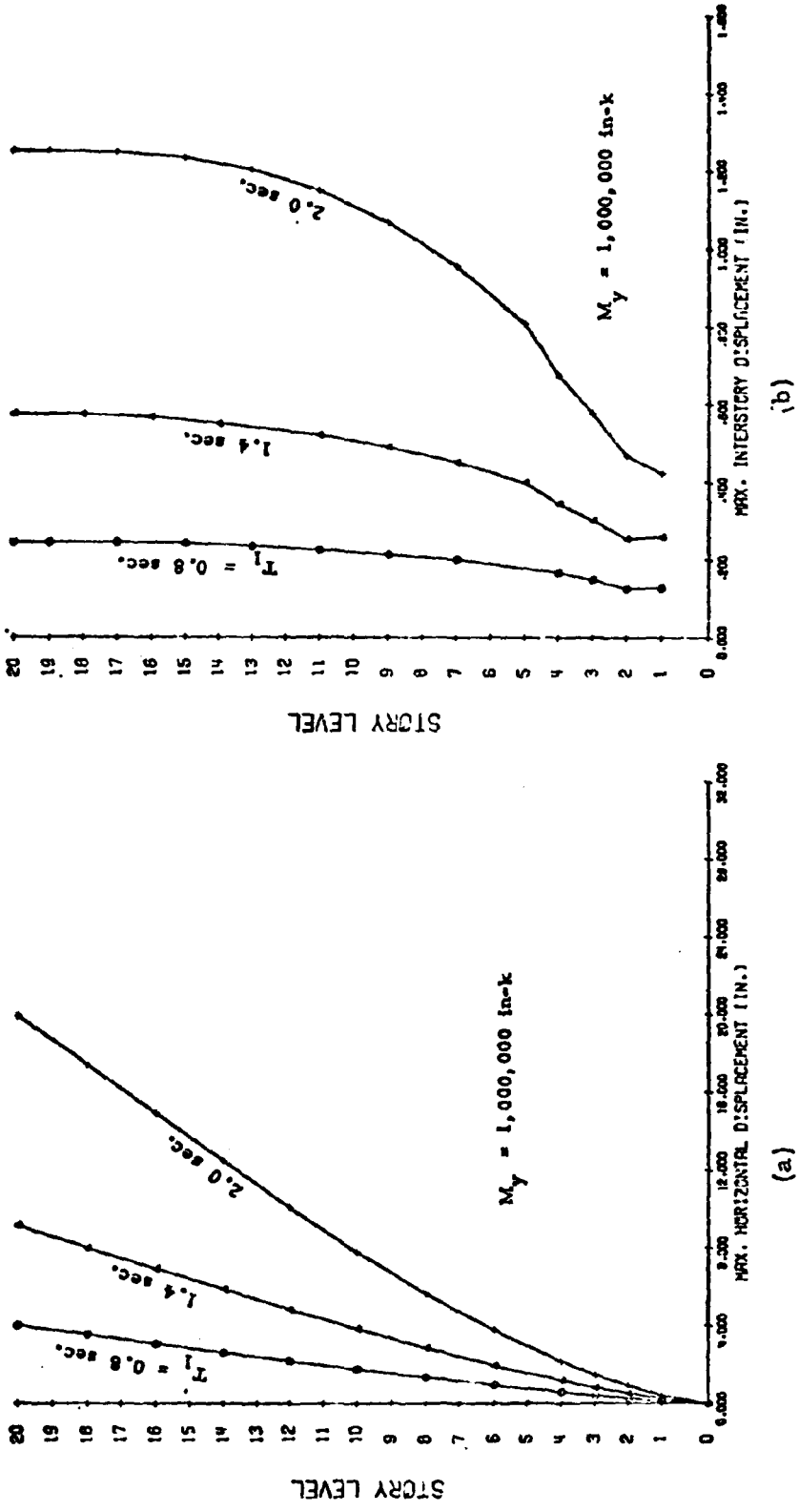

Fig. 40 Effect of Fundamental Period of Vibration, T_1

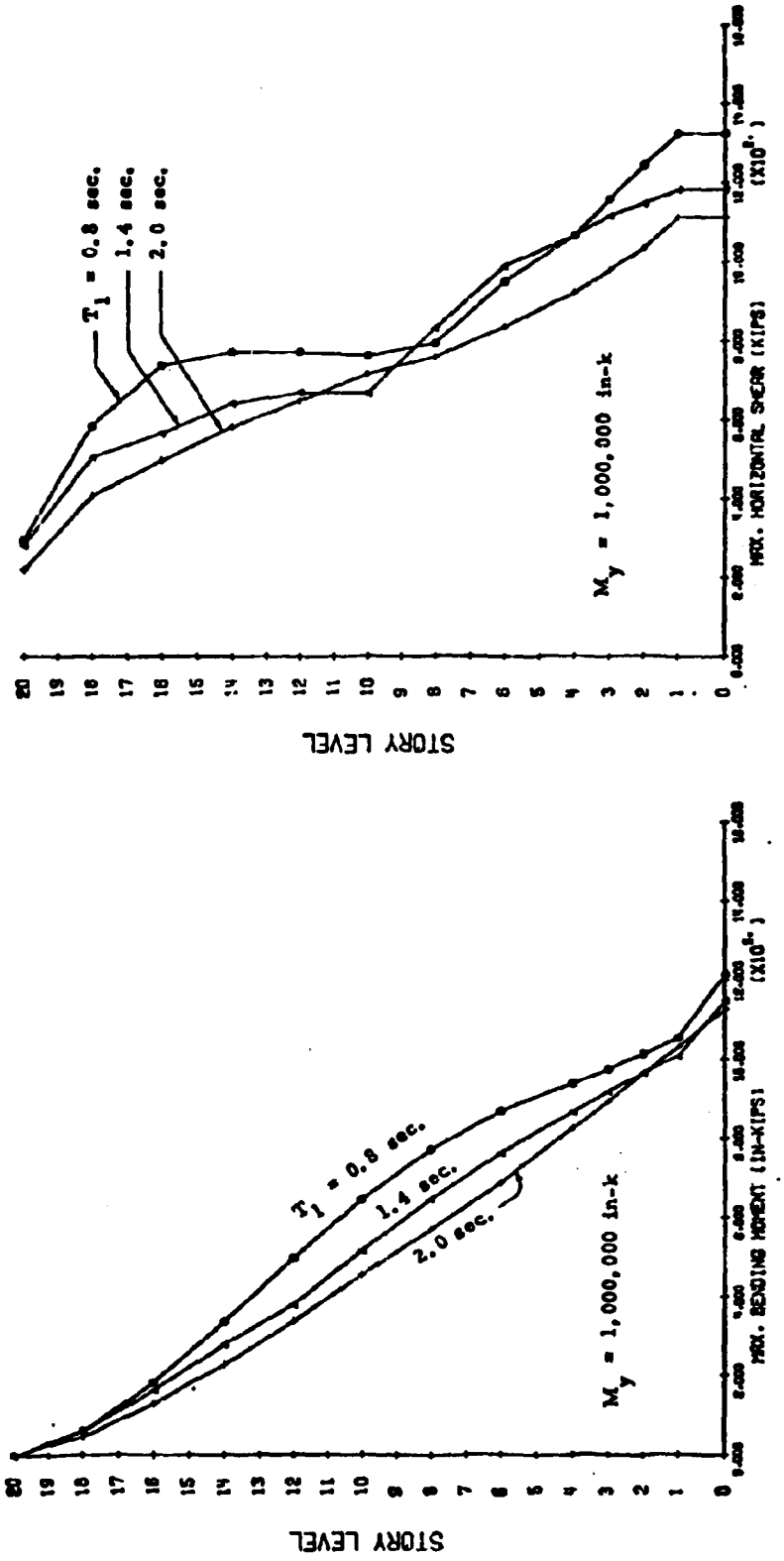

Fig. 40 (contd.) Effect of Fundamental Period of Vibration, T_1

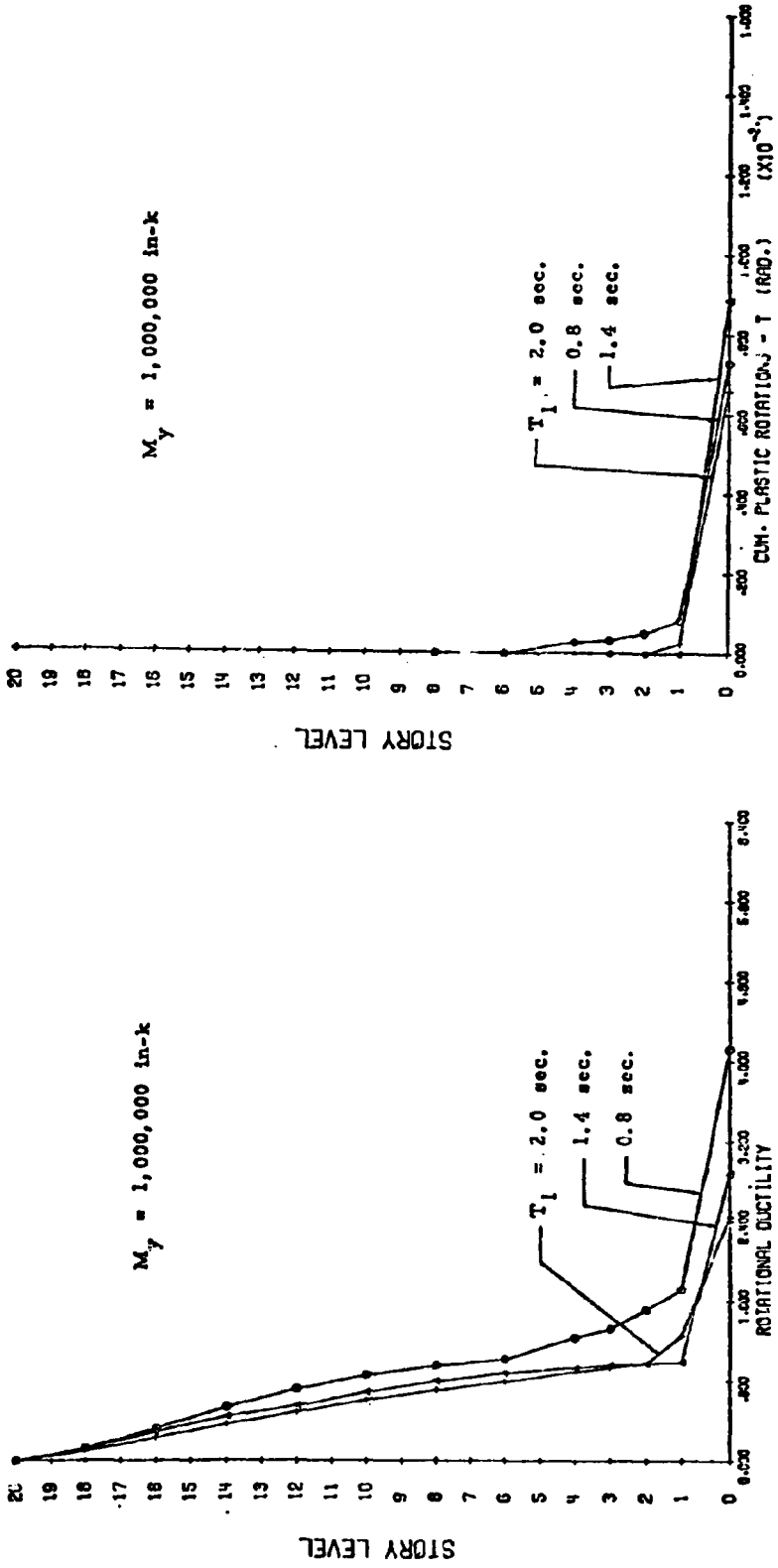

Fig. 40 (contd.) Effect of Fundamental Period of Vibration, T_1

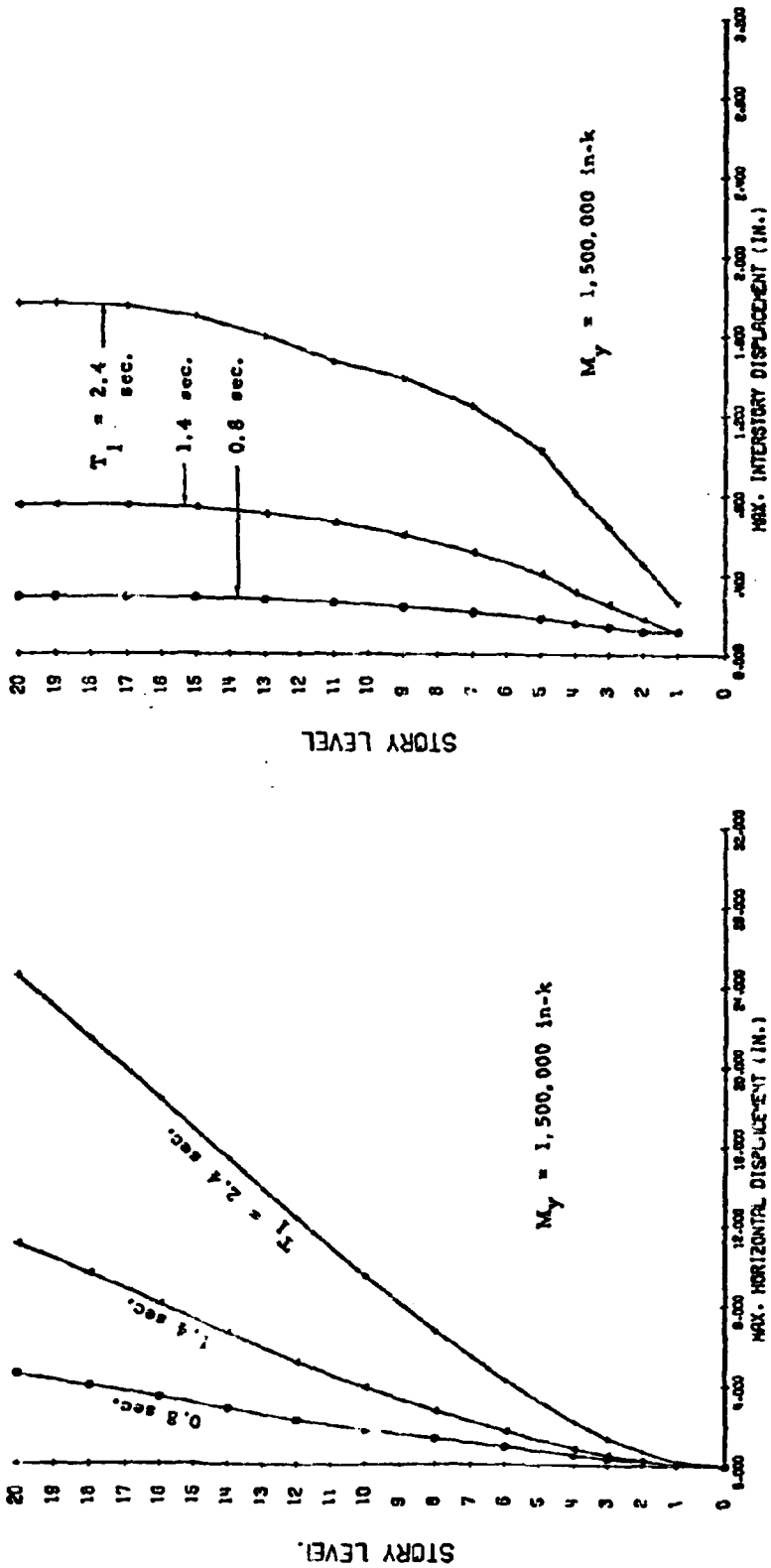

Fig. 41 Effect of Fundamental Period of Vibration, T_1

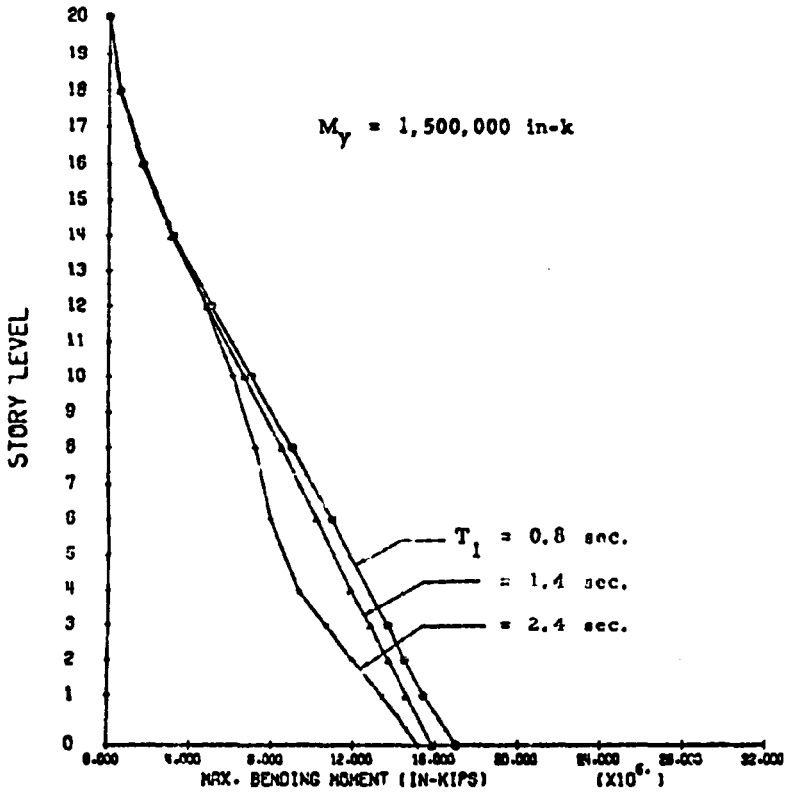

(c)

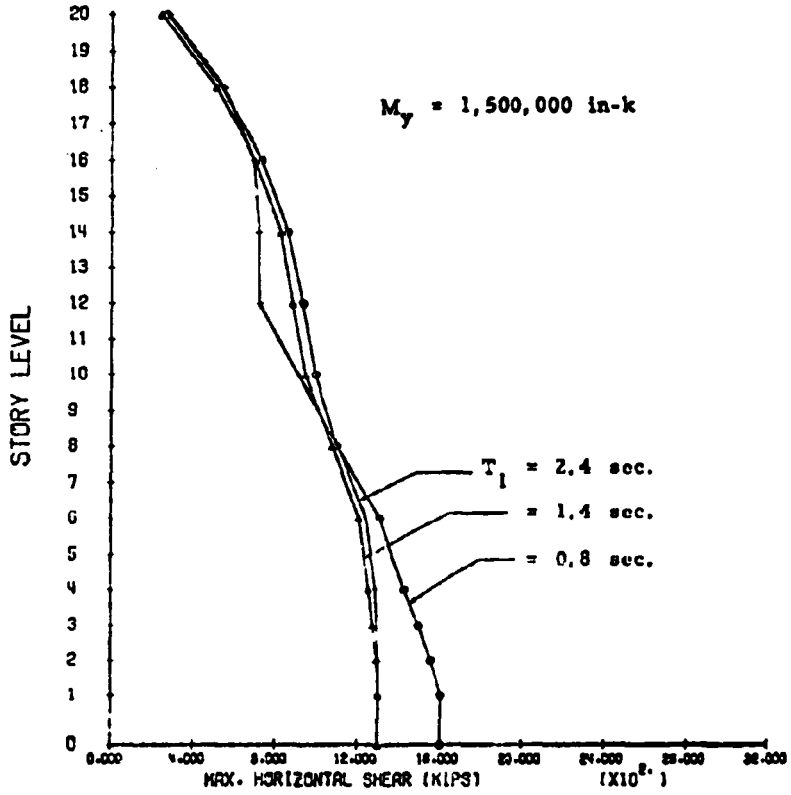

(d)

Fig. 41 (contd.) Effect of Fundamental Period of Vibration, T_1

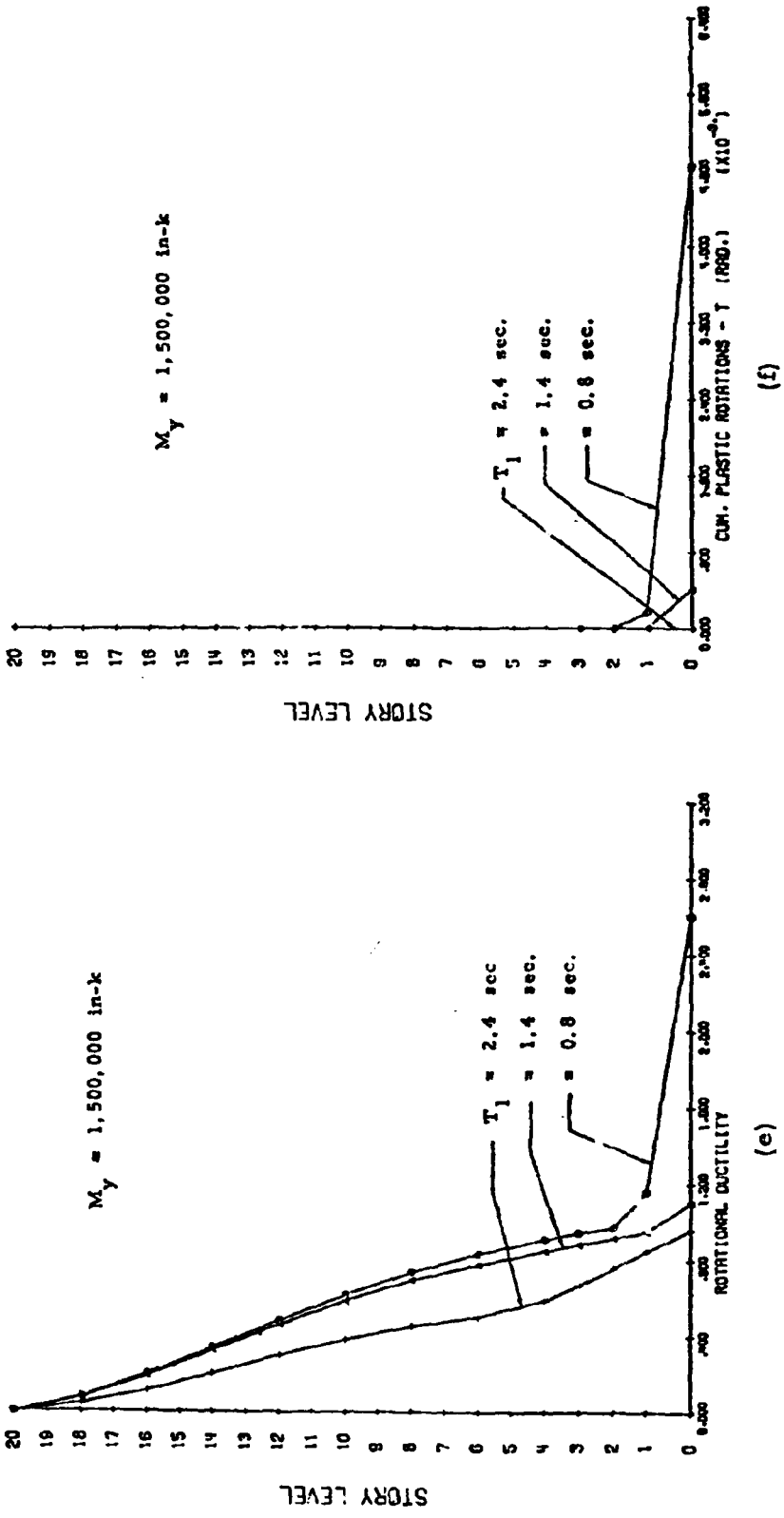

Fig. 41 (contd.) Effect of Fundamental Period of Vibration, T_1

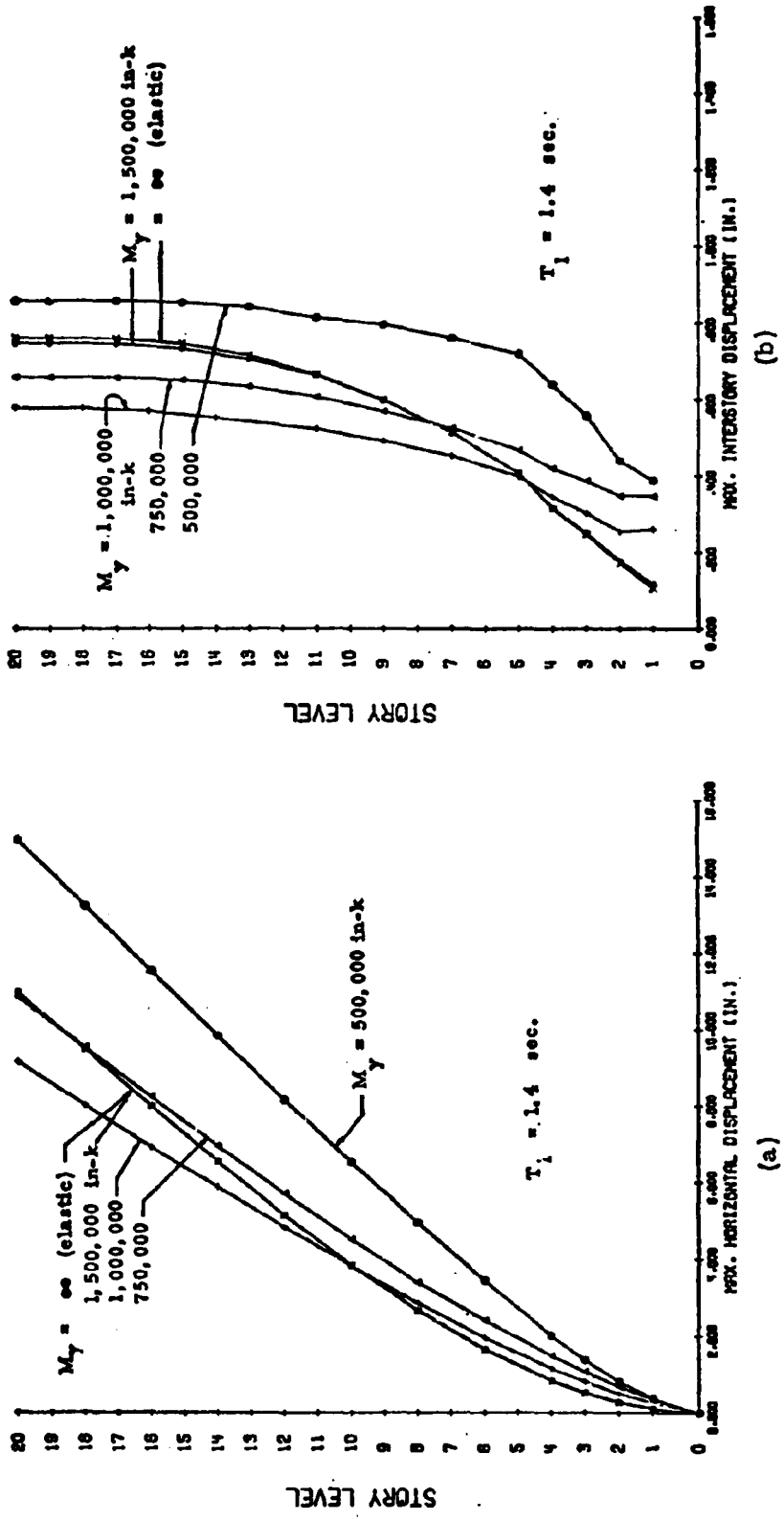

Fig. 42 Effect of Yield Level, M_y

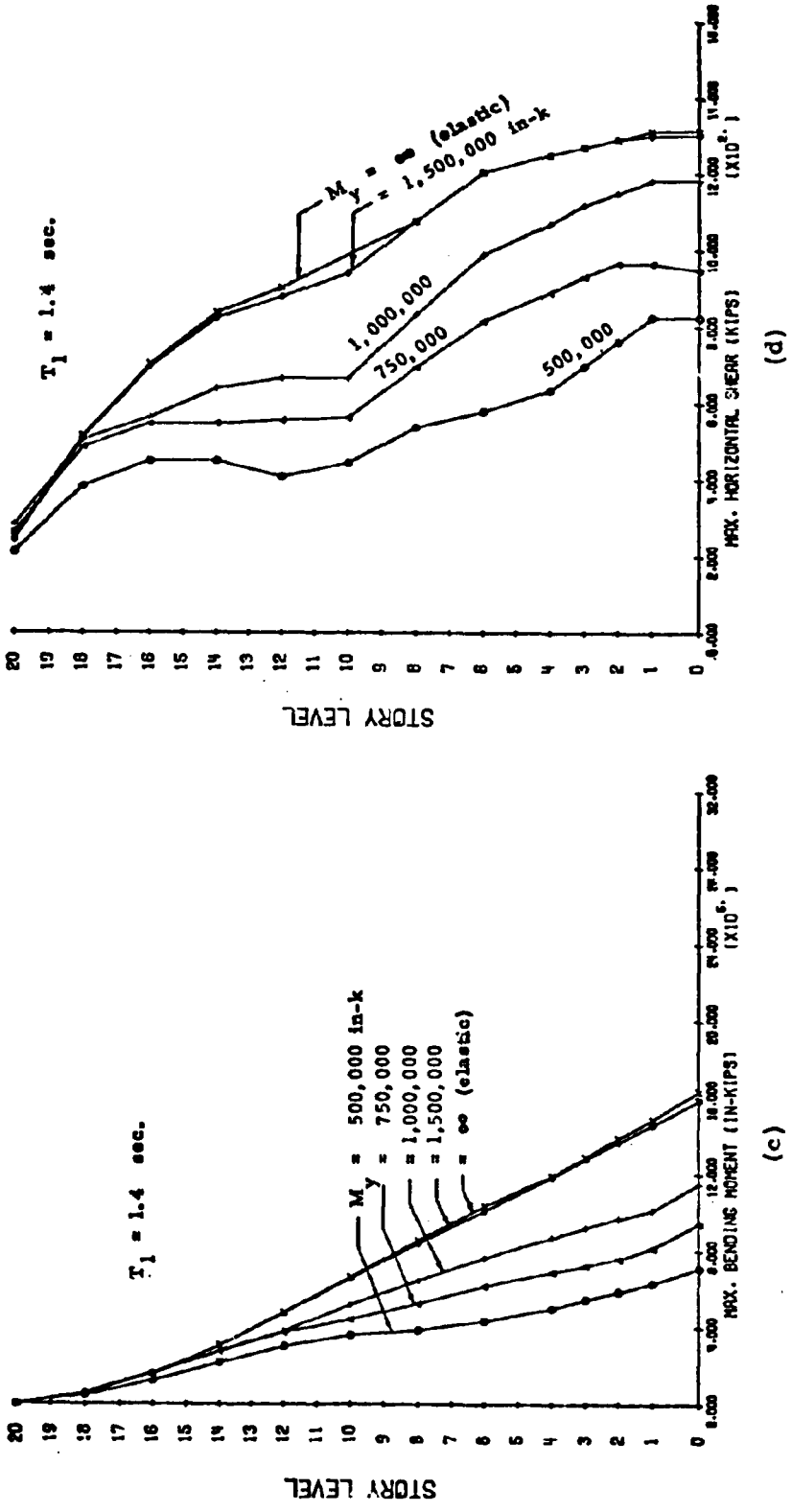

Fig. 42 (contd.) Effect of Yield Level, M_y

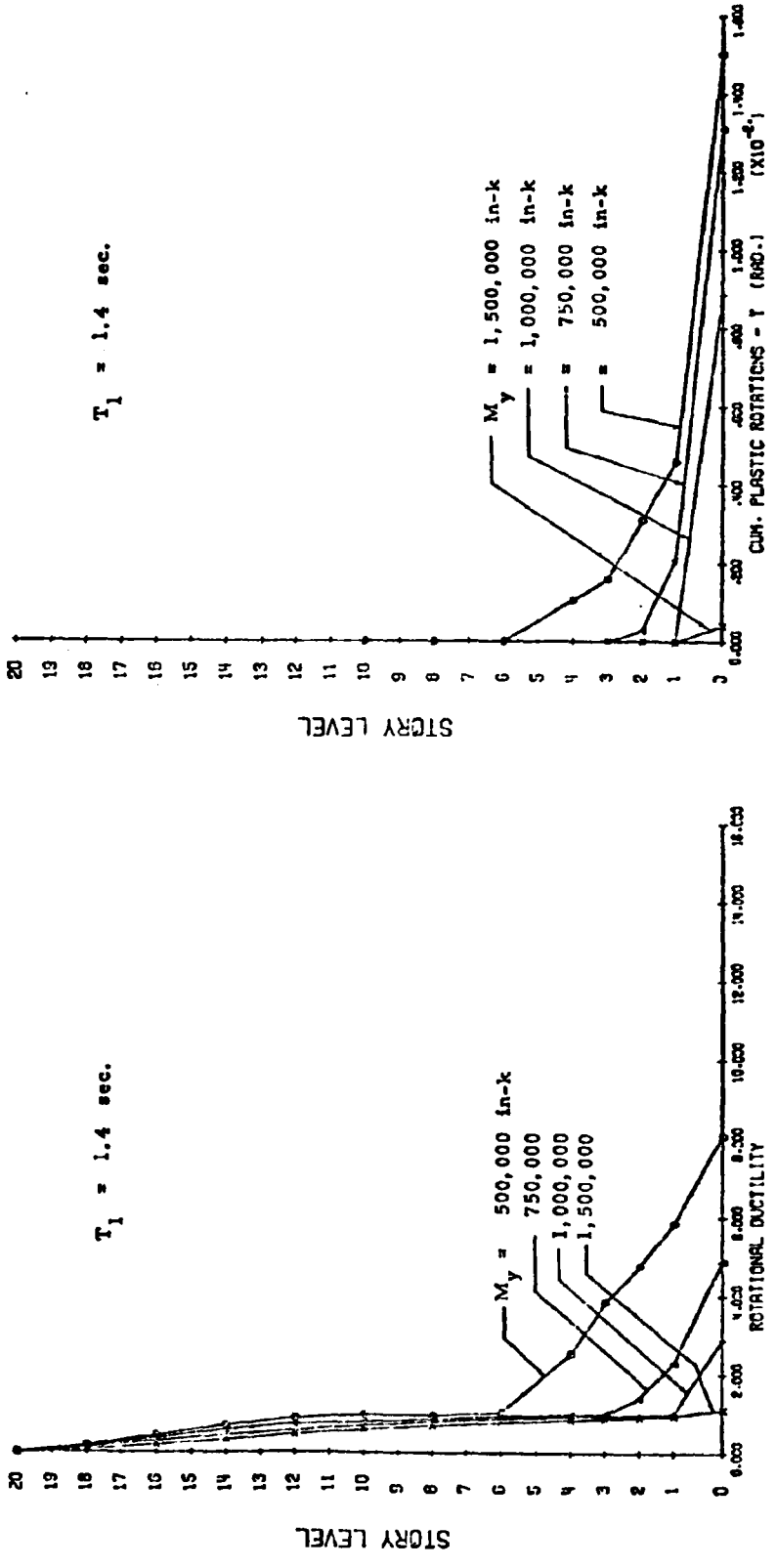

Fig. 42 (contd.) Effect of Yield Level, My

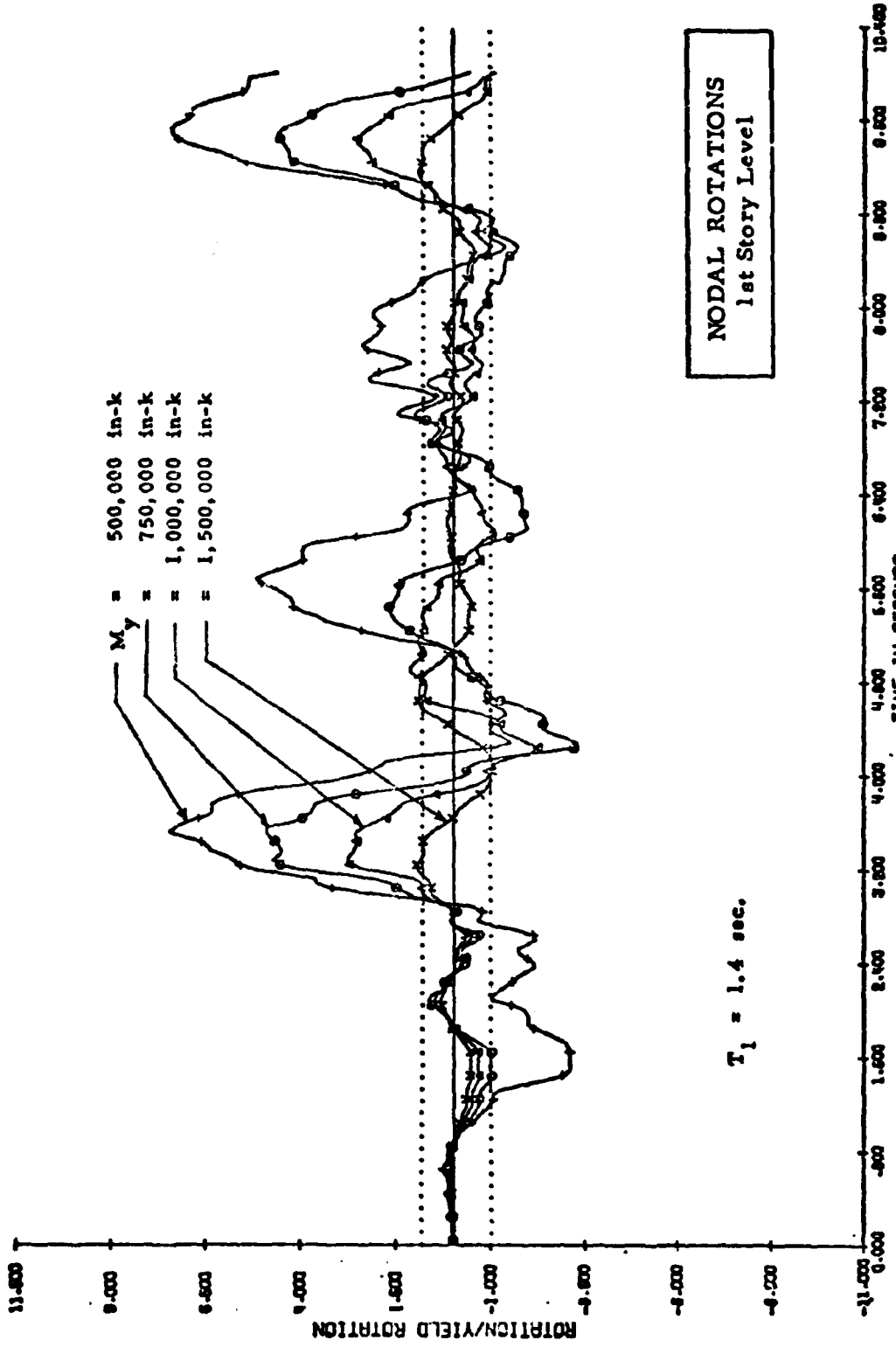

Fig. 43 Rotation in First Story vs. Time for Different Values of Yield Level, M_y

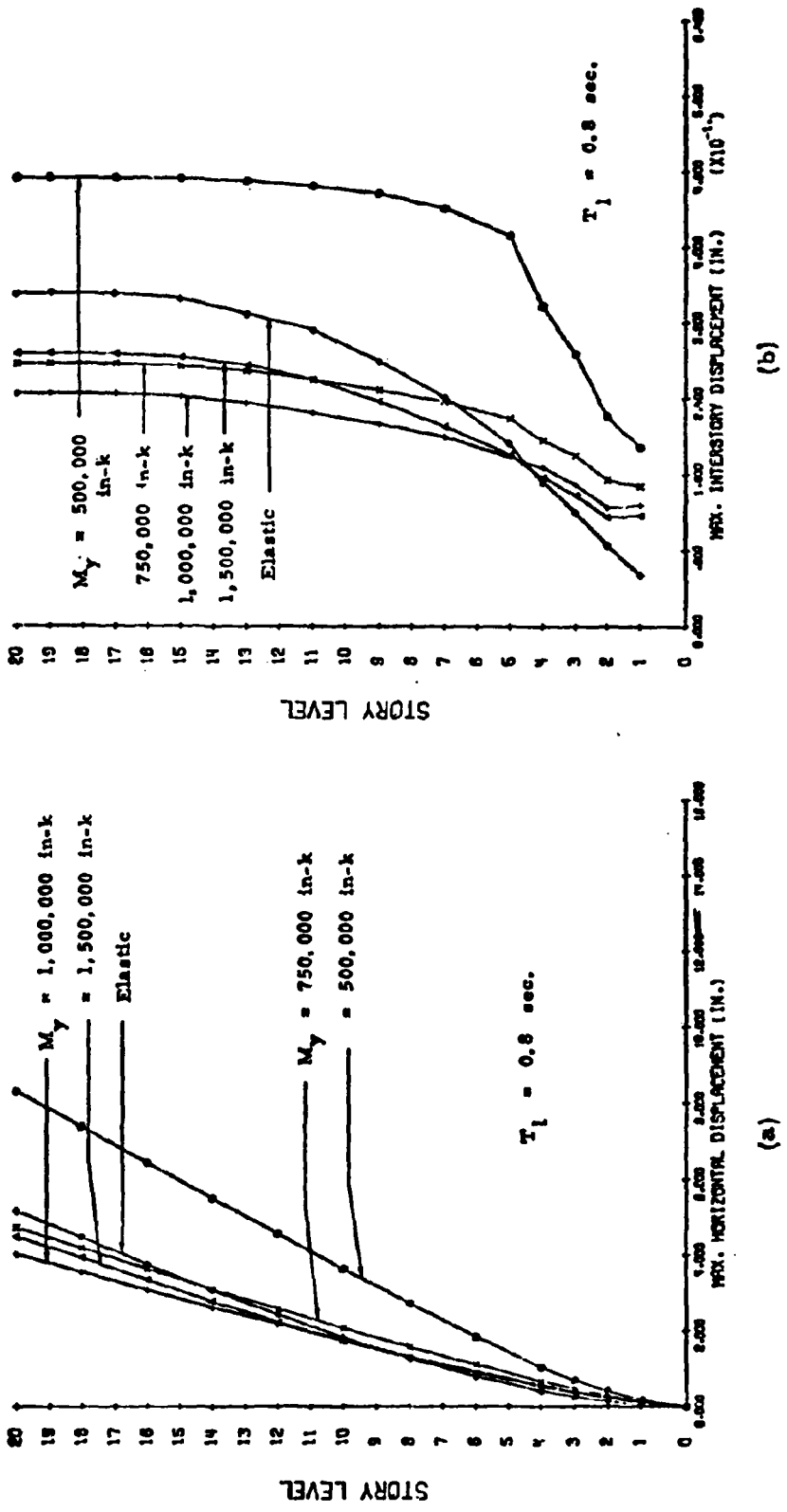

Fig. 44 Effect of Yield Level, M_y

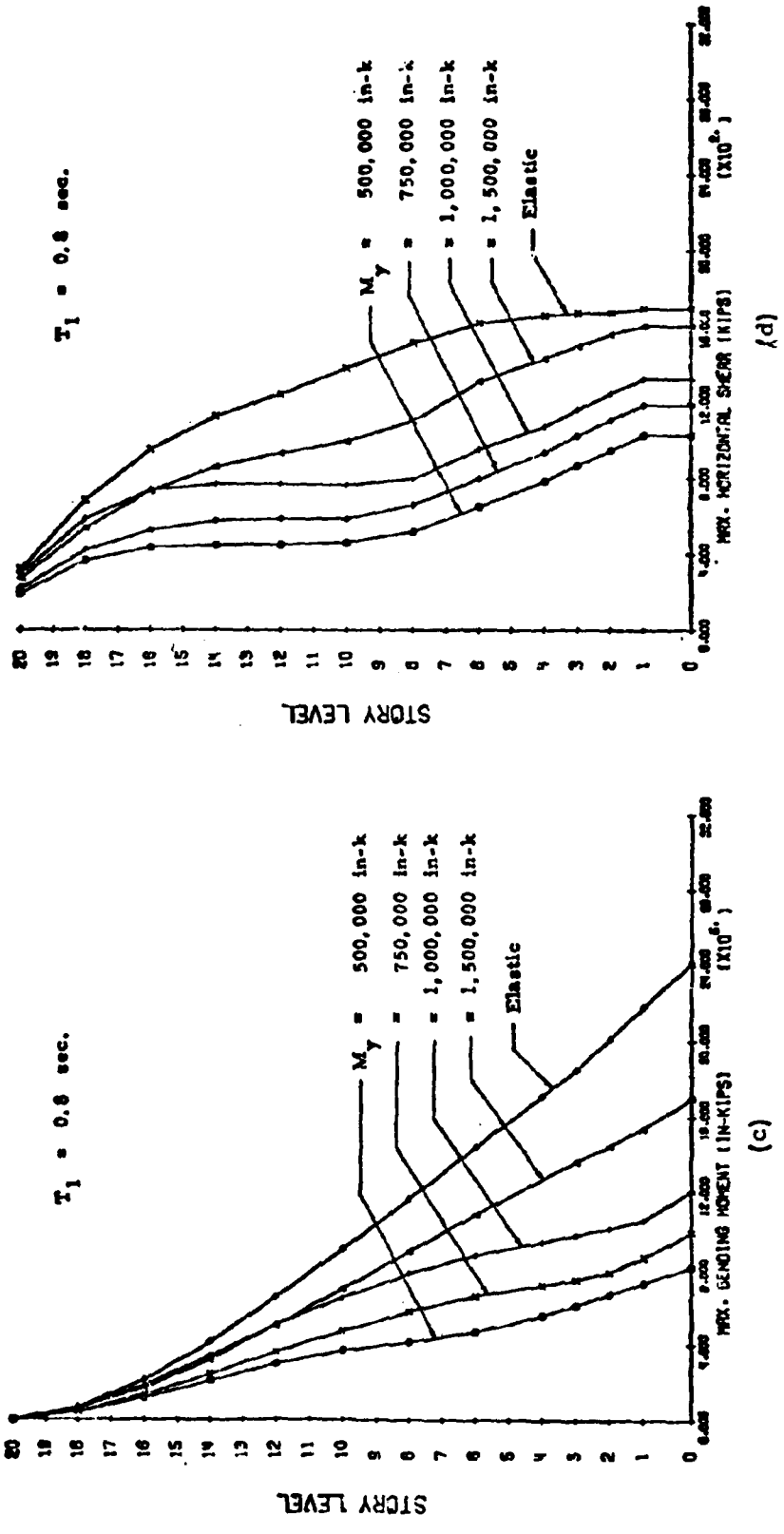

Fig. 44 (contd.) Effect of Yield Level, M_y

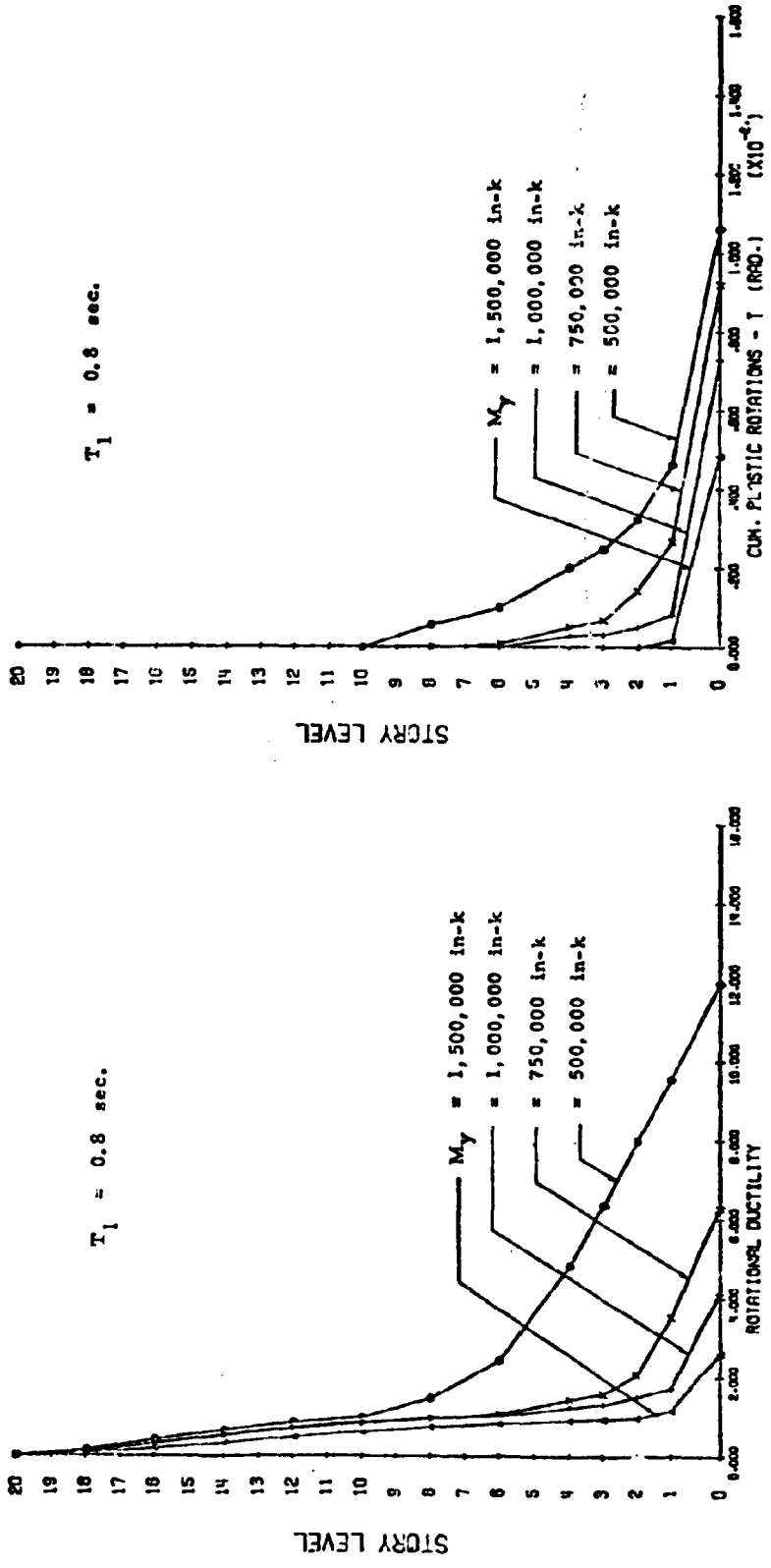

Fig. 44 (contd.) Effect of Yield Level, M_y

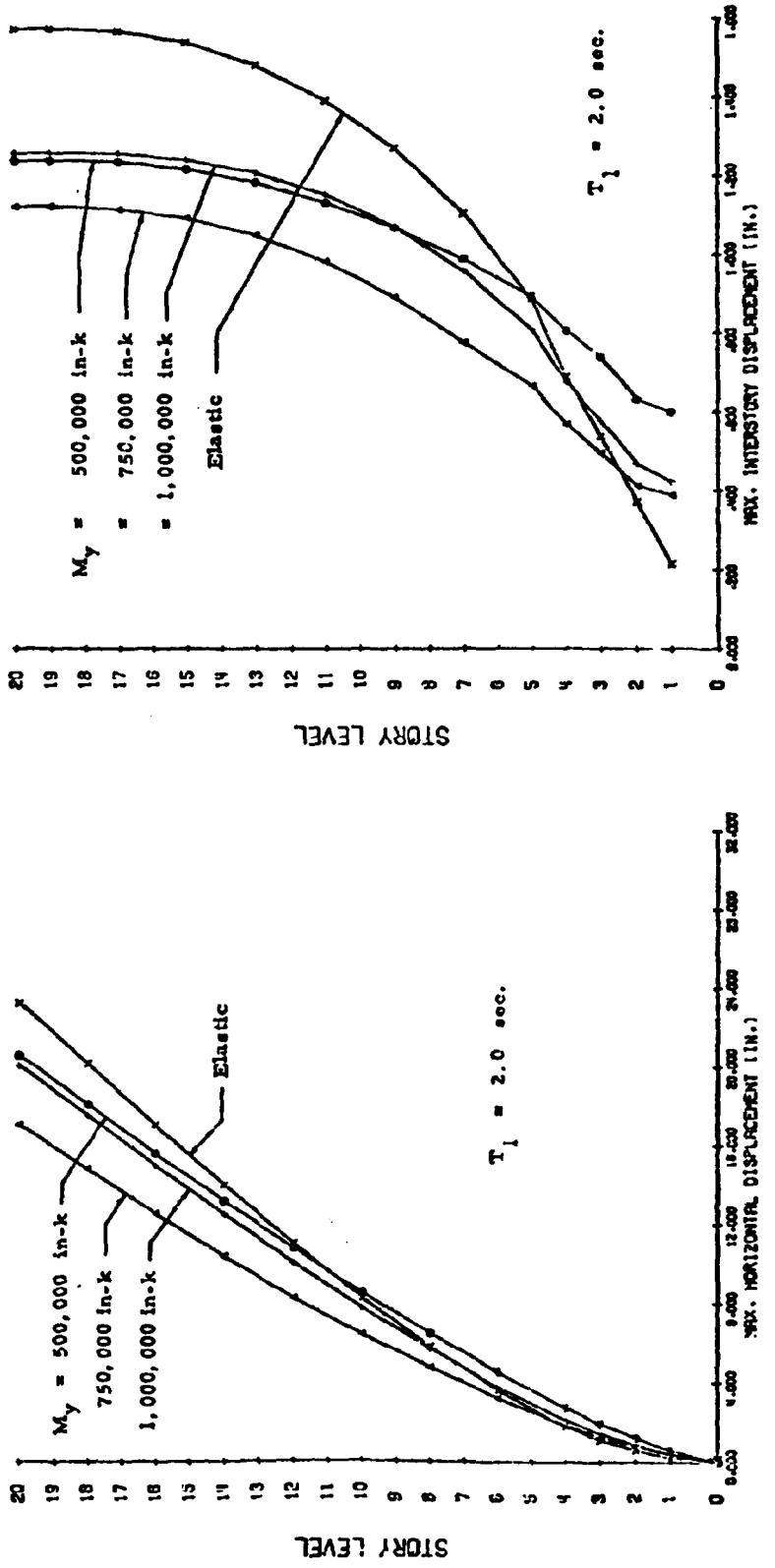

Fig. 45 Effect of Yield Level, M_y

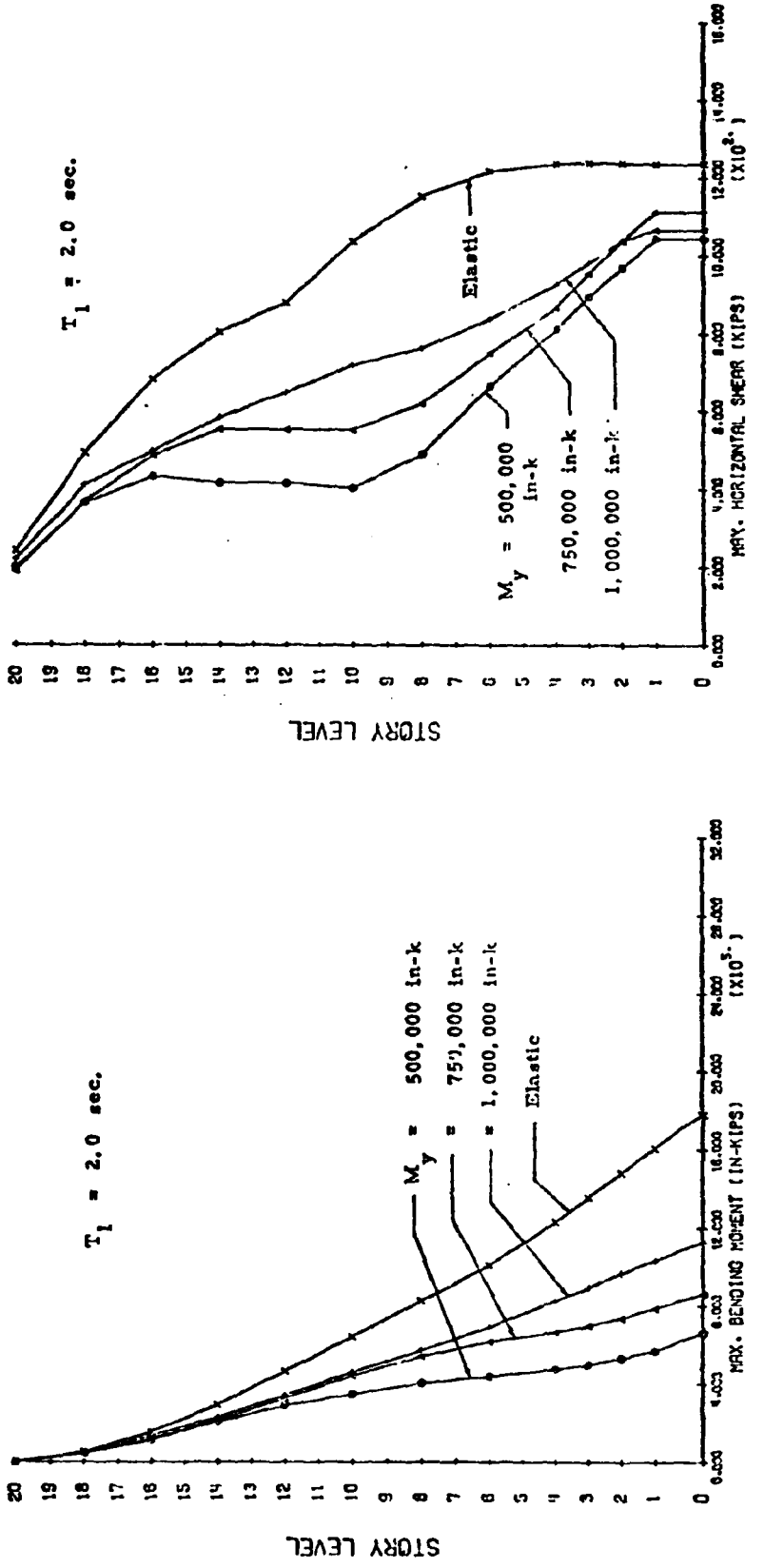

Fig. 45 (contd.) Effect of Yield Level, M_y

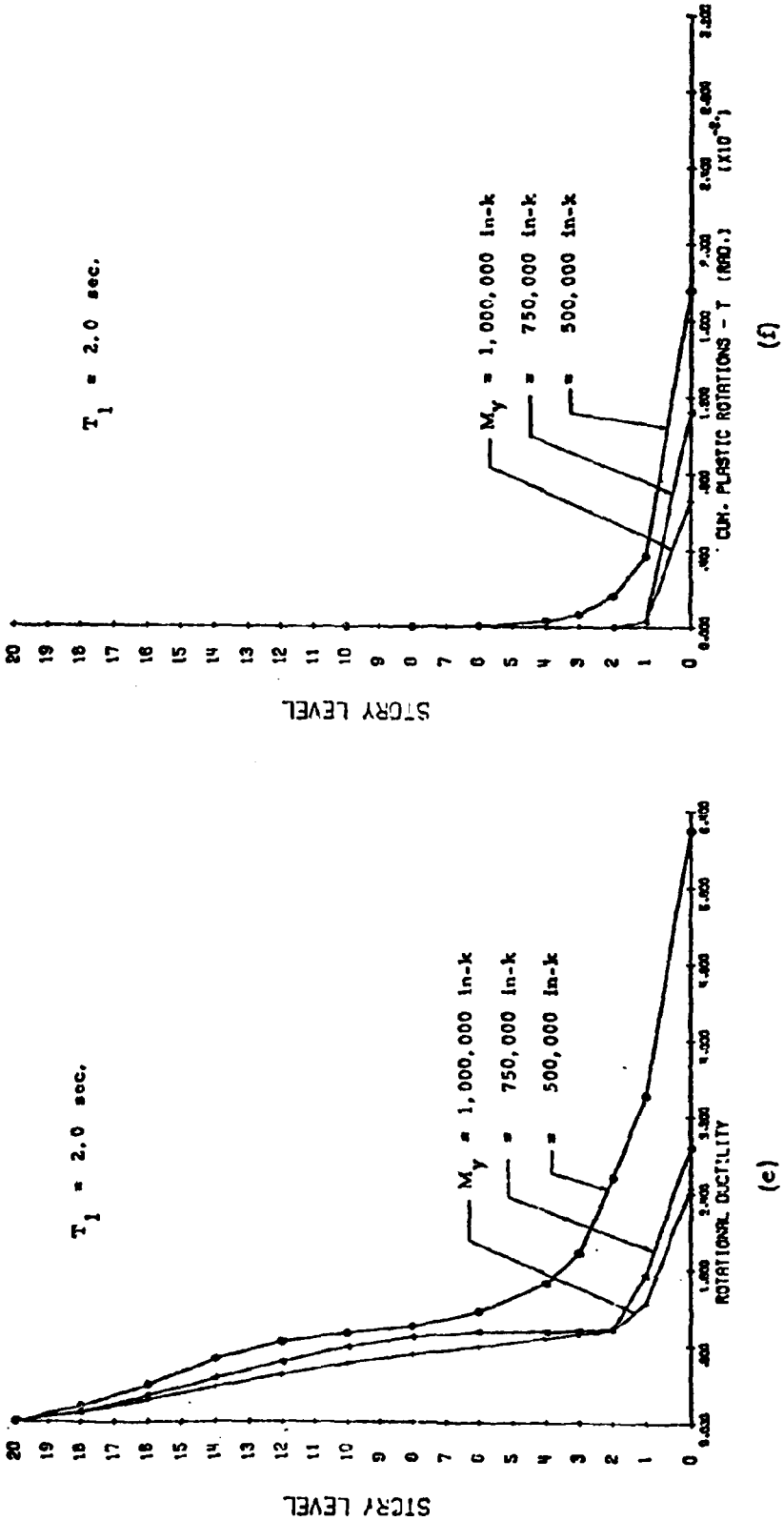

Fig. 45 (contd.) Effect of Yield Level, M_y

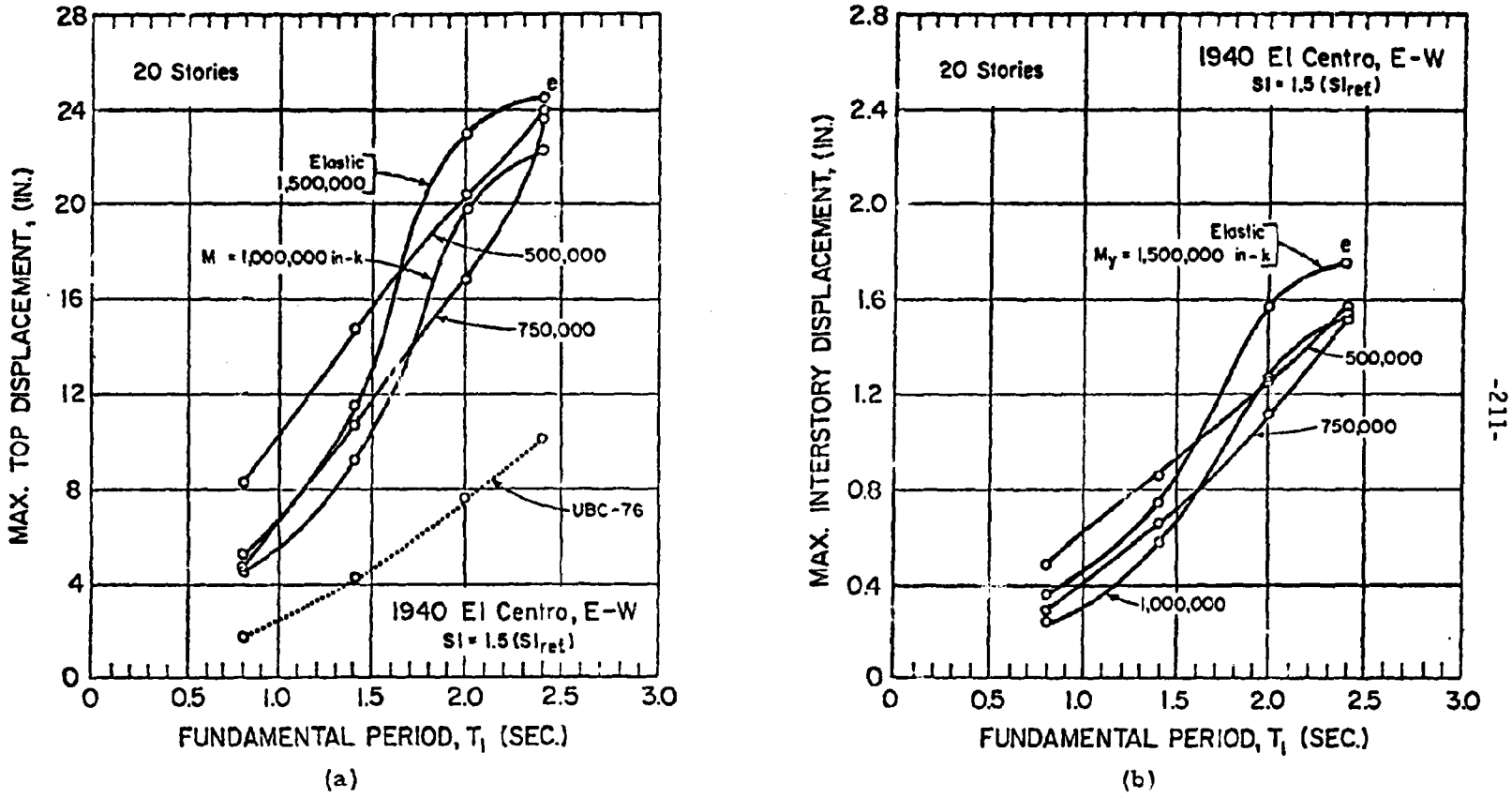

Fig. 46 Interactive Effects of Fundamental Period, T_1, and Yield Level, M_y, on Maximum Response

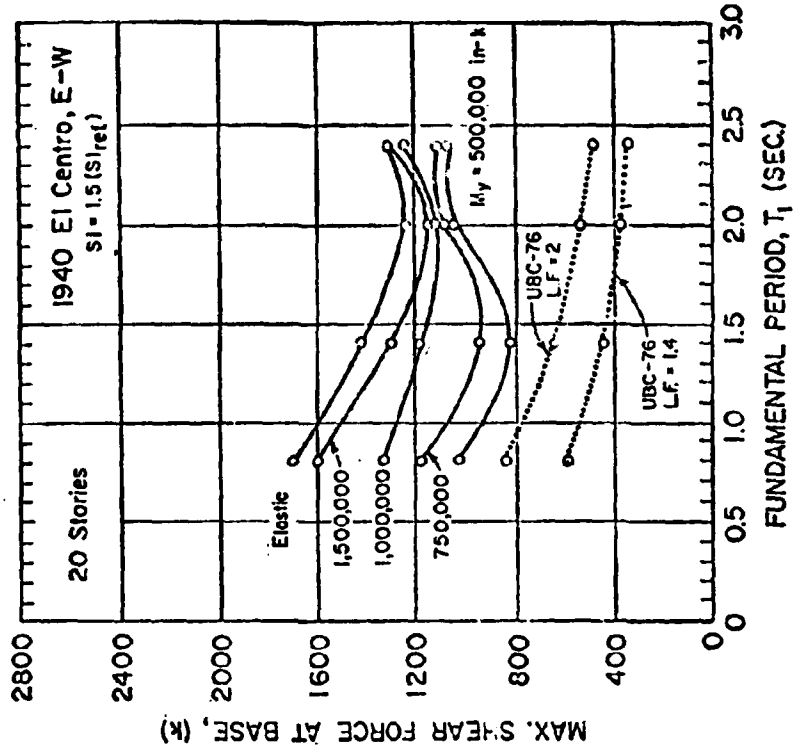

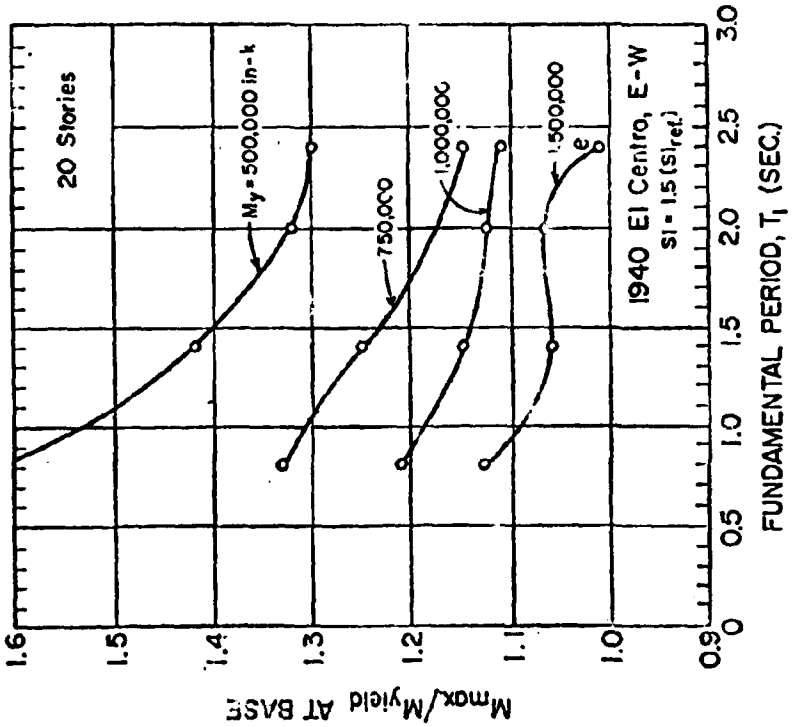

Fig. 46 (contd.) **Interactive Effects of Fundamental Period, T_1 and Yield Level M_y, on Maximum Response**

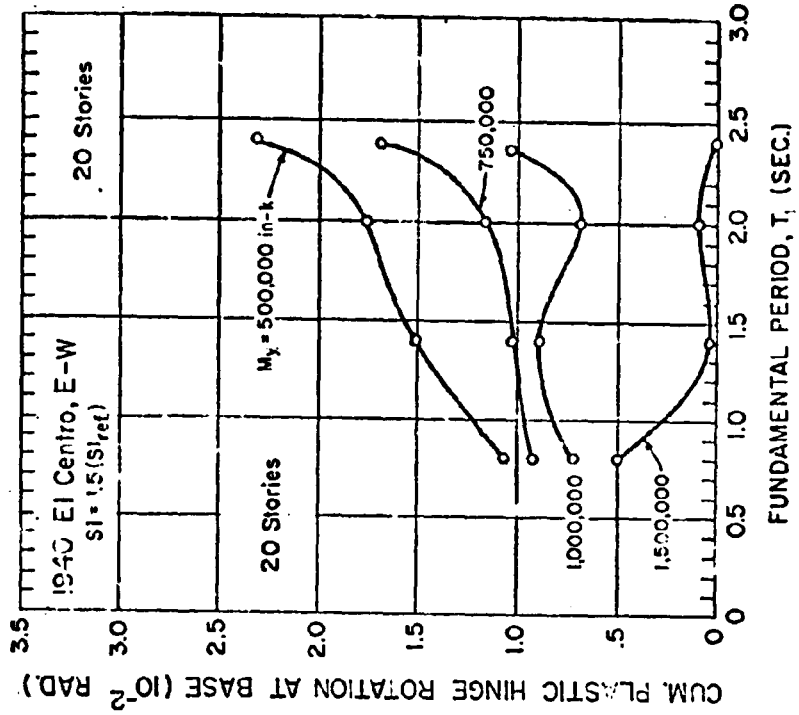

(f)

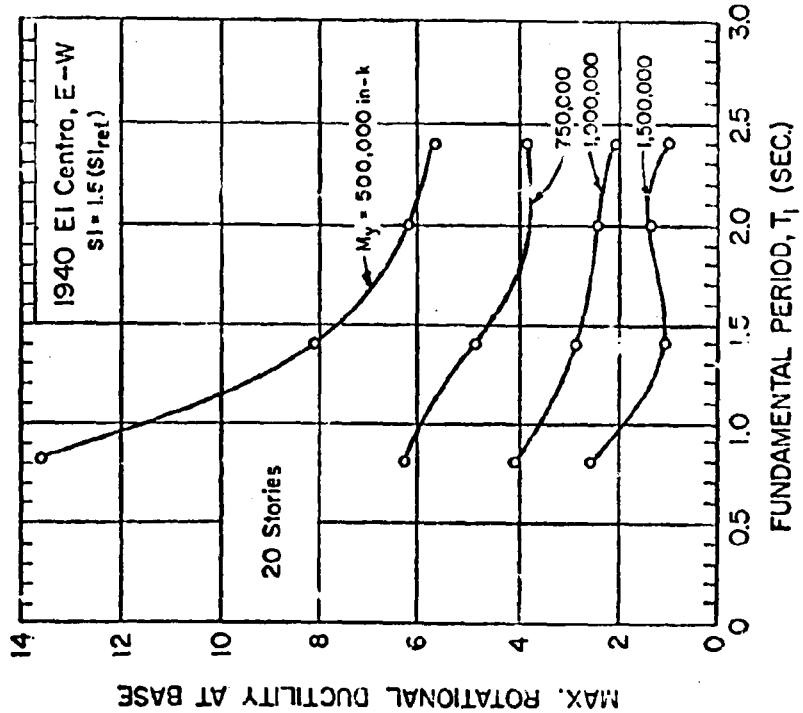

(e)

Fig. 46 (contd.) Interactive Effects of Fundamental Period, T_1 and Yield Level M_y, on Maximum Response

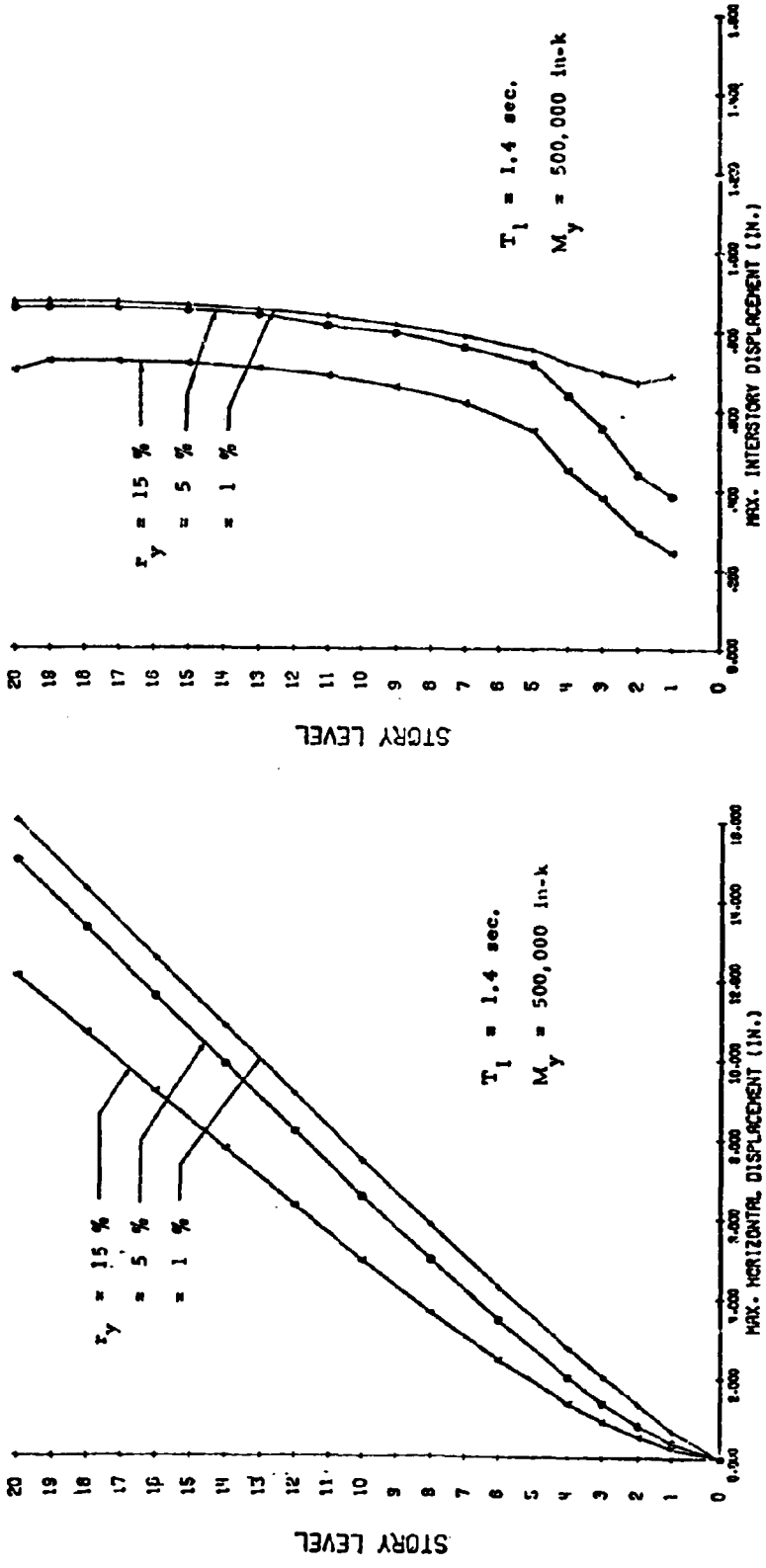

Fig. 47 Effect of Slope of Post-Yield Branch of Moment Rotation Curve

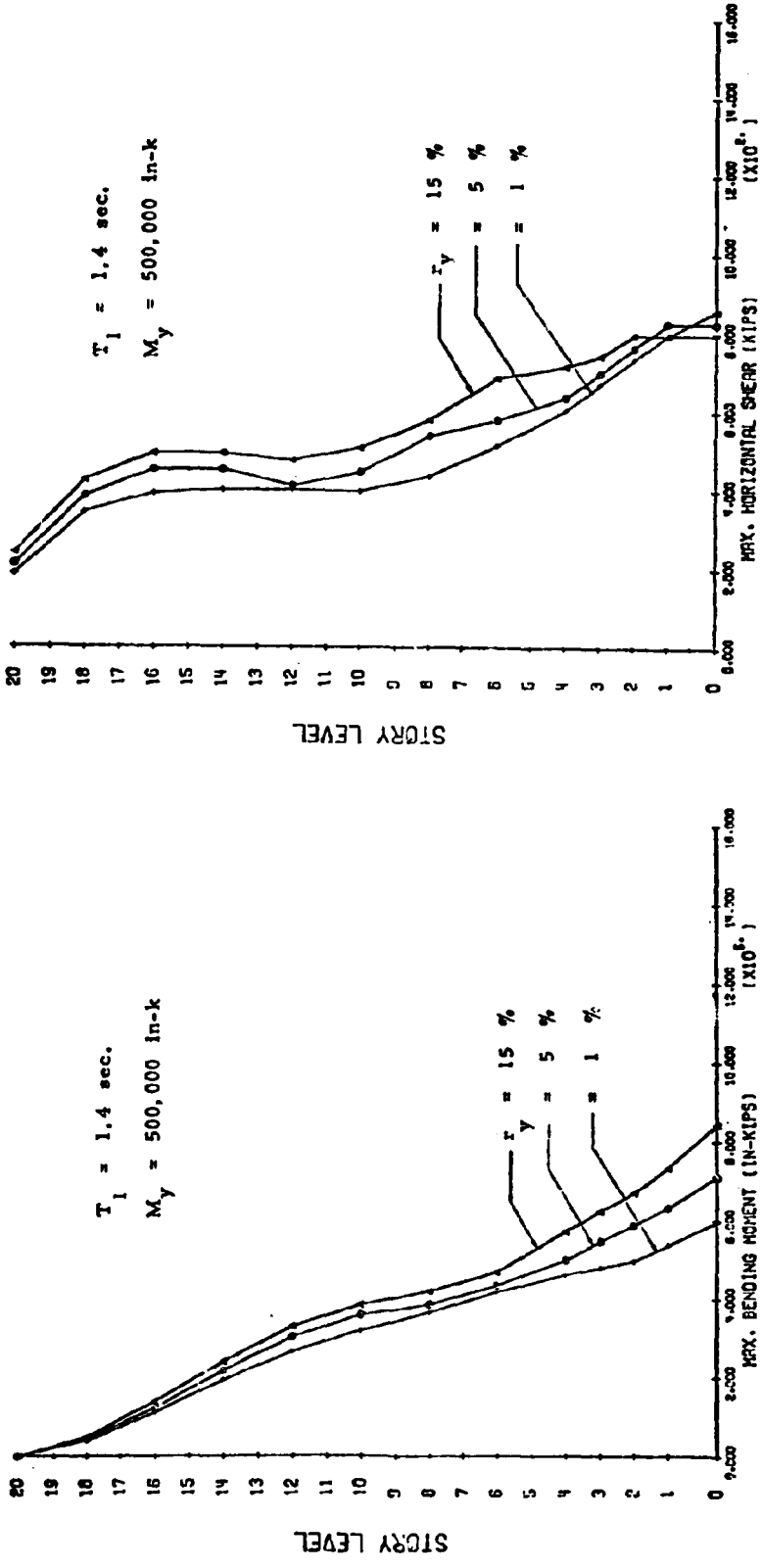

Fig. 47 (contd.) Effect of Slope of Post-Yield Branch of Moment Rotation Curve

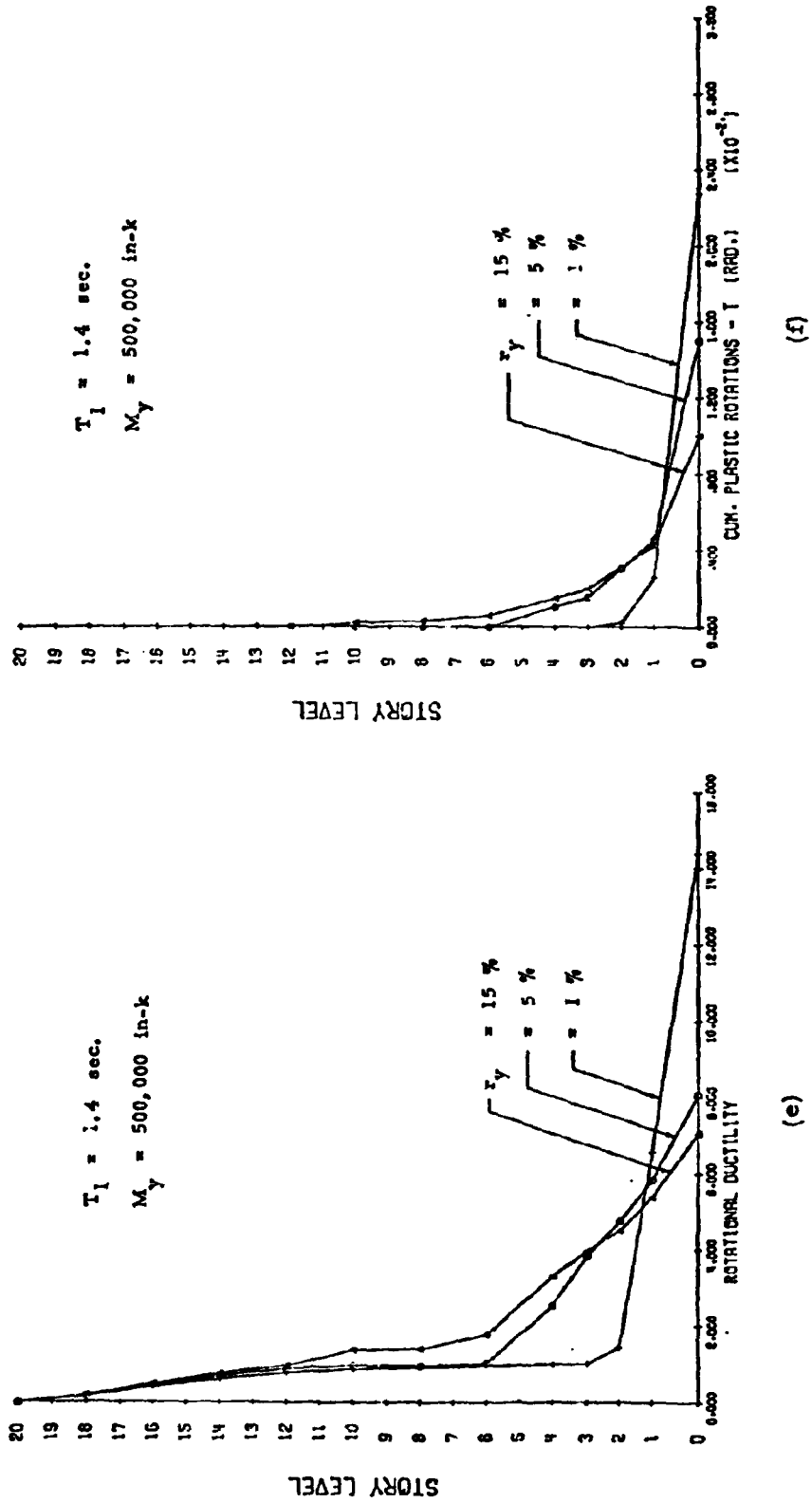

Fig. 47 (contd.) Effect of Slope of Post-Yield Branch of Moment-Rotation Curve

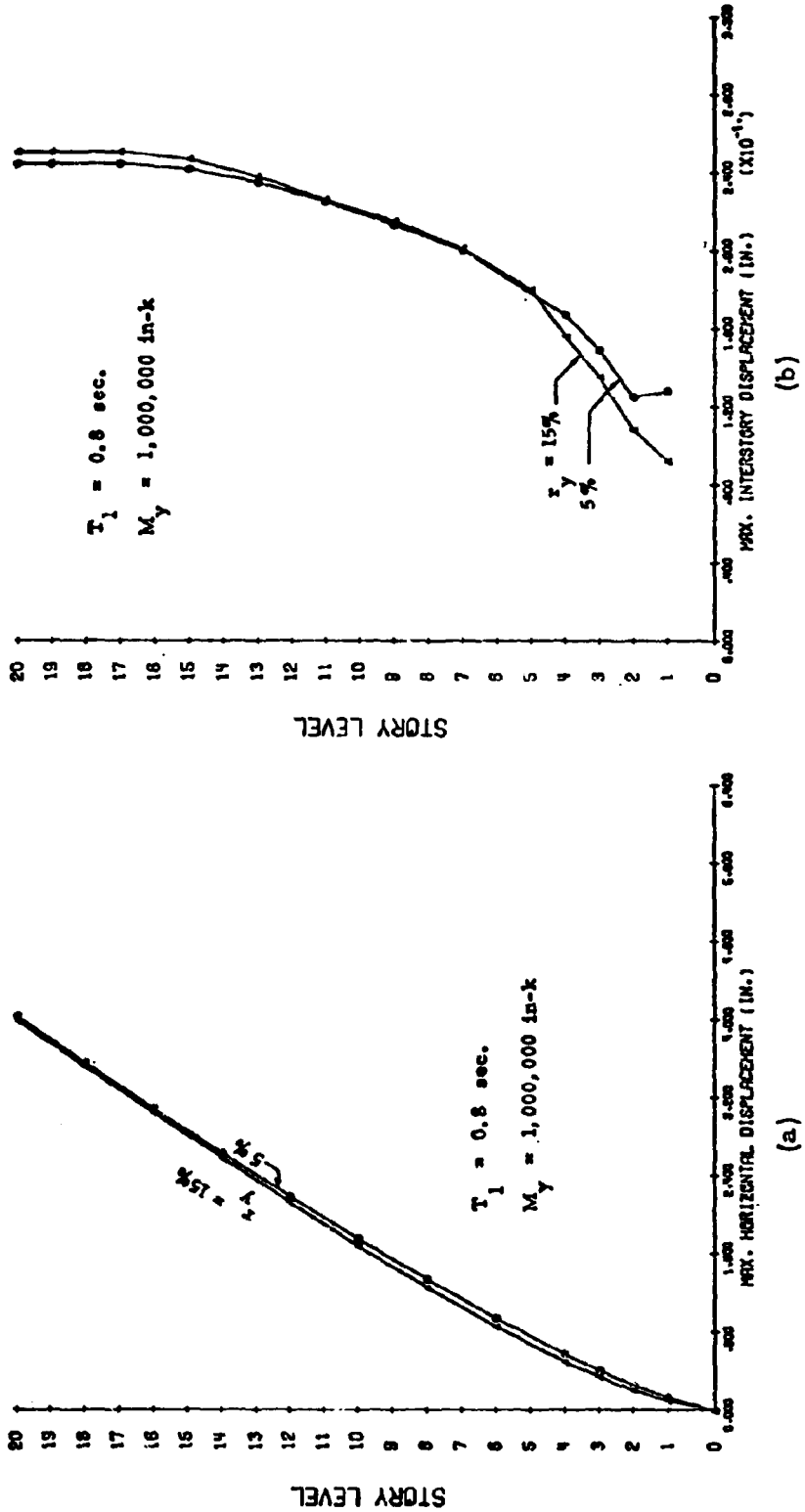

Fig. 48 Effect of Slope of Post-Yield Branch of Moment-Rotation Curve

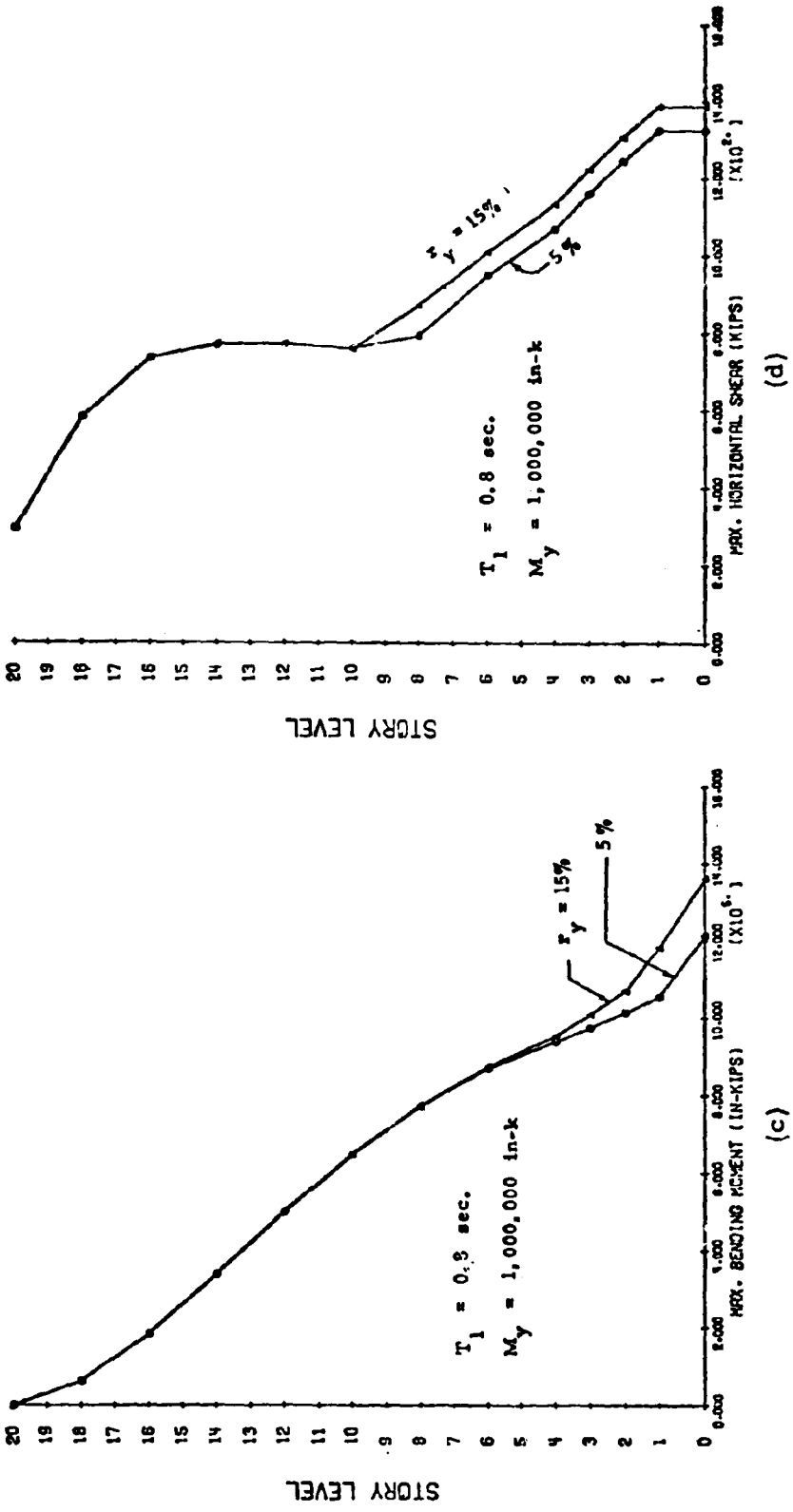

Fig. 48 (contd.) Effect of Slope of Post-Yield Branch of Moment-Rotation Curve

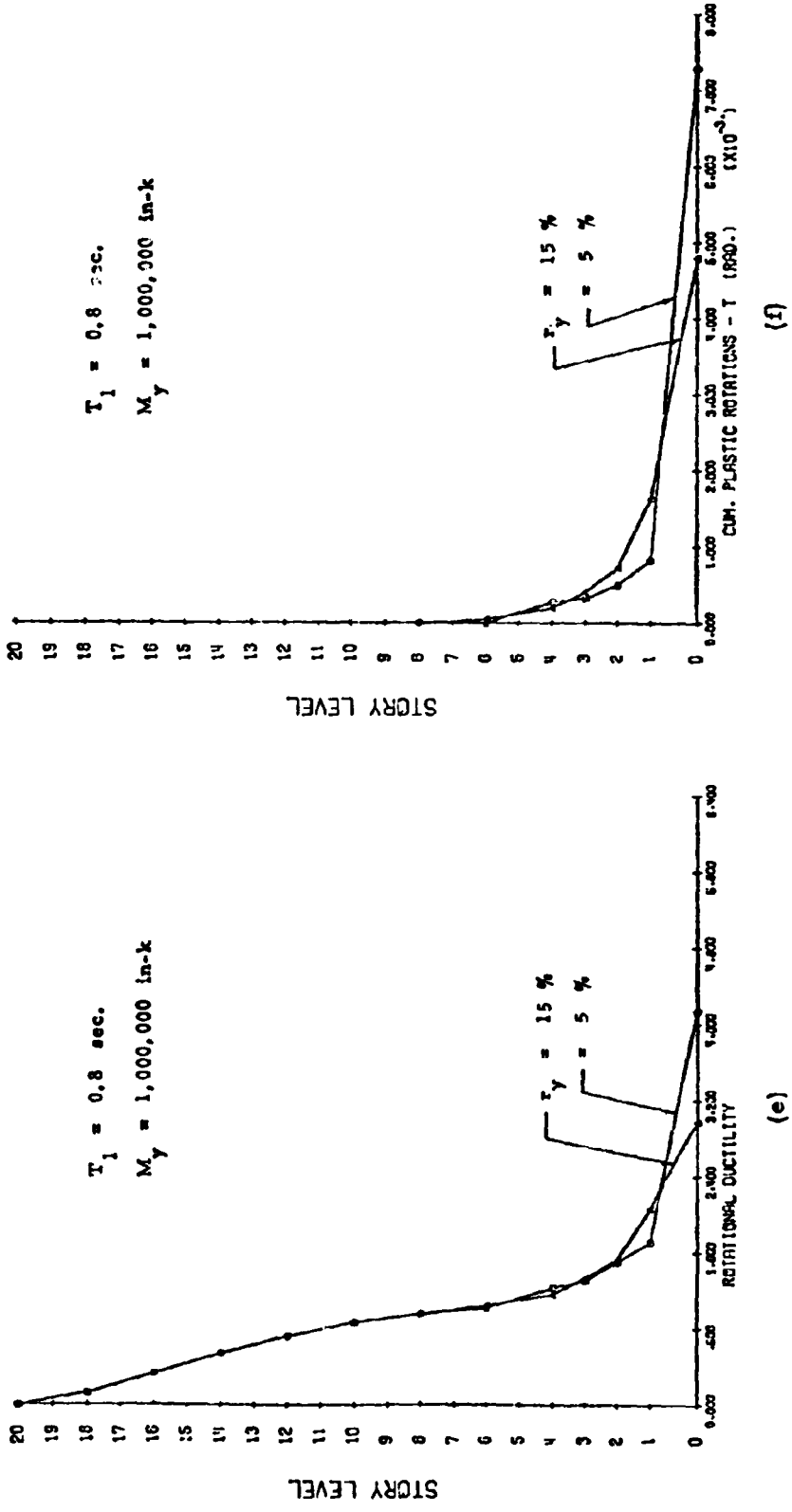

Fig. 48 (contd.) Effect of Slope of Post-Yield Branch of Moment Rotation Curve

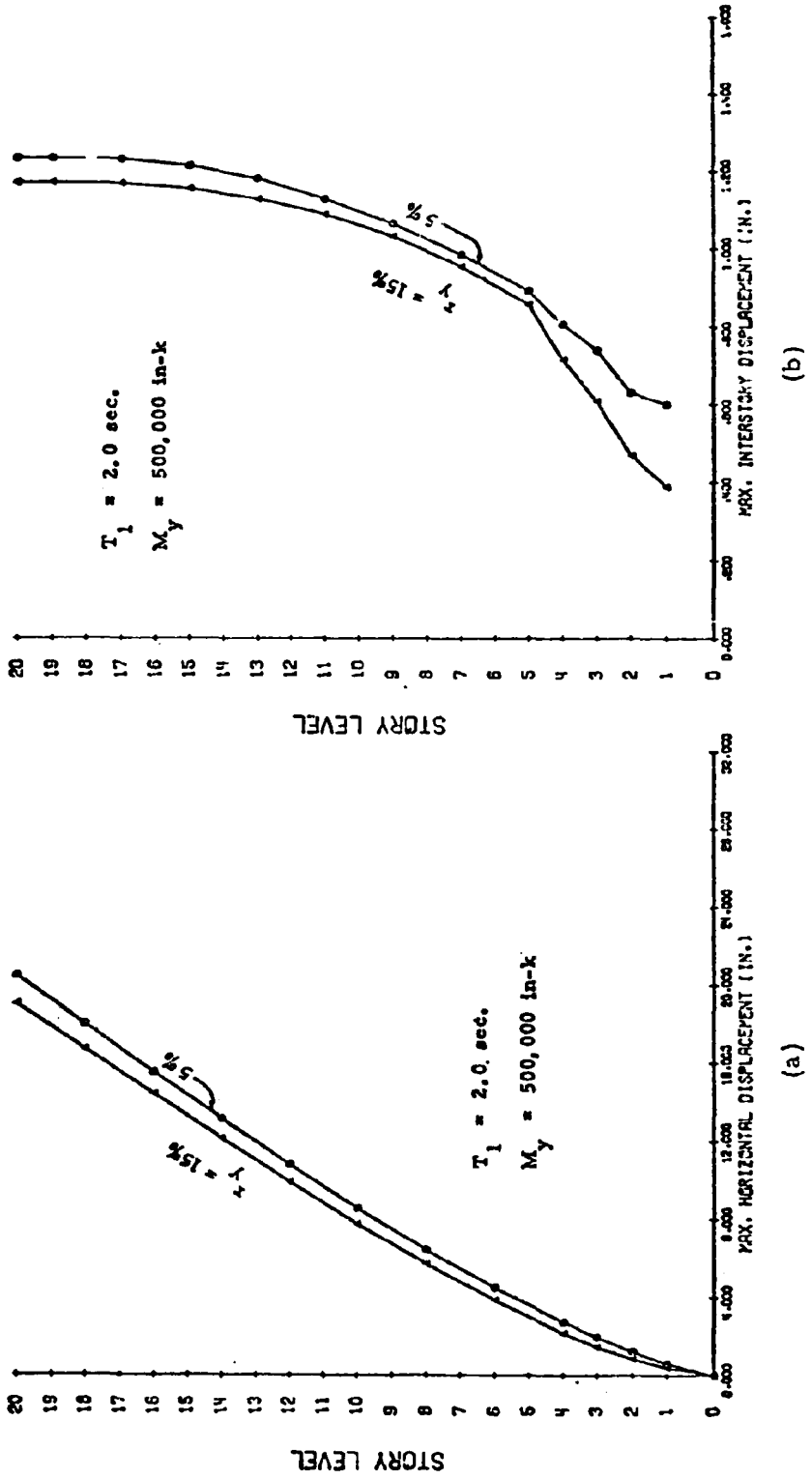

Fig. 49 Effect of Slope of Post-Yield Branch of Moment-Rotation Curve

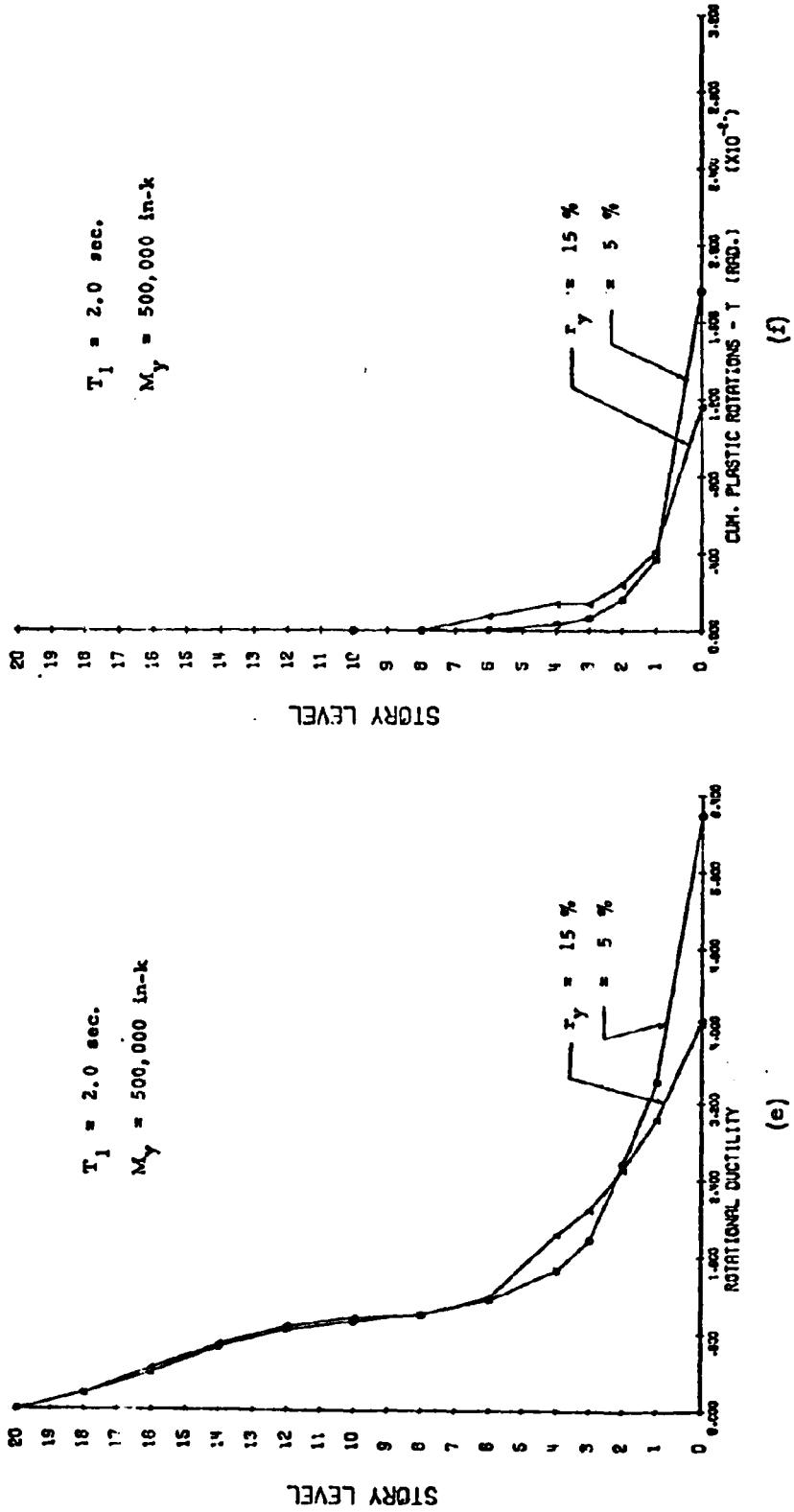

Fig. 49 (contd.) Effect of Slope of Post-Yield Branch of Moment-Rotation Curve

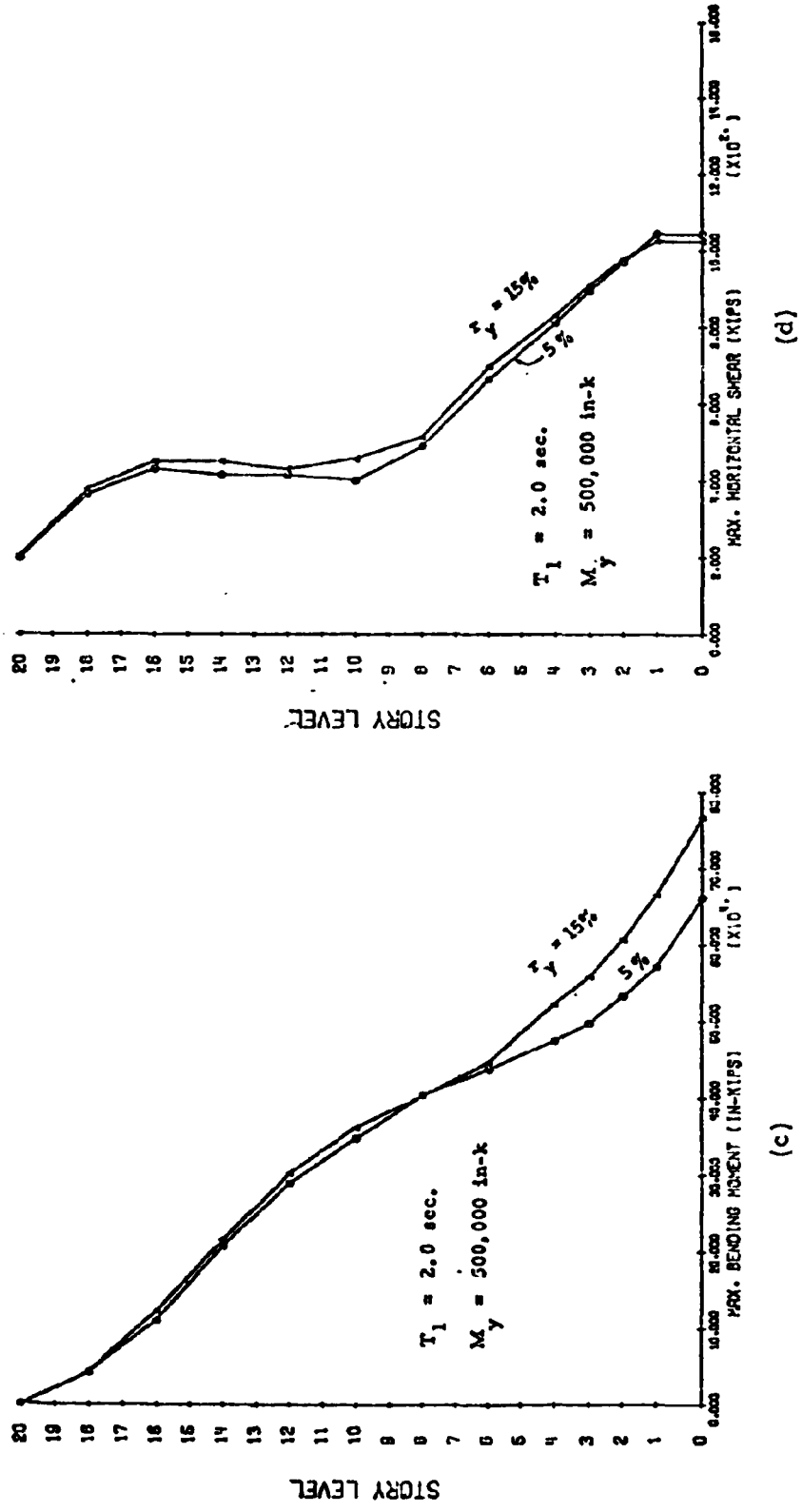

Fig. 49 (contd.) Effect of Slope of Post-Yield Branch of Moment-Rotation Curve

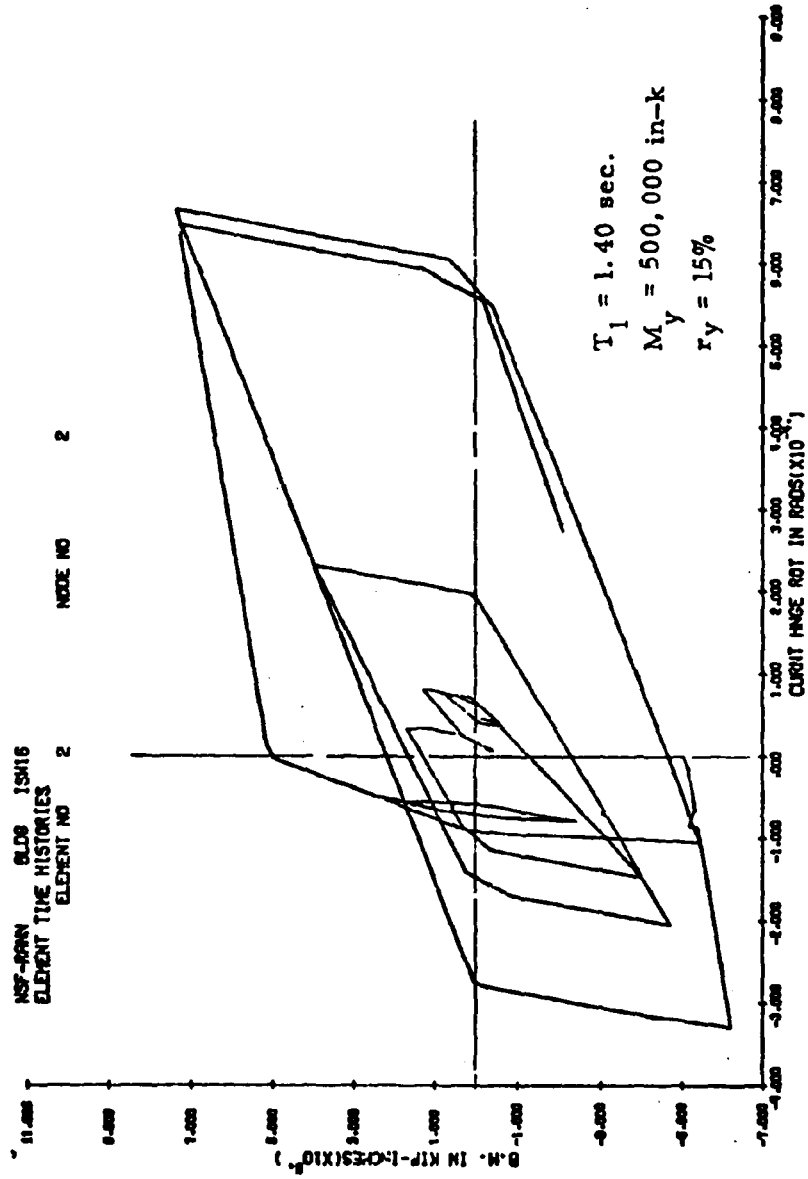

Fig. 50 Moment-Rotation Loop for First Story Hinge

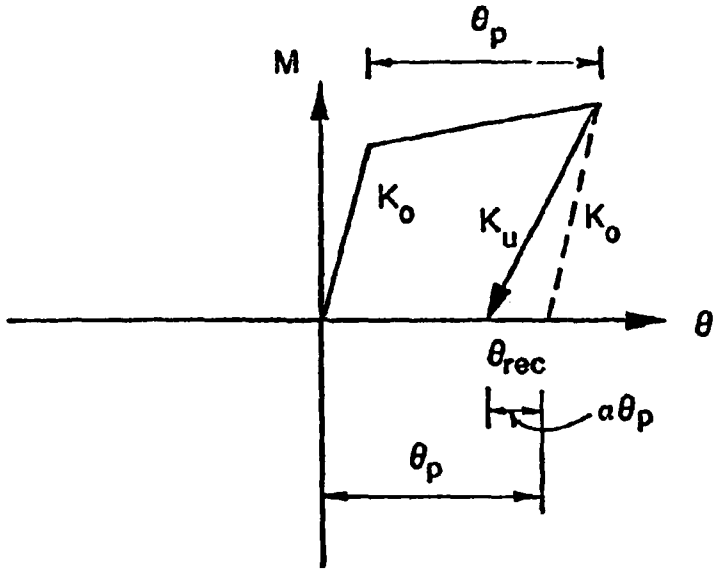

(a) unloading stiffness

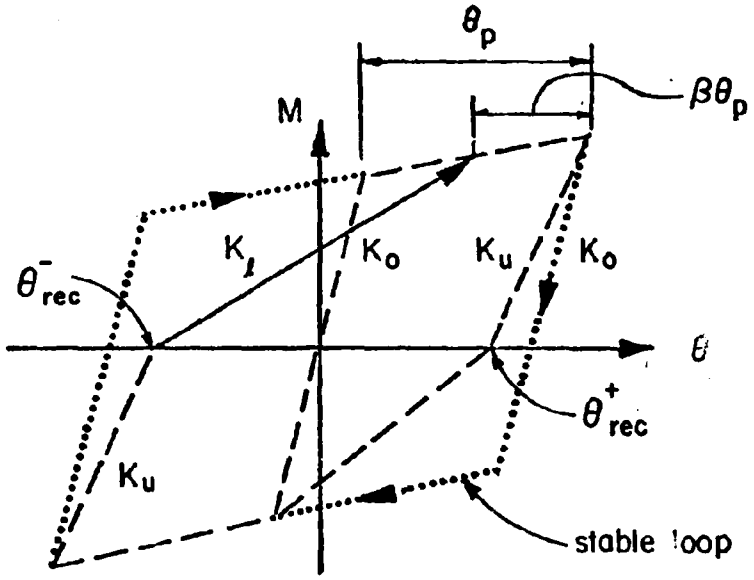

(b) reloading stiffness

Fig. 51 Takeda Model Parameters α and β.

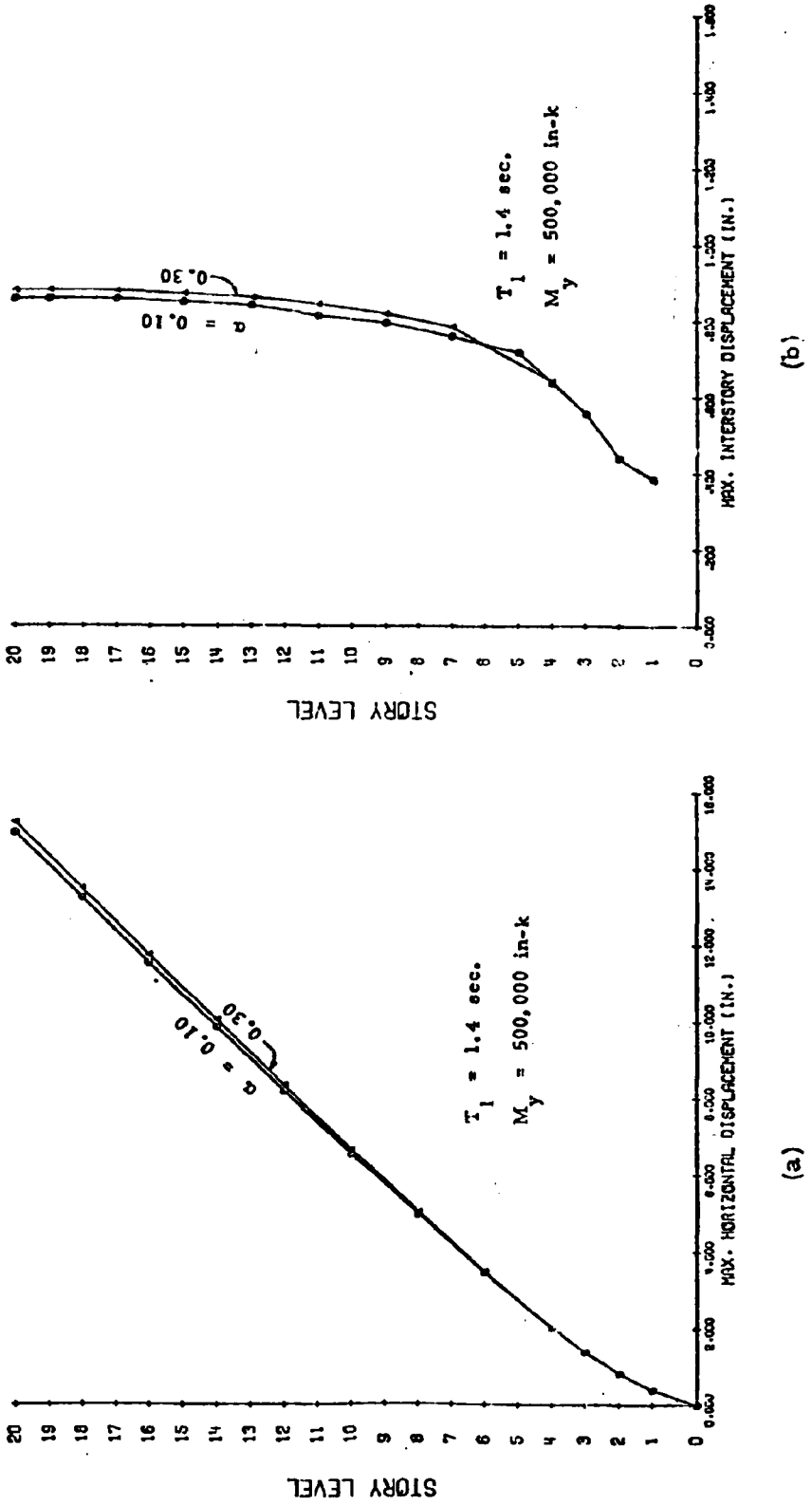

Fig. 52 Effect of Plastic Hinge M-θ Hysteretic Loop Unloading Parameter α

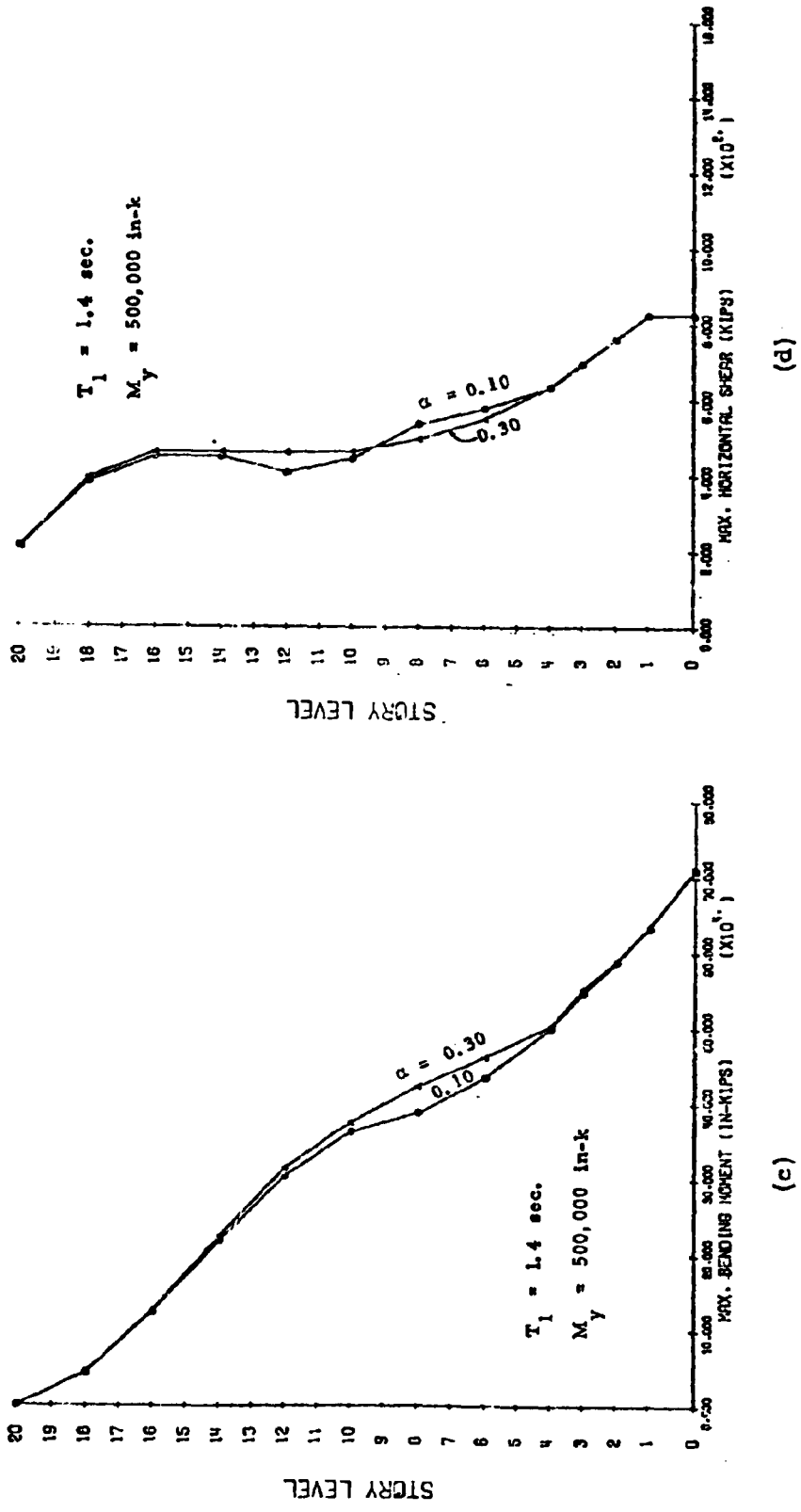

Fig. 52 (contd.) Effect of Plastic Hinge M-θ Hysteretic Loop Unloading Parameter α

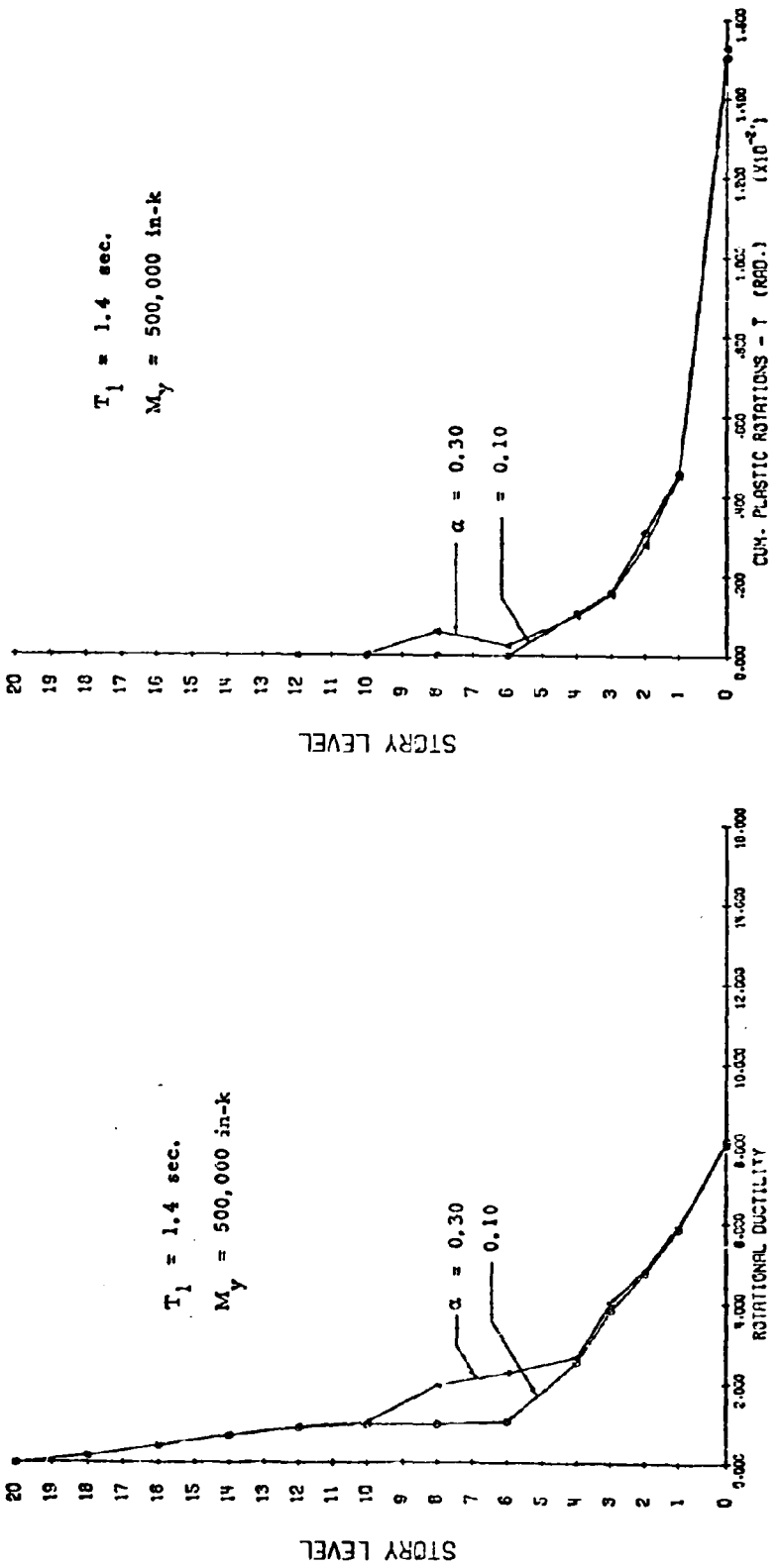

Fig. 52 (contd.) Effect of Plastic Hinge M-θ Hysteretic Loop Unloading Parameter α

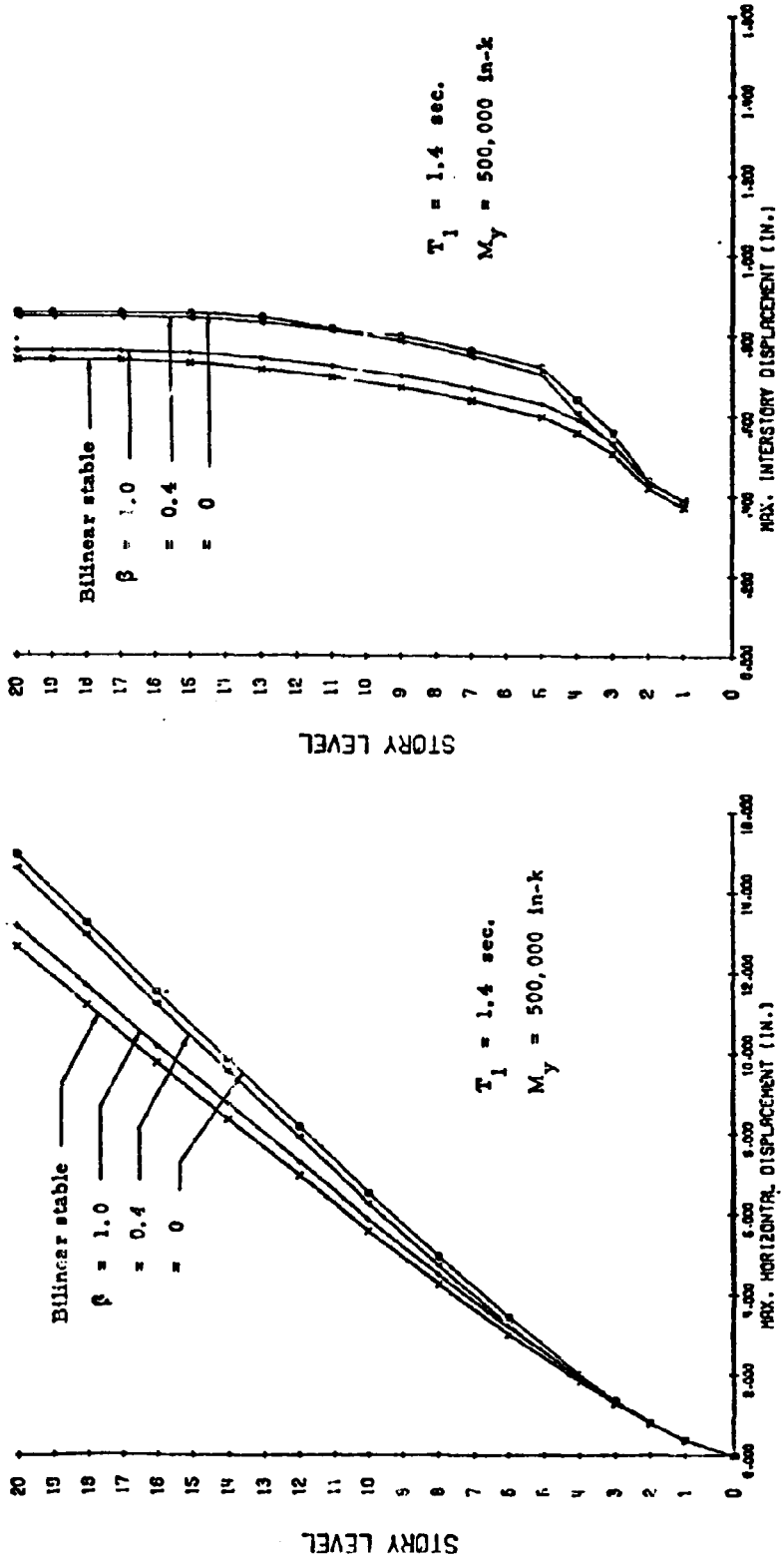

Fig. 53 Effect of Plastic Hinge M-θ Hysteretic Loop Reloading Parameter β

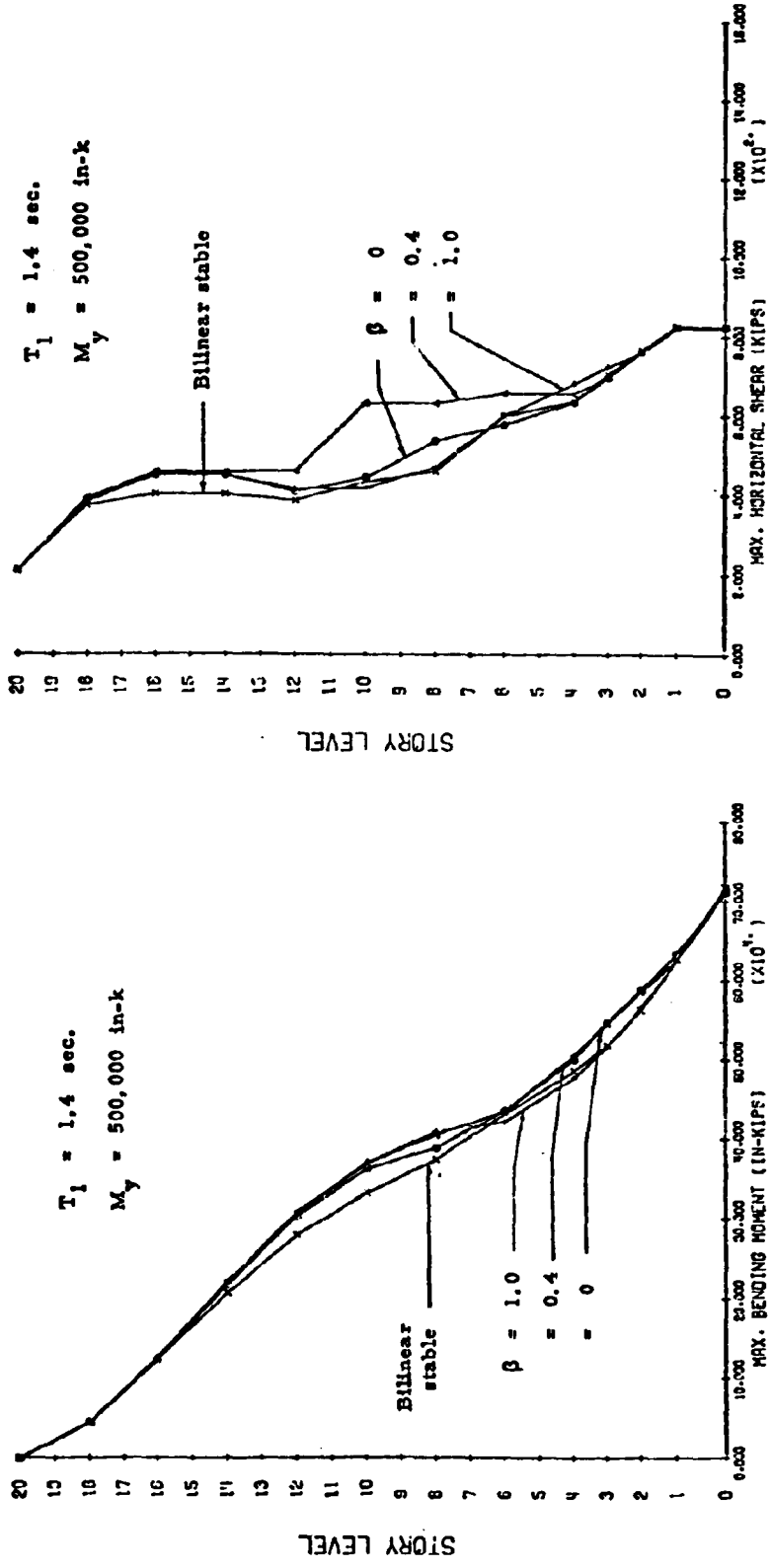

Fig. 53 (contd.) Effect of Plastic Hinge M-θ Hysteretic Loop Reloading Parameter β

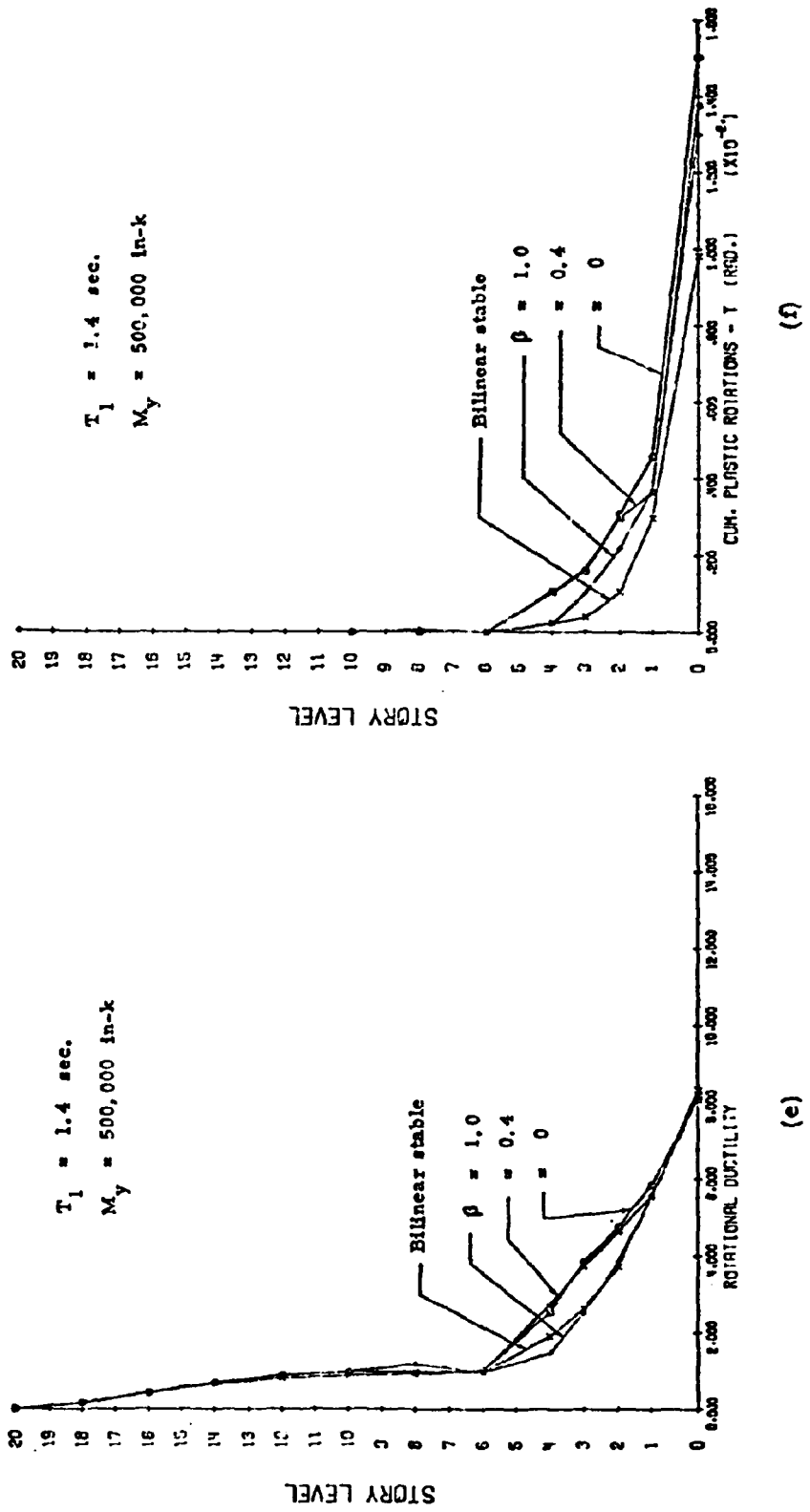

Fig. 53 (contd.) Effect of Plastic Hinge M-θ Hysteretic Loop Reloading Parameter β

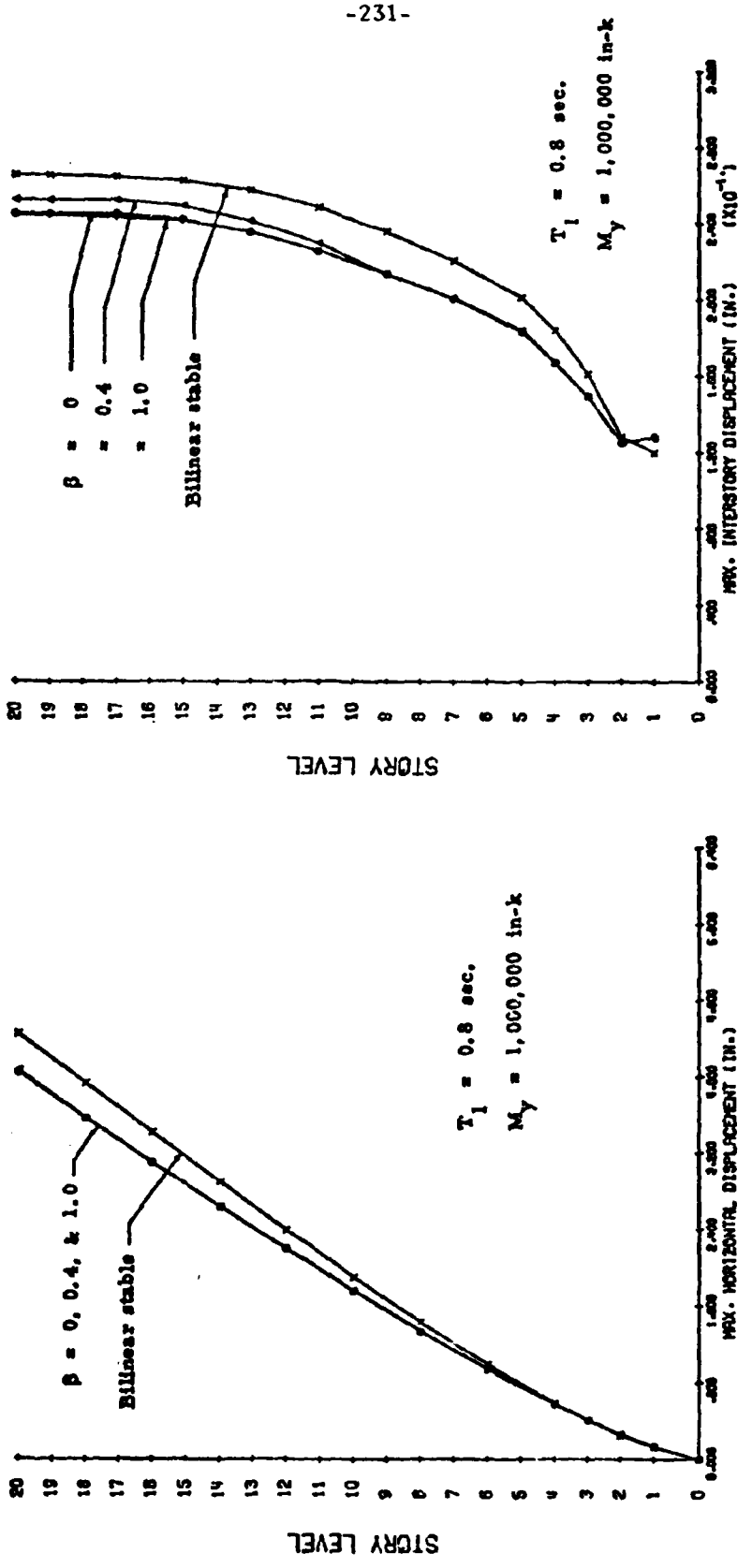

Fig. 54 Effect of Plastic Hinge M-θ Hysteretic Loop Reloading Parameter β

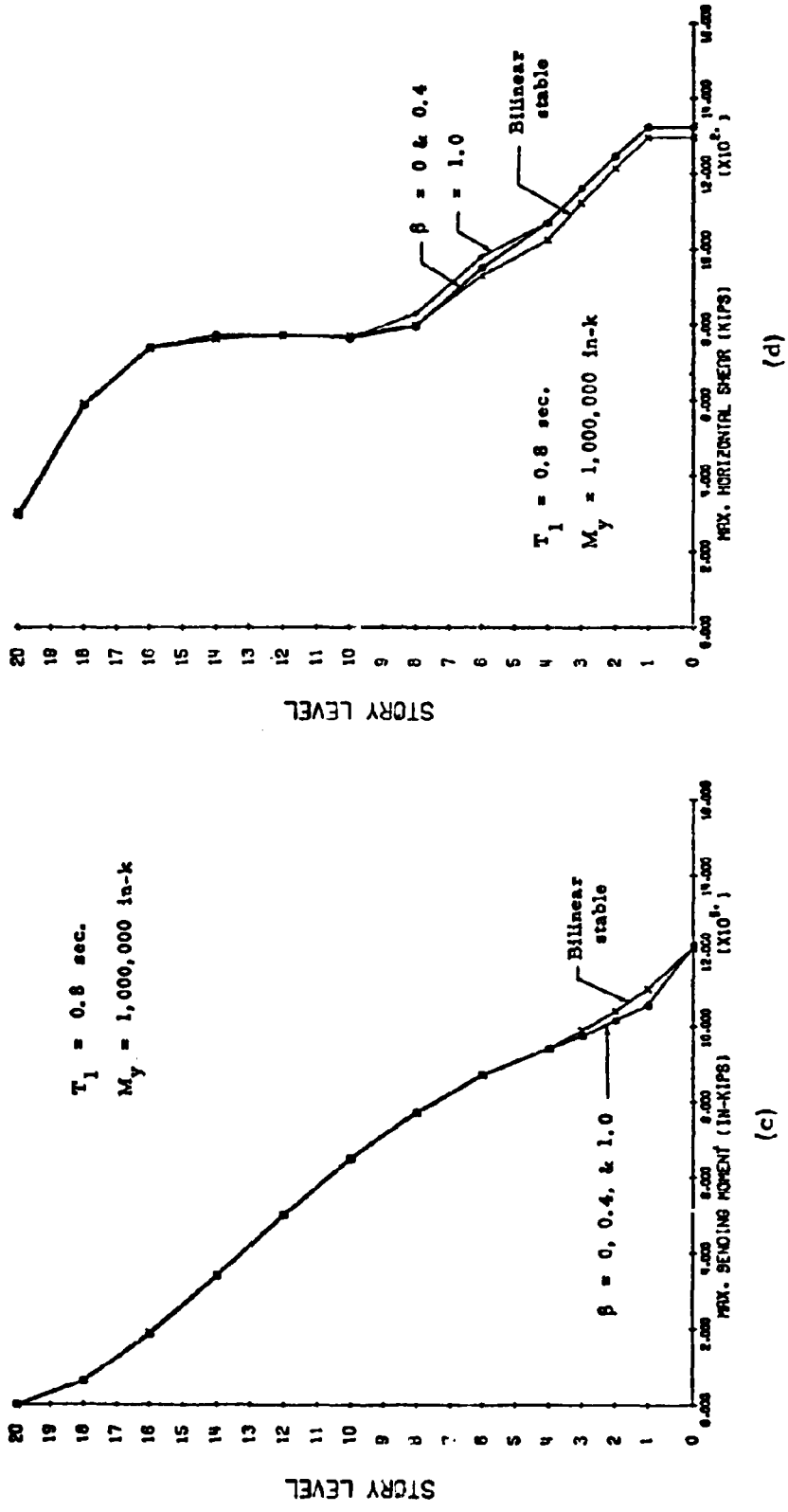

Fig. 54 (contd.) Effect of Plastic Hinge M-θ Hysteretic Loop Reloading Parameter β

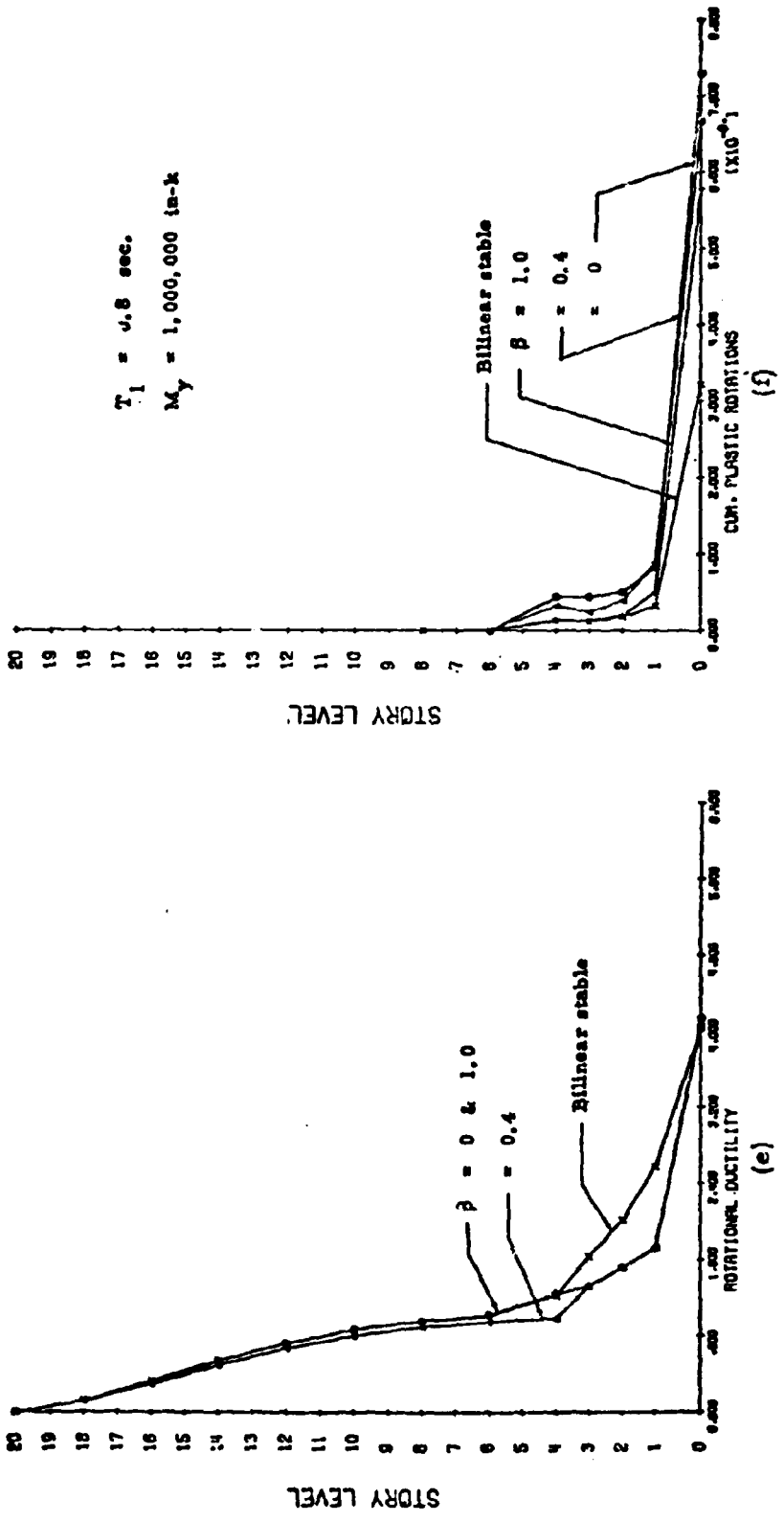

Fig. 54 (contd.) Effect of Plastic Hinge M-θ Hysteretic Loop Reloading Parameter β

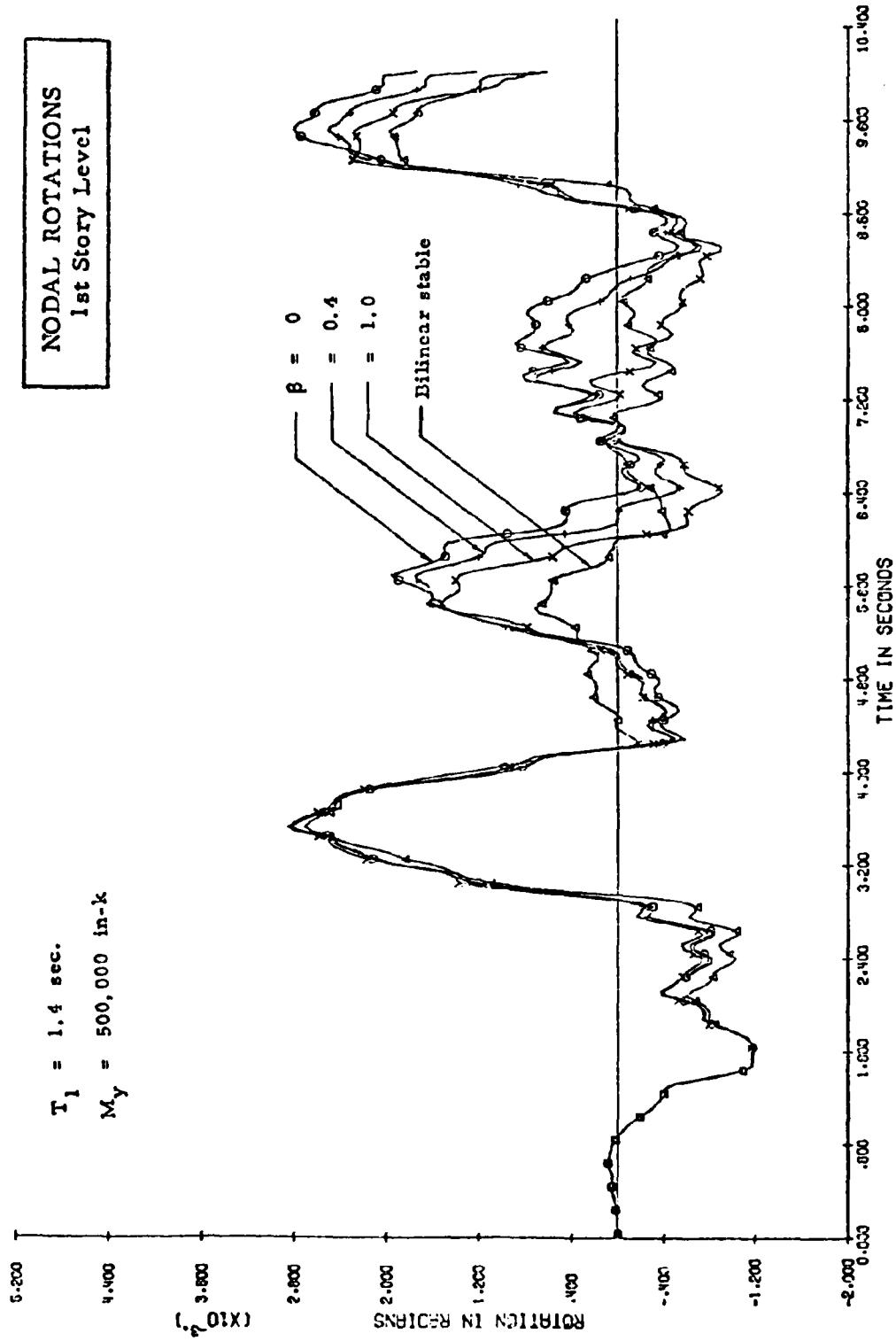

Fig. 55 Rotation in First Story vs. Time for Different Values of the Plastic Hinge M-θ Hysteretic Loop Reloading Parameter β

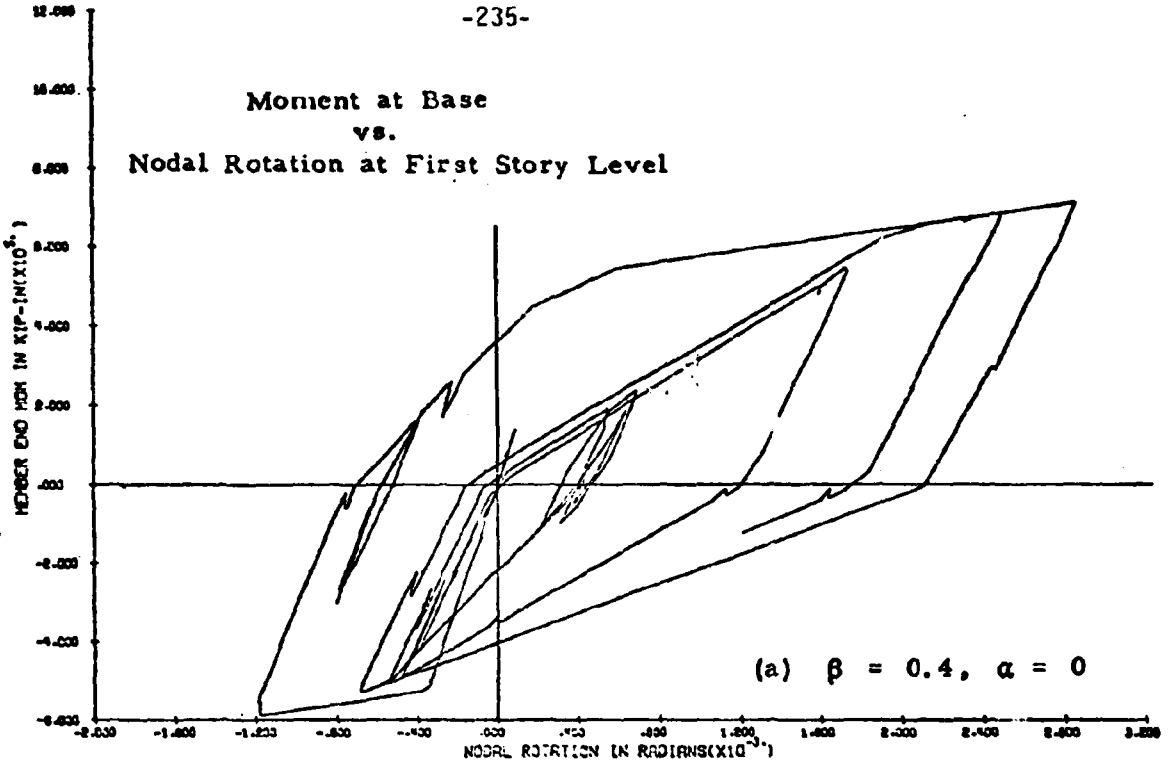

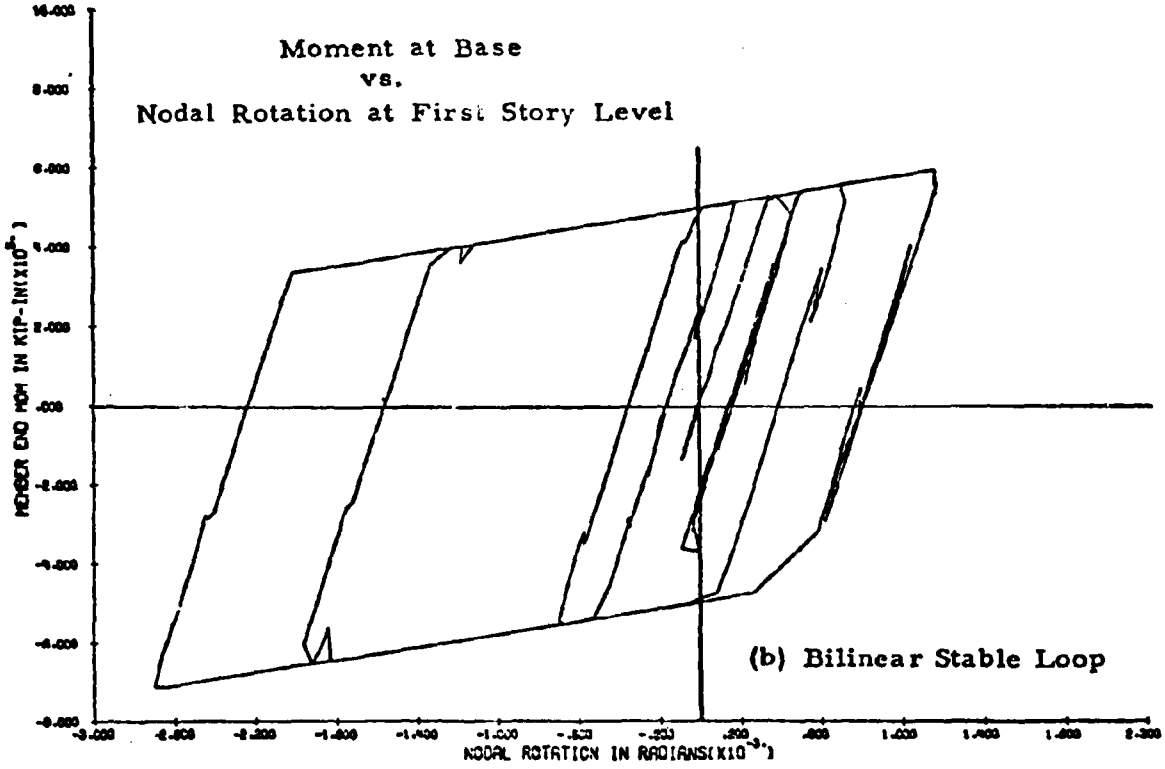

Fig. 56 Moment at Base *vs.* Nodal Rotation at First Story Level for Different M-θ Curve Characteristics

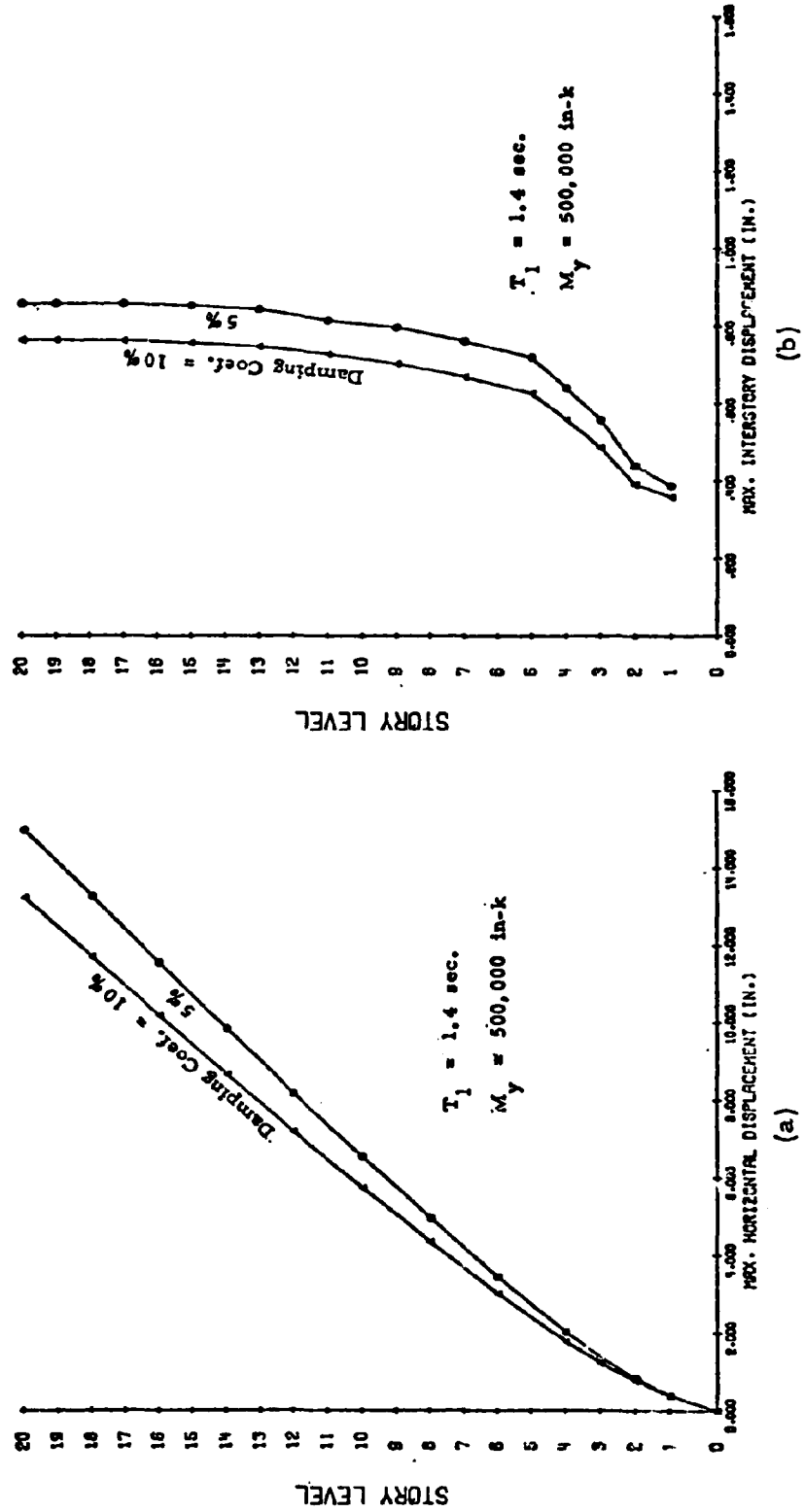

Fig. 57 Effect of Damping

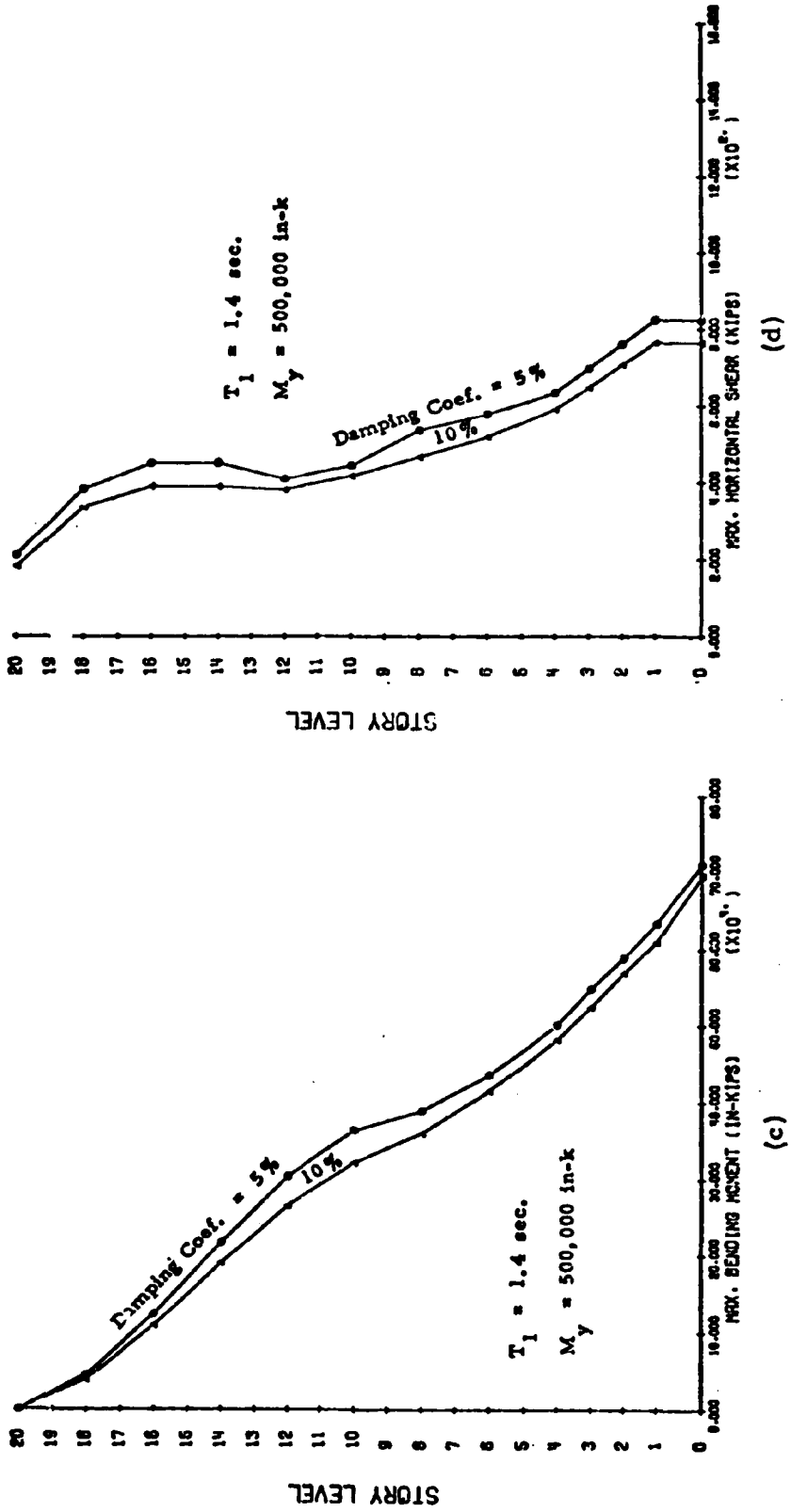

Fig. 57 (contd.) Effect of Damping

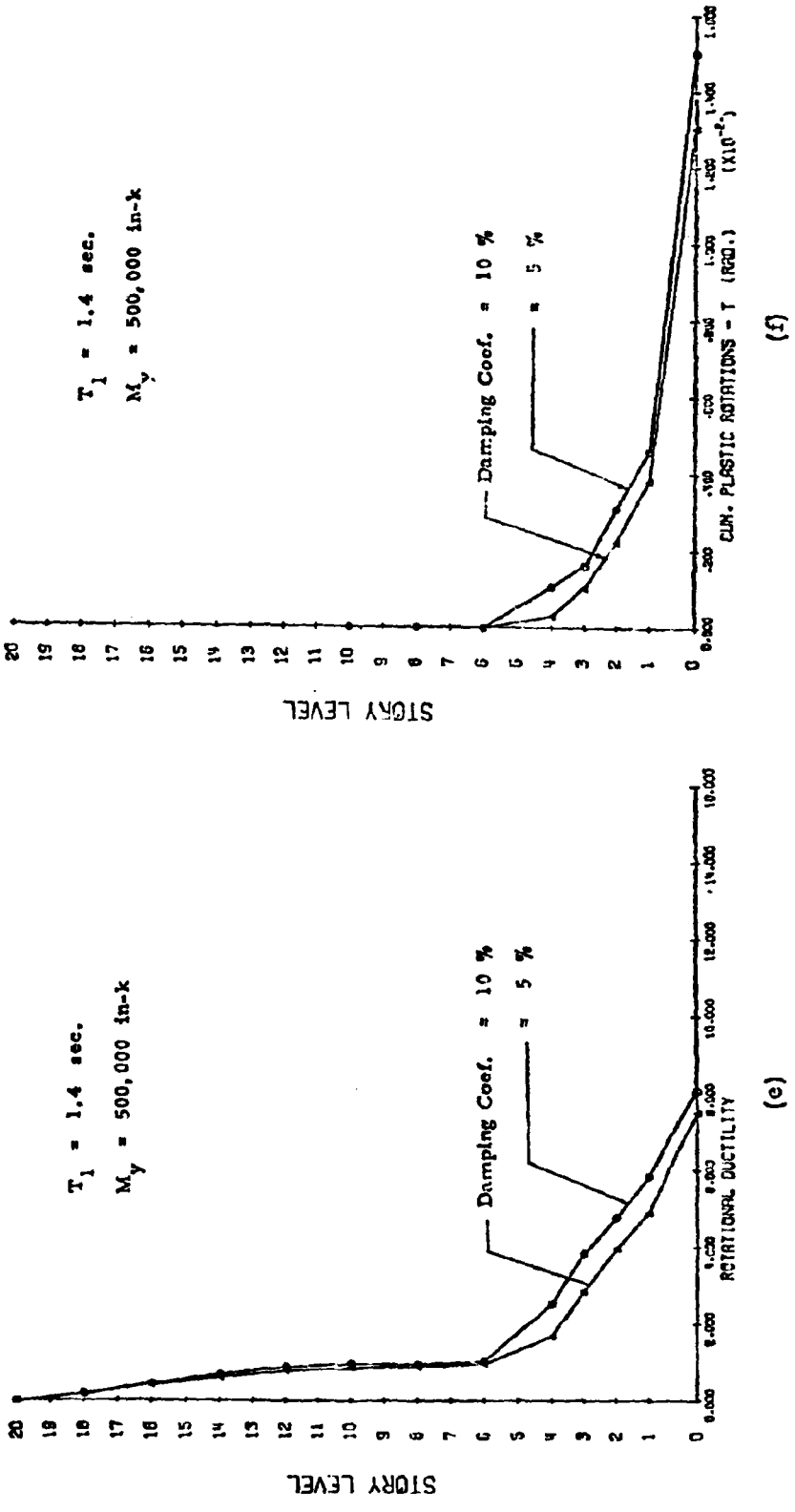

Fig. 57 (contd.) Effect of Damping

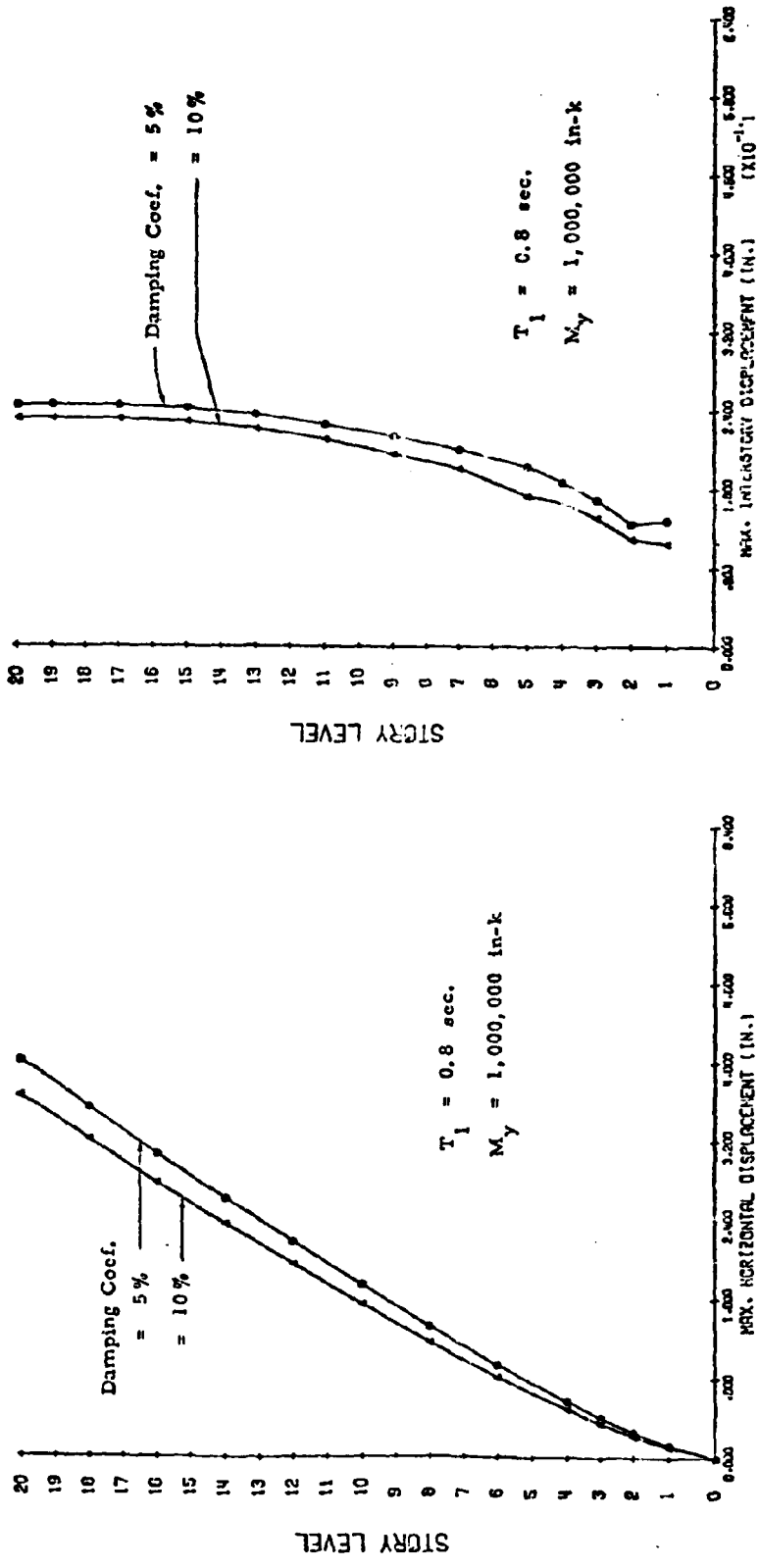

Fig. 58 Effect of Damping

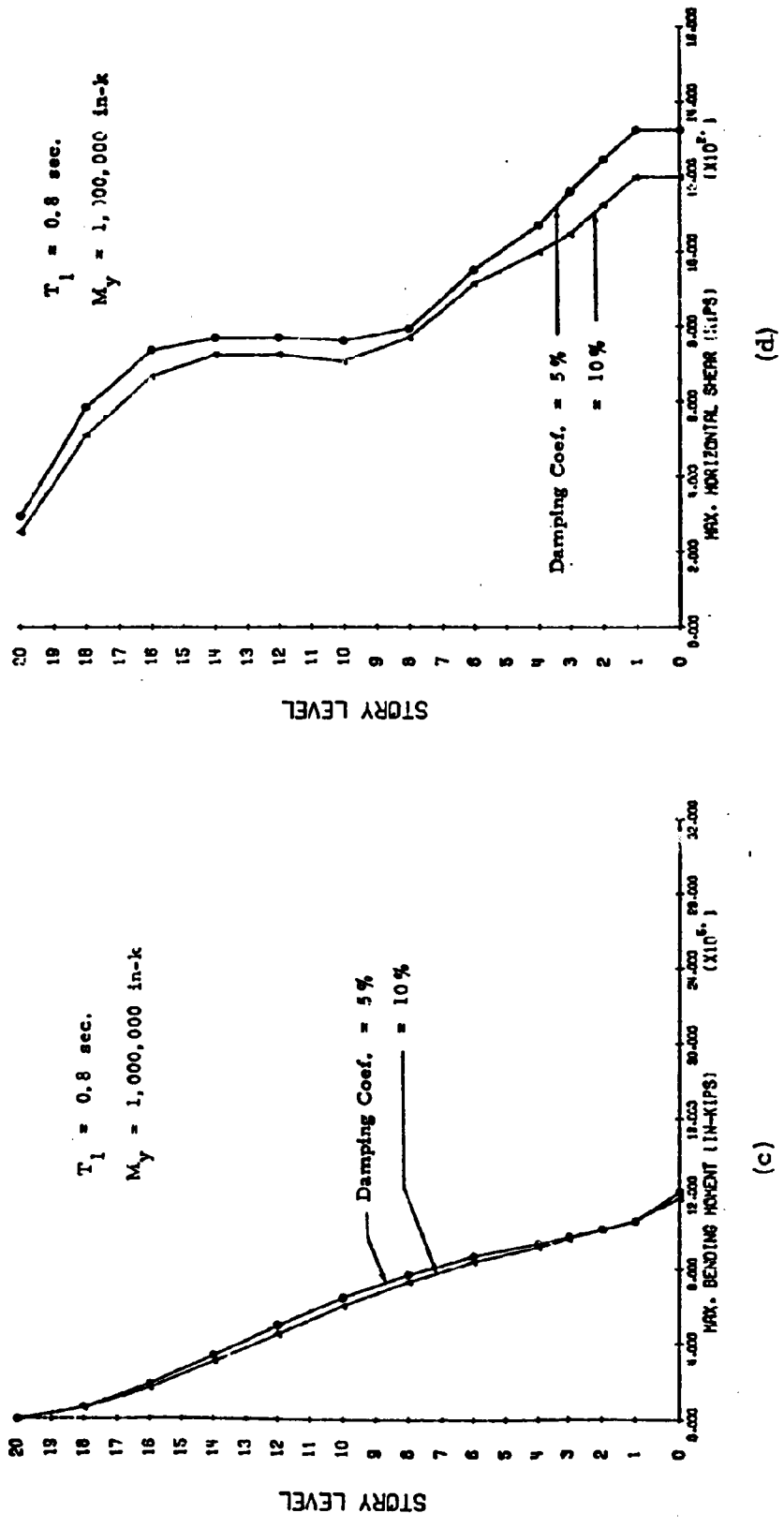

Fig. 58 (contd.) Effect of Damping

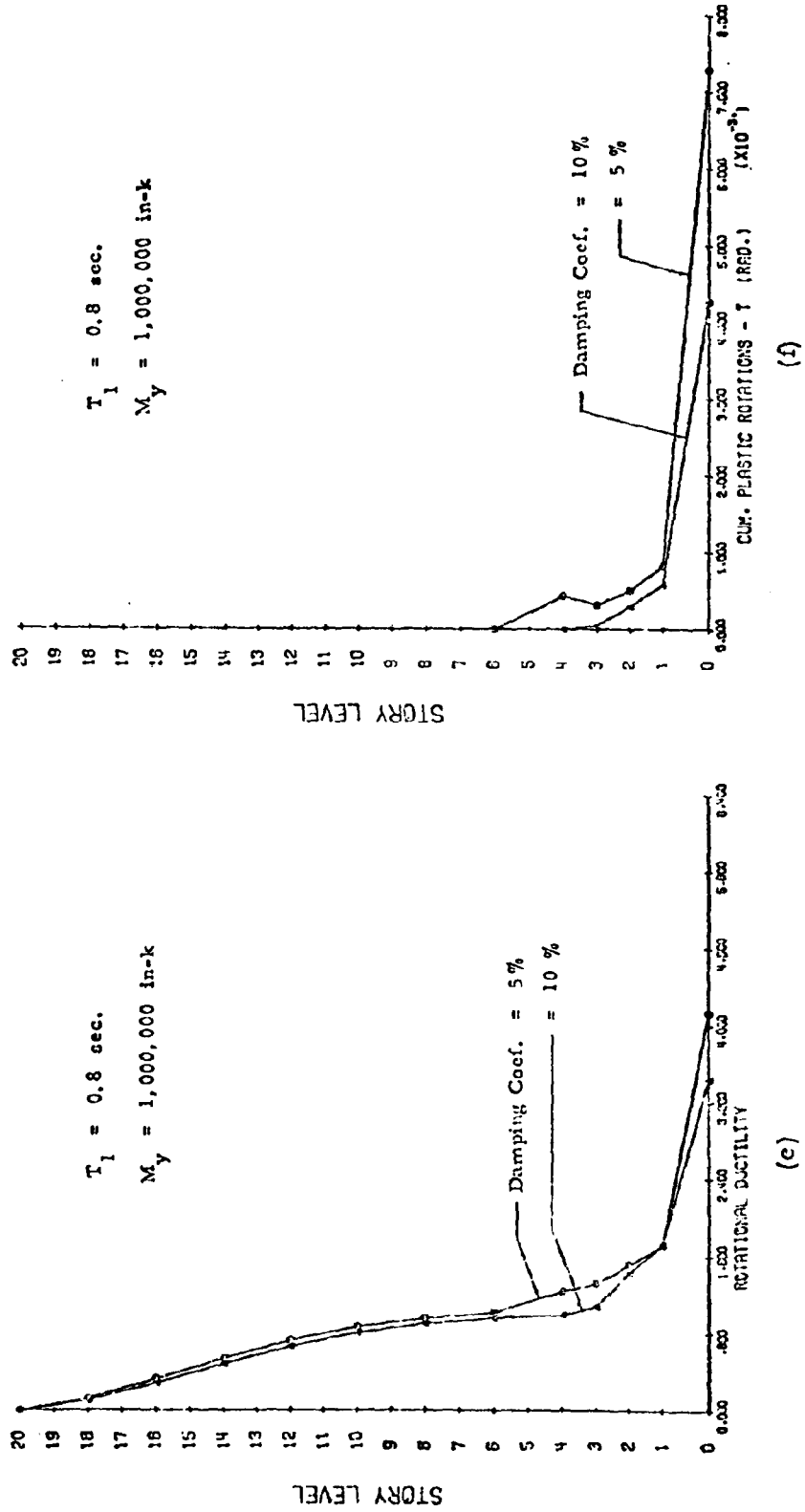

Fig. 58 (contd.) Effect of Damping

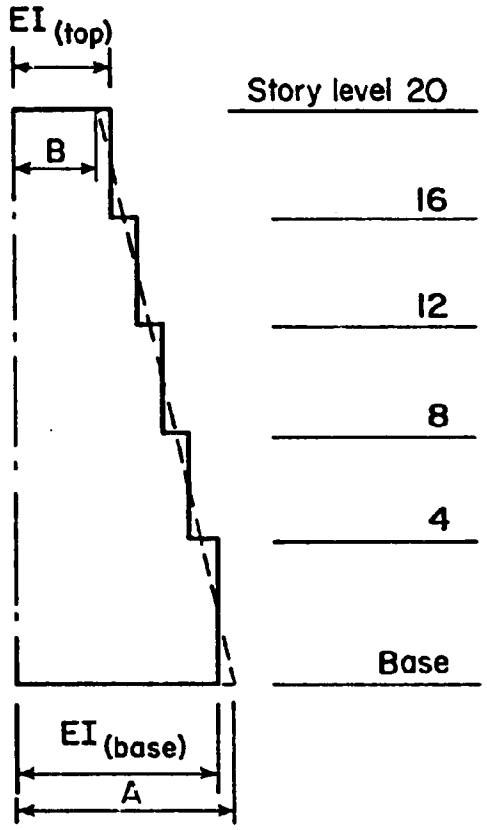

Fig. 59 Stiffness taper

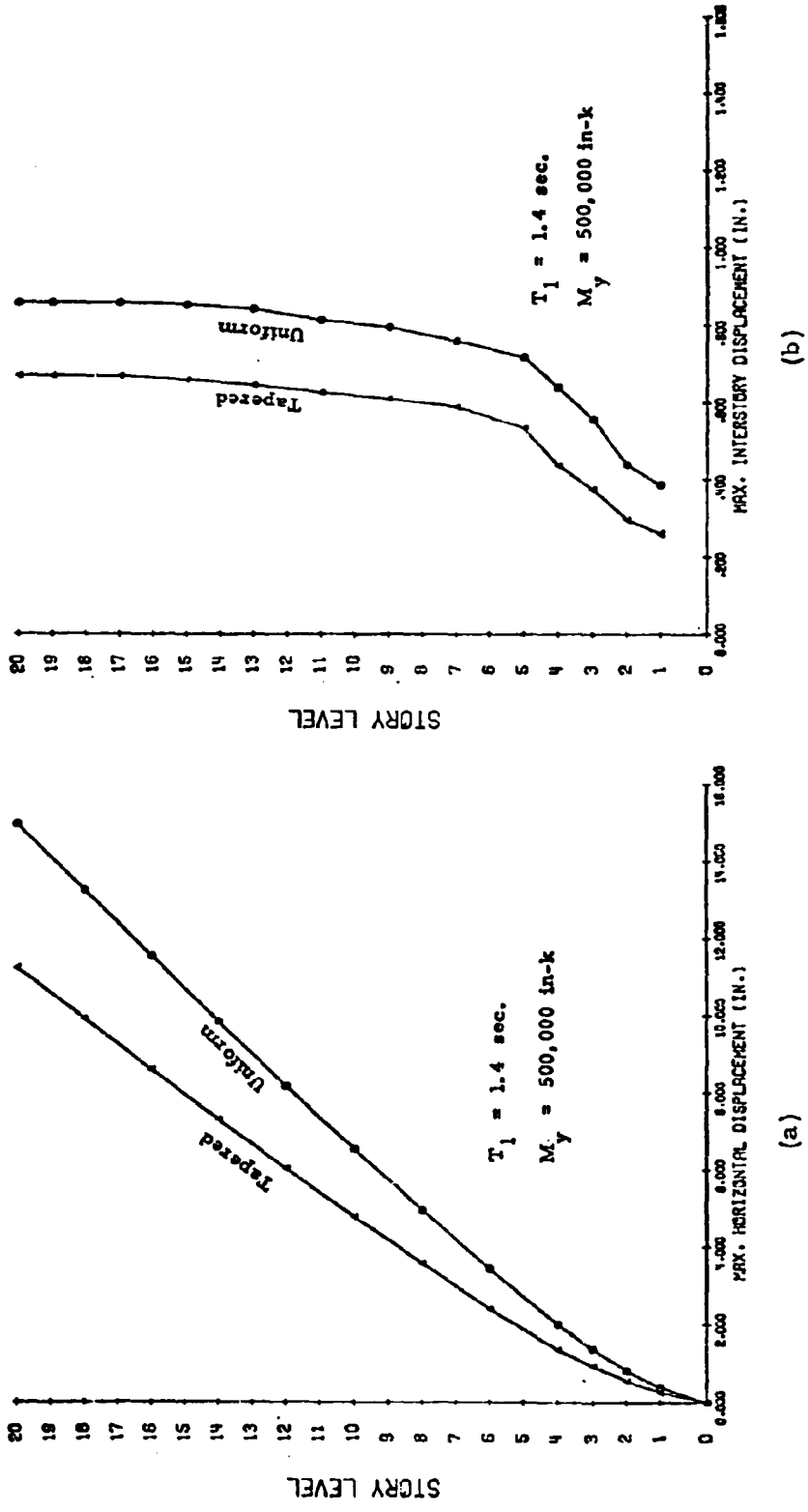

Fig. 60 Effect of Stiffness Taper

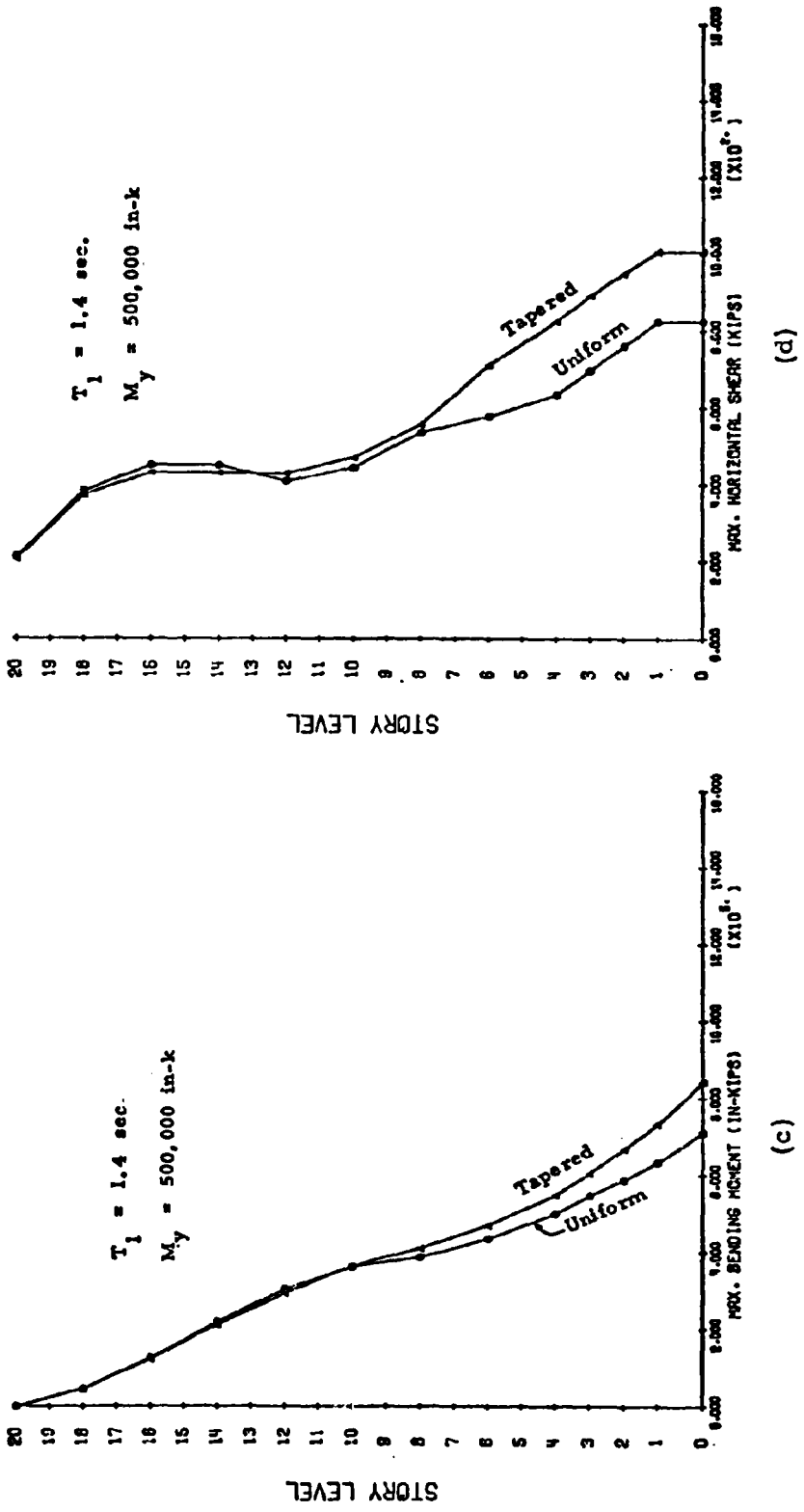

Fig. 60 (contd.) Effect of Stiffness Taper

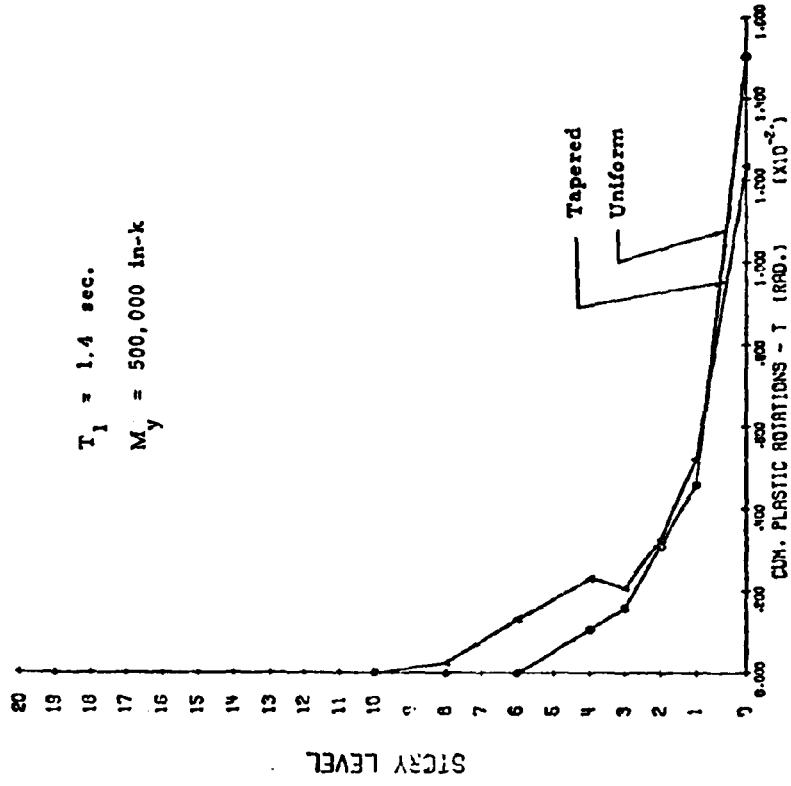

(f)

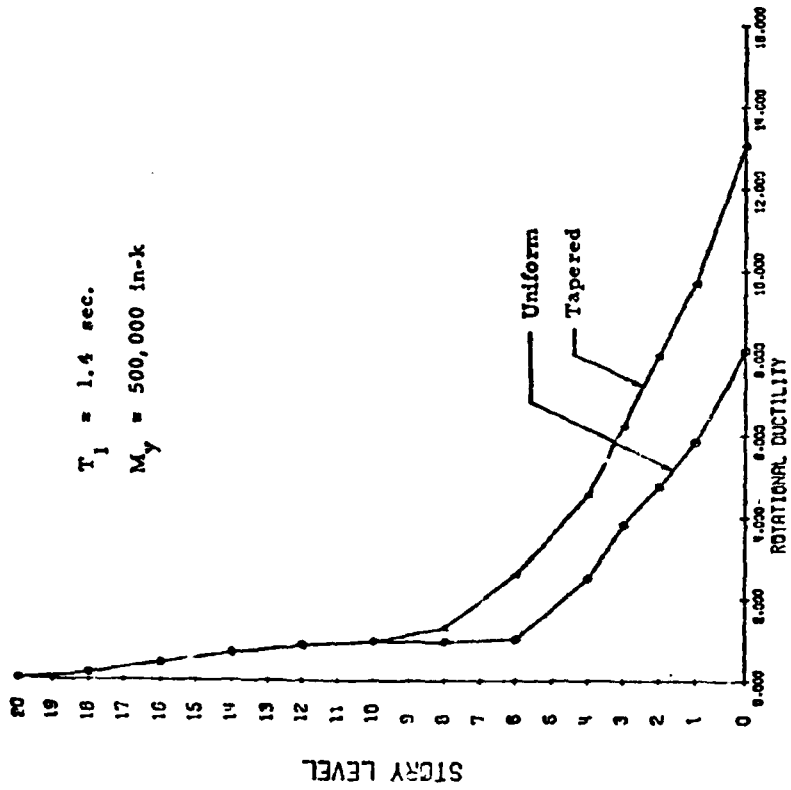

(e)

Fig. 60 (contd.) Effect of Stiffness Taper

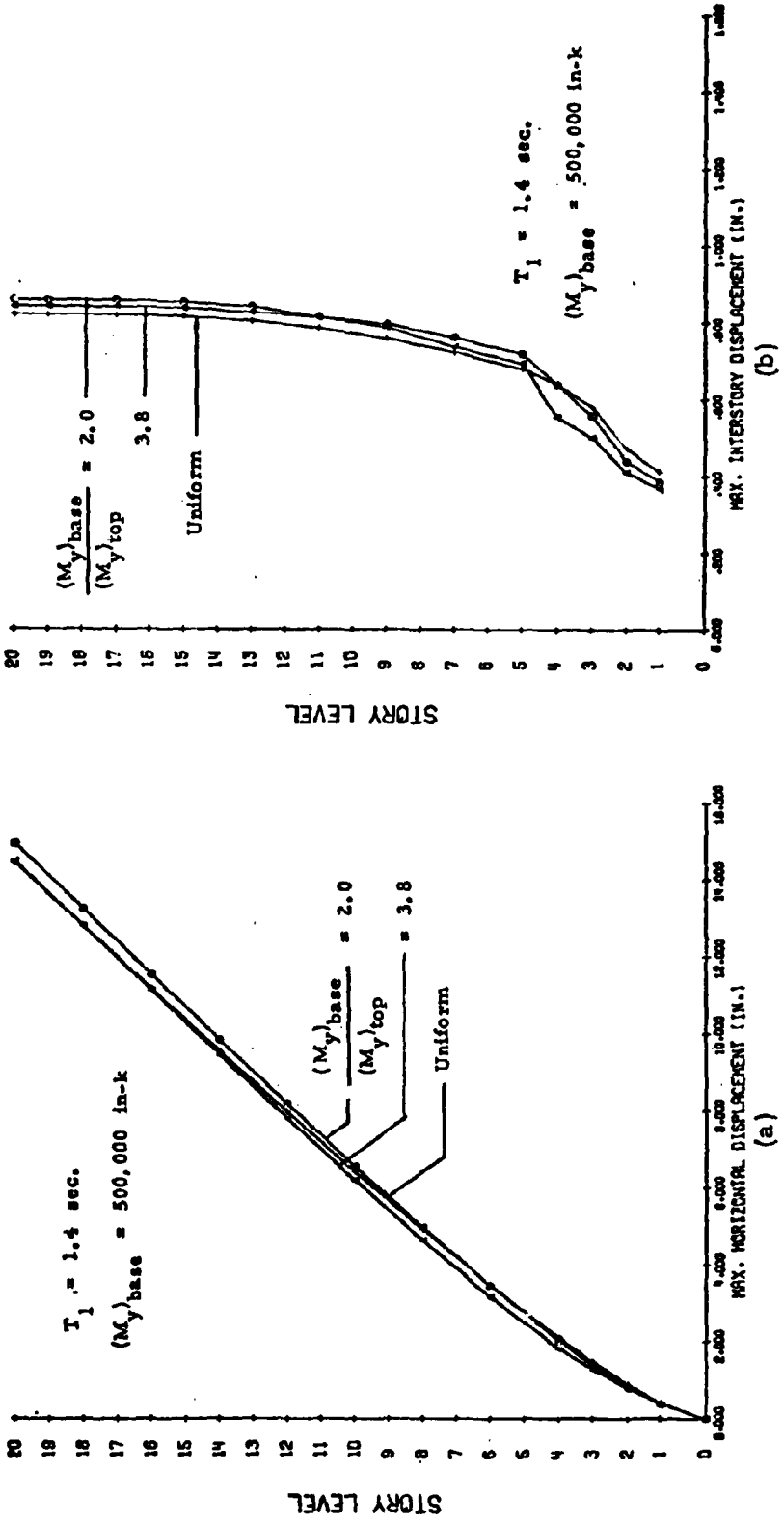

Fig. 61 Effect of Strength Taper

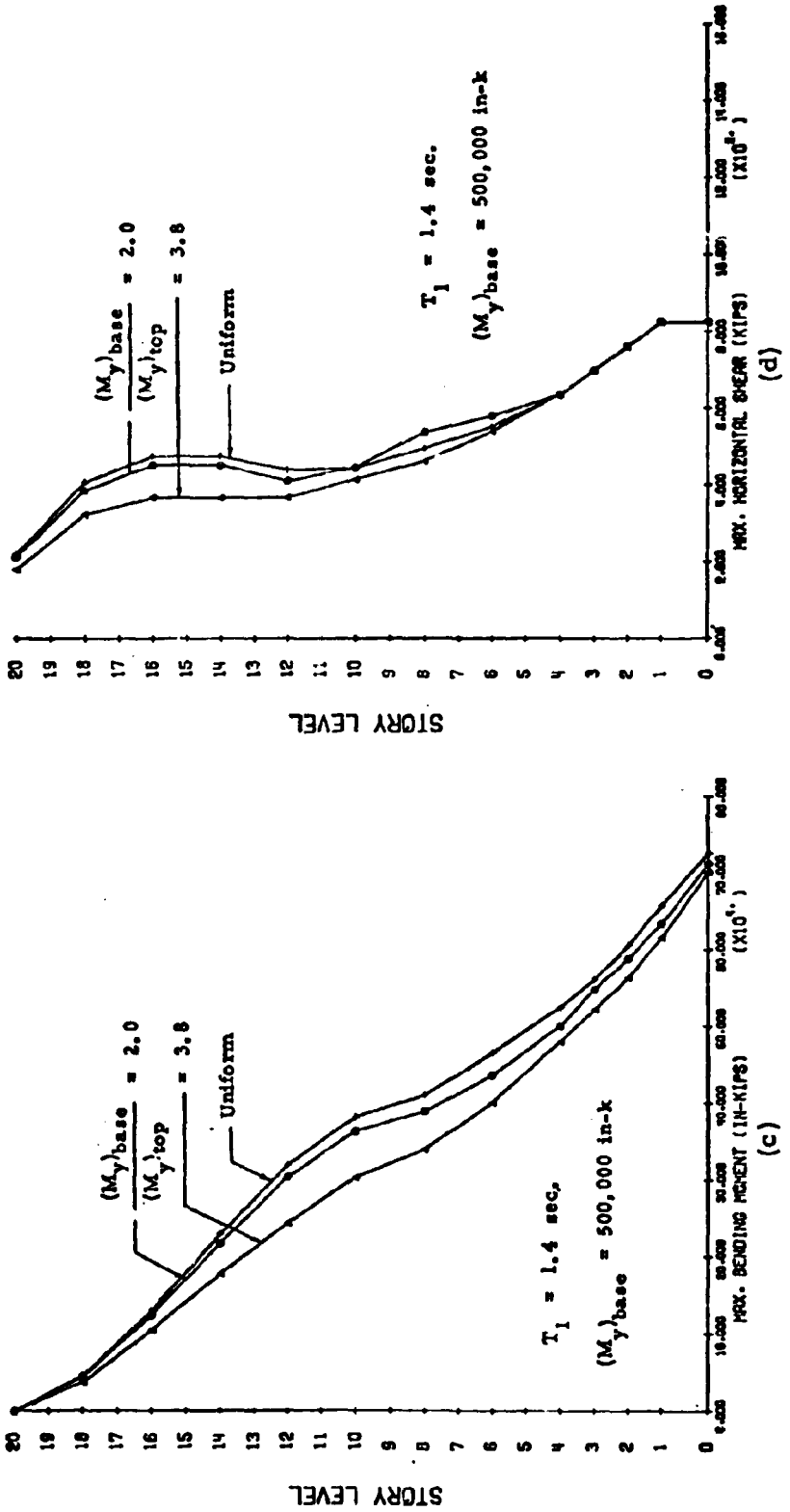

Fig. 61 (contd.) Effect of Strength Taper

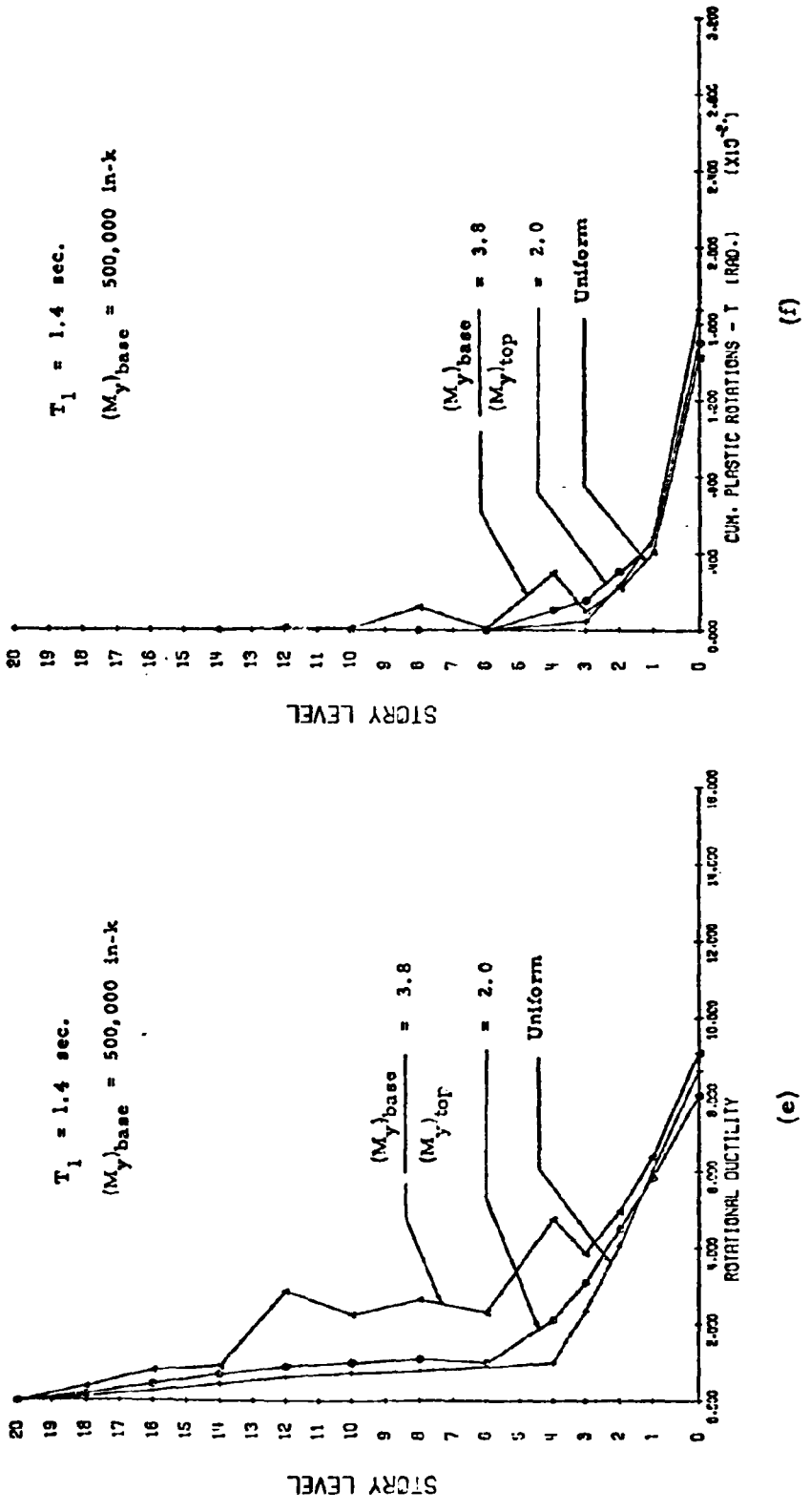

Fig. 61 (contd.) Effect of Strength Taper

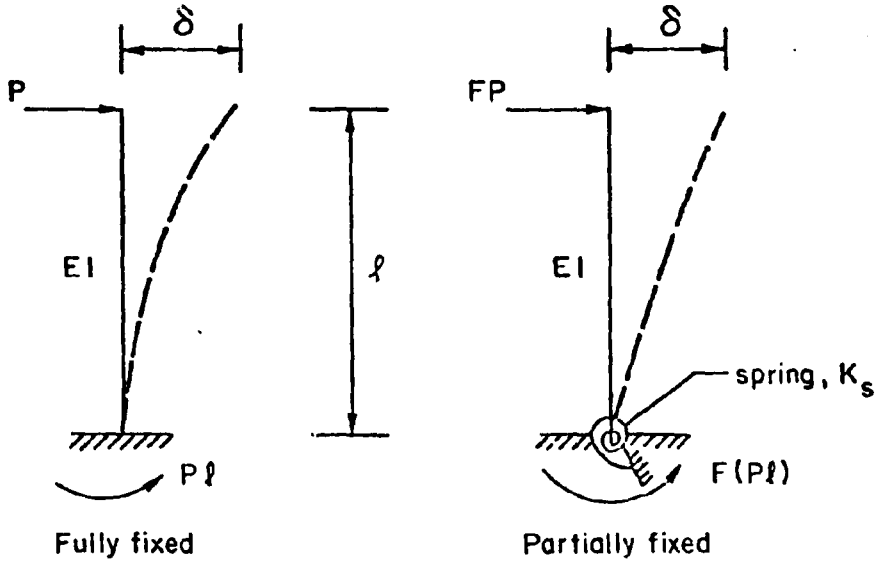

Fig. 62 Definition of Base Fixity Factor, F

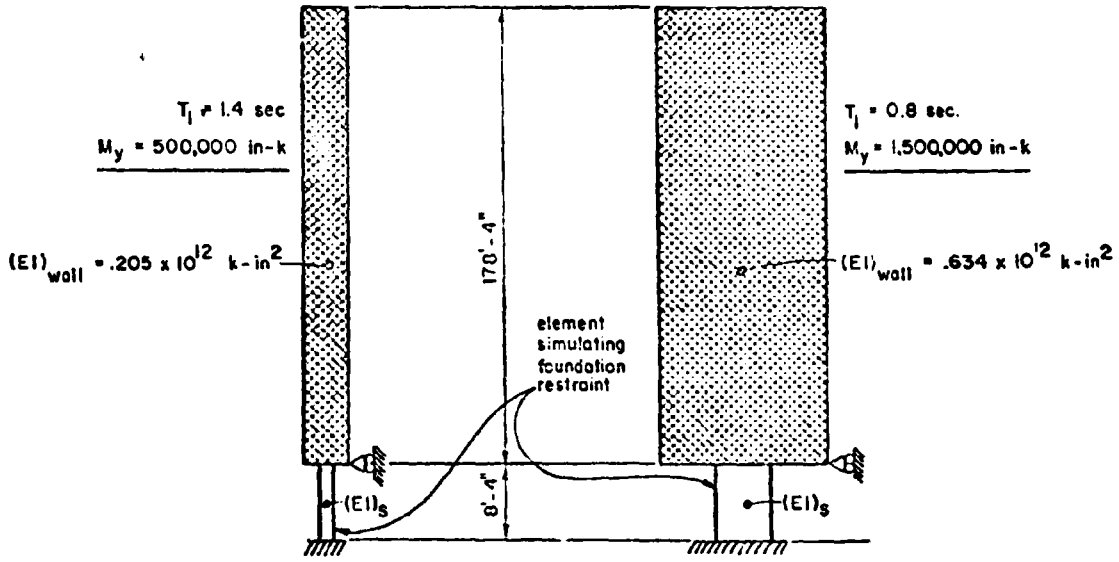

Base Fixity (%)	$(EI)_s$ k-in^2	T_1 (sec.)
100	∞	1.40
75	.31 x 10^{11}	1.43
50	.104 x 10^{11}	1.52

Base Fixity (%)	$(EI)_s$	T_1 (sec.)
100	∞	0.60
75	96 x 10^{11}	0.83
50	.32 x 10^{11}	0.88

Fig. 63 Models Used in Study of Effect of Base Fixity Condition

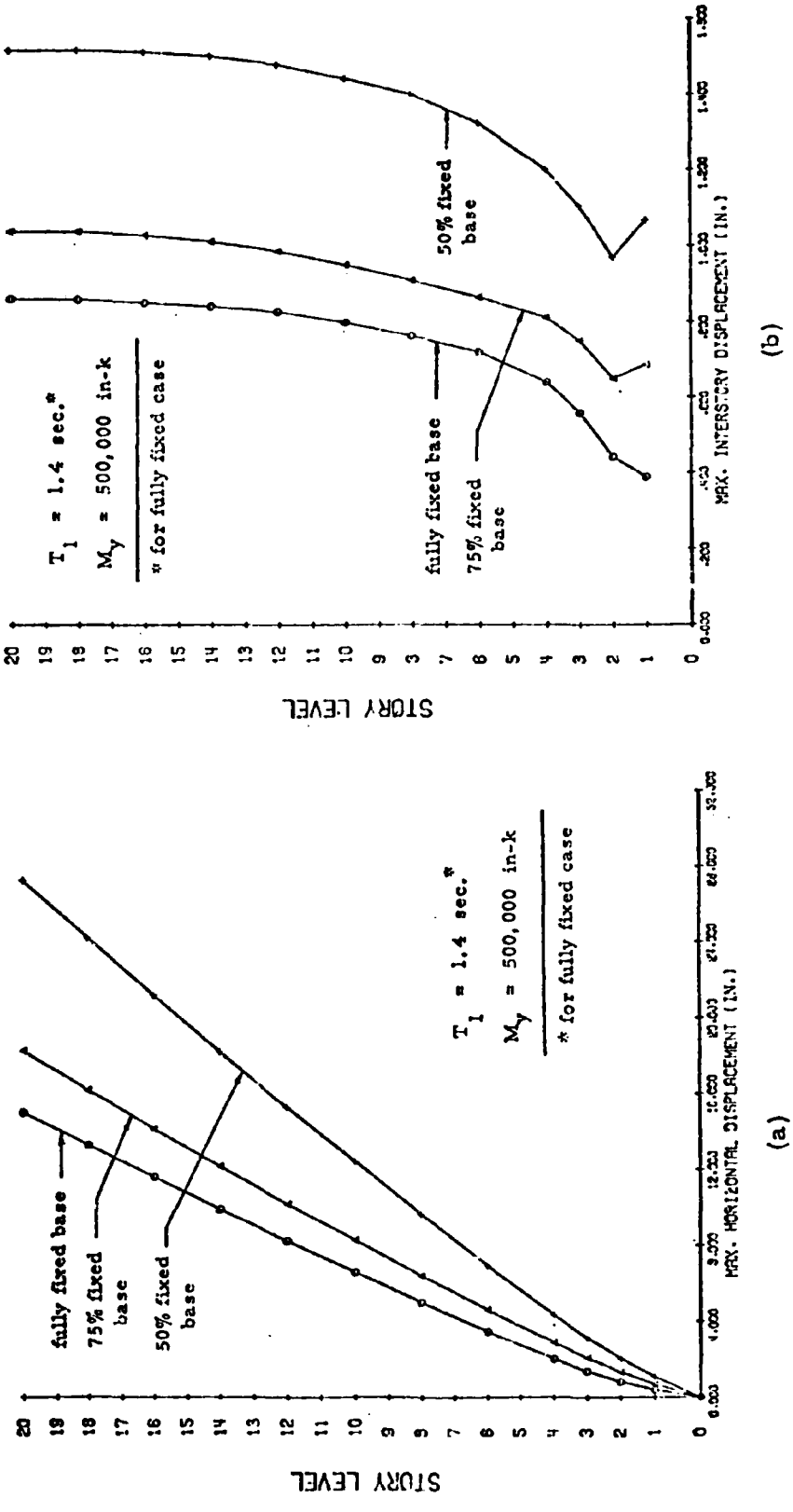

Fig. 64 Effect of Base Fixity Condition

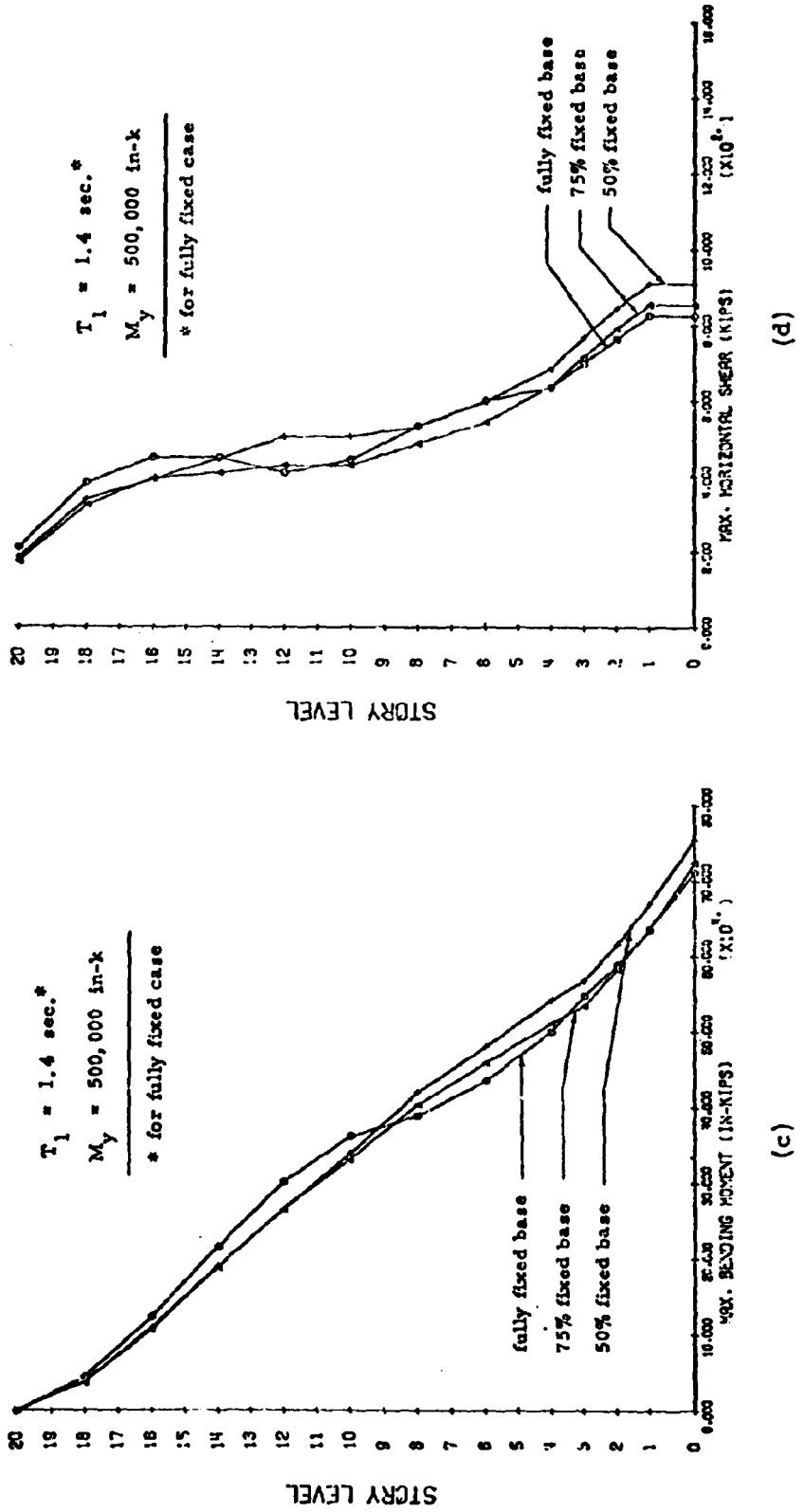

Fig. 64 (contd.) Effect of Base Fixity Condition

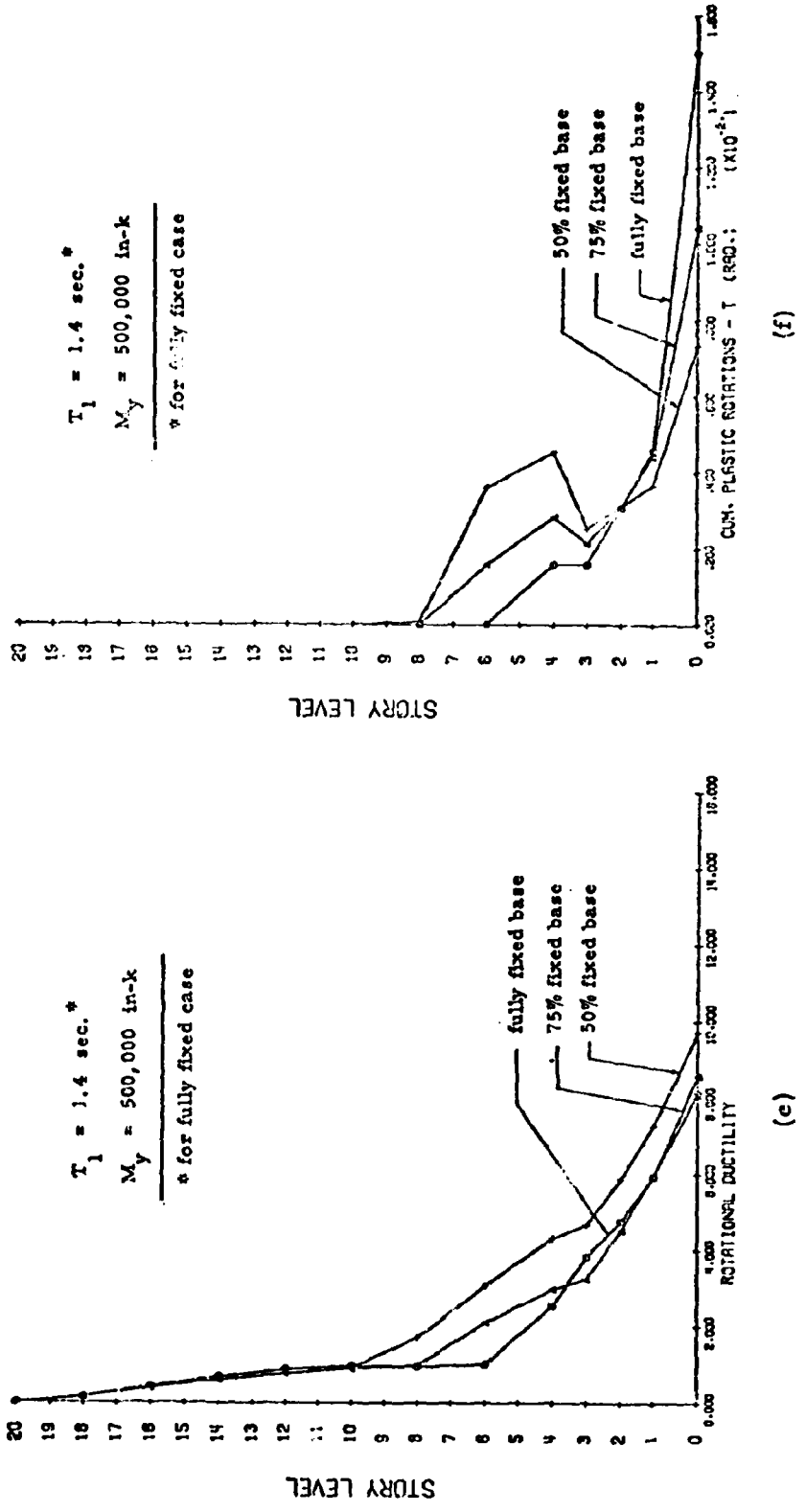

Fig. 64 (contd.) Effect of Base Fixity Condition

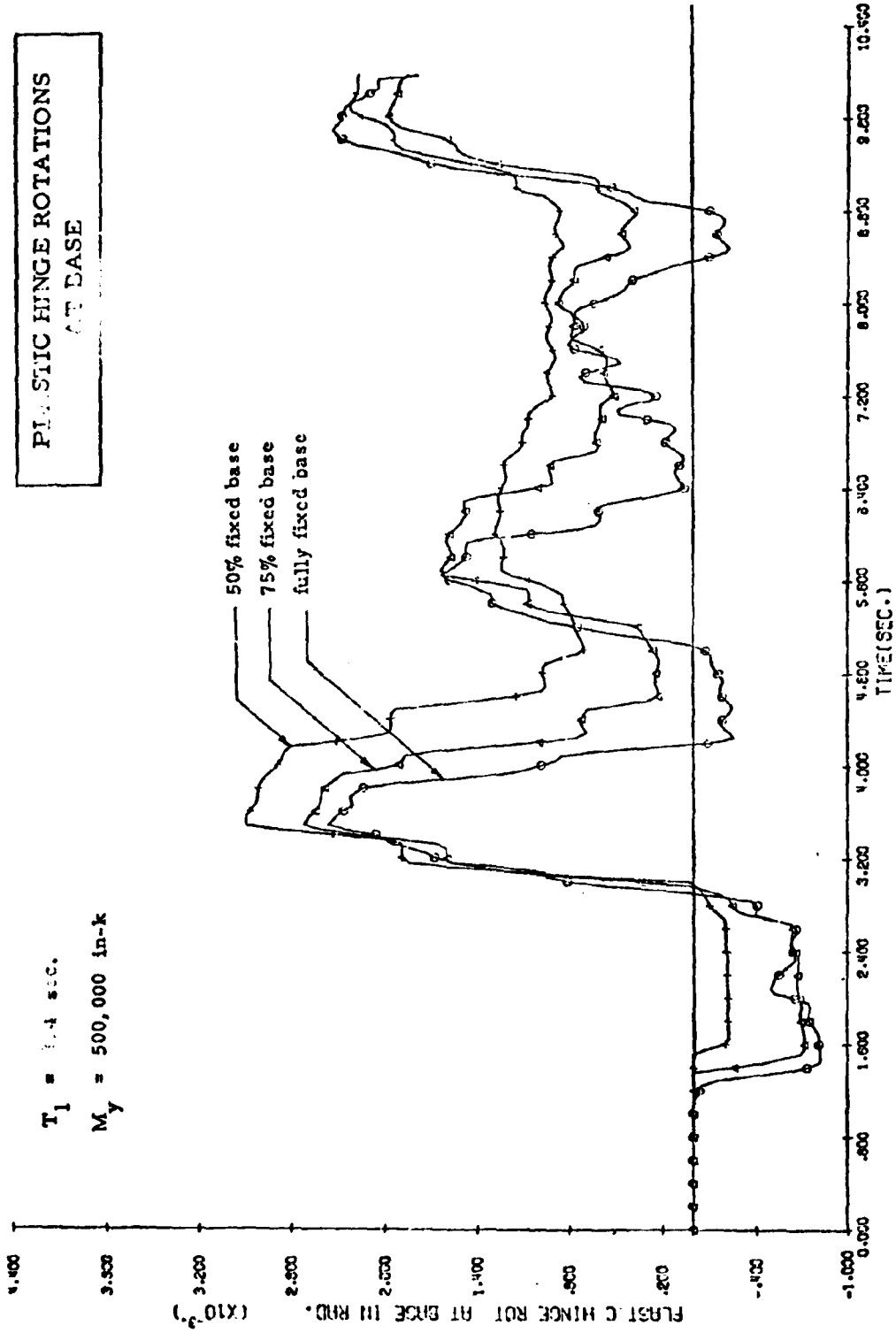

Fig. 65 Plastic Hinge Rotations at Base vs. Time for Different Degrees of Base Fixity

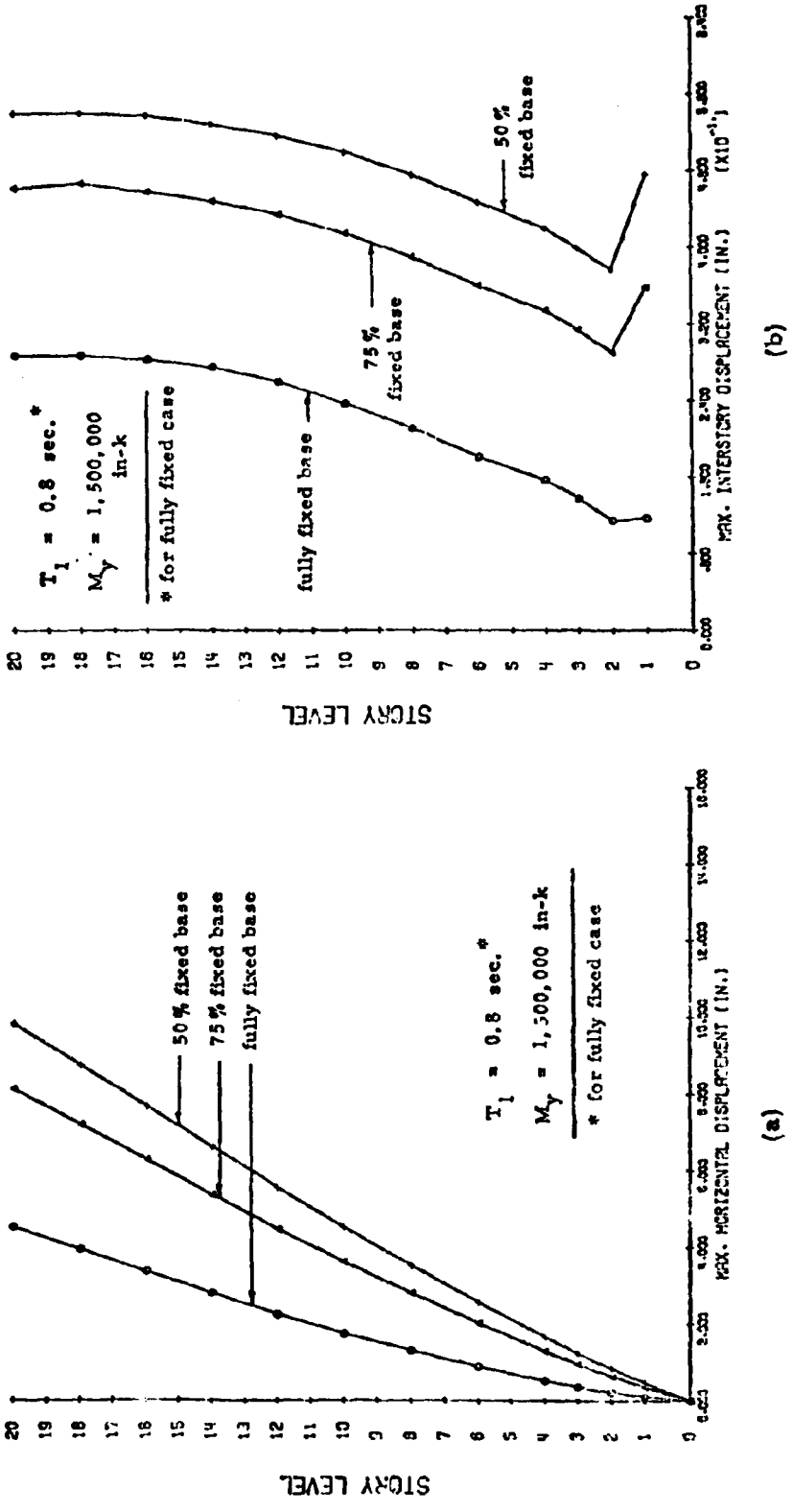

Fig. 66 Effect of Base Fixity Condition

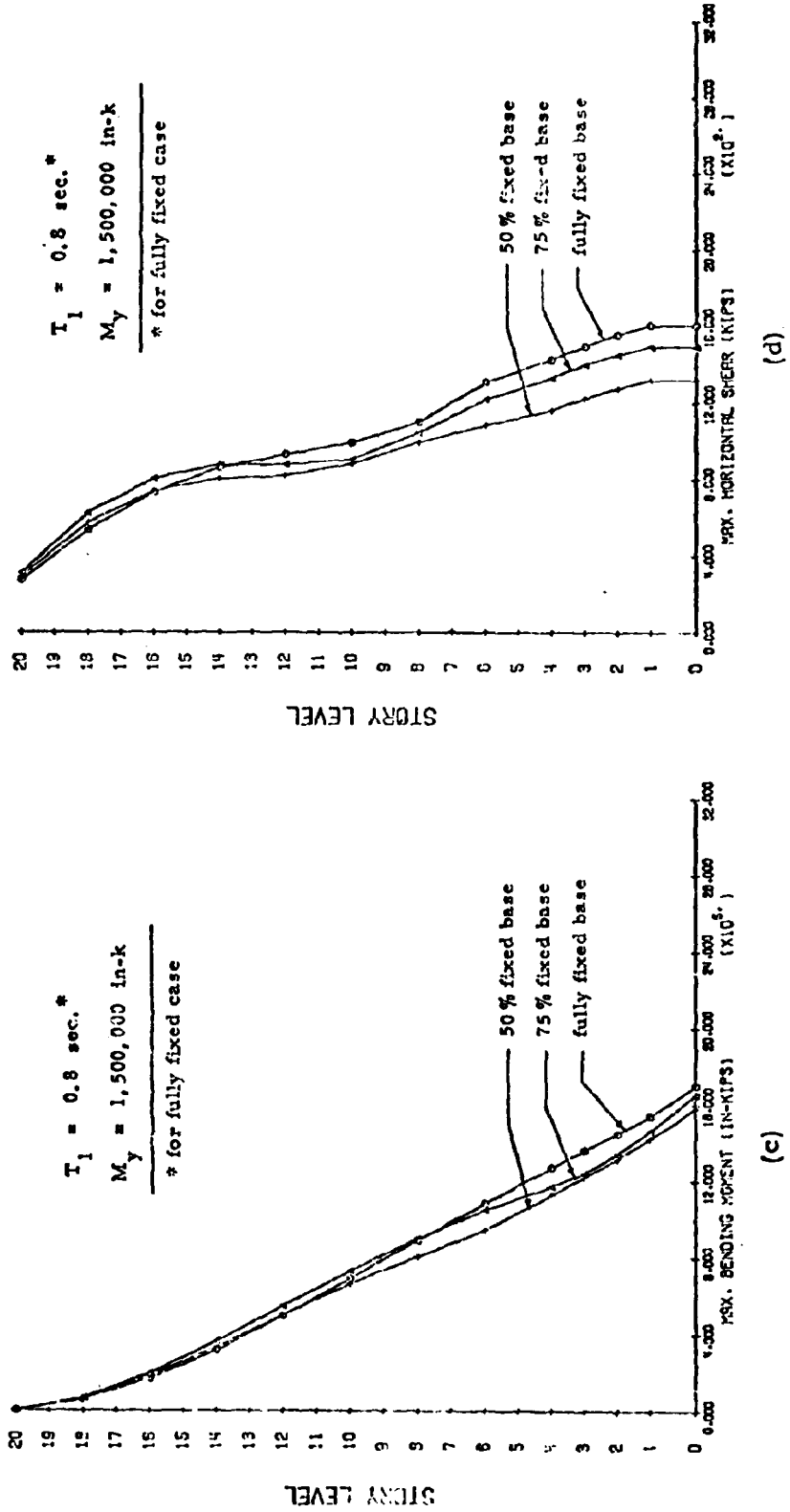

Fig. 66 (contd.) Effect of Base Fixity Condition

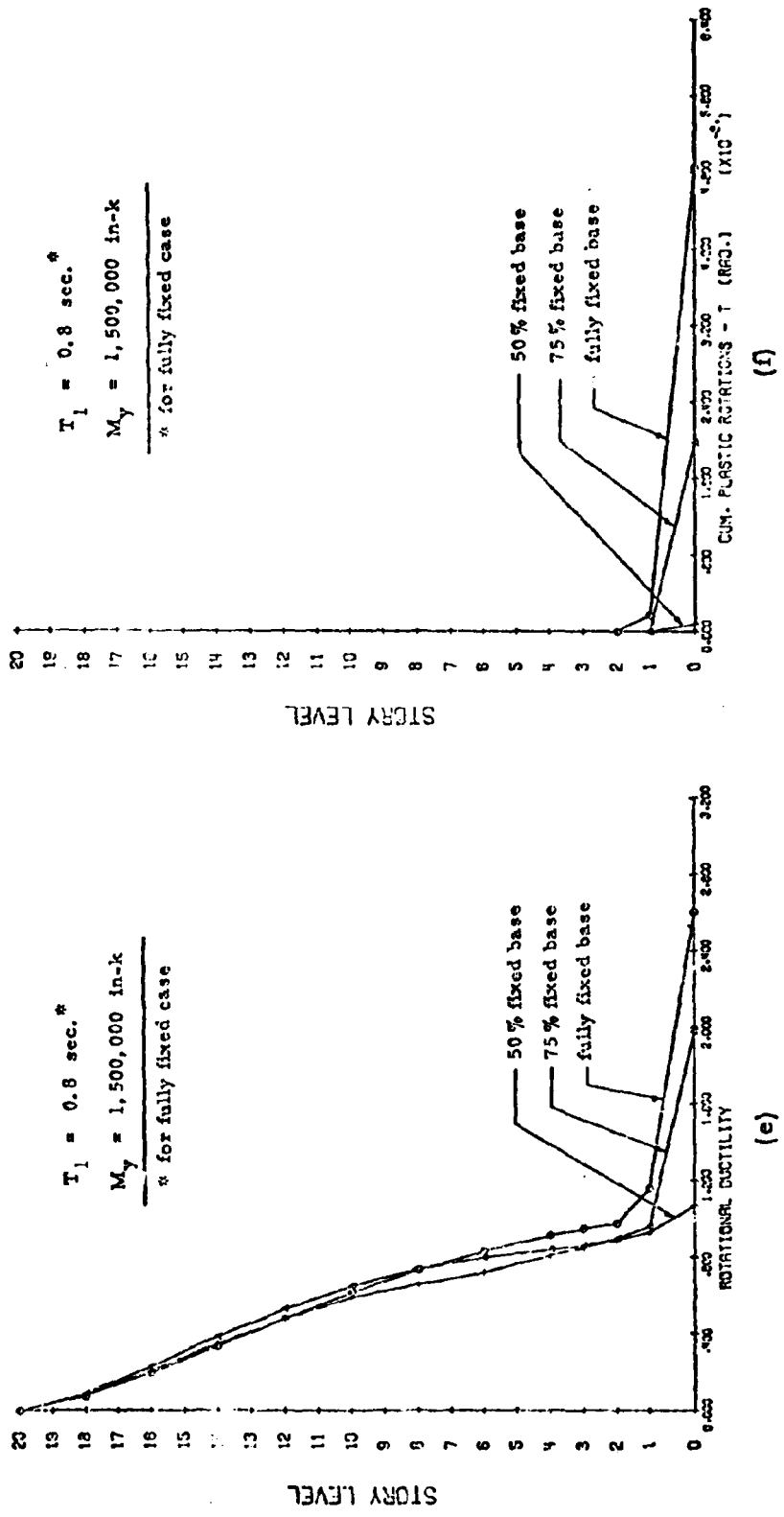

Fig. 66 (contd.) Effect of Base Fixity Condition

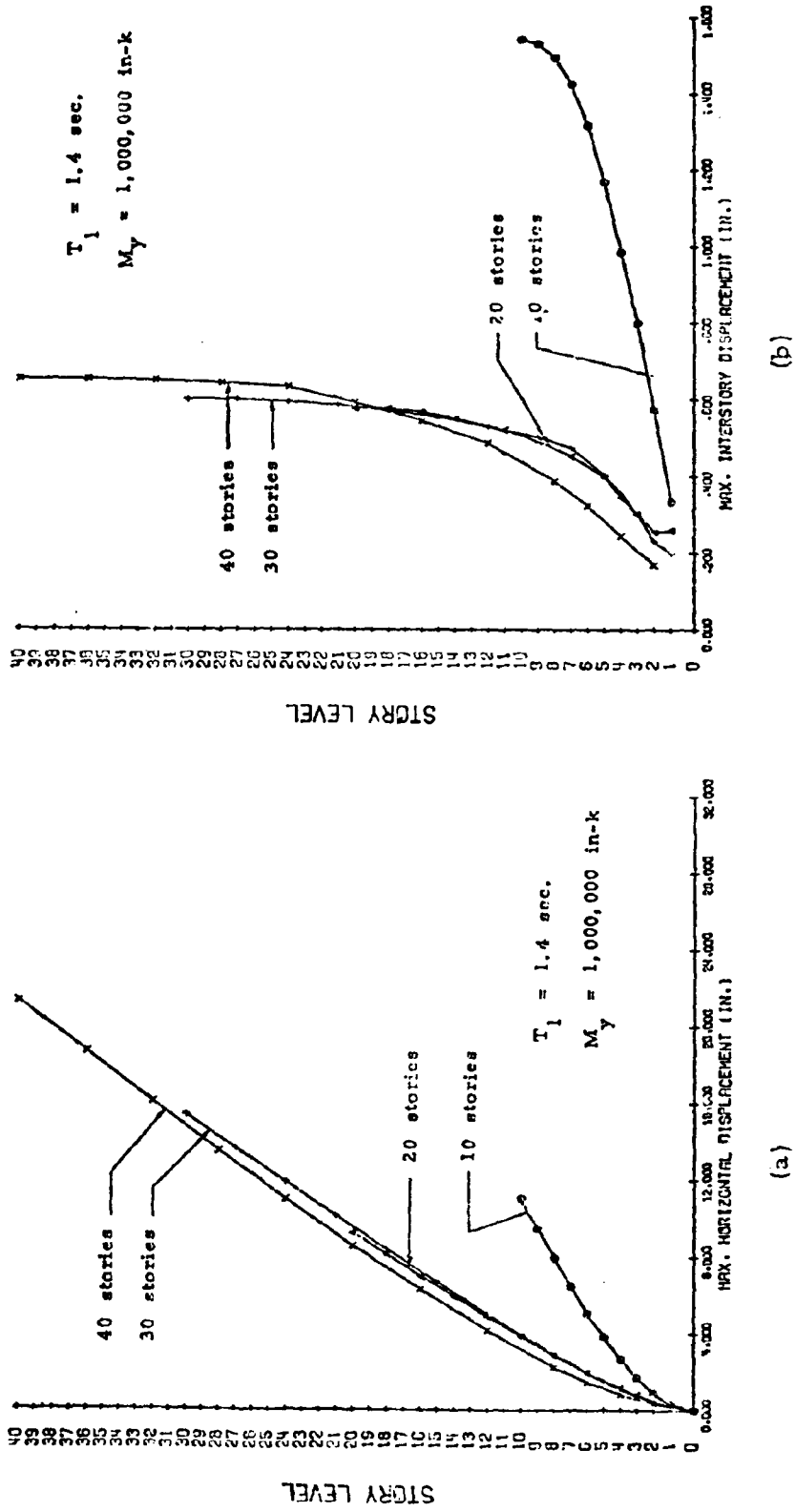

Fig. 67 Effect of Number of Stories

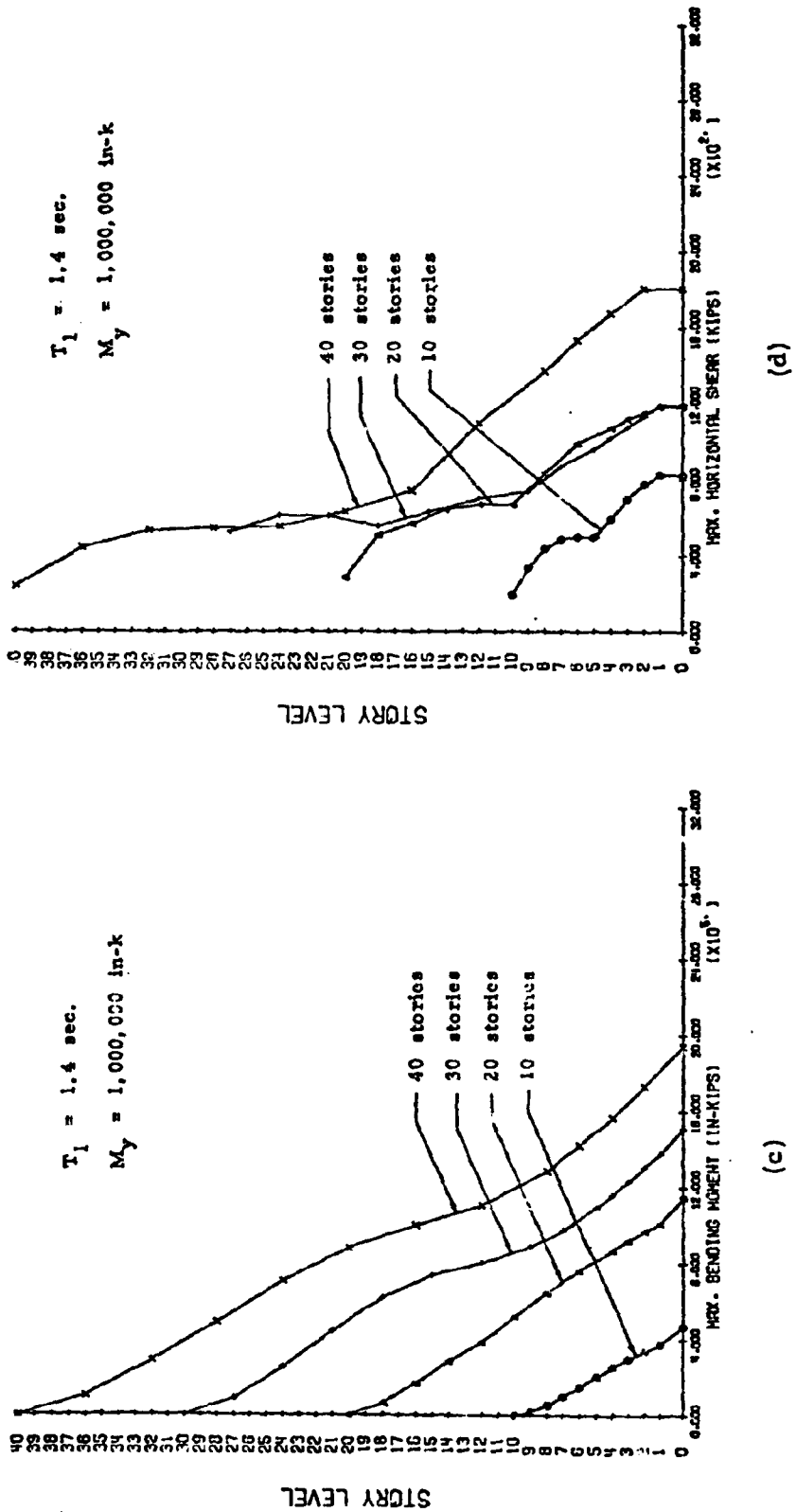

Fig. 67 (contr.) Effect of Number of Stories

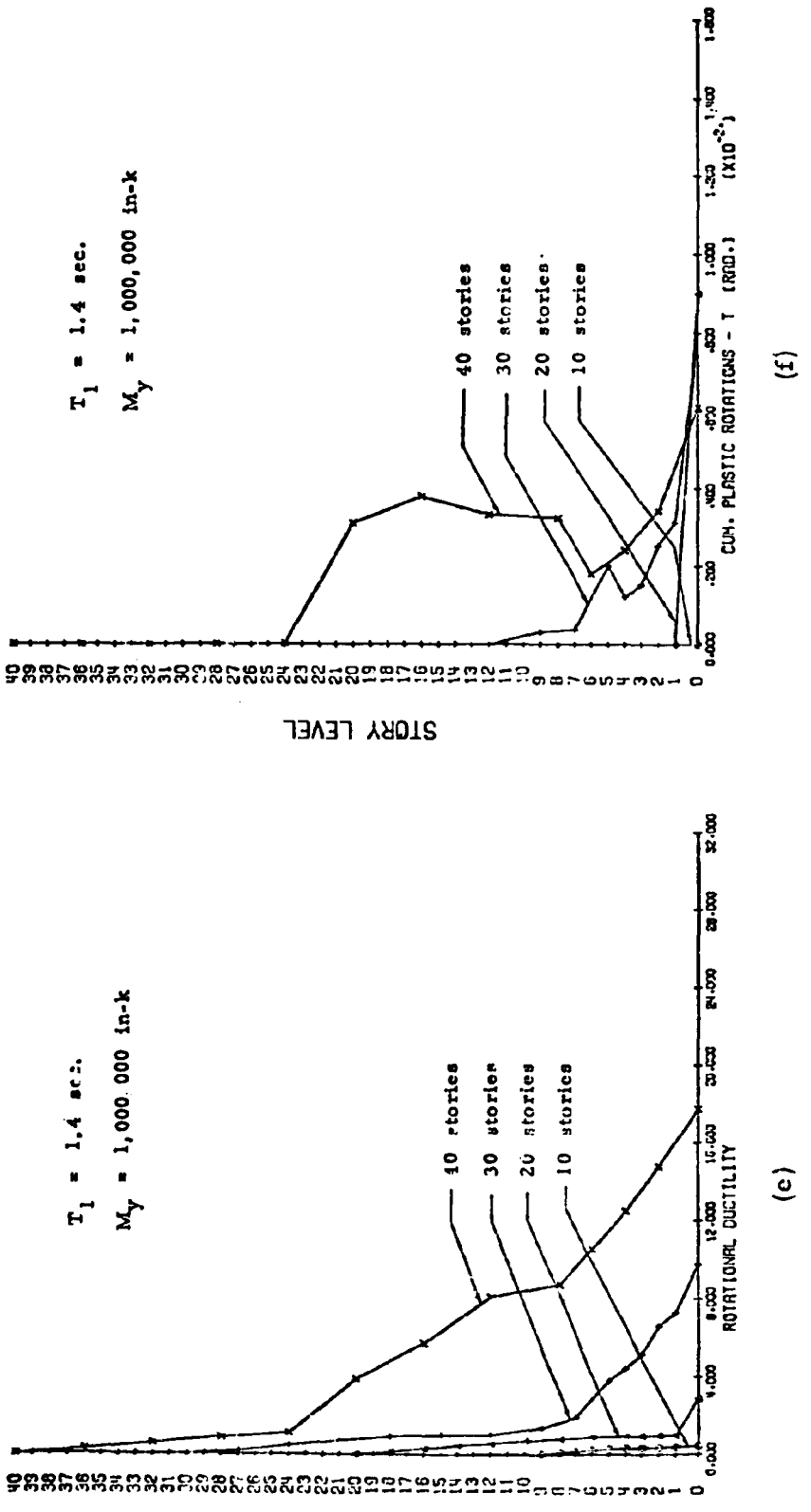

Fig. 67 (contd.) Effect of Number of Stories

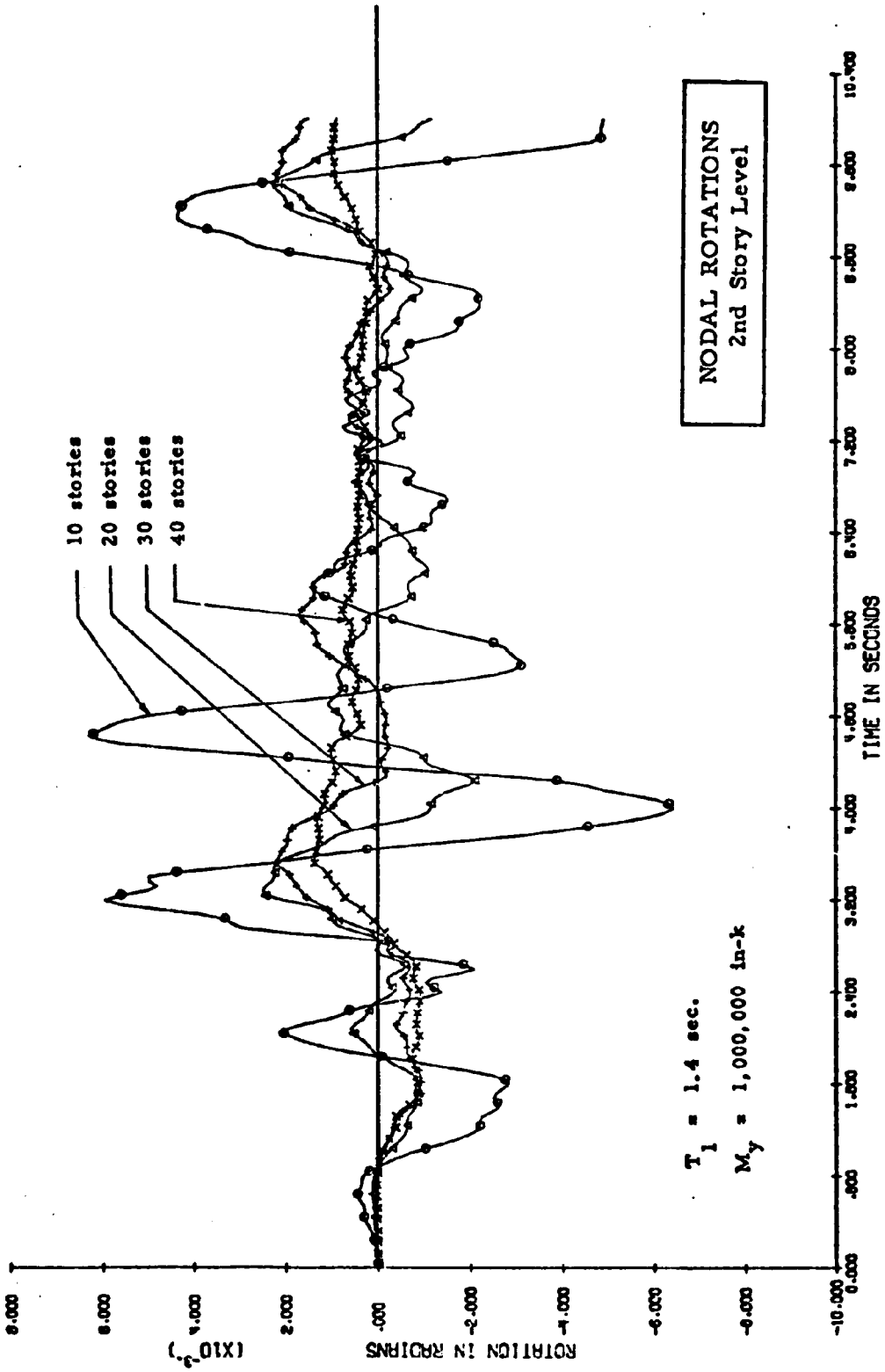

Fig. 68 Nodal Rotations at Second Story Level vs. Time for Different Heights of Structure

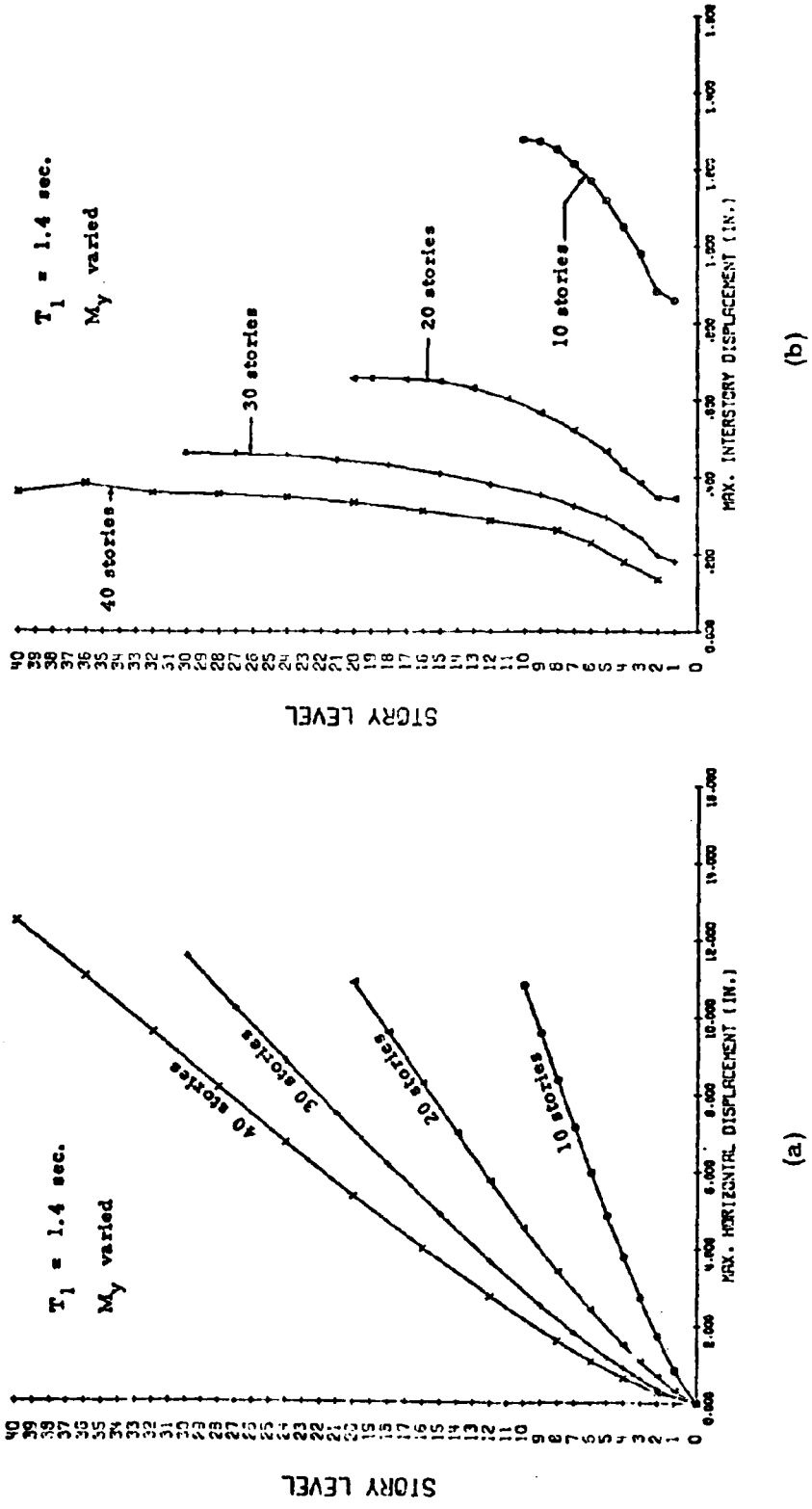

Fig. 69 Effect of Number of Stories

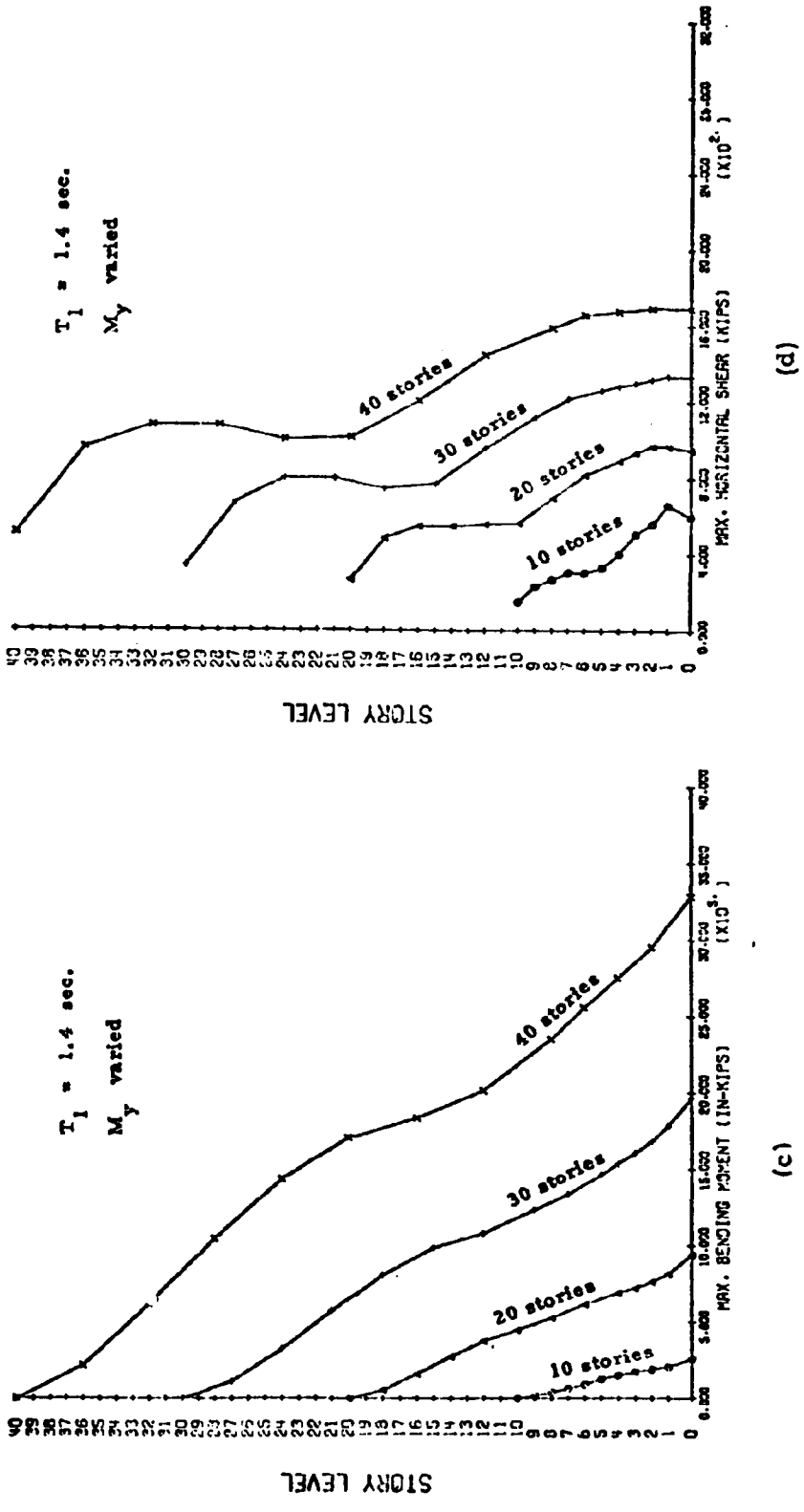

Fig. 69 (contd.) Effect of Number of Stories

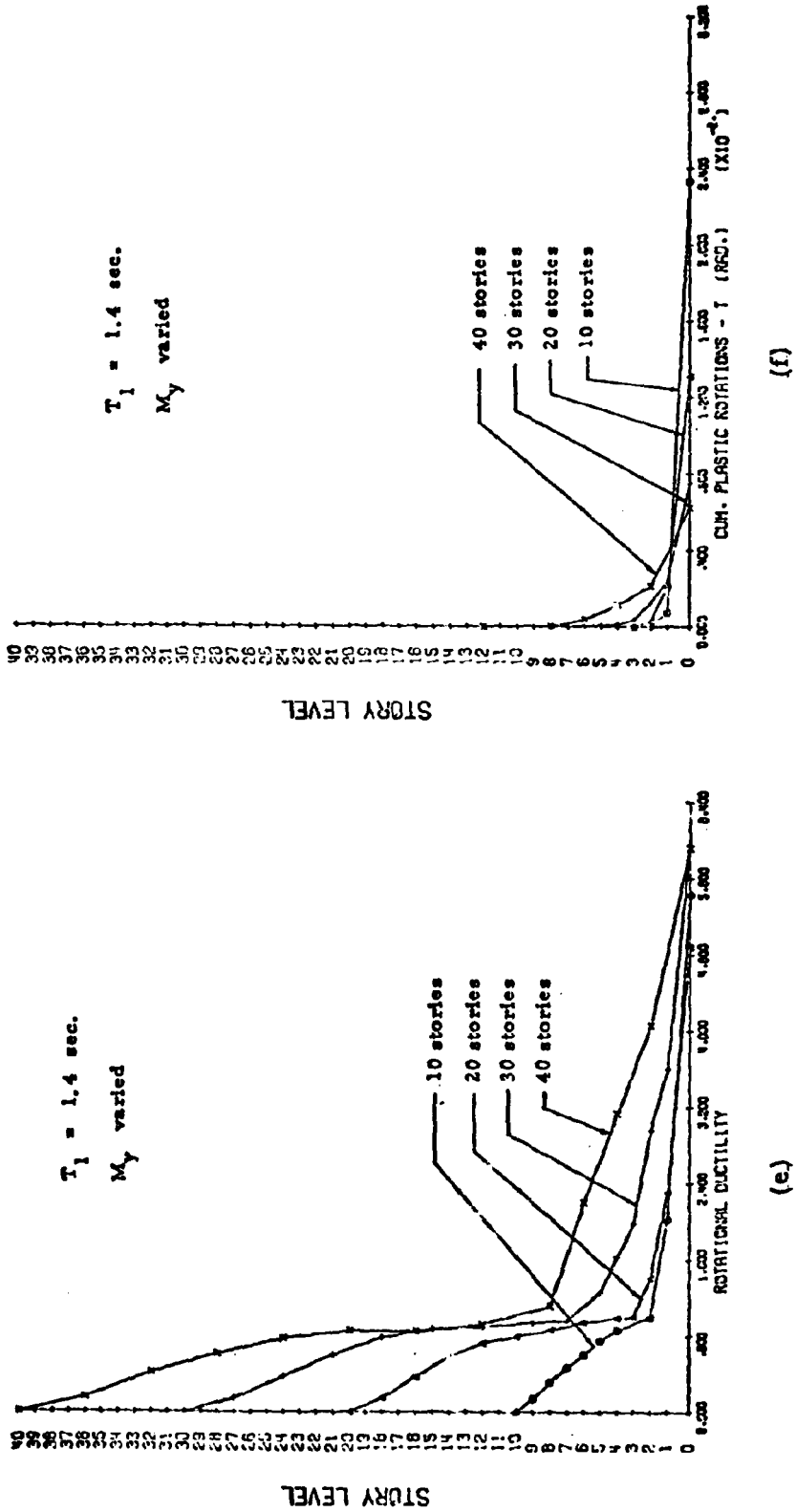

Fig. 69 (contd.) Effect of Number of Stories

APPENDIX B

This Appendix presents a compilation of normalized time-histories of the rotation in the first story of structural walls corresponding to variations in specified parameters. Unless specifically indicated, the ground motion used was the first 10 seconds of the E-W component of the 1940 El Centro record, with intensity normalized to yield a spectrum intensity equal to 1.5 $(SI)^*_{ref.}$

$^*SI_{ref.}$ (reference spectrum intensity) = the area under the 5%-damped relative velocity response spectrum corresponding to the first 10 seconds of the N-S component of the 1940 El Centro record, between periods of 0.1 sec. and 3.0 sec. $SI_{ref.}$ = 70.15 inches.

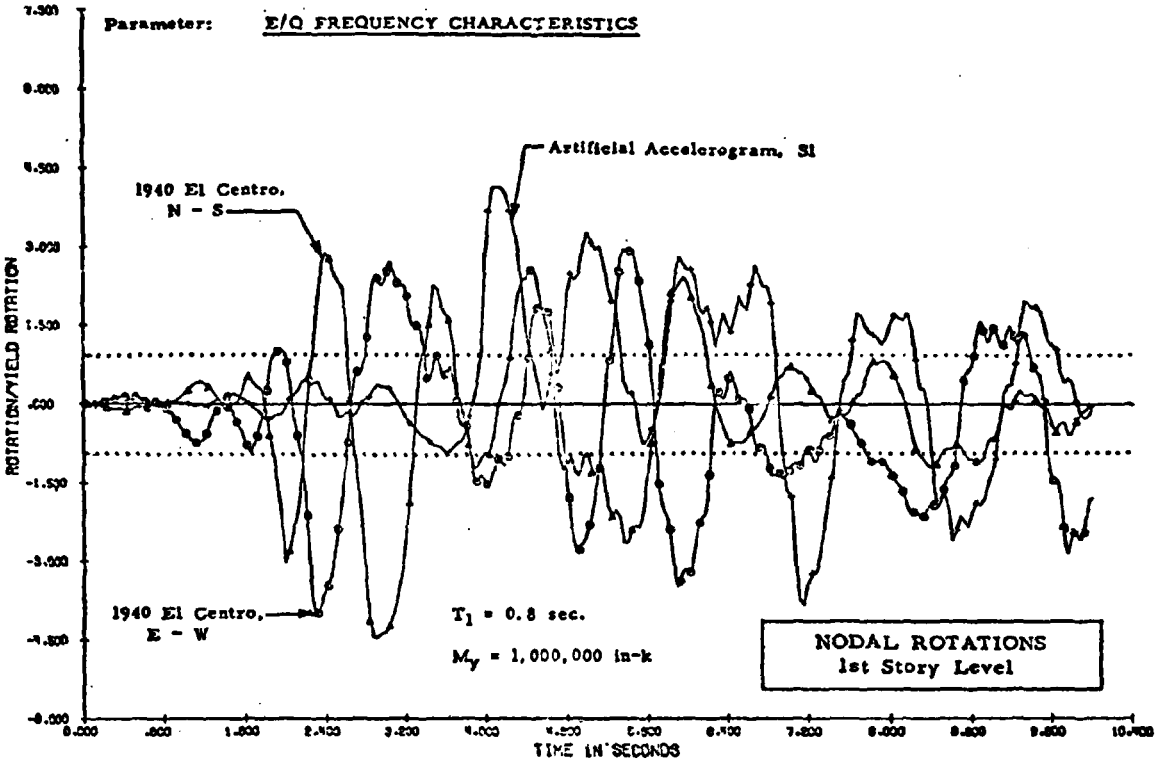
Parameter: E/Q FREQUENCY CHARACTERISTICS
Artificial Accelerogram, S1
1940 El Centro, N - S
1940 El Centro, E - W
T_1 = 0.8 sec.
M_y = 1,000,000 in-k
NODAL ROTATIONS
1st Story Level
ROTATION/YIELD ROTATION
TIME IN SECONDS

Fig. B1

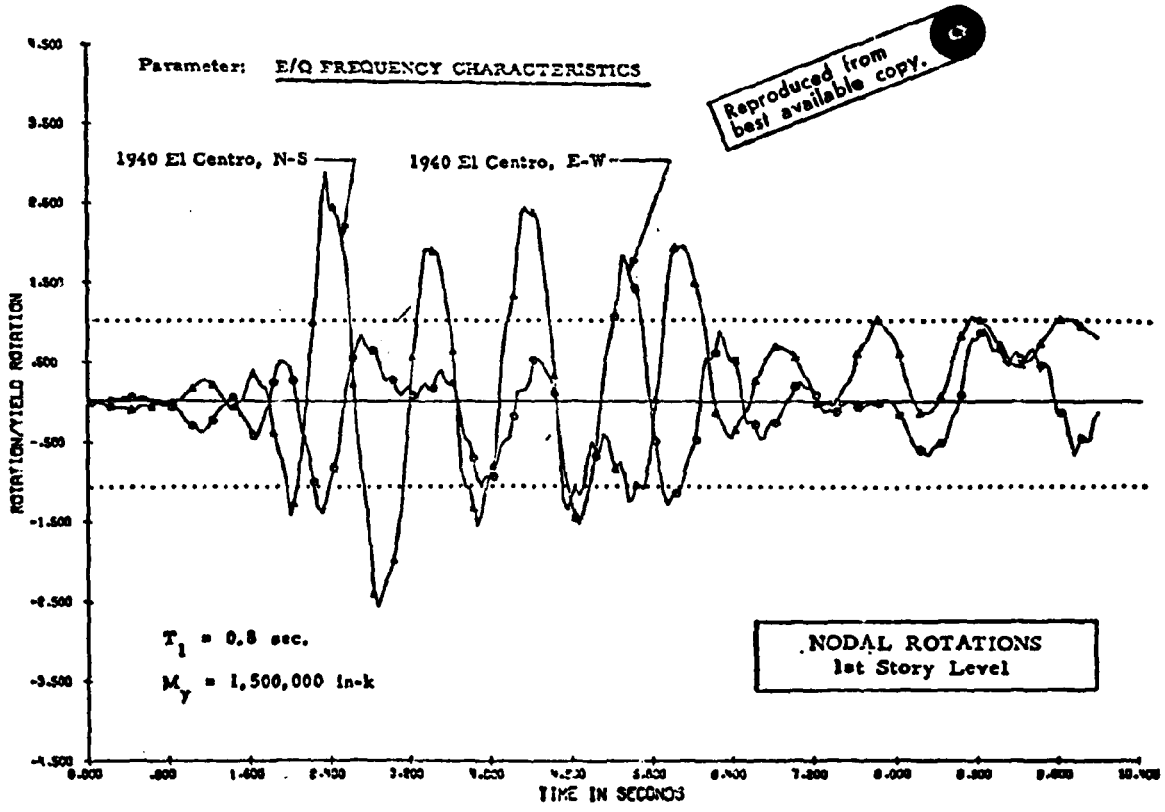
Parameter: E/Q FREQUENCY CHARACTERISTICS
Reproduced from best available copy.
1940 El Centro, N-S
1940 El Centro, E-W
T_1 = 0.8 sec.
M_y = 1,500,000 in-k
NODAL ROTATIONS
1st Story Level
ROTATION/YIELD ROTATION
TIME IN SECONDS

Fig. B2

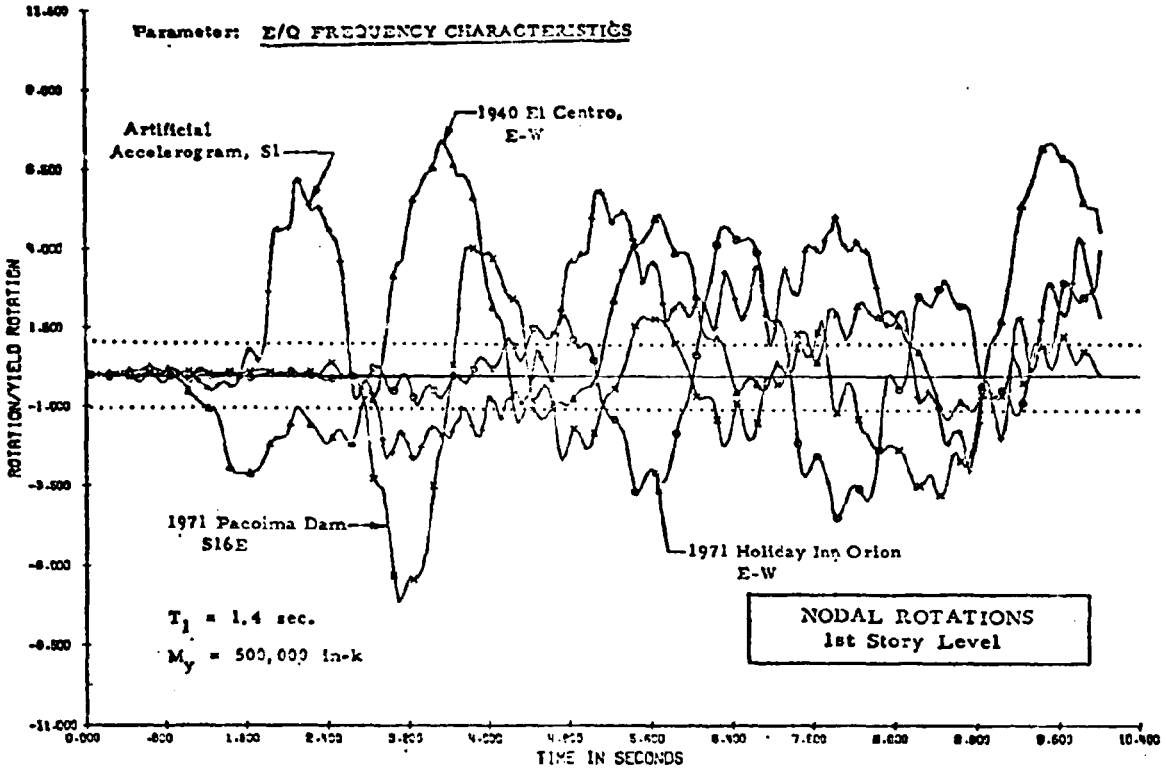
Parameter: E/Q FREQUENCY CHARACTERISTICS
Artificial Accelerogram, S1
1940 El Centro, E-W
1971 Pacoima Dam S16E
1971 Holiday Inn Orion E-W
T_1 = 1.4 sec.
M_y = 500,000 in-k
NODAL ROTATIONS 1st Story Level
ROTATION/YIELD ROTATION
TIME IN SECONDS

Fig. B3

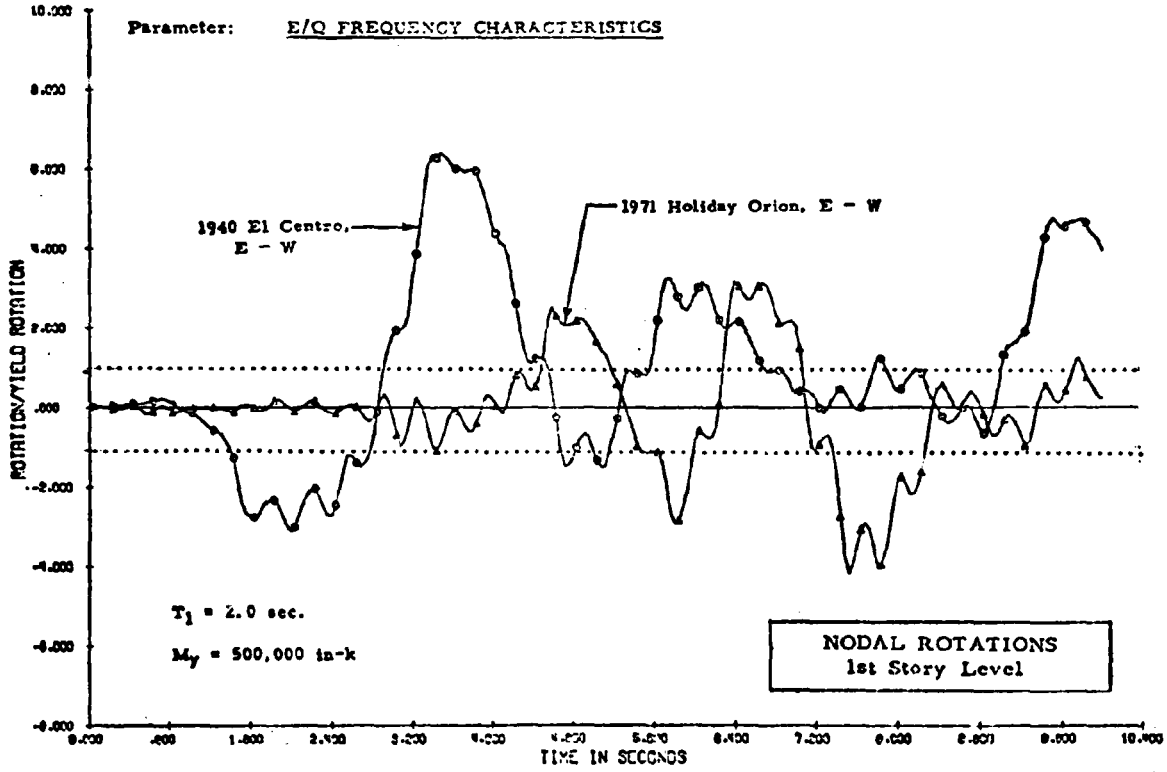
Parameter: E/Q FREQUENCY CHARACTERISTICS
1940 El Centro, E - W
1971 Holiday Orion, E - W
T_1 = 2.0 sec.
M_y = 500,000 in-k
NODAL ROTATIONS 1st Story Level
ROTATION/YIELD ROTATION
TIME IN SECONDS

Fig. B4

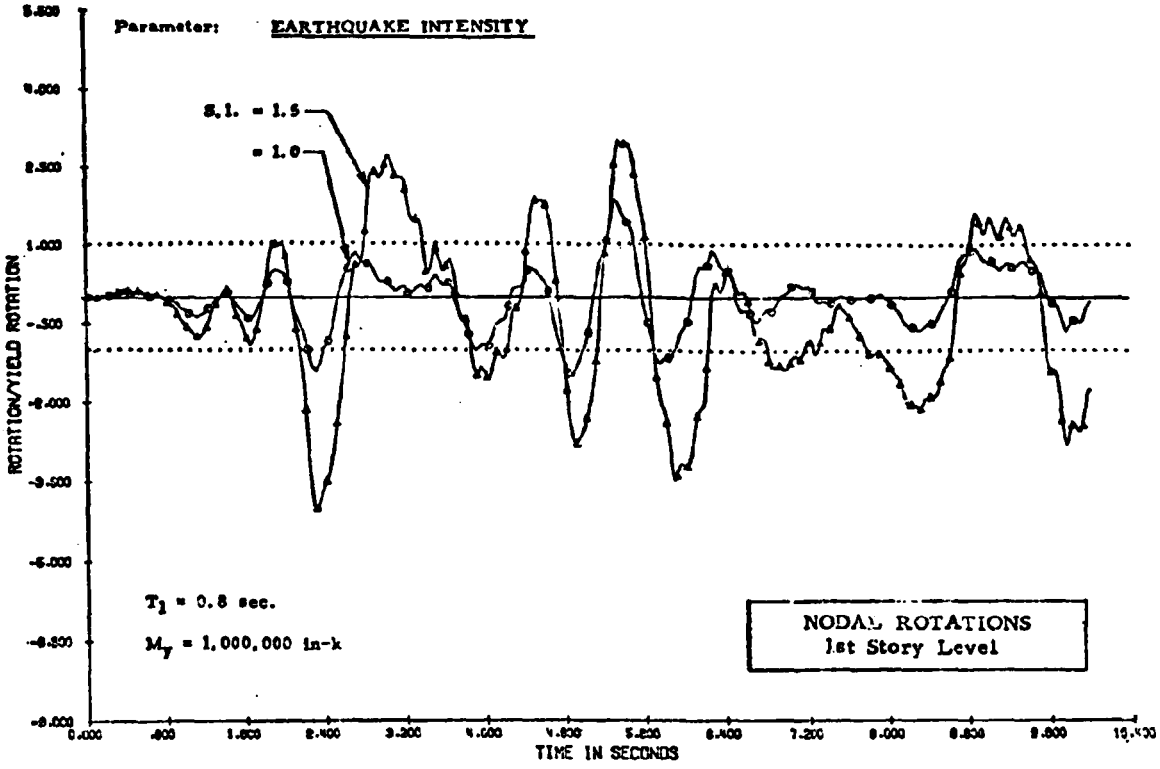
Parameter: EARTHQUAKE INTENSITY
S.I. = 1.5
= 1.0
ROTATION/YIELD ROTATION
T_1 = 0.8 sec.
M_y = 1,000,000 in-k
NODAL ROTATIONS
1st Story Level
TIME IN SECONDS

Fig. B5

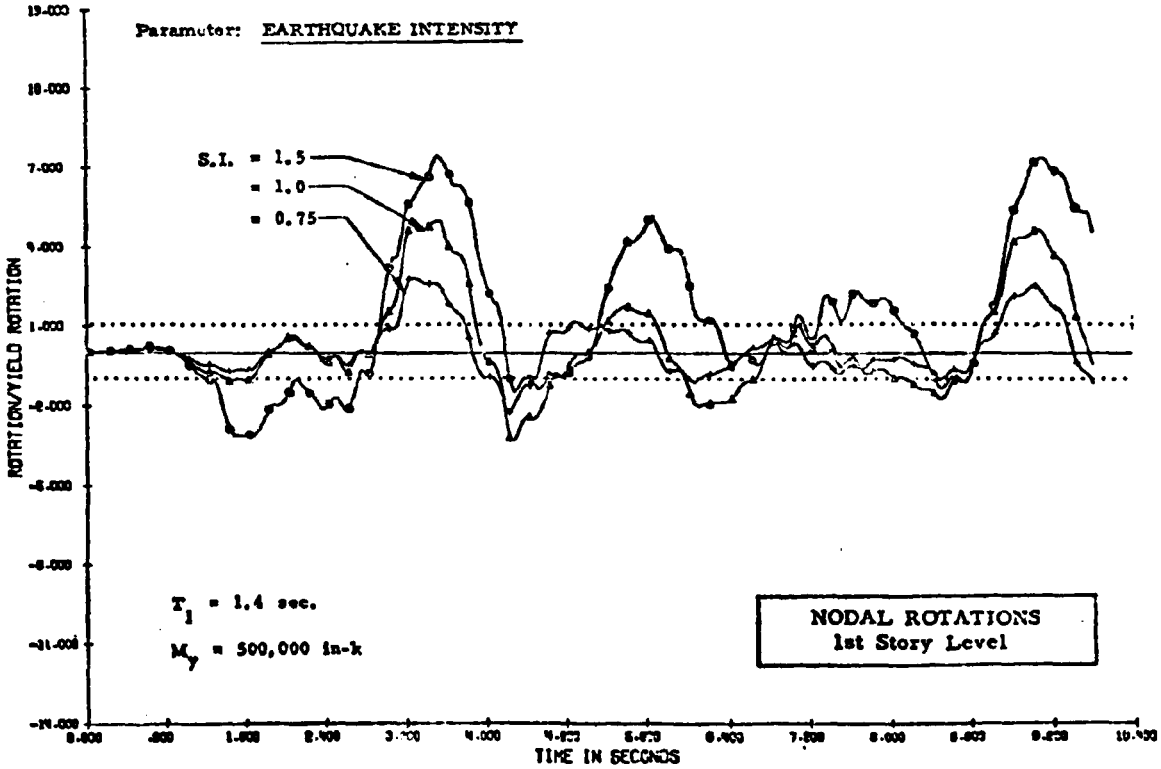
Parameter: EARTHQUAKE INTENSITY
S.I. = 1.5
= 1.0
= 0.75
ROTATION/YIELD ROTATION
T_1 = 1.4 sec.
M_y = 500,000 in-k
NODAL ROTATIONS
1st Story Level
TIME IN SECONDS

Fig. B6

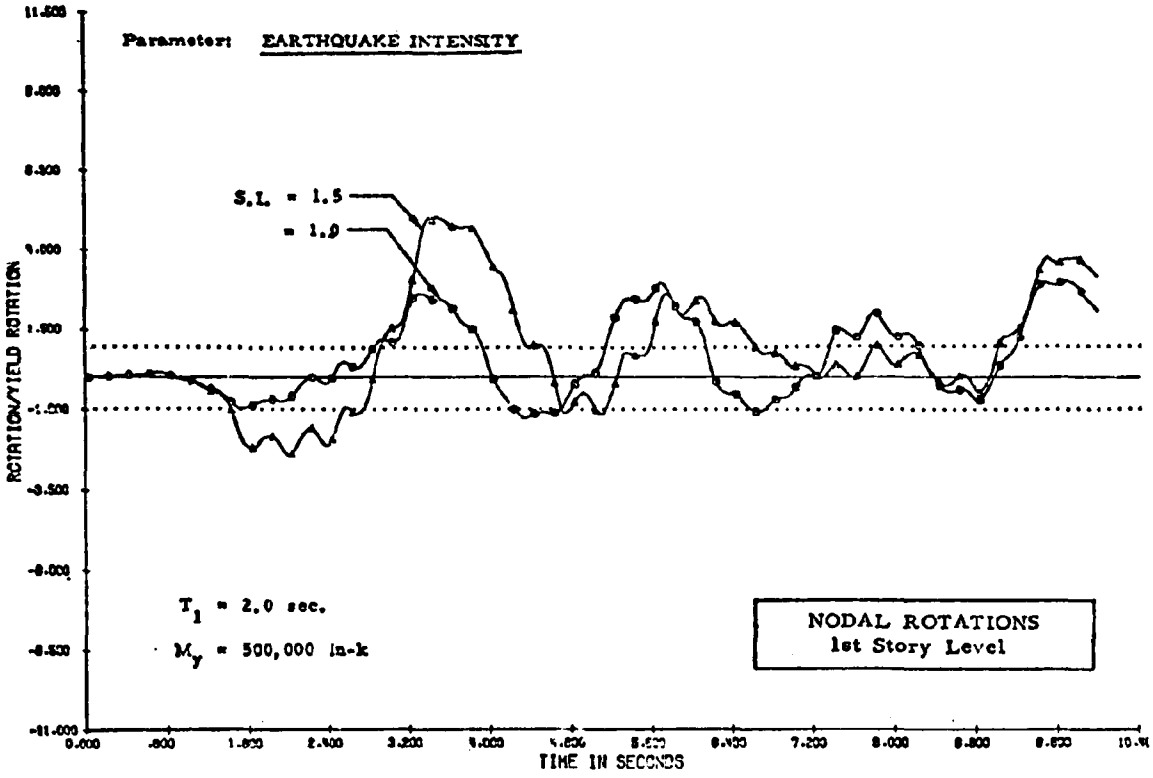
Parameter: EARTHQUAKE INTENSITY
S.I. = 1.5
= 1.0
ROTATION/YIELD ROTATION
T_1 = 2.0 sec.
M_y = 500,000 in-k
NODAL ROTATIONS
1st Story Level
TIME IN SECONDS

Fig. B7

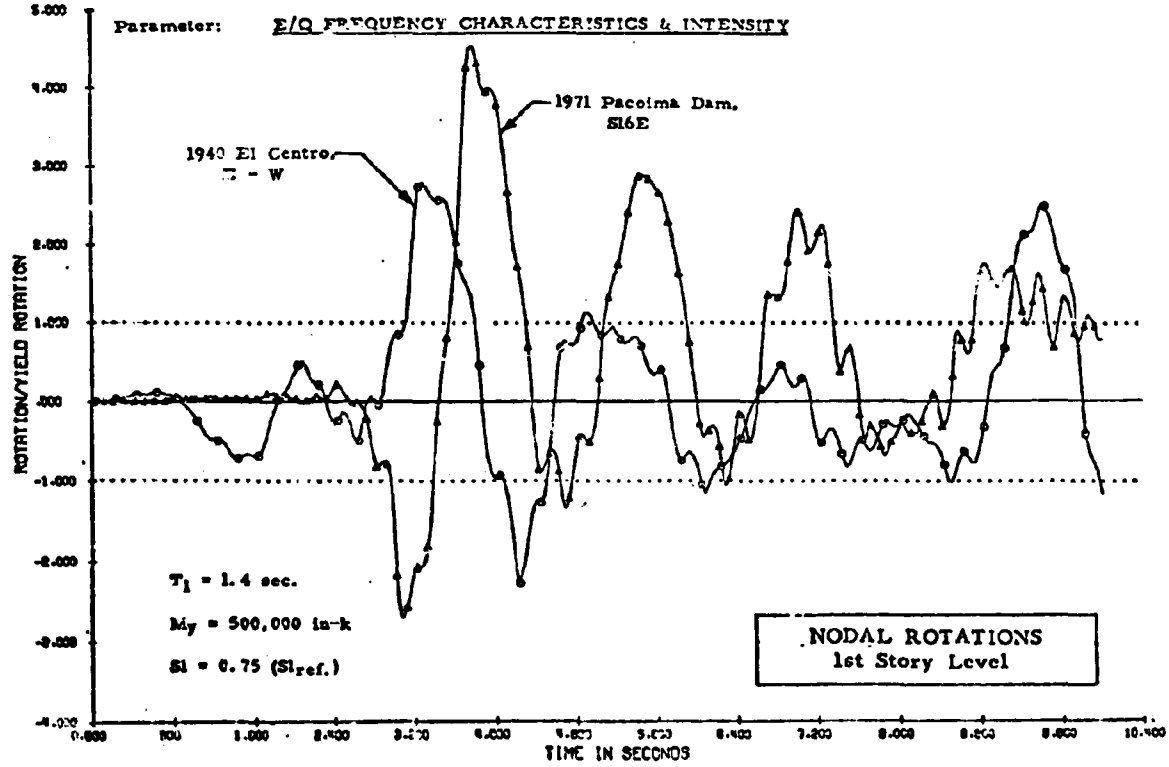
Parameter: E/Q FREQUENCY CHARACTERISTICS & INTENSITY
1971 Pacoima Dam, S16E
1940 El Centro, E - W
ROTATION/YIELD ROTATION
T_1 = 1.4 sec.
My = 500,000 in-k
SI = 0.75 ($SI_{ref.}$)
NODAL ROTATIONS
1st Story Level
TIME IN SECONDS

Fig. B8

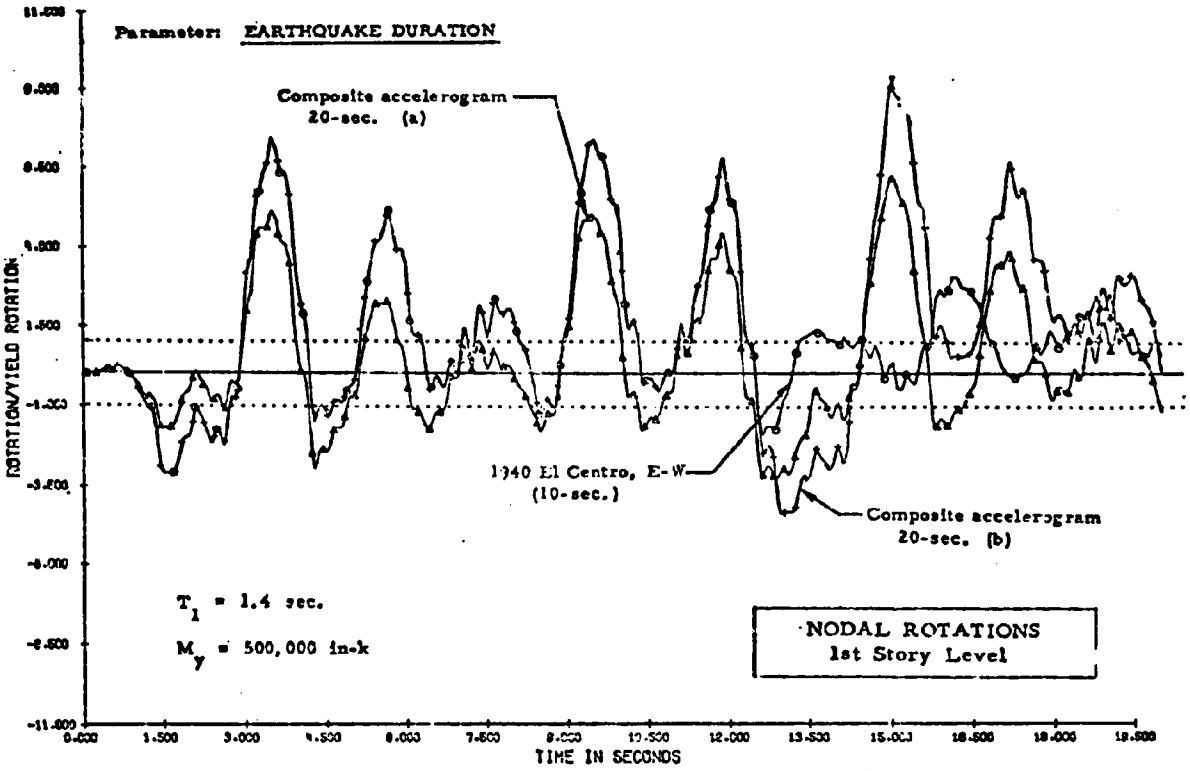

Fig. B9

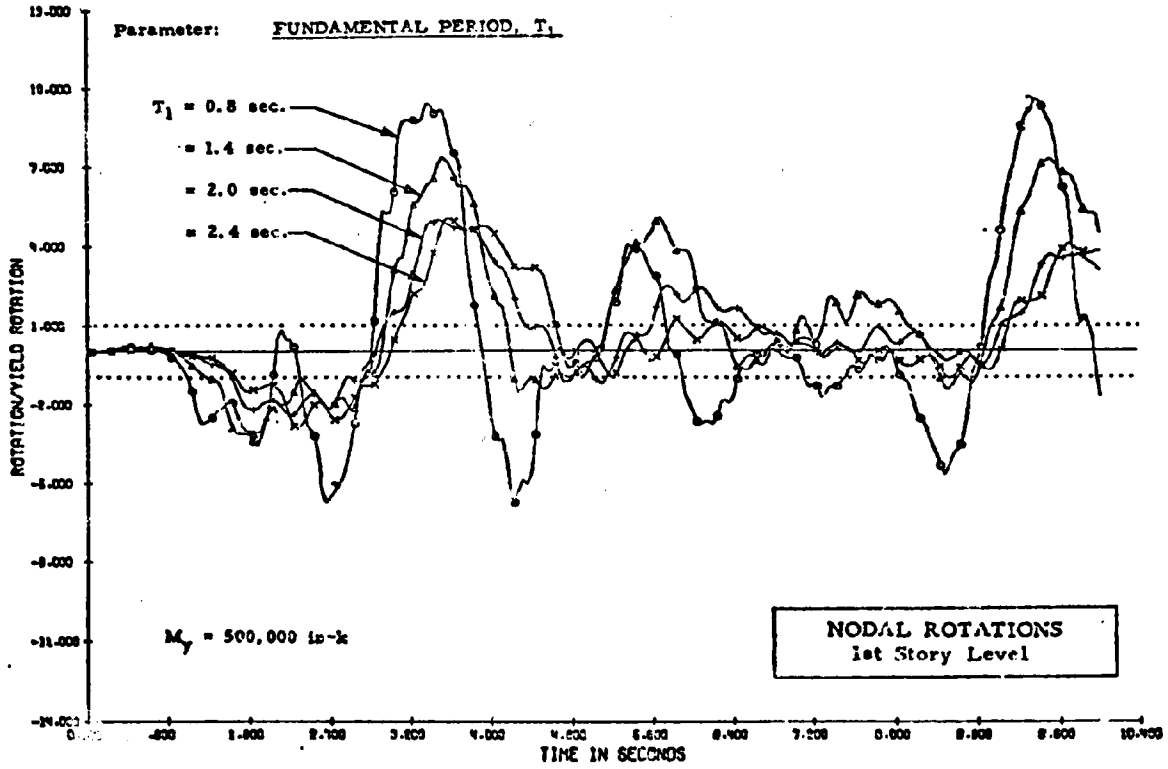

Fig. B10

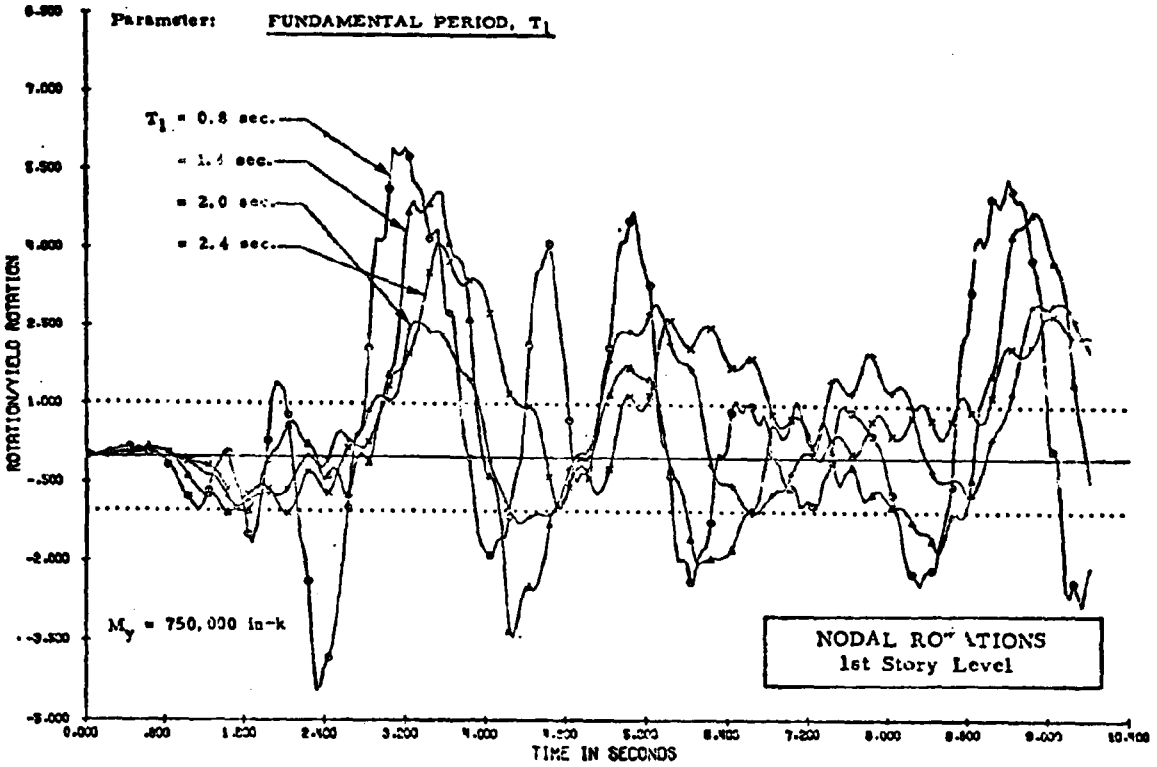

Fig. B11

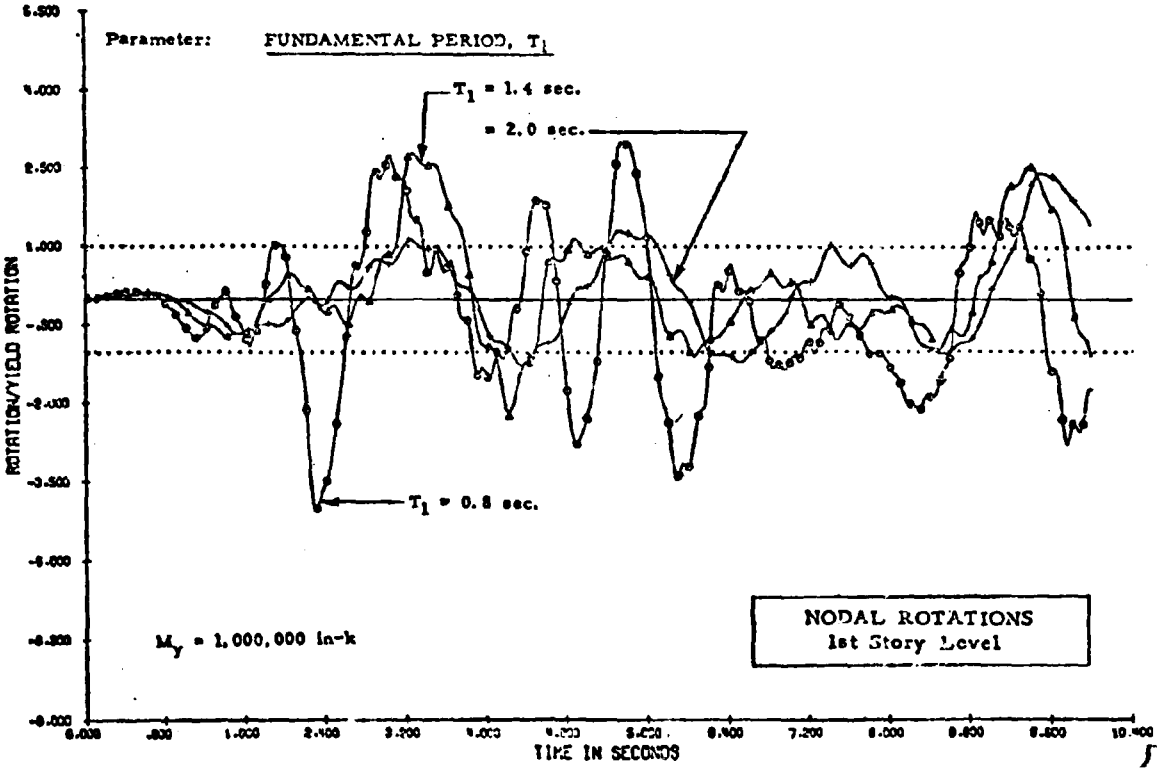

Fig. B12

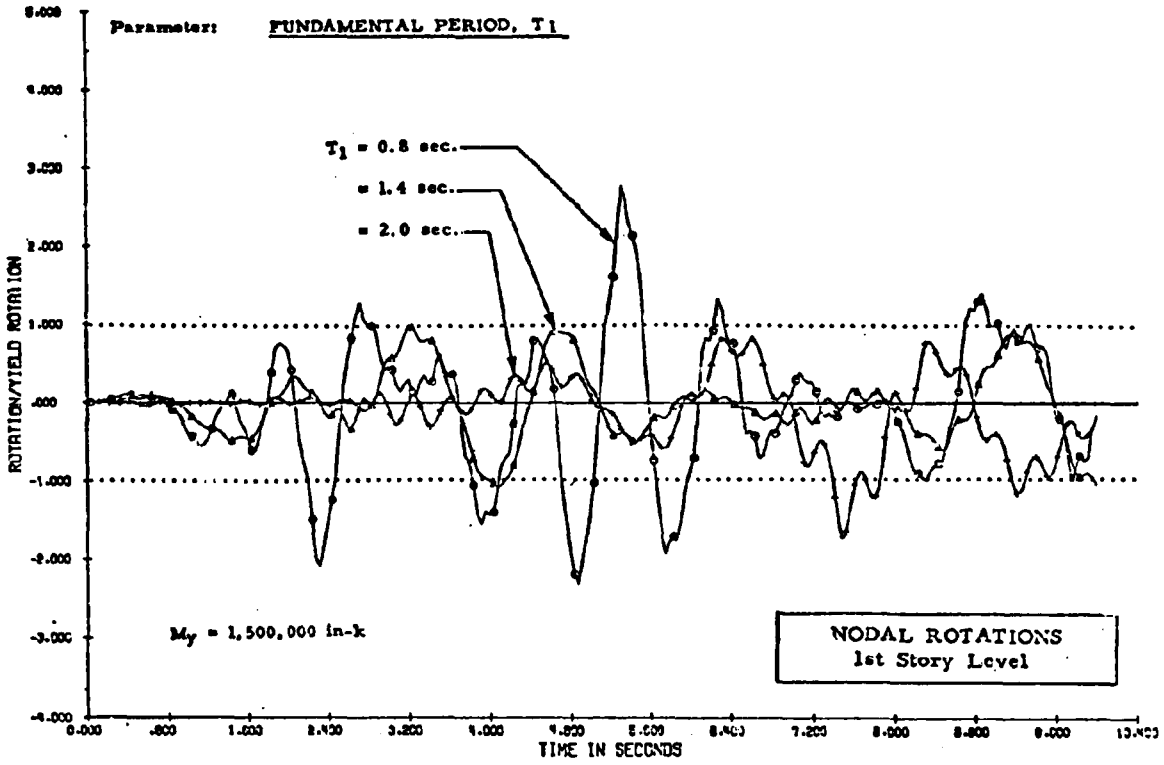

Fig. B13

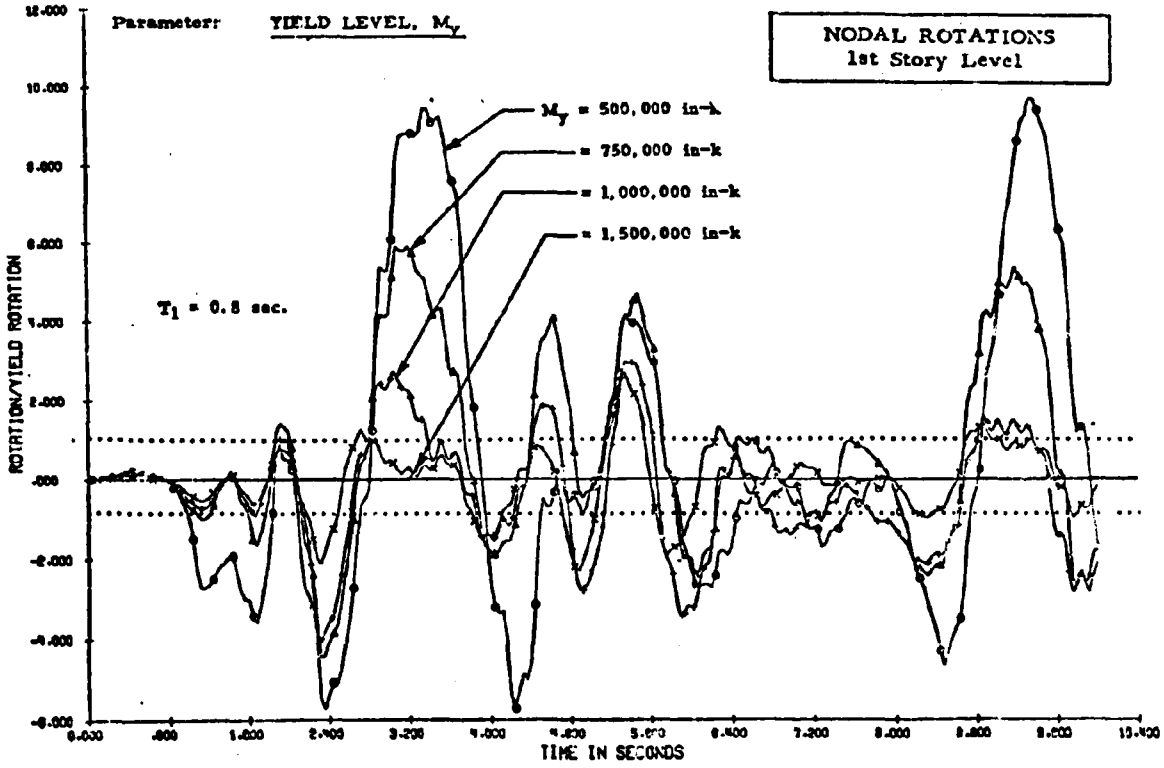

Fig. B14

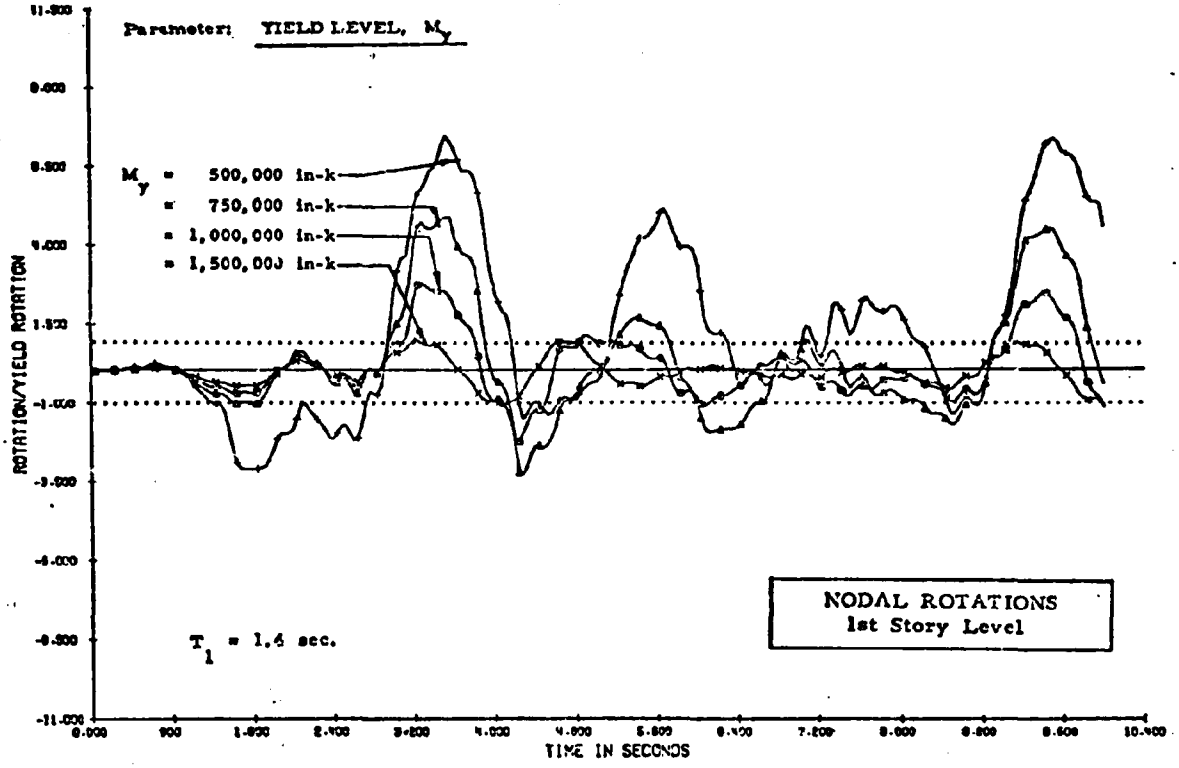

Fig. B15

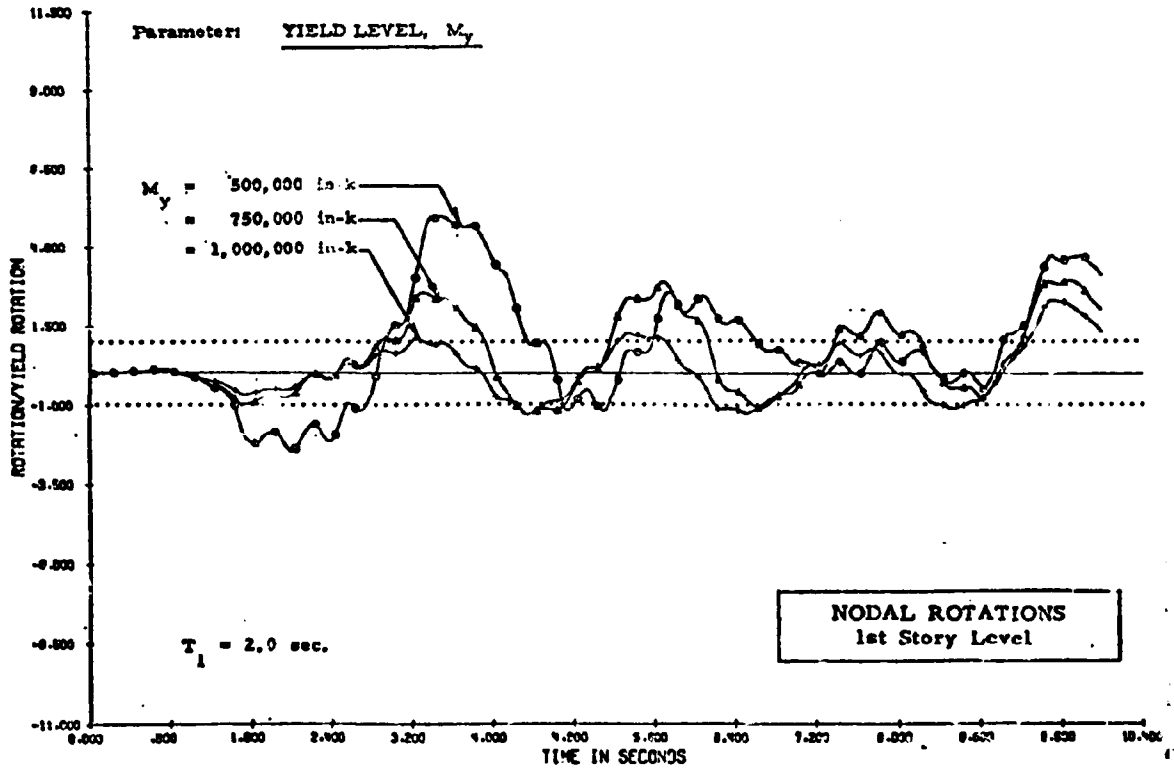

Fig. B16

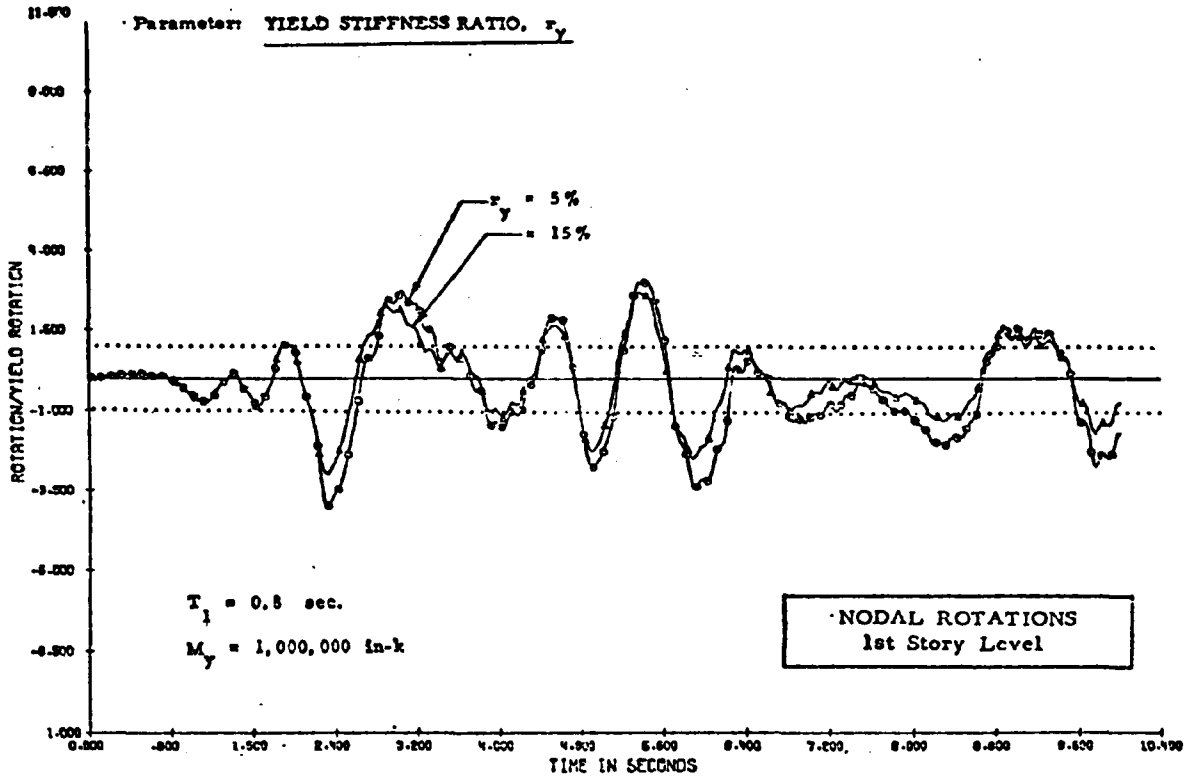

Fig. B17

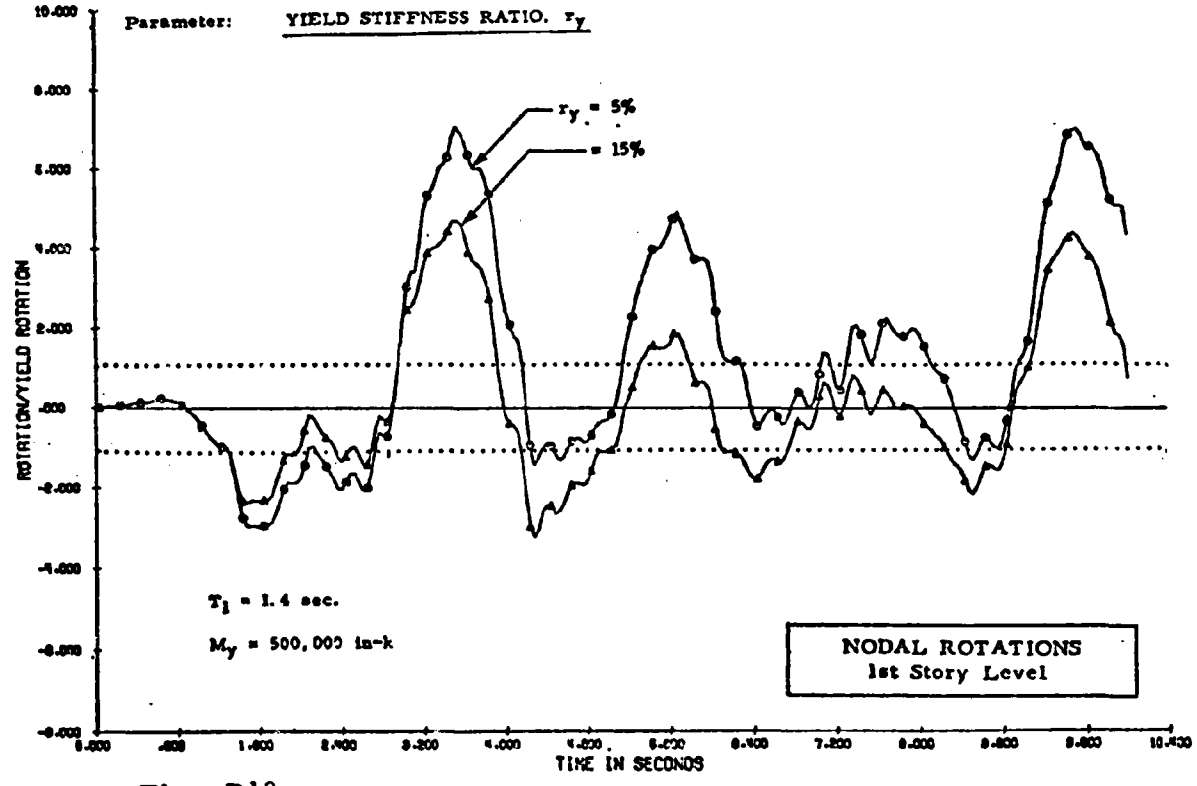

Fig. B18

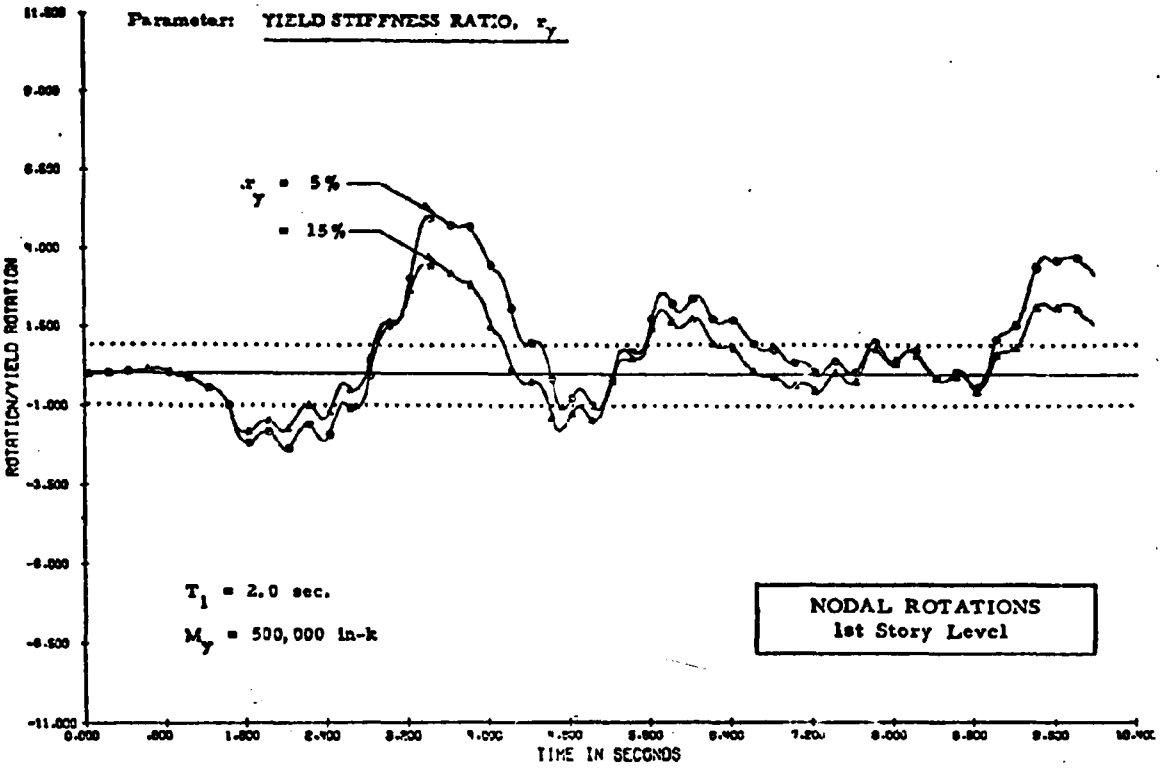

Fig. B19

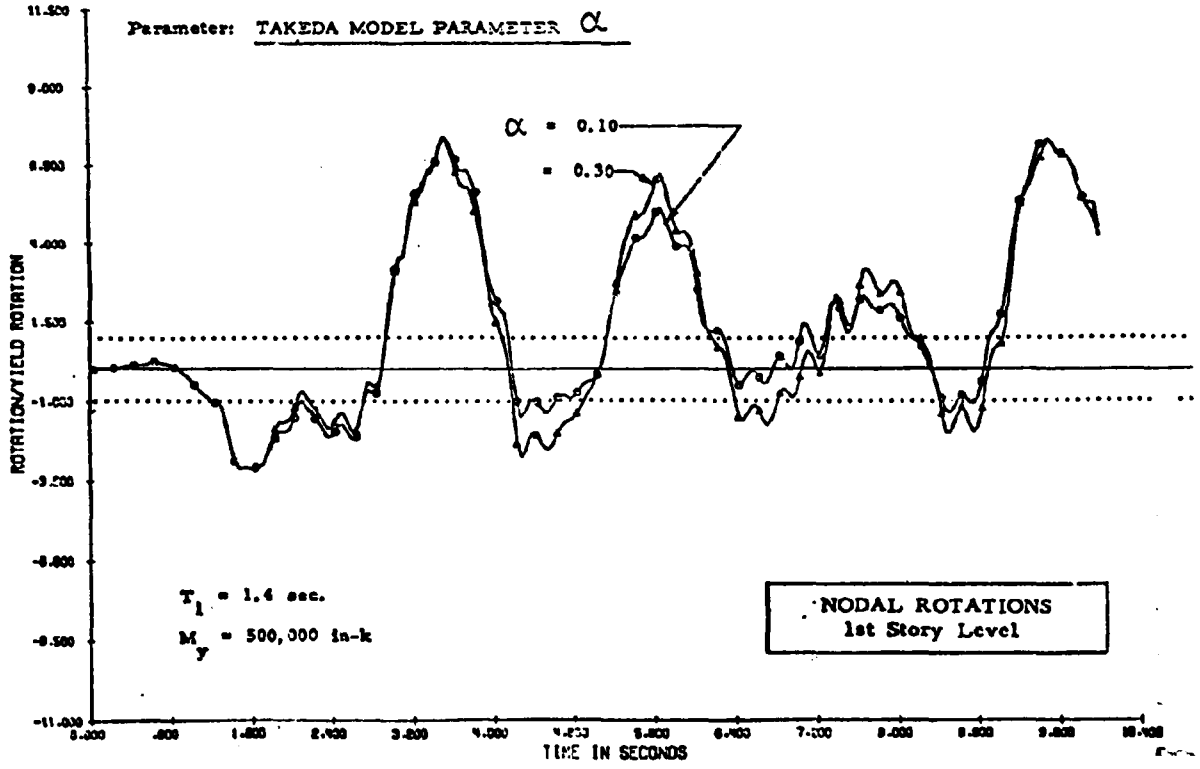

Fig. B20

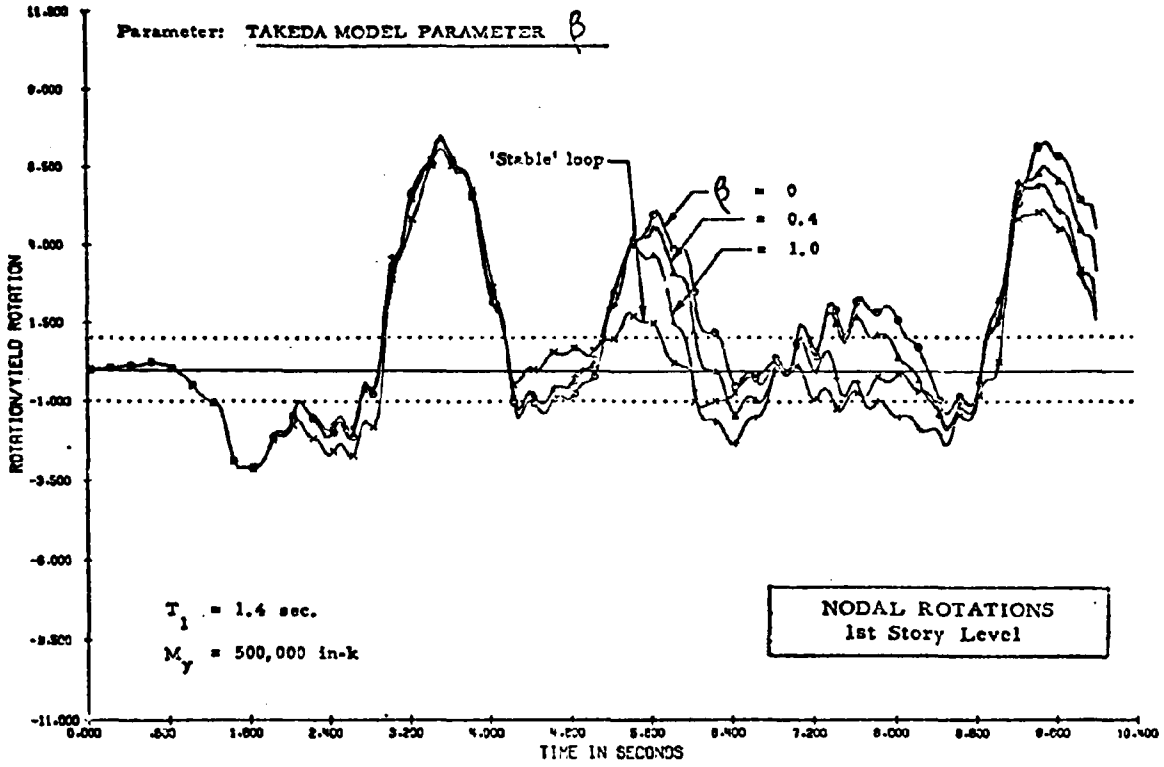

Fig. B21

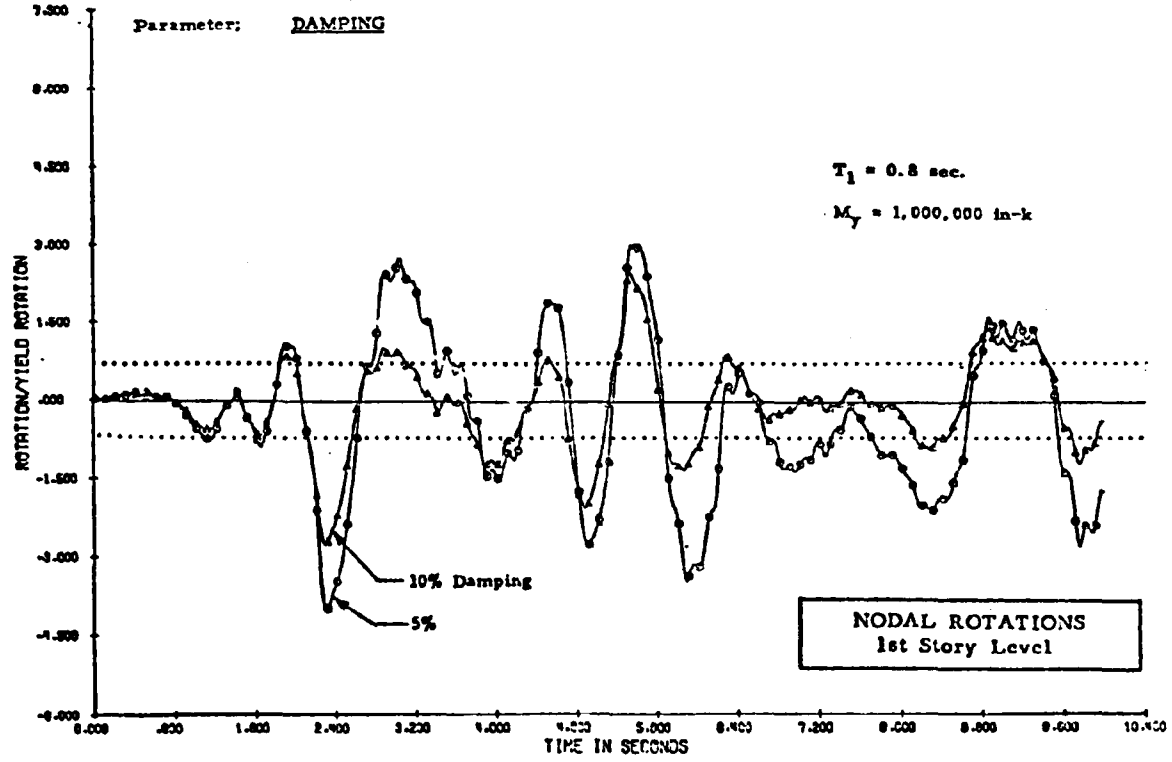

Fig. B22

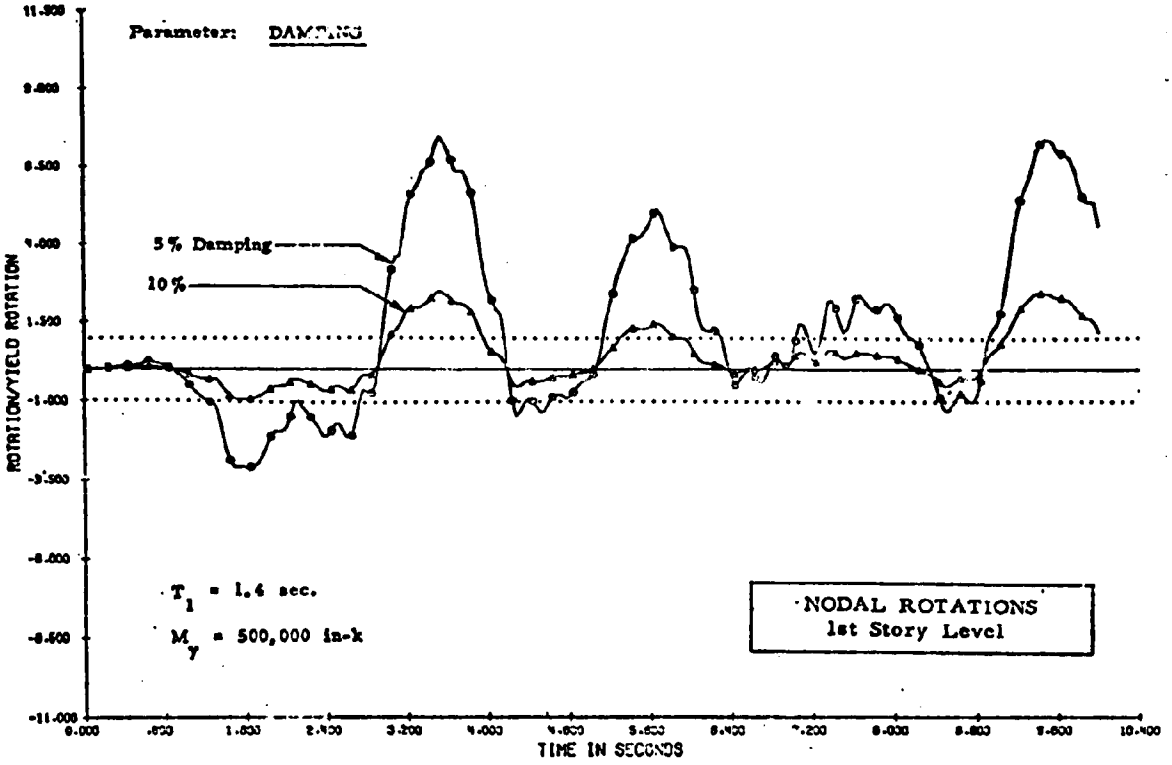

Fig. B23

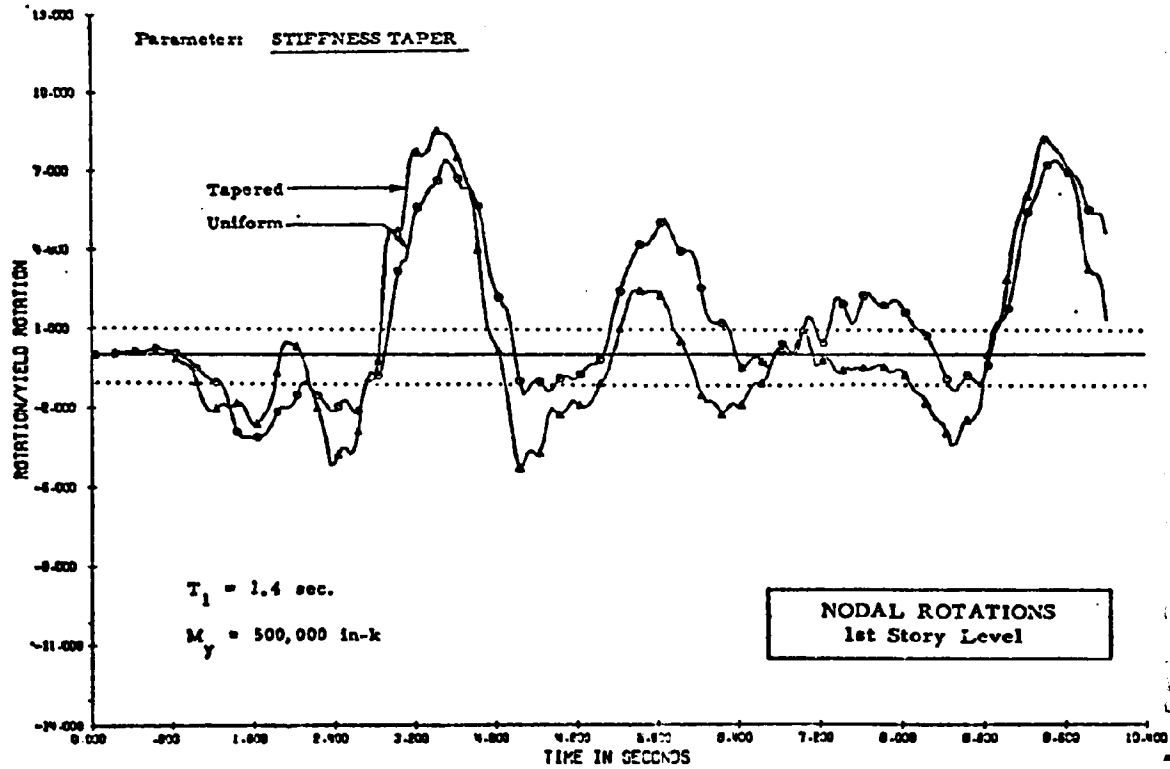

Fig. B24

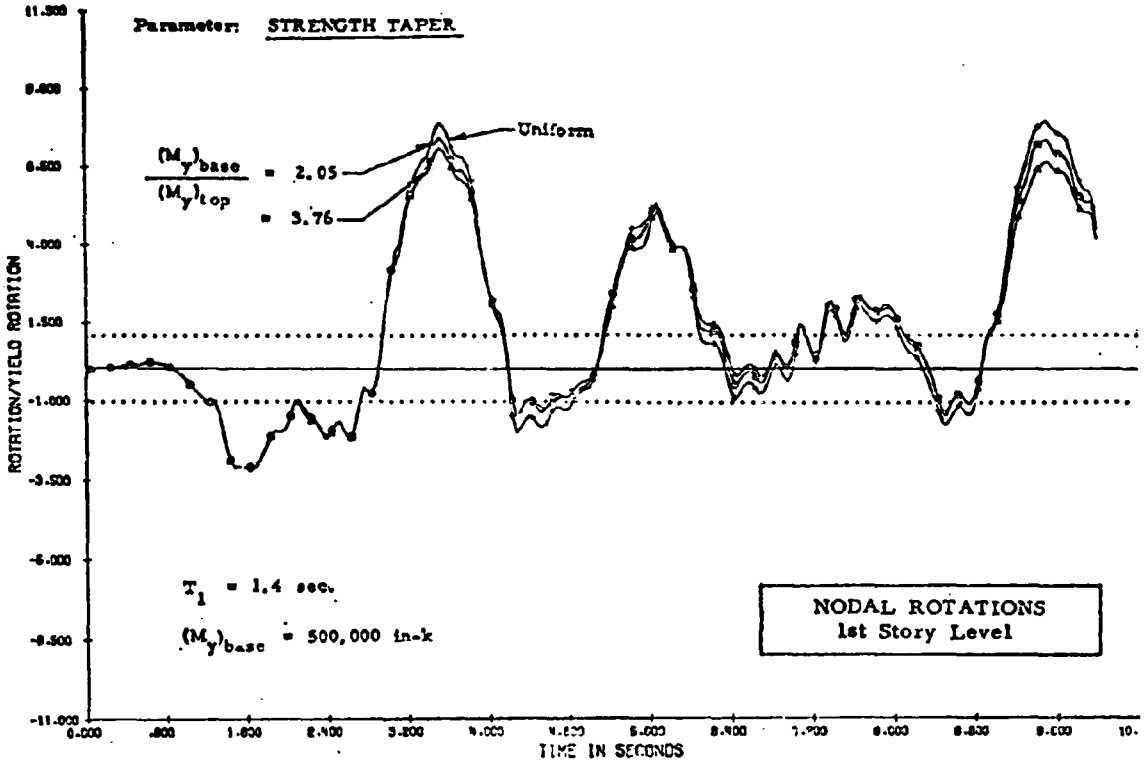

Fig. B25

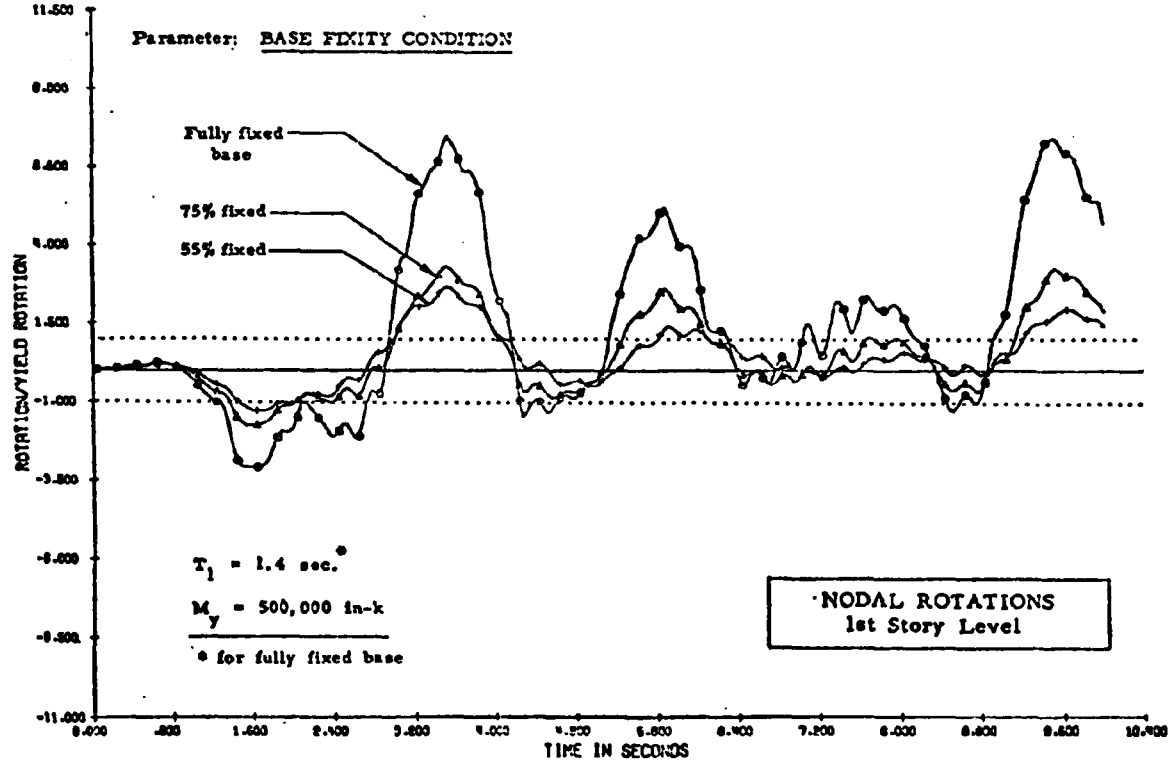

Fig. B26

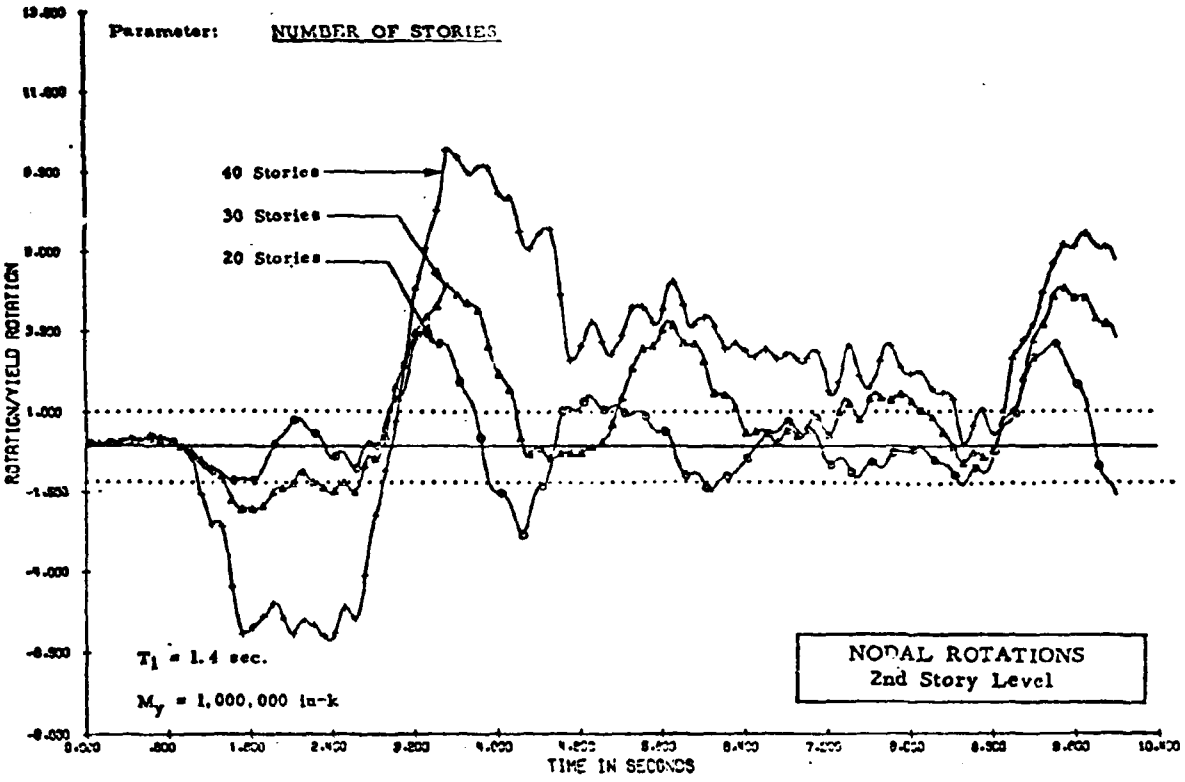

Fig. B27

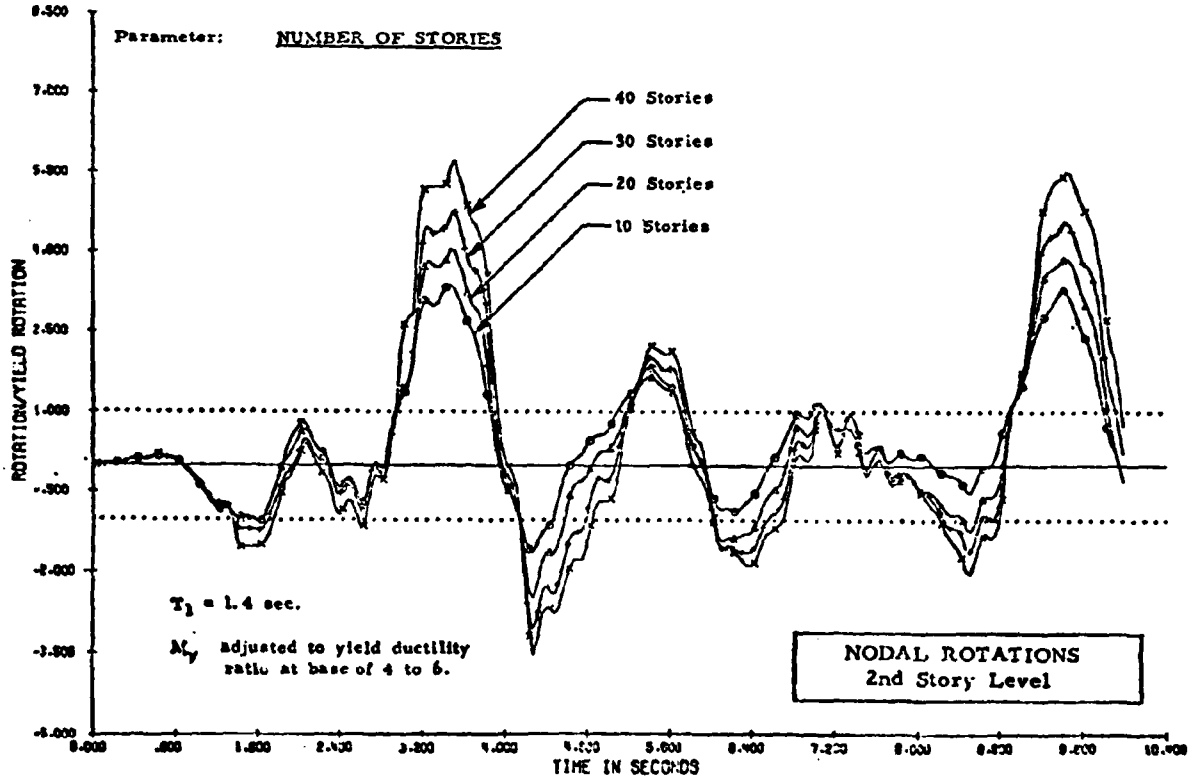

Fig. B28

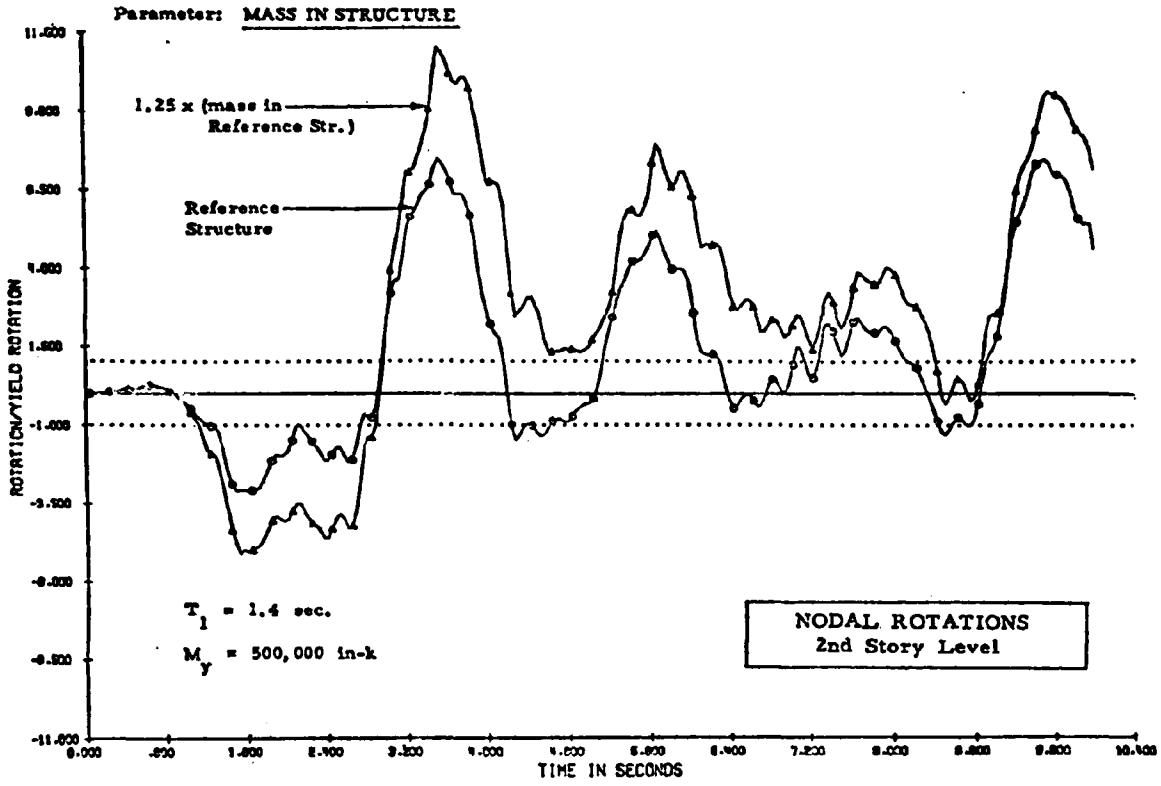
Parameter: MASS IN STRUCTURE
1.25 x (mass in Reference Str.)
Reference Structure
ROTATION/YIELD ROTATION
T_1 = 1.4 sec.
M_y = 500,000 in-k
NODAL ROTATIONS
2nd Story Level
TIME IN SECONDS

Fig. B29